N°: **42129**

PhD Thesis

MODIFIED LIGNIN AS FLAME RETARDANT FOR POLYMERIC MATERIALS

PhD defended at

UNIVERSITE LILLE1 SCIENCES ET TECHNOLOGIES

École doctorale Sciences de la Matière, du Rayonnement et de l'Environnement, UFR de Chimie

To obtain the grade of

DOCTEUR

Specialty: Materials Sciences

by

Benjamin PRIEUR

Graduated Engineer of Ecole Nationale Supérieure de Chimie de Lille

PhD thesis supervised by

Prof. Serge Bourbigot and Prof. Gaëlle Fontaine

Defended on October, 18th 2016 in front of the following dissertation committee:

Prof. Sophie Duquesne	Université Lille 1	President
Prof. Giovanni Camino	Politecnico di Torino	Reviewer
Prof. Luc Avérous	Université Strasbourg	Reviewer
Dr. Roland Klein	Fraunhofer Institute LBF	Examiner
Prof. Serge Bourbigot	Université Lille 1	Director
Prof. Gaëlle Fontaine	Université Lille 1	Co-Director

Acknowledgement

First, I would like to thank Prof. Alexandre Legris, head of the UMET laboratory, and Prof. Serge Bourbigot, head of the group ISP and the team R2F (Reaction and Resistance to Fire). I would like to thank them for giving me the opportunity to join this laboratory, work on this project and achieve this PhD in excellent job conditions. I extend my thanks to Mr. Bernard Fontaine, head of the École Nationale Supérieure de Chimie de Lille (ENSCL), where the laboratory is located.

Obviously I would like to thank my supervisors, Gaëlle and Serge, who gave me the possibility to work with them and to pass my PhD thesis in the R2Fire lab. Working with them was a great pleasure throughout these three years, on both the PhD thesis and the PHOENIX project. Their encouragement and support helped me to progress. I appreciated their scientific knowledge and their availability, whenever it was needed. Was it a great experience? "YES YES YES"!

I am very grateful to Prof. Sophie Duquesne who agreed to chair the jury, and to Prof. Luc Avérous, to Prof. Giovanni Camino as well as to Dr. Roland Klein who accepted to take their time, to bring their expertise as reviewers of this work and to be part of the jury.

I would like to acknowledge all the industrial and academical partners of the PHOENIX consortium. Obviously for the work we achieved together, but also for all these awesome social events we shared during these three years. In particular, I would like to thank Roland Klein, Matthias Wittemann and Marcel Meub from Fraunhofer LBF for our collaboration about lignin, the support they provided me and the constructive discussions we had together. Finally, I especially want to thank Begoña, Hristin, Christof and Nicolas (aka PS, for more details please ask Serge).

I also sincerely thank all current and former members of the R2F team for all the moments we shared in easy-going atmosphere. First, thanks to those who left before me but brought me a real pleasure to work in the beginning of this PhD: Bastien, Marianne, Marion, Caroline, Nico Renaud, Gwen, Trang, Francis and in particular Carmen. Thanks to all the lab's permanent members: Gaëlle, Sophie, Serge, Fabienne, Mathilde, Michel, Maude, Charaf', Catherine, Severine. Of course many many thanks to Bridgie, for her support, her good mood and most of all her patience.

Table of contents

Abbreviations

ABS	Acrylonitrile Butadiene Styrene
APP	Ammonium polyphosphate
ATR	Attenuated total reflectance
CC	Cone calorimeter
CP	Cross polarization
DSC	Differential scanning calorimetry
DTG	Derivative thermogravimetry
EPMA	Electrom probe microanalyzer
EVA	Ethylene-vinyl-acetate
FR	Flame retardant
FTIR	Fourier Transformation Infrared
GC	Gas chromatography
GW	Glow Wire
HPDEC	High power decoupling
HRR	Heat release rate
IS	Intumscent system
LIG	Neat Kraft lignin
LOI	Limiting Oxygen Index
MAS	Magic angle spinning
MLC	Mass loss cone
MS	Mass spectrometry
NMR	Nuclear magnetic resonance

PCFC	Pyrolysis combustion flow calorimeter
P-LIG	Phosphorylated LIG
pHRR	Peak of HRR
PHY	Phytic acid sodium salt hydrate
PLA	Polylactide
POSS	Polyhedral oligomeric silsesquioxane
PP	Polypropylene
PS	Polystyrene
Py	Pyrolyzer
SEC	Size-exclusion chromatography
SEM	Scanning electron microscopy
STA	Simultaneous thermal analysis
SUCC	Succinic acid
TGA	Thermogravimetric analysis
THF	Tetrahydrofuran
THR	Total heat release
TPU	Thermoplastic polyurethane
TTI	Time to ignition
XPS	X-ray photoelectron spectroscopy
XRD	X-ray diffraction

General introduction

The petrochemical boom of the second half of the last century has marked the beginning of a new area for chemistry. The use of oil-based platform molecules offered a large diversity of possibilities, and the opportunity to develop an infinity (or almost) of chemical compounds used as fuel, polymers, additives, medicines. Oil-based chemical products are now found in plenty of domains, such as health, transportation, building or textile industries. However, an increase of the awareness of the human society coupled with the decreasing of fossil resources feedstock in the last decades force the scientific community to find alternative solutions. Therefore, a strong interest has been growing on considering sustainable resources, especially in the energy and materials areas [1], these domains consuming oil-derivatives products in a large extent.

In the context of using sustainable resources, a specific attention has been called for biomass. Biomass is biological material derived from living, or recently living organisms. In the context of biomass for energy or material science, this is often used to mean plant based materials, even if it can be equally applied to both animal and vegetable derived material. Among biomass, lignocellulosic material is particularly of interest because it is not in competition with food applications. Moreover it is a renewable feedstock, available in a large amount on Earth [2]. Cellulose, lignin and hemicellulose are the three main components of the lignocellulosic biomass. The composition however depends on the botanical origin and is presented in Figure 1 [3]. Cellulose and hemicellulose are used in plenty of applications, such as textile and pulp industries. Nonetheless, concrete applications of lignin are rare.
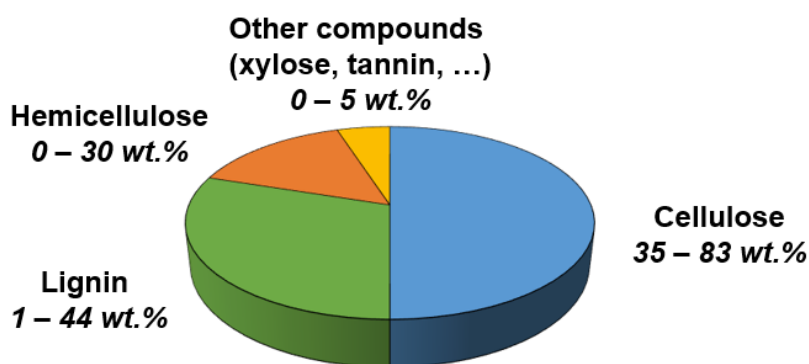
Figure 1. Schematic representation of contents of the lignocellulosic biomass

Because historically considered as a low value product, lignin is predominantly obtained as by-products of the pulp industry and varies in it chemical and physical properties depending on isolation methods and plant origin [4]. As a consequence the majority is used as fuel and only about 2 wt.% is employed for concrete applications such as binders and surfactants [5]. But taking into account that biosphere contains 3×10^{11} tons of lignin and that is increasing annually, major efforts were undertaken in the last decade to take advantage of this material. This interest in lignin is reflected by the significant growing number of scientific papers shown in Figure 2. This is explained by the fact that until 2000, lignin was mainly studied in regard with the pulp industry (isolation and extraction processes for example). Now, lignin is involved in many other domains and therefore the amount of publications grows significantly. The creation of international cooperation such as the EUROLIGNIN project illustrates this interest in lignin [6]. Moreover, the concept of biorefinery emerged and high value lignin becomes available in a large extent [7]. Because lignin is a polyphenolic macromolecule, it can be used in several ways for different applications [8]. Researches are mainly focused on using lignin, neat or chemically modified, as chemicals source (fragmentation of the structure), low or high value additive for polymers (UV stabilizer, antioxidant) or as building elements in the design of bio-based materials (lignin-based materials such as polyurethane or epoxy).
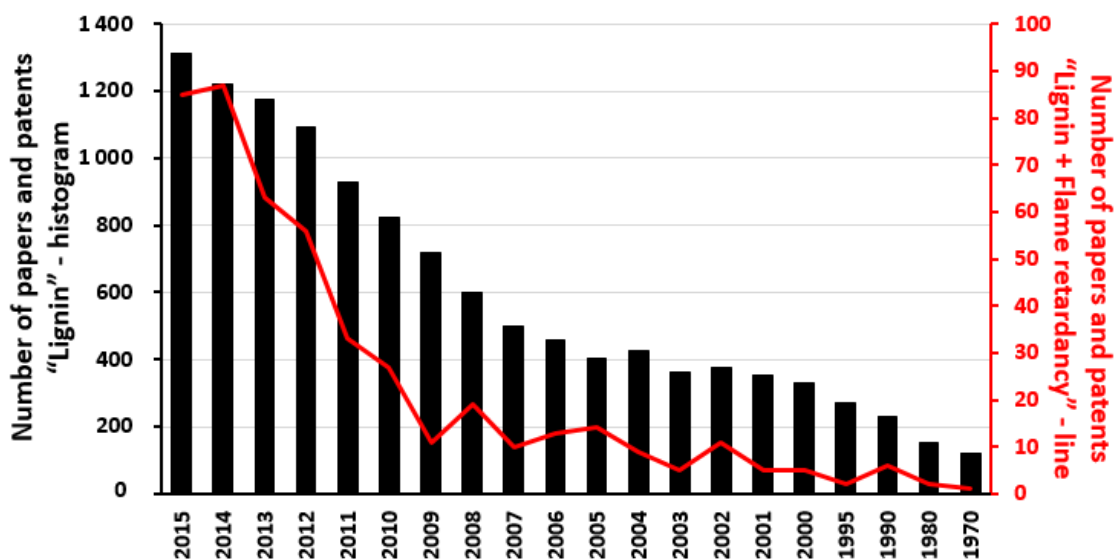
Figure 2. Number of papers or patents for "Lignin" and "Lignin + Flame retardant"

(Scifinder July 2016)

Among these applications, lignin exhibits promising performance when used as flame retardant additives for plastics. It is noteworthy that the production of plastics grew fast in the 1950s and never decreased since that time, except during the oil shocks in 1973 and 1979, and because of the crisis in 2008 [9]. In spite of their properties and the variety of their uses, plastics exhibit one major drawback: they are highly flammable. In case of fire, these materials will tend to release fuel and toxic smokes. Statistics in the US report that 1,240,000 fires occurred in 2013 [10]. In that frame, it has become really necessary to develop Flame Retardants (FR) to reduce the risk inherent to the use of plastics. FR additives represent a large group of chemicals consisting mainly in organic and inorganic compounds based on halogens, nitrogen, boron, phosphorus, sulfur, metals (mainly aluminum and magnesium) (Figure 3) [11]. As the general trend in chemistry slowly shifts towards the use bio-based chemicals, studies are undertaken to find sustainable FR additives, and lignin may be considered as carbon source and/or charring agent. Because the global consumption of FR reached about 2 million tons a year in 2011, and growing, it represents a real market opportunity for valorization of lignin (Figure 2).
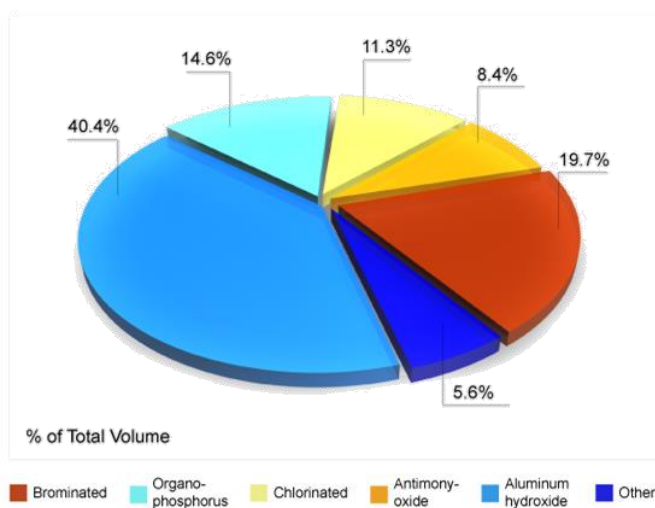
Figure 3. Global consumption of flame retardants by type (2011 data) [12]

However, even if more and more interesting papers deal with the use of lignin as FR for polymers (see Figure 2), each study dealt with different types of lignin and/or various polymers. As a consequence, the conclusion about lignin as FR vary from one author to another. At the moment, there is clearly a lack of homogenized results. In this context, lignin was considered in the European FP7 project called PHOENIX. This project is a consortium of fifteen academic and

industrial partners, which aims to find a solution to substitute the halogenated flame retardant (HFR) additives used in flame retarded (FR) thermoplastic and thermoset materials. One of the objectives is to develop new FR additives from lignin. To overcome the problem of homogenized results, a unique source of lignin, Kraft lignin, was considered, as it is one of the most available on the market. As phosphorylation of lignin appears to be promising for FR applications [13,14], Kraft lignin was phosphorylated in the frame of the PHOENIX project by the Fraunhofer LBF. This PhD thesis is part of this project, and more specifically involved in the understanding of how lignin can act as FR in polymers.

The PhD thesis is organized into five different chapters. The first chapter gives a general background about lignin and the influence of both botanical and extraction processes on its chemical structure. The usual characterization techniques, its properties and the common application of lignin are also investigated. Then, the chapter details reviews of the use of lignin as FR additive in polymers. This section gives, when applicable, lignin's mode of action proposed in different papers. Finally, the strategy of the PhD, based on the literature survey, is detailed.

The second chapter presents the materials used in this study. The polymer and flame retardant additives as well as the material preparation are described. Then, characterization methods will be presented. Tests to characterize lignin, properties of the composites and fire properties as well as experimental techniques to investigate the fire retardant will be depicted.

The third chapter is dedicated to the characterization of neat and phosphorylated lignin. Neat lignin chemical structure and properties are first characterized. The influence of the phosphorylation on lignin's structure and properties are then discussed. The last part is focused on the understanding of the thermal decomposition mechanism of lignin, and how the phosphorylation impacts the thermal stability.

Chapter four presents a screening of lignin incorporated in different polymers. The objective of this chapter is to find a polymer in which a lignin-based system exhibits the best fire performance. First, neat lignin is incorporated into different polymers and the FR performance are evaluated. Afterwards, the most promising polymers, polylactide (PLA) and acrylonitrile-butadiene-styrene (ABS), are selected and lignin-based FR systems are developed. Neat and phosphorylated lignin

are used in combination with different additives or synergists. The FR performance of these systems are evaluated.

In chapter five, a selected FR system, ABS containing lignin or phosphorylated lignin, is investigated. The aim is to elucidate the mode of action of lignin, and understand why the phosphorylation of lignin permits to further improve the FR performance of ABS. At first, material properties of the composites are evaluated. Then, fire retardant performance is assessed by different FR testing. Finally, the last part is devoted to the investigation of the thermal stability as well as the analysis of both gas and condensed phase. Afterwards, a mode of action of lignin and phosphorylated as FR is proposed.

At the end of this work a general conclusion is given and proposal for future studies on this subject are proposed.

I- State of the art: Lignin as FR additive in polymers

In this study, lignin, an abundant bio-polymer, is intended to be used as potential bio-based flame retardant for polymers. In order to gain knowledge in lignin materials and to further develop it as FR additive, a literature survey is necessary. First, a complete description of lignin is proposed. Origin, structure elucidation and main applications are presented. Then, some basics about the flame retardancy are reminded in order to better understand how lignin might be used as flame retardant. Finally, an overview of the systems involving lignin as FR in polymers is discussed.

1. Lignin materials

Lignin is a natural material found in plants and threes. If mass is considered, it is the second most abundant bio-polymer available on earth after cellulose. Lignin represents 30 % of all non-fossil organic carbon, and its availability exceeds 300 billion tons. The major supplier of lignin is the pulp and paper industry, which extracts around 50 million tons of lignin per year [8]. In 2004, the largest part of the produced lignin was directly burnt at the facilities for energy recovery. Only 2 % of it was indeed commercially used. Common applications of lignin were part of niche markets, such as dispersing and binding agents. Why lignin was under exploited? Actually, lignin's structure is very changing depending on botanical origin or extraction process, and these changing properties are the main obstacle to industrial valorization. However, the growing interest for a green and sustainable chemistry forces the scientific community to take advantage of the huge renewable feedstock that represents lignin. Therefore, significant efforts are put on lignin researches to standardize the use and find suitable applications [6]. As shown in Figure 4, the use of lignin as additive is now an important part of the applications, and will become more significant in the upcoming years. Indeed, the lignin market is expected to reach 985.5 million dollars in 2023 [15]. Lignin's valorization is therefore a topic of major interest, as the development of biorefineries becomes stronger and stronger [7].
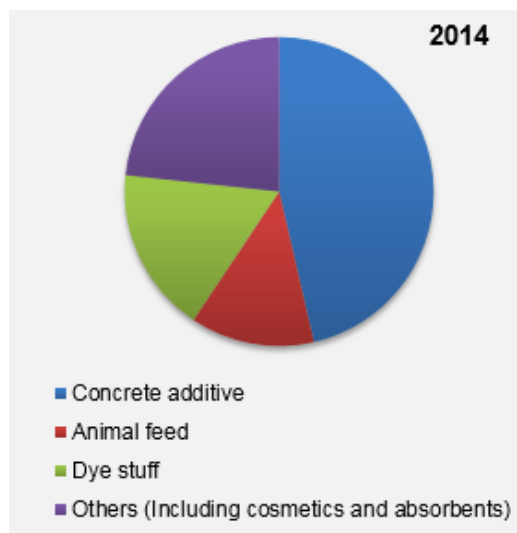
Figure 4. Global lignin market volume share by application in 2014

(Source: Transparency Market Research Analysis 2015)

1.1. Generalities

1.1.1. Origin and botanical provenance

1.1.1.1.   Origin

Lignin is the second most abundant of the three major polymers found in the biomass, and the main one is based on aromatic monomers. Among the lignocellulosic biomass, the lignin content can vary between 17 and 40% depending on the plant [16]. These three components form a highly efficient system, and lignins act as a matrix that binds the plant polysaccharide microfibrils and fibers together, thus improving the strength and rigidity of the plant which is necessary for a vertical growth. Lignin also performs other biological functions like the protection of plants against biological attacks or assisting in water transport by sealing plant cell walls against water leaks.

Its chemical structure is a randomly branched polyphenol made up mainly of three phenylpropane monomers, also called monolignols: p-coumaryl alcohol, coniferyl alcohol, synapyl alcohol (Figure 5). At the birth of a tree or a plant, after the cell growth has ceased, lignin is formed by a dehydrogenative polymerization of the three monolignols, which are produced from D-glucose [17]. Randomly linkage occurs at different locations on each phenolic unit, leading to dilignols, which are then extended to oligolignols and finally to the polymeric lignin. Therefore the three monomers units become called p-hydroxyphenyl (from p-coumaryl alcohol), guaiacyl (from coniferyl alcohol) and syringyl units (from synapyl alcohol). In the following, this monomeric units are cited as H, G or S respectively (Figure 5).
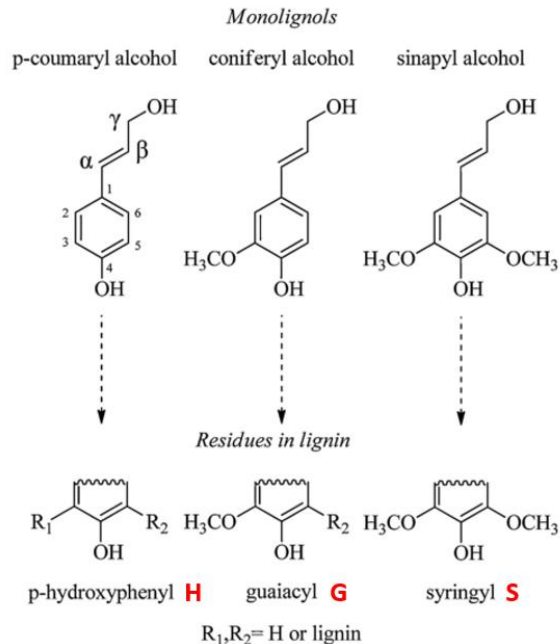
Figure 5. Monomeric lignin precursors [8]

The combination of this three monomers leads to a highly branched polyphenolic polymer with a three dimensional structure, which is particularly complex to elucidate. Models have been developed to draw lignin structures with the relative proportions of each monolignols and linkage types [18]. Whetten *et al.* investigated the possible bond types linking the monomers together, and concluded that at least 20 different linkages are present in a common lignin structure [19]. Generally the β-O-4, α-O-4, β-5, 5-5, 4-O-5, β-1, and β-β linkages are the most common bonds (Figure 6) [20]. The ether linkages are estimated to make up at least one half of the total number of native plant lignin linkages [21]. Beside typical linkages, several chemical groups are contained in the structure, such as aromatic and aliphatic hydroxyl, carboxylic, carbonyl and methoxyl groups.

So the lignin's structure is very influenced by its botanical origin. But it is also highly dependent of the extraction process, what is presented in the next section.
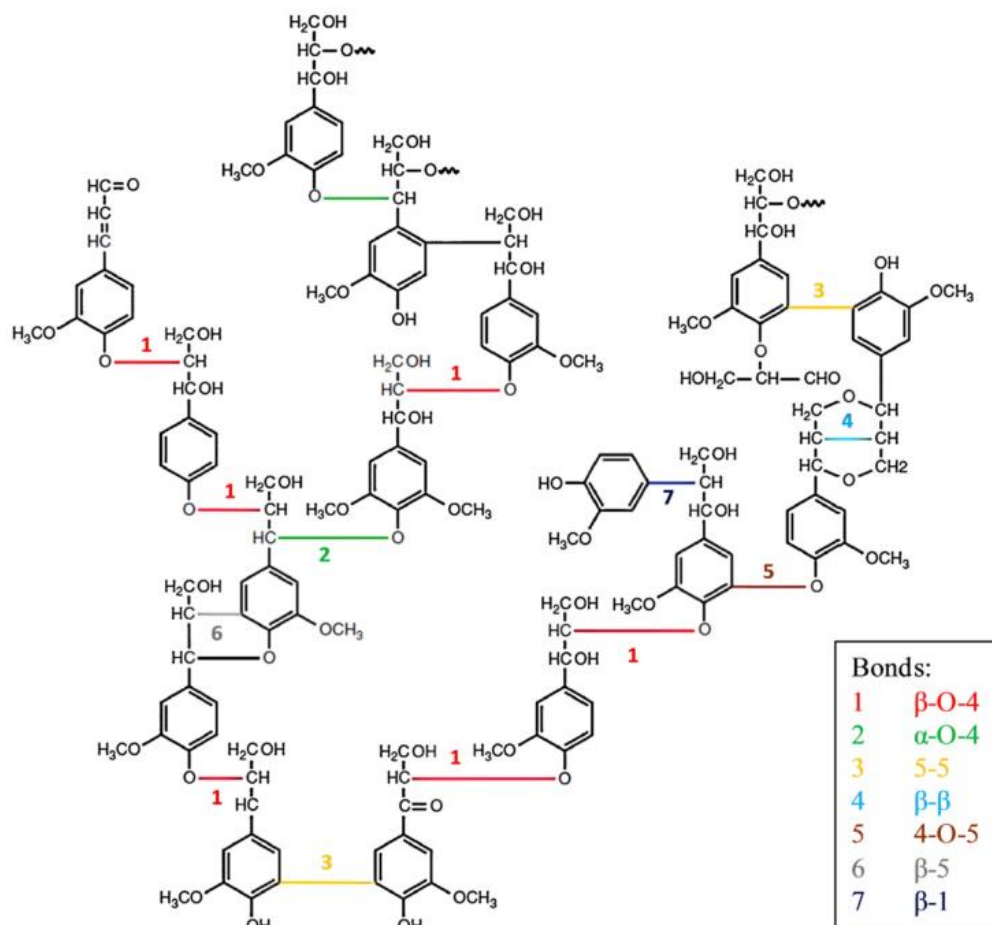
Figure 6. Structure and common intermonomeric linkages of a softwood lignin [8]

1.1.1.2. Influence of the botanical resource

Since the lignin is built from a complex enzymatic mechanism, its final structure is influenced by many parameters, such as the biological environment and the monomers concentrations. Botanical origin significantly affects the lignin architecture: monomers repartition, elementary composition as well as linkages occurrence and repartition. A typical classification differentiates hardwood (also known as angiosperm), softwood (gymnosperm) and grass lignins as seen in Table 1. Hardwood lignins derivate mostly from coniferyl (G) and synapyl (S) monolignols, while softwood lignins contain mostly coniferyl monolignols [19]. With similar G/S ratios as for hardwood, grass lignins contain also units from p-coumaryl monolignols (H) [22].

Table 1. Classification of lignin according to the botanical source

	Sources		
	Hardwood = Angiosperm	**Softwood = Gymnosperm**	**Grass**
Units in lignin's structures	Guaiacyl, Synapyl Ratios from 4:1 to 1:2	Guaiacyl mainly	p-hydroxyphenol, Guaiacyl, Sinapyl
Usual name	G-S lignins	G lignins	G-S-H lignins

Beside monomeric units' content, the botanical origin also may also modify the mechanism of lignin formation. Therefore, the types and the content of linkages involved in the lignin structure depend on the plant or tree. In this context, Dorrestijn *et al.* investigated this phenomena by comparing linkages occurrence in lignin from hardwood or softwood [23]. The results are listed in Table 2. Depending on the wood's type, some trends can be established. First, β-O-4 linkage is the main bond in the lignin structure and ranges from 46 to 60% of the overall amount. Accordingly to α-O-4, β-1, 5-5 and 4-O-5 linkage occurrences, softwood is more condensed than hardwoods lignins [16], and such structural difference should have an impact on the lignin material properties such as the thermal stability [24]. Such changes could be interested for fire retardant applications. So botanical origin clearly influences the lignin's structure. What about the influence of extraction process? The following section deals with these processes and which structural changes of lignin they might induce.

Table 2. Inter-unit linkages and functional groups

occurrence of spruce and beech lignin [23]

Bond types Functional groups	Proportions (%)	
	Softwood lignins	**Hardwood lignins**
Arylglycerol-β-aryl ether (β-O-4)	46	60
Noncyclic benzyl aryl ether (α-O-4)	7	7
Phenylcoumaran (β-5)	11	6
Resinol (β-β)	2	3
Biphenyl (5-5)	10	5
Diaryl ether (4-O-5)	4	7
1,2-Diarylpropane (β-1)	7	7
Other	13	5

1.1.2. Extraction of the lignin from the lignocellulosic biomass

1.1.2.1.   Extraction processes

In order to get access to the lignin, several separative techniques have been developed. Basically, it can be isolated from extractives-free wood as an insoluble fraction after hydrolytic removal of polysaccharides, for example like the Klason lignin with 72% sulfuric acid. The Klason procedure is often used to quantify the amount of lignin of lignocellulosic material [16]. Another technique is the Björkman method leading to the so called milled wood lignin. But both of these techniques only permit to produce lignin at lab-scale quantities. Actually, the largest amount of lignin produced in the world is obtained from the pulping industry, which considers lignin as by-product.

Indeed, the lignocellulosic biomass is a very abundant resource which contains a well-known polymer, the cellulose. Depending on the botanical origin, it ranges from 35-83 wt.% of the dried biomass. Because of its intrinsic properties, this polysaccharide is used as common chemical (or polymer) in numerous sectors, such as the paper industry. To get access to cellulose, lignin (representing 1-43 wt.%) has to be degraded and therefore it is considered as byproduct in such industry. To do this, many techniques are used involving mechanical, thermo-mechanical or chemical processes. The approach using chemistry is mostly preferred in the industry, and they can be split into two categories: sulfur and sulfur-free methods (Figure 7).

The sulfur processes include the Kraft and the lignosulfonate lignins. These are the most produced lignin in the world, especially the Kraft [25]. In the Kraft process, the wood is treated with a Na_2S/NaOH solution with a temperature ranges from 155 to 175°C for several hours. The cellulose is then separated from the "black liquor". This dark solution is put in a basic media (pH = 13) in which the lignin precipitates to be recovered. The sulfur-free methods are the new generation of extraction processes, and aim at the production of lignins with less degraded structures. Some processes are listed hereafter. Organosolv lignin is extracted from different organic solvent-based procedure at a high temperature/pressure. Alcell (ethanol/water), Organocell (methanol/NaOH/anthraquinone pulping), steam explosion and Biolignin© processes are some of the recent developed methods, thus leading to commercial lignins [25].
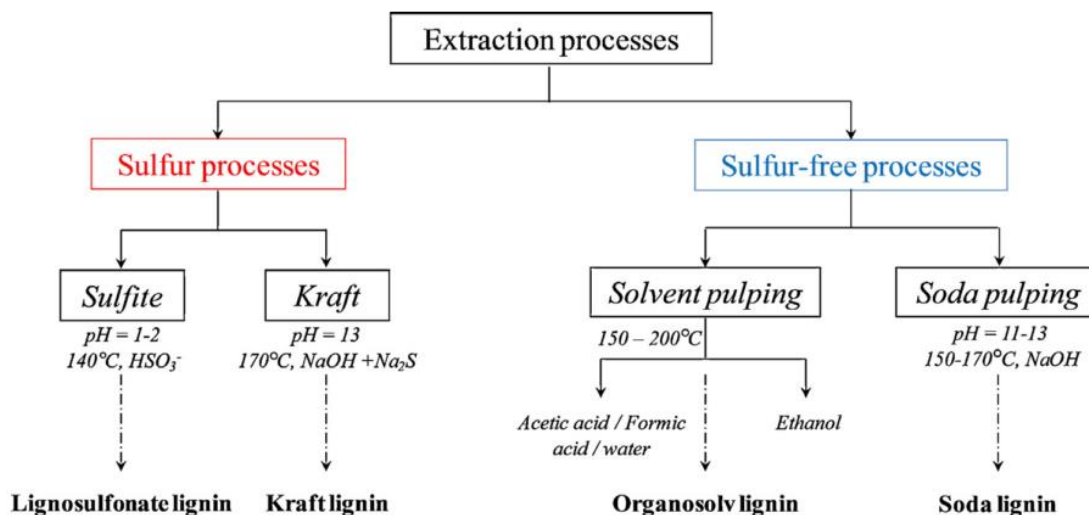
Figure 7. Different extraction process to get technical lignins [8]

All these processes do not have the same influence on the lignin structure since they use very different techniques. The next part is devoted to evaluate the impact of such processes on the lignin chemical structure.

1.1.2.2.   Influence of the extraction process

A major concern in the context of the lignin's valorization regards the numerous grades of available lignin. First it has been pointed out the role played by the botanical origin. Furthermore, the extraction processes also contribute to change the lignin's structure, so it is therefore necessary to evaluate their influence.

J. Kim *and al.* investigated the difference observed on organosolv (OL), ionic liquid (IL) and Klason (KL) processes for extracting lignins from the same botanical source, i.e poplar wood [26]. Milled lignins (ML) were used as reference [27]. First, each process yielded to different amount of lignins, which are 5.5 wt.% for ML, 3.9 wt.% for OL, 5.8 wt.% for IL and 19.5 wt.% for KL. Therefore the amount of recovered lignin is very dependent of the extraction process. In order to investigate the structure, elemental composition as well as functional groups contents were quantified. In the case of ionic liquid lignin (IL), more cleavages of the β-O-4 linkage occurred in comparison to Klason (KL) and Organosolv (OL) procedures, thus leading to a higher aromatic hydroxyl groups amount in IL. Furthermore, the amount of carbon double bonds was higher for OL, IL and KL, thus indicating a higher condensation level in comparison to ML. β-0-4 bonds represent 40 to 60% of

the bonds in lignins but were barely detected in KL and OL, that could be due to the extensive condensation occurring during sulfuric acid treatment [28]. In conclusion, OL and KL were the lignin with the highest condensed structural form. The influence of the condensation degree on the lignin's properties will be discussed in the following.

Organosolv and soda processes (both sulfur-free) were also compared [29]. From an advanced characterization by FTIR spectroscopy, it has been established that the lignin produced by the soda cooking is more oxidized than that from organosolv cooking. Indeed higher amount of carbonyl and carboxylic acid groups were detected. In conclusion, the extraction process deeply influences the structure of the produced lignin. Changes occur in terms of presence and/or amount of chemical groups and inter-units linkages, so to say the skeleton of the polymeric lignin. It is shown that the properties of lignin considered as polymeric material, such as solubility or molar mass, are considerably affected by the extraction process [8]. These properties will be commented in the part 1.2.2.2, p36.

In this context, when speaking about "lignin material", it should be mentioned from which botanical origin the lignin is and by which process it was extracted. Numerous lignins should be considered and in the frame of this work, the study is focused on lignin available at high volume. Lignin from industrial processes are therefore taken into consideration, such as Kraft lignin. The next part is then focused on the techniques for characterizing lignin usually performed, followed by an overview of the physico-chemical properties of the lignin materials.

1.2. Characterization and properties

The characterization of lignin induces used for molecules as well as for polymers. In the last part, it was shown that depending on its botanical origin and extraction process, lignin exhibits different structures thus implying changes in its properties, such as the solubility in organic solvents. Therefore, it mays cause trouble for techniques requiring samples in solution. In the following section, characterization techniques adapted for lignin analysis are described. Then, material properties of usual lignins are presented. Since the aim of the study is to develop lignin-based flame retardant additives, the thermal degradation will be particularly investigated.

1.2.1. Structural characterization

1.2.1.1.   Non spectroscopic analysis in lignin chemistry

Historically, knowing the presence and amount of lignin in wood was important to develop and adapt the process allowing to access to cellulose. Simple and quick methods were established. The easiest method to detect lignin in a sample is to use coloring reactions, like the *Mäule test* in which is one of the oldest qualitative test [30]. It also permits to differentiate hardwood from softwood lignin. In terms of lignin's quantification, the most common method is the *Klason Procedure,* which is a test of reference in the paper industry. This method is based on the fact that cellulose and hemicellulose are hydrolyzed by concentrated sulfuric acid into soluble sugar while lignin is condensed to an insoluble cross-linked polymer [16]. In order to determine the purity of a lignin sample, standards were developed. The ash content, the acid-soluble part, the Klason lignin and the polysaccharide content may be determined according to ASTM D 1102-84, ASTM 1106-96, TAPPI UM250 and ASTM D 5896-96 respectively [31].

Elemental analysis is commonly performed in order to quantify the amount of the main elements such as hydrogen, carbon, oxygen, nitrogen and potentially sulfur. From these atomic ratios an empirical formula can be drawn. But in lignin chemistry the empirical formulae is mostly given referring to the hypothetical hydroxyphenyl structural unit, the so called "C9 formula" (see Figure 5, 23). In this case, the methoxyl content needs to be quantified, by ^{1}H NMR for example [32]. Combining all the data, the C9 formula can be established and helps to compare the empirical monomer unit of different lignin [33].

From 2002 to 2005, the European project EUROLIGNIN (G1RT-CT-2002-05088) aimed to accelerate the introduction of sustainable and high-value lignin based material [6]. In this project, many characterization methods have been developed. For example, systematic analytical protocols regarding the characterization of sulphur-free lignin by non-spectroscopic methods are proposed [34]. Aqueous titrations based on sodium hydroxide or hydrochloric acid permits to quantify the carboxylic groups. Non aqueous potentiometric titration with tetra-n-butylammonium hydroxide gives the amount of both phenolic hydroxyl and carboxylic groups. Another potentiometric titration with potassium methylate quantifies only the phenolic hydroxyls. Eventually, an HPLC analysis of saponified acetylated lignin determines the amount of

total hydroxyl groups. The molar mass was measured either by high pressure size exclusion chromatography (HPSEC) (in dimethylformamide) or vapor pressure osmometry.

The work achieved by EUROLIGNIN lignin was huge and recognized, and several protocols were adapted for other lignin's types, such as sulphur lignin (like the Kraft lignin). As an example, the molar mass determination is noteworthy in case of using lignin as polymeric material. The gas permeation chromatography (GPC, or SEC) is the common technique, however sulfur lignin is known to be hardly soluble in organic solvent. In order to avoid this issue, lignin is most of the time acetylated, thus increasing their solubility. Then the SEC can be performed in common solvents [31].

Because of their chemical structure, spectroscopy is powerful for analyzing lignin and can be considered. The use of such techniques for lignin chemistry is discussed in the next parts.

1.2.1.2.   UV and IR spectroscopies: advantages and limitations

In this part, the ultraviolet (UV) and infrared (IR) spectroscopies applied to lignin are described and compared. UV spectroscopy is used to evaluate the amount of phenolic groups. The method is based on the difference in UV absorbance maxima of phenols in alkaline and neutral solutions [35]. In alkaline solution, hydroxyls from phenolic groups are ionized and the absorbance shifts to higher wavelengths. Lignin samples with known and controlled phenolic content were used to calibrate the absorbance. Depending on the fact that the phenolic group is conjugated or not, three characteristic maxima at 250, 300 and 350 nm are commonly observed in the spectra (Figure 8). In spite of the simplicity of the UV measurements, the samples preparation is laborious and time-consuming. Even if some quick protocols were further developed [36], the use of this technique is limited only for phenolic groups. It is not sufficient for this this work, because aliphatic hydroxyl and other chemical groups are considered.
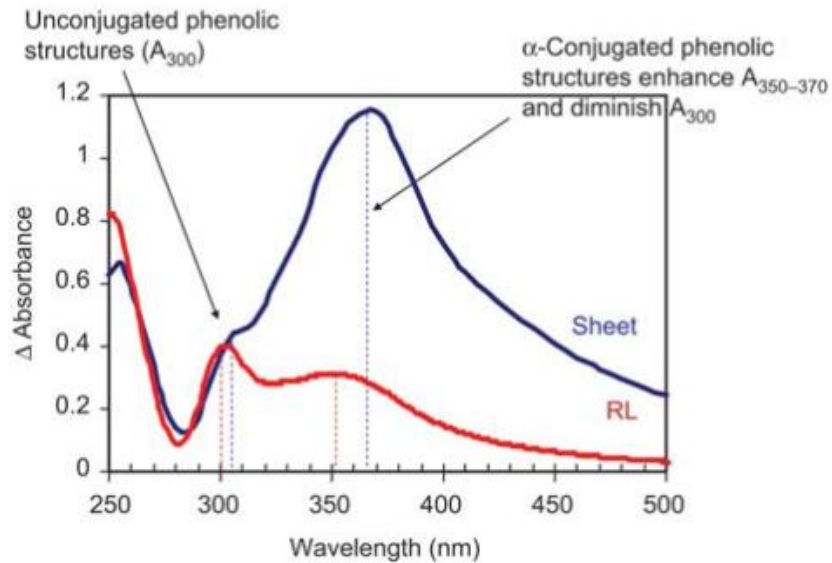
Figure 8. Ionization difference spectra measured for different lignin samples [36]

The IR spectroscopy is used most of the time in reflectance on solid sample (embedded in KBr or not). This makes the IR spectroscopy a universal method since many lignins are not soluble in aqueous or organic solvents. Therefore, this technique is commonly used to compare several lignin. IR spectroscopy gives information about chemical groups and specific bonds. Because of the complexity involved by the lignin's structure, only significant changes on specific bands can provide reliable information. Many researches intended to assign bands to specific linkages providing spectra library for different kind of lignins [29,37–39]. An example is given in Table 3, comparing absorption bands of softwood and hardwood lignins. Significant changes are mostly observed from the vibrations of syringyl units which are only observed for the hardwood lignin at 1340 and 1125 cm^{-1} (refer to section 1.1.1.2, p24). If the spectra are correctly normalized, conclusions can be drawn about hydroxyl groups or S,G and H monomers amounts. In order to compare the condensation degree of several lignins, a condensation index can be calculated from the spectra [31].

Table 3. Comparison of specific absorption bands in IR spectroscopy for different lignins [29]

Absorption band location cm^{-1}		Type of vibration
Softwood lignin	Hardwood lignin	
3500 – 3100		Stretching vibrations of alcoholic and phenolic OH groups involved in hydrogen bonds
1715 – 1710		Stretching vibrations of C=O bonds at β location and in COOH group
1665 – 1655		Stretching vibrations of the C=O bonds at α and γ location
1605 – 1595		Aromatic ring vibrations
1515 – 1500		
1430 – 1425		
–	1340 – 1330	Vibrations of syryngyl rings and stretching vibrations of C-O bonds
1272 – 1265		Vibrations of guaiacyl rings and stretching vibrations of C-O bonds
1225 – 1220		
1140	1150 (shoulder)	Deformation vibrations of C-H bonds in guaicyl rings
–	1125	Deformation vibrations of C-H bonds in syryngyl rings
1085	1085 (shoulder)	Deformation vibrations of C-O bonds in secondary alcohols and aliphatic ethers
1035 – 1130		Deformation vibrations of C-H bonds in the aromatic rings and deformation vibrations of C-O bonds in primary alcohols
945		Deformation vibrations of C-H bonds in associated to aromatic rings
870 – 850		
780		

Both UV and IR spectroscopies provide interesting information about lignin's structure, but used alone they are not sufficient to elucidate the lignin structure. Moreover such techniques are considered to make qualitative comparison mostly. Therefore, nuclear magnetic spectroscopy was widely used in order to fully characterize the structures and in a quantitative way.

1.2.1.3.   Liquid and solid state NMR: advanced characterizations of lignin

Liquid NMR spectroscopy is used for functional groups quantification and precise attribution of the structure of soluble lignin. The use of model compounds, which mimics the phenylpropanoid monomers, were used for signals attributions [40]. In the case of advanced characterization, 2D NMR is a method of choice to identify the different lignin units and the sub-unit bonds. Methods such as ^{13}C-^{1}H correlation using HSQC (hetero single-quantum correlation) , HMQC (hetero multiple-quantum correlation) or ^{1}H-^{1}H procedures are often considered [41]. 2D ^{13}C-^{1}H HSQC NMR provides information about the purity of the lignin sample by detecting the presence of fatty

chains or polysaccharides [42]. Quantitative 1D and 2D sequences as well as 3D methods can also be considered for advanced characterization [43–45]. In conclusion, combining different NMR sequences may allow a complete elucidation of the structure [46]. Despite the skeleton structure, classical ^{1}H and ^{13}C NMR were found to be effective in the determination of specific chemical groups (such as hydroxyls or carbonyls) even if discrepancies between the methods were noticed [38]. Another procedure developed by Argyropoulos and Granata [47] is widely used in hydroxyl groups determination. It consists in derivatizing with a pholpholane reagent, which reacts with all hydroxyl groups. These can be observed and quantified with ^{31}P NMR since the chemical shift of the phospholane is slightly modified, depending on which type of hydroxyl is involved. Figure 9 shows 31P spectrum obtained with this technique. Aliphatic (150-146 ppm), syringyl (144-141.5 ppm), guaiacyl (141-137 ppm) and carboxylic acids (136-134 ppm) hydroxyls signals are clearly separated and therefore can be quantified thanks to the internal standard (145.2 ppm). So Important information about lignin's structure can be obtained with this method.
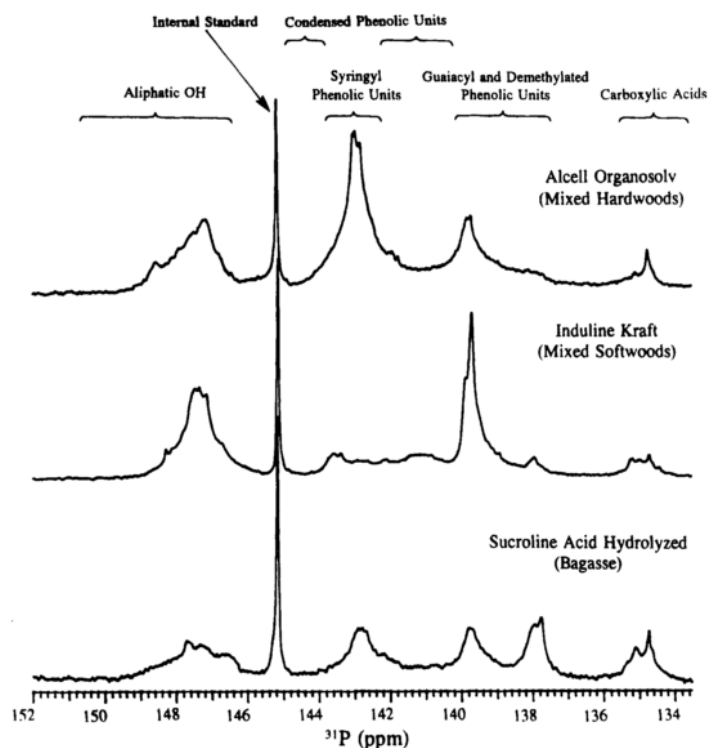

Figure 9. Comparison of hydroxyl groups content from different lignin with the Argyropoulos method [47]

Even if the liquid state NMR is well accurate and gives precise structural information, this method is limited only to soluble lignin, which were previously isolated and fractionated. With these treatments, the structure is changed in comparison to the native lignin. Therefore, solid state NMR spectroscopy (ssNMR) was applied to lignin chemistry, even if line broadening constitutes a problem for chemical shift attribution [48]. Some issues, intrinsic at the solid state NMR, are especially observed in the lignin characterization, like the low abundance of the ^{13}C or the spinning side bands. Many methods were developed in order to make ssNMR as efficient as possible for lignin's characterization. Indeed, information about bonds and specific moieties can be obtained, but not from simple methods. In order to elucidate fully a lignin's structure, combination of multiple and complex sequences is required. Distortionless Enhancement by Polarisation Transfer (DEPT), Dipolar Decoupling (DD) and Cross Polarization (CP) sequences are commonly used and combined in order to get precise information about lignin [49]. Structural information such as the influence of the extraction process were observed with this technique [50]. For other advanced characterization, direct polarization/magic angle spinning (DP/MAS), ^{13}C CPTOSS with dipolar dephasing, ^{1}H-^{13}C heteronuclear correlation (HETCOR) may be considered [51].

In conclusion, liquid and solid state NMR spectroscopy provides by far the largest amount of information with a high accuracy. Combination of different methods and sequences applied on raw lignin or fragments is a powerful tool to fully assess the chemical structure of lignins. For fine and highly precise characterization, fragmentation of lignin may be considered in order to make easier the NMR spectroscopy analysis and interpretation. The techniques of fragmentation are described in the following part.

1.2.1.4. *Fragmentation of lignin*

As it was shown in the last sections, the structural characterization of lignin is not an easy process. Several methods overcome the limitations induced by the characterization of macromolecules by fragmenting lignin. With this technique, smaller molecules are produced which are easier to analyze. Therefore, fragmentation of lignin was investigated deeply for more than 60 years. Other oxidation techniques are known and used for producing high value products, like vanillin, DMF,

methyl mercaptan or DMSO [8]. Nitrobenzene, some metallic oxides, air and oxygen are the widely used oxidant agents. Catalysis science also plays an important role in such processes [52]. A first approach to fragmentize lignin is the chemical oxidation. For example, permanganate oxidation was introduced for the analysis of lignin structure by Freudenberg in the fifties [17]. Different methodologies were established since and were reviewed, such as oxidative degradation by hydrogen peroxide followed by the esterification of the products for GC-MS analysis [53]. This technique measures the proportions of hydroxyphenyl, guaiacyl and syringyl units and also quantify the abundance of different lignin substructures. In order to evaluate the amount of alkylaryl ethers of a lignin, the thioacidolysis might be used since it involves the cleavage of the β-O-4 linkages [21].

Derivatization followed by reductive cleavage (DRFC) is one of the last well established method for chemical fragmentation of lignin [54]. The lignin is mixed with acetyl bromide, followed by a reductive cleavage with zinc dust in a mixture of dioxane, acetic acid and water. Then, the products are acetylated in order to be analyzed by gas chromatography. With this method, hydroxyphenyl, guaiacyl and syringyl units linked by α- and β-aryl ether bonds are cleaved and transformed into 4-acetocinnamyl acetate, coniferyl diacetate and synapyl diacetate.

Despite chemical fragmentation, thermal techniques such as pyrolysis are also commonly used for getting information about the lignin's structure. Depending on the process parameters, the pyrolysis generates degradation products in solid, liquid and gaseous form which are then analyzed [55]. With such technique the monoligols composition can be determined for example. Because this technique involves thermal degradation of the lignin, this will be discussed in the section 1.2.3 (p38).

1.2.2. Physico-chemical properties

1.2.2.1.   Lignin morphology

The random assembly of the three monomeric phenylpropane units gives a 3D structure, which leads to physically and chemically heterogeneous materials. Such unordered chemical structure impacts clearly the micro- and macro properties of the lignin such as the morphology of the particles.

According to its versatile structure, a typical amorphous halo pattern is observed by X-ray diffraction for several types of lignin in the solid state. This peak is used for calculating intermolecular distance having a broad distribution. In the case of milled wood lignin, the peak is broader than that of usual synthetic amorphous polystyrene [56]. This supposes that inter-molecular distance of lignin's chains is distributed in a broad range, thus suggesting random chains organization. Lignin is therefore mostly an amorphous polymeric material.

From the mesoscopic scale, lignin states as a powder, and its color ranges from light to dark brown. Smell, color and particles size distribution depends on the lignin's type. An example of alkali particles morphology is presented in the Figure 10. Spherical particles from different sizes and agglomerates are observed.
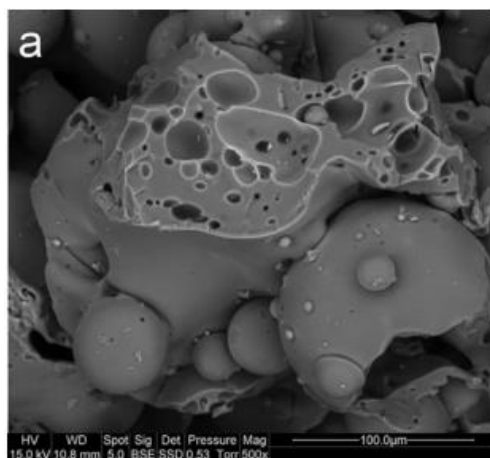
Figure 10. SEM image of alkali lignin particles [14]

1.2.2.2. Lignin properties as polymer

Because lignin is a macromolecule made of repetition of different molecules, this material can be considered as a polymer. An important information regarding polymers is their molecular mass value and distribution. The molecular mass distribution of lignin is complex to obtain in regard to its solubility in organic solvents. Because parts of lignin are cross-linked, insoluble portions of high molecular mass are necessarily obtained. As one of the most used technique is the SEC (see part 1.2.1.1, p29), the underestimation of the molecular mass has to be taken into account. Reviewing the literature, molecular mass of isolated lignin ranges from 10^3 and 10^5 g/mol, thus depending on botanical origin, extraction process and measuring method [56]. If the C9 formula of the lignin

is known, the molecular mass of the hypothetical hydroxyphenyl structural unit can be theoretically calculated and used as comparative index between lignin. For example, a M_w of 176.09 g/mol for a Kraft lignin unit may be expected [57].

Despite of the presence of aliphatic parts which could bring some flexibility, the molecular motion in the lignin's structure is limited because of the abundance of phenyl groups, the cross-linking and the numerous hydrogen bonds [56]. These increase the transition temperature. Moreover, the temperature range of lignin is broader than that of synthetic amorphous polymers, typically from 60 to 180°C. This reflects its complex and heterogeneous structure and sub-structures. Some DSC-curves of different lignins are presented in the Figure 11.
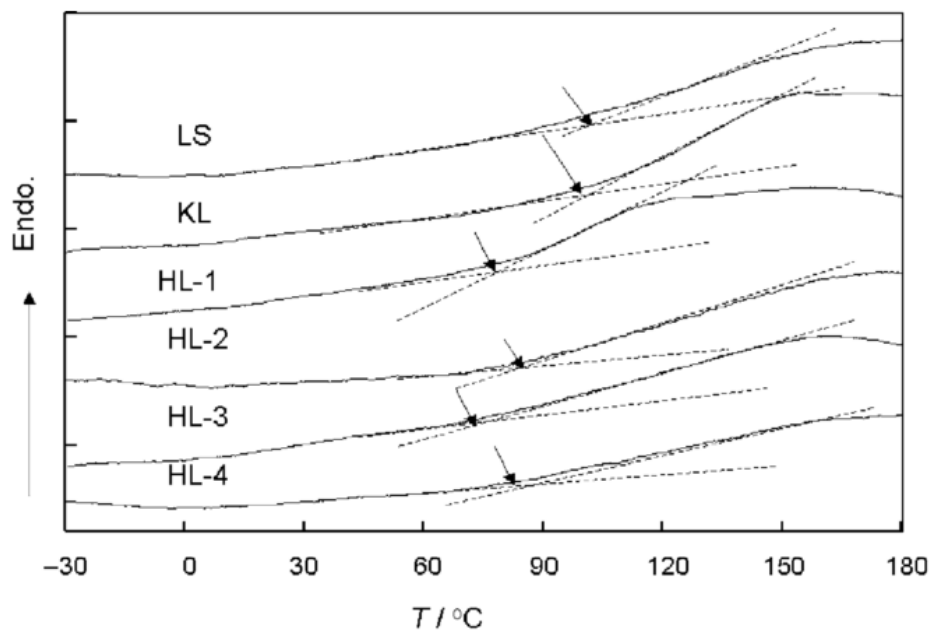
Figure 11. DSC curves of lignosulfonates (LS), kraft lignin (KL) and hydrolyzed lignin (HL), Heating rates = 10°C/min [56]

As for all amorphous polymers, lignin shows enthalpy relaxation when glass transition slowly takes place. The same effect as slow cooling can be obtained by annealing at a temperature set close to the T_g. During annealing, the molecular high order changes by aggregating. Enthalpy relaxation is identified as an endothermic shoulder peak in DSC curves. The glass transition is a relaxation phenomenon and thus T_g depends on time factors (frequency, heating rate). At the

same time, rate of glassification also affects the heat capacities of the glassy state due to enthalpy relaxation.

This part showed that usual polymer properties can be used to compare one lignin to another. Indeed, the chemical structure deeply influences these properties. Laurichesse and Avérous [8] compared the properties of widely used lignins, and the results are listed in the Table 4. For example, Kraft lignin is not soluble in water, which is not the case of lignosulfonates. Glass temperature ranges from 90 to 150 °C, and the polydispersity can vary from 1.5 to 8. This table clearly shows that depending on the lignin's type, different polymeric properties are obtained. So the choice of lignin's type is very important according to its final application.

Table 4. Properties of lignins provided by different extraction processes [8]

Lignin type	Sulfur-lignins		Sulfur-free lignins	
	Kraft	Lignosulfonate	Soda	Organosolv
Raw materials	Softwood Hardwood	Softwood Hardwood	Annual plants	Softwood Hardwood Annual plants
Solubility	Alkali Organic solvents	Water	Alkali	Wide range of organic solvents
Number-average molar mass (M_n – g mol^{-1})	1000–3000	15,000–50,000	800–3000	500–5000
Polydispersity	2.5–3.5	6–8	2.5–3.5	1.5–2.5
T_g (°C)	140–150	130	140	90–110

1.2.3. Thermal decomposition

1.2.3.1.   Structure information and source of chemicals

In the context of lignin's structure elucidation, pyrolysis, i.e. thermal degradation in the absence of oxygen, is a common analytical technique for characterizing lignin. Pyrolysis generates decomposition products which are related to structural parts of the initial lignin. An efficient technique is the pyrolyzer followed by a gas chromatography column coupled with a mass spectrometer (Py-GCMS). The degradation products are separated in the column and analyzed by the MS. Even if lignin produces a large number of compounds thus making the interpretation complex, interesting information such as monoligol proportion can be determined [26,58,59].

Another major and growing interest in lignin's thermal decomposition is to consider lignin as a source of chemicals [8]. Generally, pyrolysis is divided into two different approaches: the

conventional "slow" pyrolysis in which the heating rate as well as the maximum temperature are relatively low compared to "flash" pyrolysis, which involves extremely high heating rates. Depending on the pyrolysis conditions (depicted in the Figure 12), the degraded lignin generates liquids (oils), solids (char) and gaseous components (methane, carbon dioxide, phenolic compounds) in different ratios depending on the pyrolysis conditions [60,61].
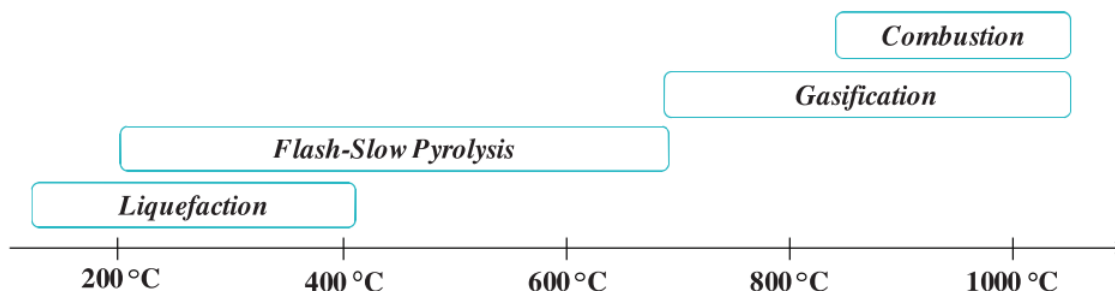

Figure 12. Temperature ranges for lignin's pyrolysis fragmentation [8]

In order to better understand how lignin degrades, the following sections are devoted to the description of lignin's thermal decomposition.

1.2.3.2.   Decomposition steps and kinetics

Temperature ranges of the different degradation steps depends on the lignin's type, as well as kinetic models of thermal degradation [62]. Once again, due to its complex structure, the thermal degradation behavior of lignin is highly affected by its botanical origin and extraction process. Moreover, the heating rate as well as the atmosphere strongly influence the thermal behavior of lignin. Therefore general conclusions about degradation temperature range, conversion and product yield have to be assumed carefully. Typical behavior in TGA is shown in Figure 13 which compares thermal stability of different lignins.

Lignin decomposes from 200 to 500°C depending on the type. Prior to lignin decomposition, water release can be noticed between 100 and 180°C corresponding to residual moisture. The DTG curves of lignin decomposition show one or many wide peaks which reveals complex and numerous reactions taking place. Heated up at 10°C/min under inert atmosphere, lignin degrades slowly and decomposition rates rarely exceed 0.3 wt.%/°C and weight loss ranges from 55 to 70

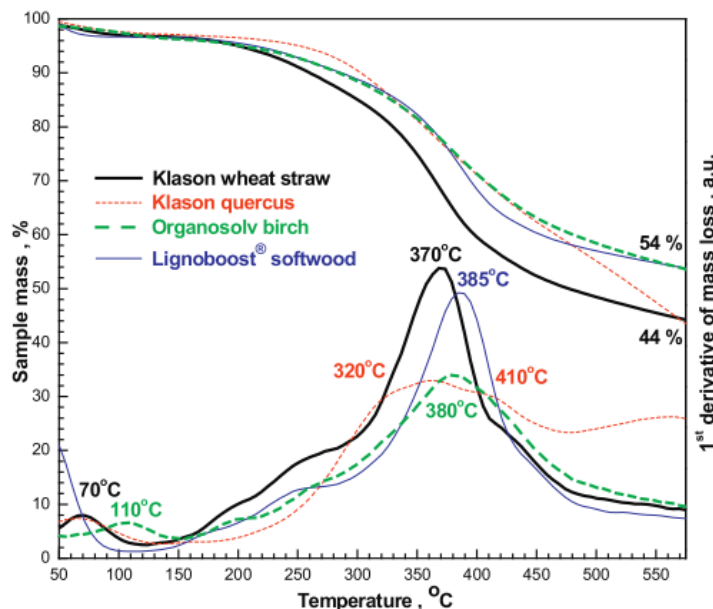at 800°C. Under thermo-oxidative atmosphere, lignin decomposes faster and no residue is left at 600°C.

Figure 13. Thermal degradation of several lignin followed by TGA (He flow, 10°C/min) [63]

Many studies investigated the kinetic analysis of lignin [64–66]. Usually, lignin decomposition is assumed to occur in a unique reaction of the first order. The conventional kinetic parameters were determined, such as the activation energy, which lies between 54 to 79 kJ/mol in the range of 244 - 309 °C, and increases to 81 kJ/mol over 327 to 1167 °C. It was also demonstrated that heat and mass transfer processes influence significantly the thermal degradation by affecting the activation energy and the pre-exponential factor [67]. More complex models were developed, involving for example three parallel reactions in the primary step (decomposition of the raw material) and an additional reaction for the secondary step (reaction between the primary volatiles) [68].

1.2.3.3.   Mechanisms and products of thermal degradation

The temperature range of degradation is broad because various chemical functions and linkages constitute the lignin, therefore scissions occur at various temperatures during pyrolysis [67]. Low molecular compounds evolution is attributed to the cleavage of functional chemical groups, while the rearrangement of the structural backbone leads to char formation and release of volatile

products. Finally, the cleavage of the abundant aryl-ether linkages produces unstable free radicals leading to products with increased thermal stability after rearrangement reactions [69]. Figure 14 summarizes the decomposition products generated when lignin is thermally degraded.

The degradation starts slowly between 200 and 275°C. Dehydration occurs first from 200°C [70]. From 230 to 260°C, degradation of the propanoid side chain leads to the formation of methyl-, ethyl- and vinyl-guaiacol and potentially vanillin as well as ferrulic acid. At higher temperatures (275-350°C), many reactions occur. C-O bonds such as the aryl-ether linkages (β-0-4, α-O-5, …) cleave, and so do the C-C and β-β inter-monomeric linkages. It results from these rearrangements the production of guaiacyl and syringyl compounds and the separation of the aliphatic side chains from aromatic rings. When the temperature increases up to 350-450°C, the demethylation of the dimethoxy-groups involves the conversion of phenols into pyrocatechols. Eventually, rearrangement of the backbone occurs between 500 and 700 °C, producing an aromatic structure like char, and may explain the large amount of residue (30 – 45 wt.%).

Despite typical lignin's degradation products, acetic acid and non-condensable gases also evolve during the pyrolysis [67]. CO is formed the first from 230°C. It is followed by CH_4, both gradually increasing up to 500°C. The presence of H_2 can be noticed at high temperature. Evolution of CO at low temperature is attributed to the cleavage of aryl-ether linkages, and increases at higher temperature since diarylether bonds also break. Methane is originated from the weakly bonded methoxy group ($-OCH_3-$). In conclusion, decomposition of the substituted groups and aliphatic structures induces the release of CO_2, H_2O from the hydroxyl groups, CO from the weakly bonded oxygen groups, and finally H_2 from the rearrangement and condensation of the aromatic rings [71].
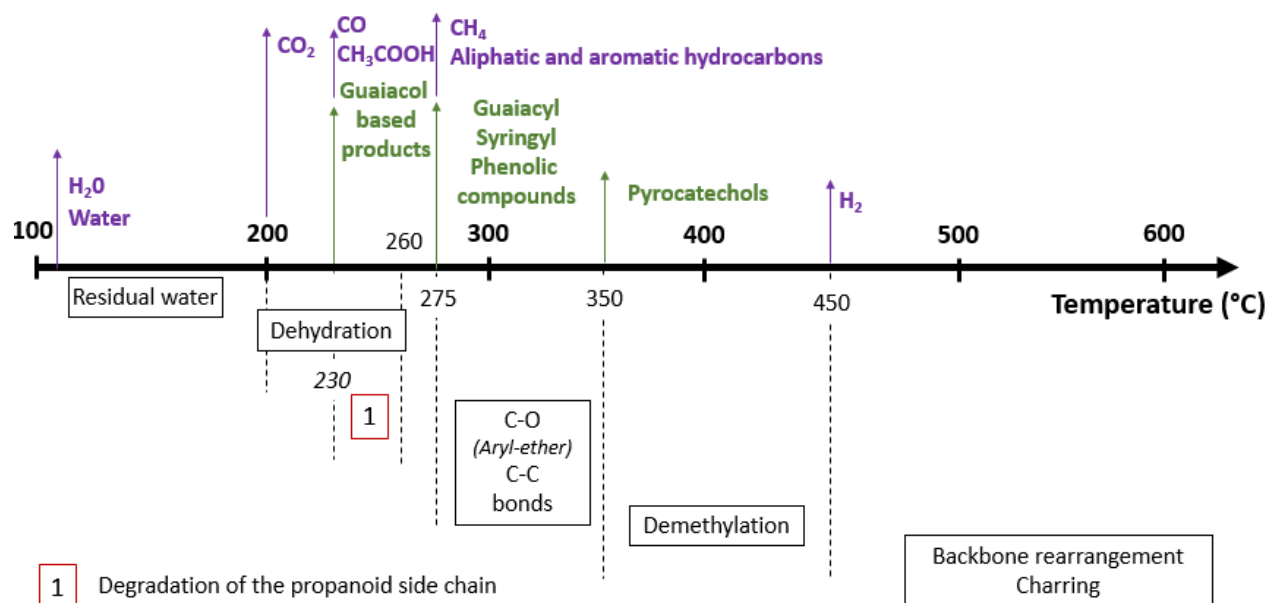
Figure 14. Overview of decomposition products evolving during lignin's thermal degradation

1.3. Applications of lignin in polymers

Valorization of lignin is a topic of interest. It has been seen previously that lignin can lead to high value products thanks to fragmentation (oxidation or pyrolysis). However, the production of high value chemicals from lignin is complex to industrialize. Another promising domain of applications is to use lignin from its initial state in polymers, as additive of monomer. Moreover, according to its structure, chemical modifications can be undertaken to tune these properties. The following section is devoted to the use of lignin in the field of polymers.

1.3.1. Chemically modified lignin

1.3.1.1.   Chemical modifications of lignin

Lignin contains different chemical reactive sites such as hydroxyl, methoxyl, carbonyl and carboxyl groups. Even if the groups' distribution depends on the lignin's type, hydroxyl groups are the first choice for chemical modifications because of their abundance and reactivity. Both phenolic and aliphatic (C-α and C-γ positions on the side chain) hydroxyl sites can be considered for chemical reaction. Esterification, etherification, phenolation, urethanization or sylilation are commonly undertaken in many studies. Moreover, in order to enlarge the range of applications of lignin,

addition of new reactive sites can be undertaken. Again, the main target is hydroxyl groups, but other abundant specific positions of aromatic moities (ortho) can also be considered. Modifications such as nitration, amination or alkylation were carried out [8].

Table 5 summarizes some usual modifications and their applications. Depending on the chemical modification, different properties can be tuned. For example, aminated lignin following a Mannich reaction with formaldehyde and amine is used as hardener in epoxy systems and esterified lignin as macromonomer for polyester or polyurethane. Increase of the amount of phenolic groups thanks to phenolation reaction permits to consider lignin in phenolic resin. Adhesive applications is a one of the market where modified lignin are more and more used.

Table 5. Usual chemical modifications of lignin

Modification	Reactants	Applications	References
Alkylation/ Dealkylation	Formaldehyde, basic media	Lignin-phenol-formaldehyde DMSO production, adhesive	[8], [72]
Acetylation	Acetic anhydride	Acetylated lignin Solubility in organic media	[34]
Amination	Amine, formaldehyde	Aminated lignin Hardener for epoxy system	[73], [74]
Esterification	Acids, Anhydrides, chlorine acids	Lignin-based polyester Macromonomers for polyesters and polyurethanes	[75], [76]
Phenolation	Phenol, phenolic derivatives	Lignin-based phenolic resin	[77]
Nitration	Nitric acid, nitrating agents	Application in polyurethanes	[78]
Sulfonation	Sulfure based	Acidic cation exchangers	[73]
Sylilation	Silanes	Lignin-silica composites	[79]
Urethanization	Isocyanates	Lignin-based polyurethanes	[80]

1.3.1.2. *Lignin derivatives for polymers synthesis*

As previously discussed, chemical modifications lead to lignin-based compounds with tuned properties, which can then be used alone or with other compounds. It results in materials with advanced properties. Polyurethanes and polyesters have been previously cited. In a general

approach, by functionalization of its hydroxyl groups or aromatic rings, lignin becomes a macromonomer as a building block unit with unique properties to elaborate innovative and functional materials.

Synthesis of lignin-based PU was extensively investigated because it is the most promising domain to find high-value application for lignin [76]. Thermoplastic, rigid or flexible foams and elastomers were produced with specific properties (see Figure 15). Lignin can also be used for replacement of synthetic phenols as binders in phenol-formaldehyde or epoxy resins [8]. Moreover, it can also be used in epoxy systems, as epoxy source after epoxidation [81] or even as hardener compounds after amination [82].
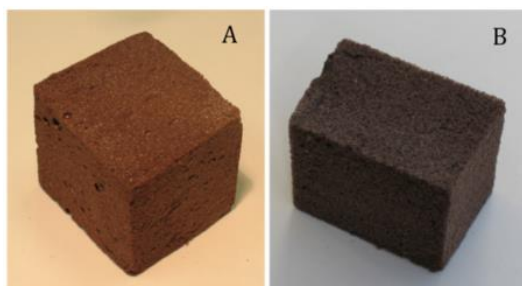

Figure 15. Rigid polyurethane foams made with lignins (A: organosolv / B: Kraft) [80]

1.3.2. Neat and modified lignin as additive in polymeric matrix

1.3.2.1. Synthetic polymers

Due to its chemical structure, lignin exhibits antioxidant properties. Because of this, many studies deal with the use of lignin in polymers. Many studies dealt with polyolefins, such as polypropylene (PP) and polyethylene (PE), in which lignin indeed exhibited antioxidant properties [83,84]. It was shown that lignin is involved in many mechanisms of degradation (processing, light or long-term heat) where it acts as stabilizer. Significant effects are observed with 10wt.% of lignin. However, an increase of the lignin's content in the polymeric matrix leads to a decrease of the mechanical properties of the composite (tensile strength for example). Morphology, crystallinity, miscibility and thermal stability of PP/lignin composites were also deeply investigated [85,86]. Addition of 20wt.% of lignin in PP leads to an enhanced thermal stability (Figure 16). Moreover, esterification

or acetylation enhance the compatibility and mechanical properties (tensile strength) of PE- and PP/lignin composites at different loadings [85,87].
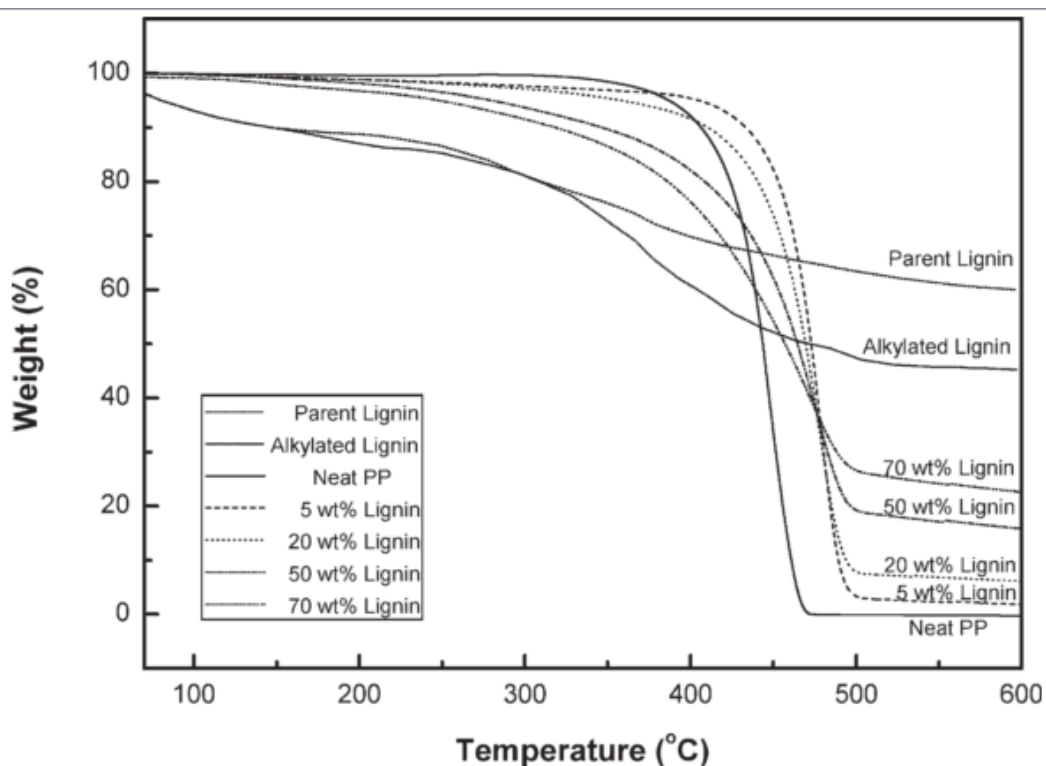

Figure 16. Thermal stability of PP/lignin composites [88]

In PVA, morphology of the blends with different lignin loadings was characterized showing good miscibility between PVA and lignin's particles. Again, the thermal stability of the blends was improved by adding lignin [89], and photo-chemical stabilizing effect attributed to the lignin were noticed [90]. Kinetic study of the thermal decomposition of PVA/kraft lignin was undertaken and revealed that complex reactions occurred under both inert and thermo-oxidative atmospheres [91]. Comparable work was done also in poly(ethylene oxide) and addition of lignin exhibited similar trends than those in PVA [92]. So it appears that lignin interacts with polymers during the thermal degradation, which could be interesting for the flame retardancy mode of action.

In order to find other polymers in which lignin could be used, Pouteau *et al.* studied the compatibility of lignins with several types of polymers [93]. It showed especially a good compatibility with polyvinyl chloride (PVC) and polystyrene (PS). Attention was paid especially to styrenics since the lignin exhibits a high aromatic structure suggesting high compatibility in those

polymers [93]. For examples, lignin loading's influence was investigated in acrylonitrile-butadiene-styrene (ABS) [94]. First, lignin can be uniformly dispersed in matrix as expected. The composites start to degrade at lower temperature that neat ABS because of the relatively low thermal stability of lignin. Nonetheless, the thermal stability at high temperature is significantly enhanced, mainly due to the char formation. Flame retardancy performance was also improved, and this will be discussed in the section 2, p48. Other technical polymers such as epoxy, thermosets materials, used modified lignin as curing agents [82,95]. Promising results were obtained which open new outlook for use of lignin in thermosets applications.

1.3.2.2.   *Bio-based polymers*

The environmental concerns and the debates about oil resources force the scientific community to put efforts and researches on the production of high performance biobased plastics. In this context, the development of biobased polymeric matrix, such as polylactid acid (PLA) or thermoplastic starch (TPS), leads to materials with more and more interesting properties. Incorporation of lignin, considered as a renewable additive, is a way to further develop functional bio-based composites. For examples, incorporation of esterified lignin in TPS permits to produce composites with improved mechanical properties and thermal stability, even if a higher water uptake was noticed [96].

As one of the most promising biobased plastics produced at the industrial scale, PLA was chosen in many studies as polymeric matrix to be used with lignin [97,98]. As for synthetic plastics, lignin exhibits antioxidant properties in PLA. Recently, Gordobil *et al.* investigated deeply the PLA/lignin composites, comparing 3 different types (alkali, organosolv and kraft) and different loading [97,99]. Some results obtained with Kraft lignin are presented in Figure 17. The thermal stability was improved and the mechanical properties not affected (around 45-50 MPa for strength at break) at low loading rates, but worsen at high loading rates. The crystallization behavior of PLA was not especially favored by adding lignin. Then, acetylation of lignin was performed and permits achieving better compatibility in PLA. Therefore, better performances in terms of mechanical properties were observed. The use of PLA grafted with glycidyl methacrylate was also studied and led to an improved compatibility of the lignin in the polymer [100].
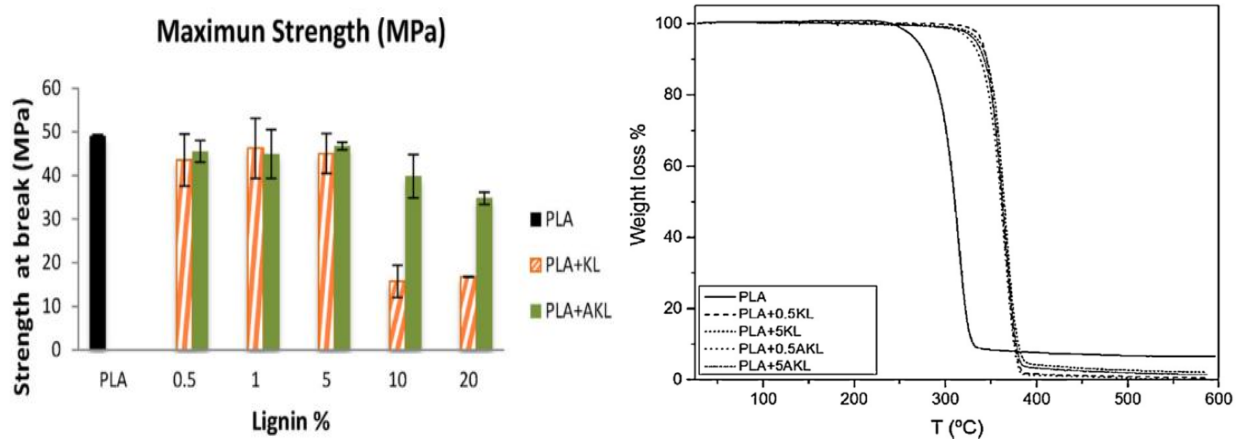
Figure 17. Strength at break and thermal stability of PLA/lignin composites (KL – Kraft lignin, AKL-Acetylated KL) [99]

1.4. Conclusion

In this part, it was seen that lignin is a particular biopolymer with a complex and versatile structure. Despite numerous researches, questions still remain about lignin formation and structure elucidation. Moreover, the lignin's structure is very changing, depending on the botanical origin and the extraction process. As a result, properties of lignin are very also varying, thus limiting its use at industrial scale. It results that lignin is considered as a byproduct of the main producing industries (pulping process mostly) and is burnt for energy recovery in the facilities. Because 50 million tons of lignin are estimated to be produced each year, the worldwide research puts significant efforts in order to valorize the second most abundant biopolymer on earth. The use of lignin as chemicals source or technical additives starts to be effective, and the lignin market tends to get bigger and bigger.

Lignin becomes regularly used in polymers applications. As building block of materials or additive in composite, lignin exhibits specific and interesting properties. These properties may be tuned by chemical modifications, for example by adding reactive chemical sites or to improve of its compatibility in a polymeric matrix. Because of this growing interest towards this renewable materials, lignin has been considered as potential flame retardant additive for polymers. The next part is devoted to the state of the art on this topic.

2. Lignin as flame retardant additive in polymers

The previous section shown that lignin may be valorized as additive in polymeric materials. Moreover, the thermal decomposition of lignin revealed that it produces char by rearrangements of unstable radicals. This intrinsic property gives us the opportunity to new possible applications for lignin as additive. Indeed, this charring ability could make lignin a flame retardant additive in polymeric materials. Flame retardancy chemicals represents an important market since it is evaluated at 5 billion $ in 2014 [101]. This is an interesting opportunity for lignin's valorization.

In the following, basics about flame retardancy of polymers are presented. As the formation of a carbonaceous layer is one of the possible mode of action to flame retard polymer, the mechanism of formation and the properties of a char issued from lignin are discussed. Finally, a state of the art of the use of lignin as flame retardant for polymers concludes this section.

2.1. Flame retardancy of polymers

This section is devoted to the comprehension of phenomena occurring when a polymer burns, thus allowing to find strategies to fireproof them. First, basics about combustion of polymers are presented. Then, strategies to limit or stop this combustion are discussed. Finally, most current FR systems for polymers are detailed.

2.1.1. Combustion of polymers

A schematic in Figure 18 summarizes the combustion process and the phenomena occurring in the flame or the polymer. The combustion process can be divided into four major steps: heating, decomposition, ignition and flame spread. Indeed, when submitted to a heat source, the material softens, or even melts in the case of thermoplastics. Then, when the energy given to the material is higher than that needed for its degradation, decomposition products, called fuel in Figure 18, are released in the gas phase from the degradation zone. These flammable gases are mixed with oxygen from the air and when the system reaches a critical concentration, ignition occurs. Part of the energy of the flame is given back to the material, so that combustion process continues without external energy. As long as degradation products are evolved and oxygen remains in sufficient amount, there is an auto-fed flame which can propagate to its surroundings. The flame

is formed by the highly exothermic reactions occurring between the radicals formed from the thermal decomposition and oxygen.
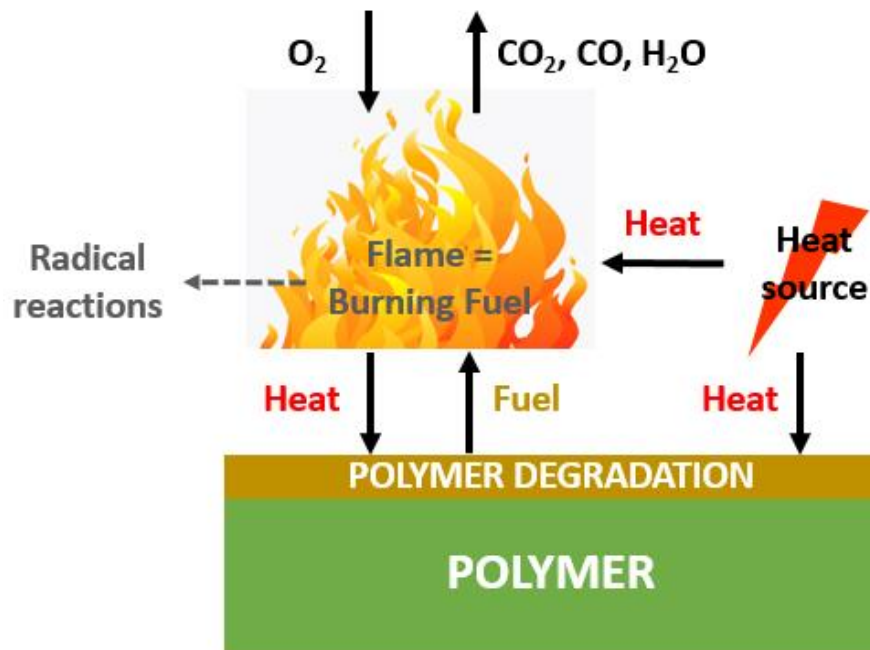

Figure 18. Combustion process and reactions occurring in the flame (R=polymer)

Upon thermal decomposition, many phenomena occur in the condensed phase: melting, hydrolyses, crosslinking, charring, dripping, diffusion of volatile products and superficial accumulation of materials. Two thermal degradation mechanisms of macromolecules can be distinguished [102]:

- The non-oxidizing thermal degradation consisting in heterolytic or homolytic chain scissions. This degradation, also called pyrolysis, occurs under the simple effect of temperature. Chain scission can occur in two ways:
  - o By formation of free-radicals, the reaction does not stop at this stage because these radicals start a chain/cascade reaction, which occurs under both oxidizing and non-oxidizing conditions.
    (example of alkanes: $R_1–CH_2–CH_2–R_2 \rightarrow R_1\text{-}CH_2{}^\bullet + {}^\bullet CH_2–R_2$)
  - o By migration of hydrogen atoms and the formation of two stable molecules
    (example of alkanes: $R_1\text{-}CH_2\text{-}CH_2\text{-}CH_2\text{-}R_2 \rightarrow R_1\text{-}CH=CH_2 + CH_3\text{-}R_2$)

- The oxidizing thermal decomposition wherein the polymer or its degradation products react with oxygen of the air. A variety of products are generated through this mechanism: carboxylic acids, alcohols, ketones, aldehydes, etc. This degradation mechanism also results in the release of radical species (i.e. $H^\bullet$ and $OH^\bullet$) that are very reactive, particularly in polyolefins. Oxidation can lead to crosslinking through recombination reactions of the macromolecular radicals. However, bond scission usually remains the dominant reaction.

2.1.2. Concepts of flame retardancy

Flame retardant systems are intended to inhibit or to stop the polymer combustion process described above by acting either physically (cooling, fuel dilution, formation of a protective layer) and chemically (reaction in the solid or gas phase). A simple schematic representation of the self-sustaining polymer combustion cycle is shown in Figure 19. Flame retardants act to break this cycle, and thus extinguish the flame or reduce the burning rate, in a number of possible ways [103]:

- **('a')** - by modifying the pyrolysis process to reduce the amount of evolving flammable volatiles. It increases the formation of less flammable gases or of char which also acts as a barrier between the polymer and the flame. Cooling of the condensed phase by endothermal decomposition of FR additive may also be considered
- **('b')** - by isolating the flame from the oxygen/air supply
- **('c')** - by introducing into the plastic formulations flame inhibitors compounds or diluting agent
- **('d')** - by reducing the heat flow back to the polymer to prevent further pyrolysis. This can be achieved by producing a protective barrier, e.g. ceramic layer, char or intumescent coating, formed when the polymer is exposed to fire conditions
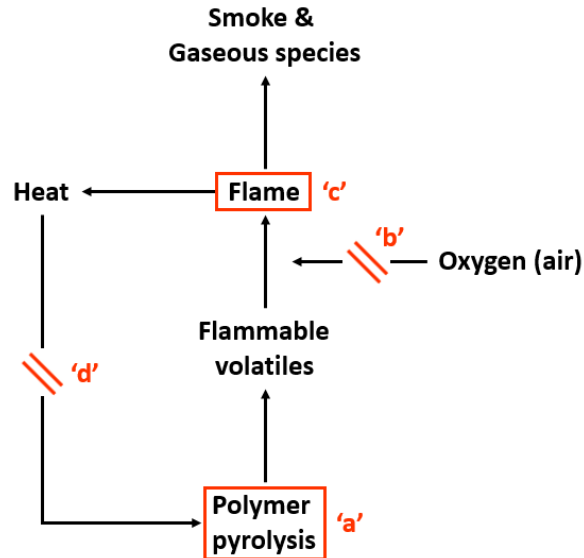
Figure 19. Schematic of potential mode of action of FRs ('a' to 'd') in the combustion cycle [103]

Flame retardants can be classified in two categories according to their processing in polymers:

- Reactive flame retardants: these are incorporated into the polymer during synthesis (as monomer for instance) or during post reaction process such as grafting.
- Additive flame retardants: these are usually incorporated in the material during the polymer transformation process. In this case, the additives have to be thermally stable and of low volatility at the processing temperatures of the particular polymer so as to avoid losses.

This study is focused on using lignin as FR for polymers, which means that lignin is considered as additive. Therefore, the following section is devoted to detail the main class of FR additives commonly used for polymeric materials, and their mode of action.

2.1.3. Solutions and mode of action of flame retardants additives

2.1.3.1.   Overview of the FR's mode of actions

In general, fire retardant additives can have a physical and/or chemical mode of action in the gas and/or condensed phase [104]. The physical action takes place through formation of a protective layer, by cooling and/or by dilution. In the first case, a protective layer with a low thermal conductivity is formed when the material is submitted to an external heat source and protects

the material through reduction of the heat and mass transfer between the external heat source and the material. Materials can also be protected by cooling through the endothermal decomposition of fire retardant additives (usually dehydration) leading to a decrease in temperature by absorbing the external heat. The protection by dilution takes place through the addition of compounds releasing inert gases, such as carbon dioxide or water, upon decomposition. These additives dilute the fuel in the condensed and in the gaseous phase and thus lower the concentration of combustible gases in the surrounding atmosphere.

The other possibility by which materials can be protected is the chemical mode of action which takes place in the condensed and/or gas phase. In the condensed phase, two types of reactions can occur. First, the formation of a carbon layer (charring) on the polymer surface limiting the volatilization of the fuel. It also limits oxygen diffusion and insulates the polymer underneath from the external heat (heat barrier). The second possibility is the acceleration of the polymer decomposition which causes a pronounced flow of the polymer and, hence, a withdrawal from the sphere of influence of the flame that breaks away. The chemical mode of action of flame retardants in the gas phase takes place through inhibition of the radical mechanism of the combustion process by flame retardants or by their decomposition products (e.g. radical scavengers). As a result, the exothermic processes that occur in the flame are stopped and the system cools down. Consequential, the supply of flammable gases is reduced or even completely suppressed.

Table 6 summarizes the previously described mode of action with their related mechanism and the flame retardants used for this purpose. It is possible that fire retardants (e.g. aluminum hydroxide and magnesium hydroxide) show exclusively a physical mode of action, but flame retardants acting exclusively through a chemical mode of action are rare. Chemical mechanisms are often accompanied by one or several physical mechanisms, most commonly endothermic dissociation or dilution of fuel. Charring is the most common condensed phase mechanism.

Table 6. FR additives types and their mode of action

Mode of action	Mechanism	Flame retardant
Gas phase		
Flame extinction	Radical inhibition	Halogen- and Phosphorus-based compounds, antimony trioxide
Decrease of the flame temperature, flame cooling	Dilution of the combustion gas	Compounds releasing carbon dioxide, water (Mineral fillers) or ammonia (melamine)
Condensed phase		
Cooling down the polymer	Endothermic degradation	Metallic hydroxides
Limitation of the fuel supply	Dilution of the polymer	Inert fillers (talc, chalk)
Reducing heat exchanges and fuel supply with the polymer	Creation of a physical (O_2 and fuel) and thermal (heat) protective barrier	Intumescent of vitrifying systems

2.1.3.2.   Flame retardants additives: current solutions

Halogen-containing flame retardants act in general by interfering in the radical chain reaction that takes place in the gas phase [105]. Iodine (C-I bonds not stable enough) and fluorine (C-F too much stable) containing FR are not used. Chlorine and bromine containing additives are the most effective. The flame retardant (RX) breaks down in the flame (Equation 1) and the halogen radical ($X^•$) reacts with the polymeric chain to form the hydrogen halide (HX) that is used to trap the high-energy radicals ($H^•$ and $OH^•$) present in the flame (Equation 2).

$$RX \rightarrow R^• + X^•$$

Equation 1. Break down of the flame retardant

$$X^• + RH \rightarrow R^• + HX$$

$$HX + H^• \rightarrow H_2 + X^•$$

$$HX + OH^• \rightarrow H_2O + X^•$$
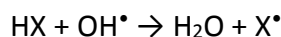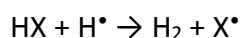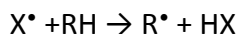
Equation 2. Reaction of HX with high-energy OH and H radicals; X = Cl or Br, R = polymer chain

Regarding the effectiveness of the hydrogen halides, it appears that hydrogen bromide (HBr) has a higher fire retardant effect than hydrogen chloride (HCl). HBr is evolved over a narrow temperature range at high concentrations. HCl instead is evolved over a wider temperature range. Consequently, a lower concentration is available in the flame zone. Moreover, higher quantities of chlorine compounds are required to reach the same fire retardant effect as bromine containing compounds. Because of their high efficiency, loading rates in polymers of halogenated FR additives are relatively low. Indeed, the loading of such additives rarely exceeds 30 wt.%. Due to relatively recent environmental concerns (REACH in Europe), there is a continuing trend toward the development of non-halogenated materials to replace these systems.

Mineral fillers such as aluminum hydroxide (ATH) or magnesium hydroxide (MDH) are widely used as fire retardant additives in polymers [106]. Hydrotalcite, Boehmite and calcium sulfate dehydrate (Gypsum) can also be considered. To achieve good fire retardant properties, high loadings (higher than 50 wt%) are required. However, high loadings drastically change the mechanical properties of the material. To overcome this disadvantage, several solutions are possible. The surface of the mineral fillers can be treated to improve lack of mechanical properties. Another possibility is the use of processing aids which change mechanical properties of the material. Finally, the combination of mineral fillers with other conventional flame retardants to develop synergist effects can also be investigated. Mineral fillers have three different fire retardant effects, which can occur alone or in combination [107]:

- They decompose endothermally and so absorb heat. This phenomenon leads to a "cooling effect", which cools down the surrounding polymer.
- Mineral fillers generally release inert gases during the combustion process. These gases, e.g. water or carbon dioxide dilute the fuel and thus reduce the concentration of the flammable gases.
- They built an inert protective layer at the surface of the decomposing polymer and thus protect the material from the external heat. Moreover, this layer acts as barrier preventing the diffusion of gases and heat from the material to the fuel.

Phosphorous containing flame retardants are widely used as alternative solution of halogenated fire retardants [108]. The class of phosphorous compounds includes ammonium polyphosphate

(APP) and red phosphorus as well as phosphinate, phosphonate, phosphate ester (pyrophosphate and polyphosphate) (Figure 20), in which the phosphorus content in the phosphorus containing flame retardants can vary from few percent to 100 % (red phosphorus).
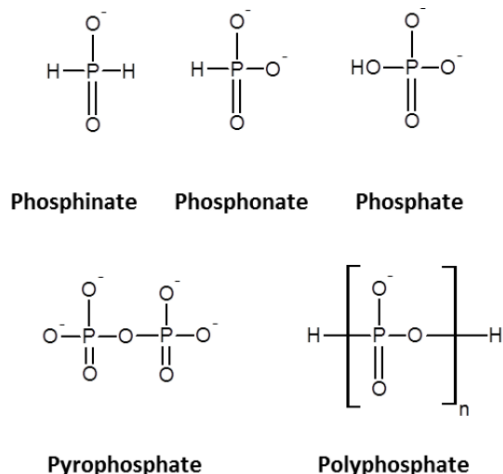

Figure 20. Different structures for organophosphorus flame retardants

Nguyen *et al.* [109] investigated a relationship between the structure and the fire retardant effect of different phosphorus based additives as well as the mode of action of the different organic phosphorous compounds. It was postulated that compounds containing P-CH$_3$ or P-H bonds have a fire retardant action in the gas phase due to the generation of small phosphorus containing species arising from the weak bond to the P atom. Due to the fact that phosphorus containing compounds are usually not chemically bonded to the final products they are supposed to have an environmental impact. Phosphorus compounds containing also halogens were already found in indoor air, house dust, drinking water, sediment and biota, whereas non-halogenated phosphorus compounds were only found in indoor environments, like offices, hospitals or schools [110]. Combination of phosphorus-based additives with nitrogen-containing products like melamine cyanurate, melamine phosphate or melamine polyphosphate exhibits high performance because of synergistic effects [111].

Halogens, hydroxides and phosphorus-based materials represent the major part of FR's additives used for flame retard polymers. Others materials can also be a solution for FR systems. Silicone-based materials are considered as a new family of FR additives [112]. Silicon is used in many areas such as organic, inorganic, organometallic, polymer chemistry. Many forms of silicon compounds have been explored as potential FR to polymeric materials: silicones and silanes, polyhedral oligomeric

silsesquioxane or silica and silicate. Such additives are considered as "environmentally friendly" and they have been already used in industrial products, such as protective coatings [113]. Boron-based products are also of interest in fire retardancy [114]. Since the 1980's, materials such as zinc borate, melamine borate or boron phosphate are commonly used as FR additives or synergists in polymers. They can act as flame retardants, smoke suppressants, afterglow suppressants and anti-tracking agents. Another area regards the use of nanocomposites in fire retardancy [115]. Nanoparticles incorporated into polymeric matrix actually display a fire retardant behavior because they avoid fire propagation by dripping of hot and flaming polymer particles thus reducing the rate of combustion. The mechanism involved is based on formation upon heating of an insulating layer resulting from the accumulation of nanoparticles.

2.1.4. Intumescent systems

Even if Gay-Lussac worked in 1821 with ammonium phosphate on cotton making an intumescent system (it was not mentioned in his paper) [116], the first comprehensive paper was published in the early 70s by H. Vandersall giving the fundamentals of intumescence [117] but only considering coating. The first researches to extend intumescent science to polymeric materials belong to G. Montaudo and co-workers [118,119] and G.Camino and co-workers [120–123]. The schematic in Figure 17 illustrates the intumescence on the polymeric substrate. Basically intumescence consists in the expansion of a foam upon heating in order to protect the underlying substrate. In fact, an intumescent material heated beyond its critical temperature, degrades by swelling. The intumescence process [69] results in the formation of an expanded multicellular barrier (called char) able to protect the substrate from the flame. This layer acts as insulating and protective barrier reducing heat, fuel and mass transfers between the heat source and the polymer. The formation of an intumescent char is a complex process involving several critical aspects: rheology (expansion phase, viscoelasticity of char), chemistry (charring) and thermophysics (limitation of heat and mass transfer) [124]. Flame retarding polymers or textiles by intumescence are essentially a special case of a condensed phase mechanism [125].
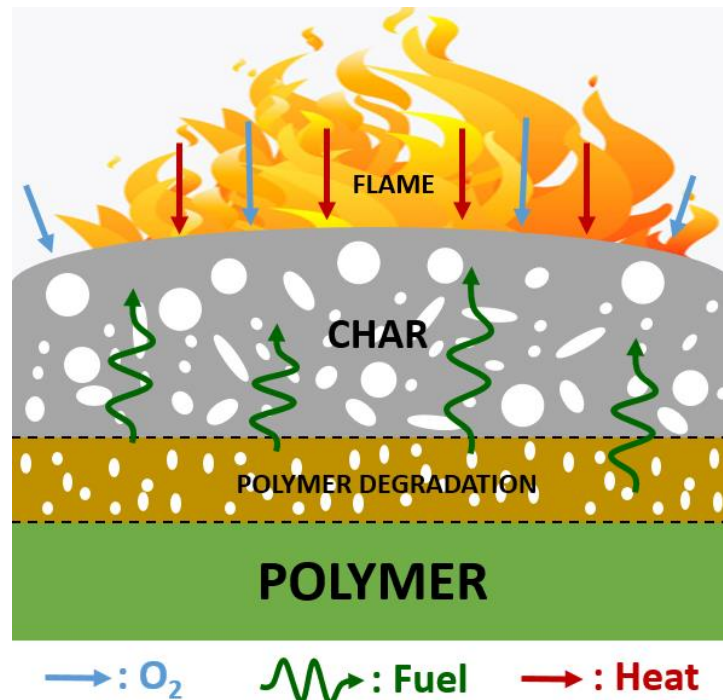
Figure 21. Development and mode of action of an intumescent system

The fire protection depends on the properties of the char i.e distribution and size of the cells, thickness of the walls, expansion, mechanical resistance, rheology, chemical composition, etc. The mechanical properties of the intumescent shields developed in the case of fire are particularly important since internal pressure (due to degradation products) or external environment can easily destroy it leading to a loss of insulating properties of layer. These properties can be tuned by playing with the intumescent formulations. Vandersall listed the ingredients required to create intumescence [117]:

- An acid source that promotes the dehydration of carbonizing agent. It is a specie able to release acidic compound (e.g. phosphoric acid) when there is a rise of temperature. It is released below the decomposition temperature of the carbonizing agent

- A carbonizing agent that is dehydrated by the acid source to form a char. The amount of char depends on the number of carbon atoms, on the rate of dehydration and on the number of reactive hydroxyl sites of the carbonizing agent

- A blowing or swelling agent that contributes to the expansion of polymer and to the formation of a swollen multicellular layer by releasing gas. Gas must be released during

the thermal decomposition of the carbonizing agent in order to allow the expansion of the carbonized layer.

Some compounds can combine two actions, such as ammonium polyphosphate (APP) which acts both as acid source and blowing agent. Table 7 presents a non-exhaustive list of common chemicals used in intumescent systems for polymers. Acid sources are commonly classical acids, ammonium salts, amines-amides or organophosphates. Carbonizing agents can be either additives or polymers which could easily be dehydrated and produced char. Finally, blowing agents are often amine-based compunds.

Table 7. Non-exhaustive list of classical additives used in intumescent systems [125]

Acid source	Carbonizing agent	Blowing agent
Acids : phosphoric, sulfuric, boric	Carbohydrates : starch, dextrin, sorbitol, pentaerythritol, mannitol, methylol melamine, phenol-formaldehyde resins	Amines/amides: Urea, urea-formaldehyde resins, melamine, dicyandiamine
Ammonium salts : phosphates, polyphosphates, borates, sulfates, halides		
Amines-amides : urea with phosphoric acids, melamine phosphate	Others (charring polymers) : polyamide 6, polycarbonate, polyurethane,	
Organophosphates: Tricresyl phosphate, alkyl phosphate		

Due to recent environmental concerns, there is a continuing trend towards the development of bio-based materials. In this context, lignin is considered as potential carbon source in FR formulations. The following parts deal with the char forming ability of lignin, then the current systems using lignin as flame retardant additive in polymeric materials, and the strategies to improve these systems.

2.2. Lignin: a promising charring agent for FR systems in polymers

Lignin produces naturally a remarkable char residue at high temperature (see section 1.2.3, p38). Since char formation is one of the solution to flame retard polymers (see section 2.1.4, p56), lignin could be considered as a flame retardant additive.

2.2.1. Definition and properties of char

In general, char is a highly cross-linked carbonaceous structures and looks like a porous solid which acts as a heat insulator. For example, these thermal and mechanical properties are a key aspect of ablative heat shields used for spacecraft when reentering in the atmosphere at high velocities. Usually made from carbon phenolic resins, such heat shields do burn, forming a residual char which insulates the interior of the vehicle from further heating [126]. The process of char formation as well as its resulting structural, mechanical and thermal properties are then very important.

The char formation takes place when a charring material is exposed to an external heat source. Chemical decomposition, cross-linking as well as bubble formation and mass transport are phenomena occurring during char formation [127]. During the combustion of a charring system, the carbonaceous structure evolves from disordered polycyclic aromatic hydrocarbons to a more ordered structure, meaning lower amount of amorphous phase, higher aromaticity and larger crystallite size [128]. The char formation can be investigated by chemical, dynamical and morphology characterizations.

Chemical characterization of the carbonization can be undertaken mostly by solid state NMR, Raman and X-Ray photoelectron spectroscopy (XPS). Since charred structures are poorly soluble, most of the techniques used are solid-state analysis often carried out ex-situ, meaning that the char residue is analyzed after combustion. Dynamic characterization (dynamic viscosity, expansion, char strength) is also very interesting, especially in the case of intumescent systems. The char expansion occurs via a semiliquid phase with gas formation and the final properties of char depends strongly on this stage. This one has to be strong enough to avoid crack formation or char collapse leading to the loss of FR performance. Finally, chemical composition and dynamic properties of the char directly influences its morphology. Analyzing the morphology (mostly X-

Ray diffraction and microscopy) appears to be interesting in order to better understand the relation between structure and properties [127].

2.2.2. Properties of a char produced from lignin

Lignins are made of phenylpropanoid units linked mainly via ether and carbon-to-carbon linkages (see section 1.1, p22). Li *et al.* [129] investigated the thermal degradation and char formation of manchurian ash lignins. The FTIR analysis (Figure 22) showed clearly that the relative absorbance of ether C-O-C (1120 cm^{-1}), phenolic and aliphatic OH (1327 and 1033 cm^{-1} respectively) and vibration of aliphatic carbon C-H (2940 cm^{-1}) decreased when the temperature increases. This evolution proves that the cleavage of ether bridges between the monomeric units took place first during heating. Such degradation leads to a reorganization of the carbonaceous structure into more conjugated groups via crosslinking reactions, which is confirmed with the increase of the relative absorbance of the aromatic ring vibration (1596 cm^{-1}) while heating. In addition, the extent of the crosslinking can be studied by measuring the increase of the relative intensity of C1s by XPS analysis [130]. The relative intensity of C1s and O1s measurements showed a good char forming ability of the lignin.
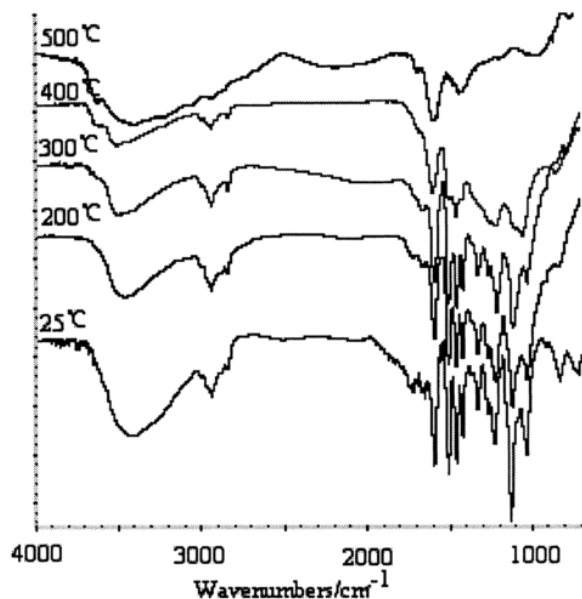

Figure 22. FTIR spectra of the manchurian ash lignin treated at different temperatures [129]

Sharma and al. [131] detailed the mechanisms occurring during pyrolysis of a polymeric Kraft lignin and were able to describe the different steps of the char formation. Lignin starts degrading from 150 to 250 °C depending on the type. Partial removal of organic products takes place [63], leading to vesicle formation. When the temperature reaches 350°C, the O/C ratio falls, suggesting some decarboxylation together with dehydration and the beginning of the char formation. The maximum of char's expansion occurred around 350°C-400°C and appears to be associated with the completion of the solidification stage. Above 400°C, the carbonization is detrimental and leads to porous structure in the char, which means that the vesicle formation continues until 750°C. That could lead to fragile char in fire conditions. During the pyrolysis, the amount of non-aromatic carbons decreased exponentially whereas the aromatic carbons only decreased by ca. 10% (Figure 23). Thus, most of the weight loss was due to the volatilization of the non-aromatic carbon. Since only a few amount of aromatic carbon was lost, lignin chars appears to be highly refractory and very resistant to thermal degradation, which should be beneficial for fire retardancy. Characterization of the char will therefore be a key point in understanding the mode of action of lignin as flame retardant.
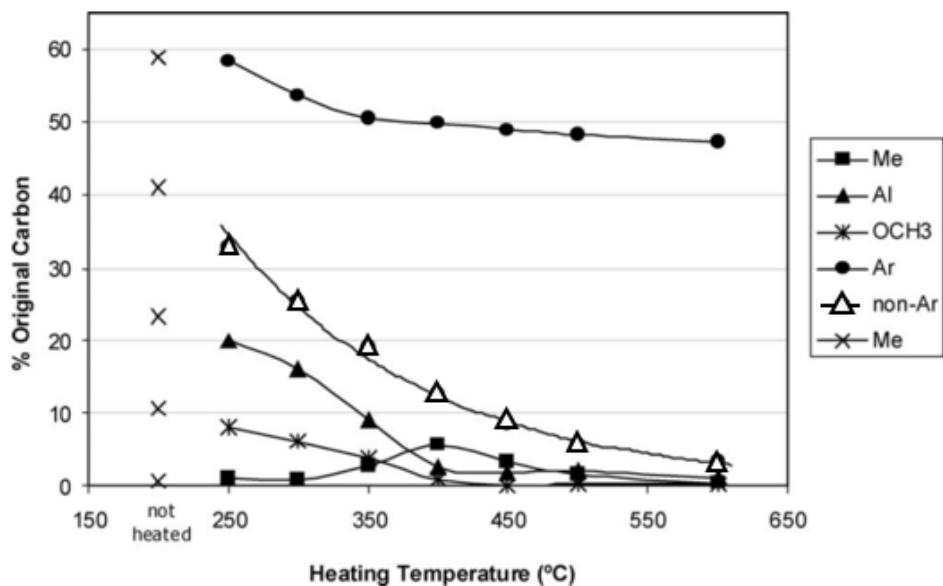

Figure 23. Type of carbons obtained by analysis of ^{13}C CPMAS NMR [131]

Me – methyl, Al – aliphatic, OCH$_3$ – methoxy, Ar – total aromatic, non-Ar – all non aromatic

carbons

As seen previously (see section 1.1, p22), the lignin history influences its structure and therefore its char residue after combustion. The comparative study between larch and manchurian lignin done by Li *and al.* [132] noticed some differences of the char properties. XPS measurement of C1s and O1s intensities showed that the C/O ratio increases for both sources while heating, in a strongest way for manchurian ash lignin. To conclude, even if larch lignin produces more char residues (due to a high C-C initial content), the manchurian ash lignin showed a good ability of crosslinking, thus forming a highly stable conjugated char. So lignin has to be chosen carefully in FR systems as lignin's type will govern the properties of the char formed in fire condition. In this context, the following section deals with the use of lignin as FR polymers.

2.3. Lignin as FR additive in polymeric materials

It was previously shown that lignin can be used as additive in polymers. In many cases the thermal stability at high temperature of the composites with lignin is improved in comparison to the neat polymer. Moreover, as lignin exhibits an interesting thermal degradation behavior and is a charring material, it has been considered as a potential flame retardant additive for plastics. Chemical modifications can also be undertaken in order to improve the FR properties of lignin. In the following sections, state of the art about lignin used as FR is presented for common polymers.

2.3.1. Polyolefines

Polyolefins are large distribution plastics and used in a plethora of applications, some of them requiring FR performance. So polyolefins are targets of choice for FR research to develop new FR systems. In the previous parts, it has been shown that numerous studies were achieved regarding incorporation of lignin as additive in PP (see section 1.3.2.1, p44). Hence PP-lignin composites are well known, and their fire retardancy performance have been extensively investigated.

2.3.1.1. Neat lignin and coadditives

The first study dealing with lignin as FR in PP was done by Gallina *et al.* [133] at the end of the 1990's. The FR performance was assessed by cone calorimetry (CC), which is one of the most representative lab-scale testing simulating the condition of a fire. It is important to notice that this test was performed on thick sample (6 mm), as the thickness influences significantly the CC

results (changes of heat and mass transfer) [134]. At 20 wt.% loading of steam exploded lignin in PP, the peak of heat release rate (pHRR) is interestingly decreased by 66 %, but the combustion time is much longer. Moreover, the time to ignition of the composites is shortened to 45 s in comparison to 80 s for the neat PP. The authors concluded that such FR performance was achieved thanks to the char formed during the test.

Based on this promising results, De Chirico *et al.* [135] went on with the investigation. Prior to fire testing, a complete study was done dealing with the influence of the lignin's loading rate on the composites. Physico-chemical, mechanical and thermal properties of the composites were studied with 5, 10, 15 and 20 wt.% of lignin in PP [86,135,136]. Thermo-Gravimetric Analysis (TGA) gives similar trends about the thermal stability of PP-lignin composites than those presented in Figure 16, p 45. Indeed, lignin permits to improve the thermal stability of the composites by shifting the maximum of degradation towards higher temperature and producing some carbonaceous residue.

From these results, lignin loading was set at 15 wt.% and FR properties of the composites with or without coadditives were investigated with cone calorimetry (Figure 24). Diminution of pHRR of about 70% is achieved when adding 15 % of lignin in PP and this reduction was mostly attributed to the formation of a char. Poly(vinyl alcohol) (PVA), melamine phosphate (MeP), aluminium hydroxide (Al(OH)$_3$), monoammonium phosphate (AHP) and ammonium polyphosphate (APP) were used as coadditive materials combined with lignin to further enhance FR performance of PP. Again, the time to ignition is shortened in comparison to neat PP, attributed to the rapid degradation of the additives. However, it could also be due to a change of absorptivity induced by the presence of lignin, which would lead to faster heating in the sample, and therefore promoting the degradation. Best FR performance (according to the reduction of the pHRR) was reached by combining lignin with phosphate-based co-additives (AHP, APP). In terms of smoke opacity, the association of lignin with Al(OH)$_3$ or PVA offers the best results, and the lowest CO yield evolving during the combustion. So considering suitable coadditive in FR based lignin systems leads to promising FR performance.
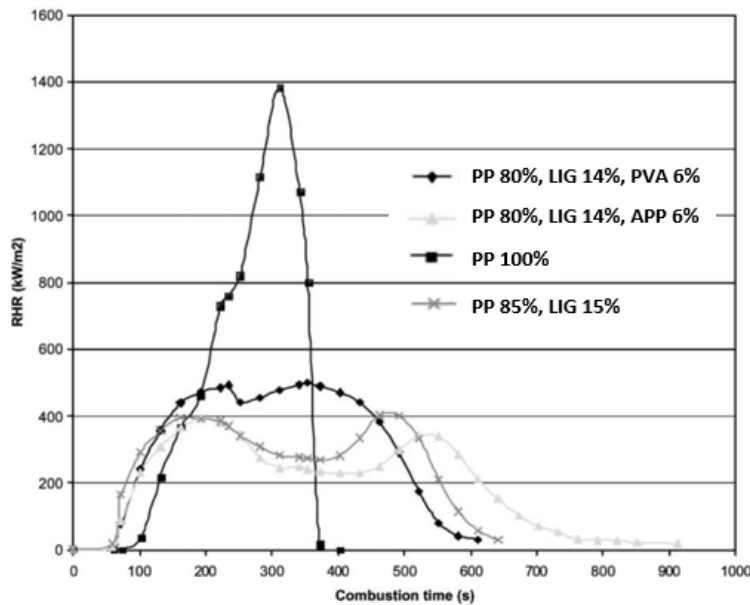
Figure 24. HRR curves of PP-lignin composites (6 mm thick, 25 mm, 25 kW/m²) [135]

2.3.1.2. Modified lignin

As seen previously, lignin can be chemically modified in order to tune its final properties (see section 1.3.1, p42). In the field of FR research, typical chemical elements are known for being responsible of the good FR performance of additives, such as phosphorus and nitrogen. For example, Yu *et al.* [13] functionalized lignin with P- and N-groups (PN-lignin) and the chemical routes are presented in Figure 25. In order to increase the amount of reactive sites hydroxyl groups, hydroxymethylation was performed prior to further FR functionalization. 8.1 and 7.2 wt.% of P and N were found respectively in the PN-lignin structure. Before to present the performance of such modified lignin, it is important to notice that PN-lignin were only characterized by XPS and FTIR, which is not sufficient to prove chemical bonding between the FR groups and the lignin structure. Conclusion must therefore be drawn carefully.
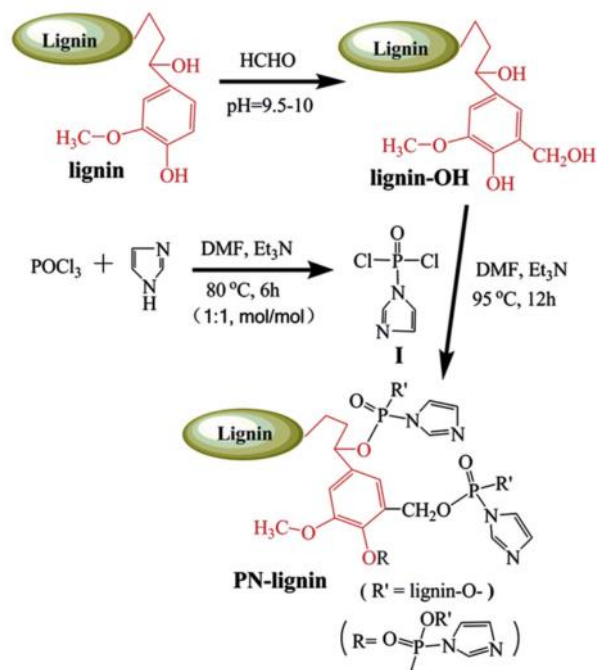
Figure 25. Chemical modification routes to get PN-modified lignin [13]

The thermal stability of lignin under inert atmosphere was significantly improved thanks to the modifications, and the amount of residue was particularly enhanced up to 61 wt.% (+ 20 wt.% than neat lignin). As a result, the functionalized lignin can enhance the thermal stability of PP at 20 and 30 wt.% of loading (with 5 wt.% of compatibilizer, PP grafted with maleic anhydride, PP-MA). Presence of lignin clearly increased the char yield, and even more significantly with PN-lignin. These composites were then tested by cone calorimetry test in order to assess their behavior to fire. The curves are presented in Figure 26.
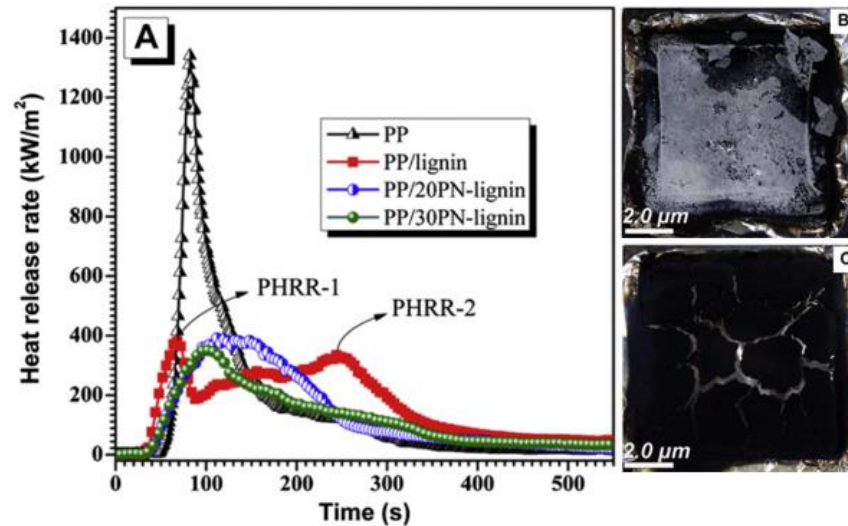
Figure 26. FR performance of PP blended with modified lignin according to CC testing (3 mm thick, 35 kW/m², 25 mm)

A- CC curves / B- Char of PP-lignin / C- Char of PP-20PN-lignin [13]

Similar reductions of pHRR of almost 70 wt.% were observed for the composites. However, the combustion behavior changes when lignin is modified or not. In the case of neat lignin, a bimodal curve is noticed, showing that the char is formed (pHRR-1) but then collapses (pHRR-2) [134]. When the modified lignin is used as FR, only one peak of combustion is observed. The results indicate that the char layer formed during the combustion is much more resistant than that with neat lignin. On the picture displayed in Figure 26, it appears that PN-lignin leads to a more cohesive char, which is partially responsible of the improved FR performances.

Yu and its team followed the study of using PN-lignin with metal-based synergists [137]. CC test results are shown in Table 8. Nickel, cobalt and zinc acetates were introduced with PN-lignin as flame retardant additives in PP (mass ratios PP/PP-MA/PN-lignin/Catalyst: 75/5/18/2). Slight reduction of the thermal stability of the composites was noticed in presence of the catalysts, but on the contrary, FR performances were a little bit improved. The best results were obtained with Ni-based catalyst, which was involved in the char-forming process. Such synergists can therefore be considered as char former catalysts in FR lignin formulations.

Table 8. CC and LOI data of PP blended with PN-lignin and synergists (3 mm thick, 35 kW/m², 25 mm) [137]

sample ID	t_{ign} (s)	PHRR (kW/m^2)	THR (MJ/m^2)	Char (wt%)	LOI (vol.%)
Pure PP	49 ± 1	1350 ± 80	87.3 ± 0.5	3.1 ± 0.3	17.5
PP/20PN-lignin	38 ± 1	380 ± 15	74.2 ± 0.4	16.0 ± 0.5	22.5
PP/20PN-lignin-Ni	31 ± 1	330 ± 10	69.5 ± 0.3	22.9 ± 0.5	26.0
PP/20PN-lignin-Co	37 ± 1	362 ± 12	72.8 ± 0.3	18.0 ± 0.5	24.5
PP/20PN-lignin-Zn	38 ± 1	368 ± 13	73.5 ± 0.4	14.2 ± 0.4	23.0

2.3.2. Styrenic polymers

This class of polymers is highly flammable and extensively used in many applications. Because lignin contains a high amount of aromatic groups, an interesting compatibility with styrenic polymers may be expected. Composite's morphology study of lignin blended in polystyrene or acrylonitrile-butadiene-styrene confirms this assumption [93,94]. Therefore, using lignin as FR additive in styrenics can be considered. In this context, Song *et al.* [94] investigated the effect of alkali lignin on thermal and FR properties of ABS composites. The influence of lignin's loading as well as the use of a compatibilizing agent (Styrene ethylene-co-butadiene styrene-grafted-maleic anhydride) were studied. TGA curves are shown in Figure 27, while cone calorimeter data are listed in Table 9.

Lignin can be evenly dispersed in the ABS matrix. Incorporation of lignin in ABS only slightly reduces the initial degradation temperature of the composite in comparison to the neat polymer. However, the thermal stability for temperatures above 400°C was enhanced in both inert and thermo-oxidative atmospheres. The amount of transient char (air atmosphere) and the final residue (nitrogen atmosphere) were definitely increased. FR performance measured by cone calorimetry was improved using lignin. Indeed, a reduction of 32% of the pHRR was observed with only 20 wt.% of lignin. When a compatibilizer is used at 10 wt.% with 20 wt.% of lignin, pHRR is therefore reduced by 44%. As for polyolefins, the main mode of action of lignin as FR is attributed to the formation of a carbonaceous layer. The free radical-trapping capacity of lignin mays also contribute to such FR performance.
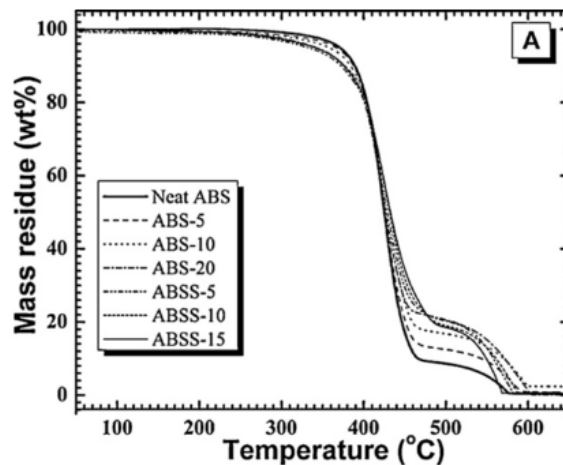
Figure 27. Thermal stability of ABS-lignin composites [94]

Table 9. CC data of ABS-lignin composites [94]

Run	t_{ign} (s)	PHRR (kW/m^2)	PHRR reduction (%)	THR (MJ/m^2)
ABS	24 ± 2	775 ± 40	Non	71.2 ± 1.2
ABS-5	28 ± 3	640 ± 32	18	69.1 ± 1.0
ABS-10	30 ± 4	550 ± 31	29	65.4 ± 0.6
ABS-20	23 ± 2	526 ± 30	32	65.1 ± 0.7
ABSS-5	23 ± 2	463 ± 28	40	61.3 ± 0.5
ABSS-10	24 ± 3	440 ± 30	44	63.4 ± 0.8
ABSS-15	24 ± 2	428 ± 22	45	63.7 ± 0.9

2.3.3. Polyurethanes

Many researches are undertaken to use neat or modified lignin as macromonomers in the conception of bio-based polymeric materials (section 1.3.2, p42). It has been seen previously that polyurethane lignin based are particularly of interest. Indeed, the lignin can substitute the usual polyol source in the process. Gao *et al.* [138] prepared polyurethanes foams from hydroxylated calcium lignosulfonates as one of the polyols and commercial flame retardants such as flame retardant polyol, microencapsulated ammonium polyphosphate (MAPP) and organically modified layered double hydroxides (OLDH) were incorporated in the composites. The fire behavior of the composites was improved according to CC testing. For example, diminutions of 65 % of pHRR and 50 % of THR were achieved with MAPP combined with OLDH.

Another approach consists in modifying the lignin macromonomers with FR groups. Zhu *et al.* [139] developed polyurethane foams flame retarded with lignin. They proceeded by first

modifying the lignin with melamine phosphate in order to add P and N elements, followed by a copolymerization of the free hydroxyls remaining with isocyanates to produce lignin-modified-PU foams. Even if slight negative influence on the morphology and mechanical properties was noticed, significant improvements of the thermal stability (increase of the residue) as well as fire properties (LOI of 28.3 % and V-1 at UL-94, 3 mm) were noticed in comparison to neat PU foams.

2.3.4. Bio-based polymers

2.3.4.1. Polylactic acid

The bio-based plastics become more and more used. Indeed, the progress made on the development leads to biopolymers exhibiting high performance and interesting properties. The polylactic acid (PLA) is the best example, since it is now widely used in plenty of applications. Therefore, PLA needs to be flame retarded, and many solutions are available depending on its final use [140]. Réti et al. [141] worked on innovative bio-based intumescent systems for PLA. Starting from an established system (ammonium polyphosphate (APP) / pentaerythritol (PER)), the carbon source (PER) was substituted by bio-based materials. Starch and lignin were considered. A design of experiment was set up to find the best formulation regarding fire testing such as LOI, UL-94 and Mass Loss Calorimeter. The ternary diagram for LOI is presented in Figure 28. A formulation containing 10 wt.% of lignin and 30 wt.% of APP exhibited good FR performances by reaching V0 classification (3 mm) and a LOI value of 31. This systems was then extended to textile, and was applied to nonwovens composed of hemp or wool to improve their fire retardancy properties [142].
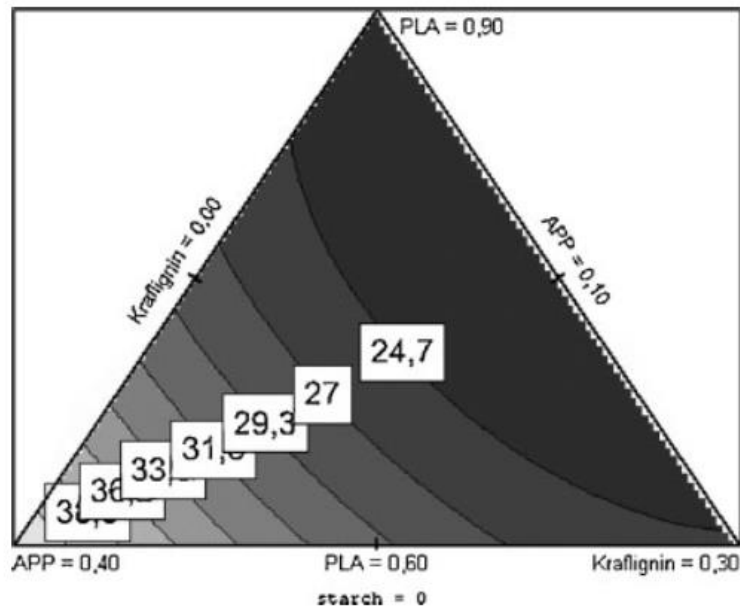
Figure 28. Ternary diagram showing the evolution of LOI value as a function of PLA, APP and lignin amount [141]

Zhang *et al.* worked on the optimization of this system in different ways. First, modifications of lignin were undertaken. Lignin-silica were prepared by sol-gel method [143], while urea-modified lignin were synthetized according to the Mannich reaction [144]. In combination with APP, these modified-lignin exhibited good FR performance in PLA according to UL-94 (V0, 3 mm), LOI (35 %) and CC testing (75 % reduction of pHRR). Another way of improvement of the system was achieved by adding organic modified montmorillonites (OMMTs) to the system as synergistic agent [145]. Different types of OMMTs were compared. An improvement of the FR properties was noticed and was attributed to the fact that OMMTs catalyze the degradation of PLA which release less combustible gases. Char was also observed to be much more cohesive.

2.3.4.2.   Polybutylene succinate

Besides the polylactic acid, new bio-based polymers are starting to be developed at the industrial scale. The biopolyester polybutylene succinate (PBS) is one of them. Because of the growing interest towards this biopolymer, researches are done to find suitable flame retardants additives to reduce its flammability. In this context, Ferry *et al.* [14] incorporated alkali and organosolv lignin in PBS. Since alkali lignin releases sulfur dioxide during decomposition, it exhibits a better FR behavior in comparison to organosolv lignin. Alkali lignin was then surface modified by

macromolecular phosphorus compounds (homoP, copoP, DHAP in Table 10). The results of CC test are presented in Table 10. The time to ignition decreased dramatically, while a reduction of 50 % of the pHRR was achieved with 20 wt.% loading of lignin. Even if the chemical modification did not further improve the FR performance, the char cohesion was enhanced according to the authors.

Table 10. Cone calorimeter data of PBS flame retarded with neat and modified alkali lignin [14]

Sample	Residue (%)	TTI (s)	pHRR (kW/m^2)	THR (kJ/g)
PBS	5.7	72	562	22.1
PBS–5% Lig Alk	6.4	61	497	20.7
PBS–10% Lig Alk	9.5	51	363	20.0
PBS–15% Lig Alk	12.5	44	329	19.7
PBS–20% Lig Alk	17.0	42	290	19.0
PBS–20%Lig Alk homoP	13.7	37	276	20.0
PBS–20%Lig Alk copoP	14.8	40	270	20.4
PBS–20%Lig Alk DHAP	11.9	41	295	19.7

2.3.5. Thermosets

Regarding the thermosets class, researches about the use of lignin are mainly focused on its chemical modifications for application in epoxy matrix. Most of the time, amination of the lignin is undertaken. Alalykin *et al.* [146] prepared FR lignin for an epoxy system. For this, hydrolyzed lignin was modified with orthophosphoric acid and urea. As seen previously, the aim is to add phosphorus and nitrogen elements to lignin for improving its FR properties. Modified lignin was then incorporated as FR additive in an epoxy resin (ED-20), cured with polyethylenepolyamine. The thermal stability (increase of the amount of residue) as well as the flammability according to oxygen index testing (from 20 to 26 %) were significantly improved.

2.3.6. Others polymeric materials

Recently, Zhang *et al.* [147] compounded lignin with hybrid-functionalized silicones to give elastomer and foam composites. Softwood lignin was modified with silicone groups according to the Piers-Rubinsztajn reaction, as shown in Figure 29. Fire performance and thermal stability of

these lignin-silicone elastomers were then investigated [148]. Without post-treatment, the composites were very flammable because of the residual Si-Hs groups. Therefore, NH$_3$ vapor treatment was undertaken and permits to remove such groups, and the composites reached V-1 at the UL-94 test (3 mm thickness). V-0 ranking was achieved after an additional thermal post-treatment of the composite. Moreover, the composites exhibited high thermal stability and low thermal conductivity that were comparable to pure silicone foams.
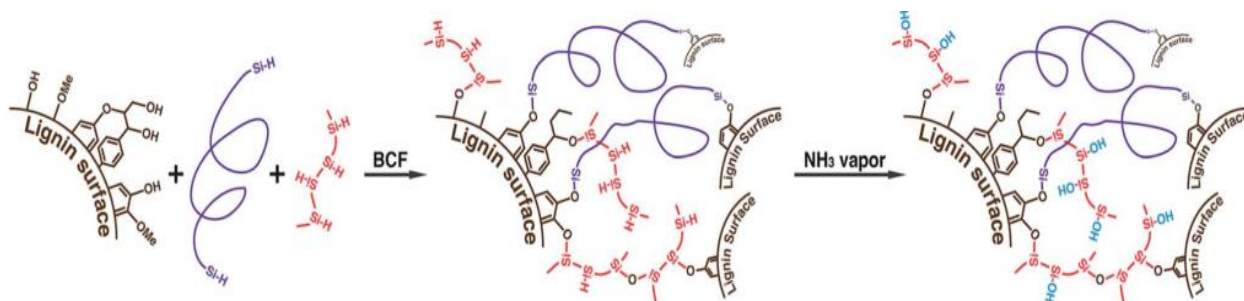
Figure 29. Schematic of lignin crosslinked network [148]

2.4. Conclusion

The use of lignin as flame retardant additive in polymers was discussed in this part. The ability of lignin to form a char during its thermal decomposition leads to consider mostly a mode of action in the condensed phase. The creation of a carbonaceous protective layer is indeed one solution to flame retard polymers. Several studies deal with lignin used as FR in polyolefines, styrenics, polyurethanes or thermosets. The formation of a char permits to improve the FR performances of the composites. Coadditives and synergists in order to enhance the FR properties of the systems were also considered. Phosphorus-based compounds for example can be used as coadditive, or metallic acetates as charring catalysts may be cited. Finally, FR groups can directly by added in the lignin's structure with chemical modifications.

This review reveals that lignin is mainly considered as charring agent in FR systems. In this context, FR formulations should be developed in order to promote the char formation from lignin and to improve the final performance of the carbonaceous residue, which is used as protective barrier. It appears that two strategies can be followed. The use of coadditives, such as acid source or

metallic compounds, which are intended to interact with lignin during the thermal decomposition. The second approach is to chemically modify lignin with chemical groups, which will promote charring of lignin, such as phosphorus or nitrogen based compounds. Even if promising FR systems with lignin were reviewed, the modes of action as FR is still unclear and remains to be elucidated.

3. Conclusion and strategy

Lignin is the second most abundant biopolymer on Earth. The pulping industry is the main supplier of lignin (> 50 million tons per year), however more than 90 % of the lignin's production is burnt for energy recovery. Indeed, lignin's structure is very changing depending on the botanical origin and the extraction process. As the knowledge about lignin increased in the last decades, a lot of efforts are put in lignin's research to find suitable valorization of this biobased materials, which presents interesting properties, for example its use as antioxidant. Today, main trends consist in considering lignin as a biosource of chemicals (fragmentation into smaller platform molecules) or as macro-monomers or additives for material applications (chemical modifications, thermal treatment). The development of such materials starts to be considered at the industrial scale. When used as additive in polymers, lignin can be used in many applications.

Lignin belonging to the family of polyphenols (full aromatic structure) could develop a char under fire conditions. Char formation is one of the mode of action to flame retard polymers. Indeed char acts as protective and insulating barrier. So valorization of lignin by using it as FR additive in polymers appears to be promising. It was seen in this chapter that several studies already deal with the use of lignin as FR additive, in PP, ABS or PBS for example. Lignin alone shows interesting FR properties, however lignin chars exhibit a low resistance when exposed to fire, thus limiting its FR performance. To overcome this drawback, the use of coadditives or chemical modifications of lignin may be considered. Several works, in epoxy or polyurethane for example, show a positive influence on char properties by adding P and N elements to lignin's structure, leading to better FR performance.

In this context, this work aims to valorize lignin, which exhibits interesting FR performance, in different systems. Valorization involves different meaning:

- Consider lignin which is commercially available, and in large quantities

- Develop systems, which contains a significant amount of lignin

- Elucidate the mode of action of lignin in the different systems

- Draw extendable conclusions, which will serve as basis for further studies

To fulfill these objectives, this work aims to develop FR lignin-based systems as proof of concept, and able to produce significant progress in the elucidation of the lignin's mode of action as FR in polymers. Kraft lignin (hereafter called LIG in this work) is chosen, since it is commercially available and produced in large quantity. It was shown that adding phosphorus in lignin's structure may improve its properties as FR additive, so phosphorylation of lignin was undertaken (P-LIG). The strategy is first to characterize in details LIG and P-LIG in order to investigate its possible mode of action as FR. Then, FR performance of LIG will be investigated in several polymers. In order to further improve the FR performance of lignin, different FR systems, using coadditives or synergists, will be develop. Finally, the better formulation in terms of FR performance will be studied and the mode of action of lignin as FR additive elucidated. The following Chapter II is devoted to the materials as well as experimental techniques used in this study.

II- Materials and methods

This chapter is dedicated to the presentation of the polymers and the additives used in this study. The preparation method of the samples is then discussed. Moreover, test methods to characterize the materials are commented. Finally, experimental techniques used to characterize FR performance, thermal decomposition, gas and condensed phase are fully detailed.

1. Materials

1.1. Polymers

Several polymers were used in this study. Technical details are available in Appendix 1, p252. Polypropylene (PP) is a standard homopolymer supplied by Lyondellbasel and referred by the producer as Moplen HP401R. Thermoplastic polyurethane (TPU) was kindly supplied by BASF under the name of Elastollan C85A. Polystyrene (PS) is a high molecular weight homopolymer provided by Styrolution with the commercial name Styrolution PS 168N/L. Acrylonitrile-butadiene-styrene (ABS) was kindly supplied by AIMPLAS in the frame of the PHOENIX project. This copolymer is commercialized by BASF under the trade name of Terluran® HI-10. Polylactic acid (PLA) is a biobased polymer which was supplied by NatureWorks LLC under tha name of PLA 4032D.

1.2. Lignin

Kraft lignin was kindly supplied by Fraunhofer LBF (Darmstadt, Germany) in the frame of PHOENIX project. Kraft lignin is produced by UPM (Finland) under the commercial name of BioPiva™ 100.
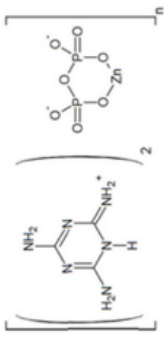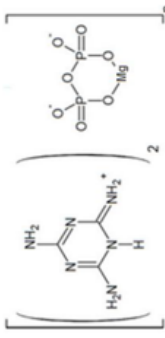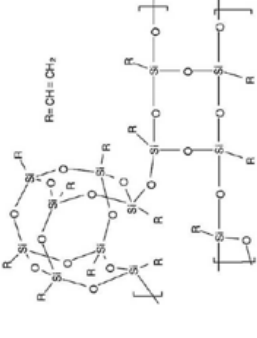
Phosphorylated lignin (P-LIG) was kindly provided by Fraunhofer LBF (Darmstadt, Germany). They chemically modified Kraft lignin in the frame of PHOENIX project. The protocol of phosphorylation is detailed in the section 1.4, p79.

1.3. FR additives

As mentioned before, this study is based on the improvement of fire retardant properties of several plastics. To do so, FR systems based on lignin are developed. In such systems, commercial FR compounds are used as coadditives or synergists. Table 11 summarizes all additives used in this work, their supplier and their chemical structure. As it can be seen, different types of compounds are considered, such as phosphorus-containing, acid source, metal-based or nanoparticles additives.

Table 11. List of additives used in this study

Chemical	Abbreviation	Supplier	Composition	Chemical Structure
AP422	APP	Clariant	Ammonium polyphosphate	
Phytic acid sodium salt hydrate	PHY	Sigma Aldrich	Phytic acid sodium salt hydrate	
Succinic acid	SUCC	Sigma Aldrich	Succinic acid	
Exolit® OP 1230	OP1230	Clariant	Aluminium diethyl phosphinate	
Iron (III) chloride	$FeCl_3$	Sigma Aldrich	Iron (III) chloride	-
Nickel (II) chloride	$NiCl_2$	Sigma Aldrich	Nickel (II) chloride	-
Safire® 200	S200	Catena – Floridienne Chimie	Melamine-poly(aluminium phosphate)	

Chemical	Abbreviation	Supplier	Composition	Chemical Structure
Safire® 400	S400	Catena – Floridienne Chimie	Melamine-poly(zinc phosphate)	
Safire® 600	S600	Catena – Floridienne Chimie	Melamine-poly(magnesium phosphate)	
Cloisite C30B	C30B	BYK Additives	Organoclay montmorillonite with surfactant	CH_2CH_2OH H_3C-N^+-T CH_2CH_2OH T = Tallow (65% C18, 30% C16, 5% C14)
POSS Firequench® 1286	POSS	Hybrid Plastics	Polyhedral Oligomeric Silsesquioxane	

1.4. Preparation of materials

1.4.1. Phosphorylation of lignin

An illustration of the simplified synthetic route leading to phosphorylated lignin (P-LIG) is shown in Figure 30. The objective of the work was the development of a process suitable for industrialization and therefore the synthetic route was kept as simple as possible. Lignin (2 kg) was dissolved in 7.5 L of tetrahydrofuran (THF). When the lignin was fully dissolved, phosphorus pentoxide (P_2O_5) was added at room temperature. The solution was heated at solvent reflux for 7-8 h in the course of which the product was largely precipitated. After the mixture was allowed to cool at room temperature, water was added in order to transform excess of P_2O_5 into phosphoric acid. Then THF was evaporated under reduced pressure at 40 °C. The phosphorylated lignin was collected by filtration and washed with water. In order to remove residual phosphoric acid, P-LIG was exhaustively extracted with water in soxhlet apparatus. Finally, the product was dried 24 h at 75 °C at reduced pressure.
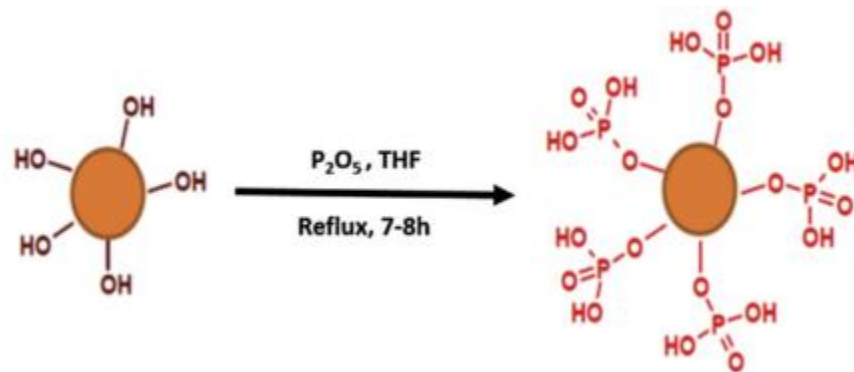
Figure 30. Synthetic route leading to phosphorylated lignin (P-LIG)

1.4.2. Processing of the composites

1.4.2.1.   Compouding by mixer

The composites were prepared using a Thermo Scientific HAAKE Reomex mixer: 200 g-batches of each material were produced. Raw materials were dried overnight at 75 °C before use. The rotors speed was set at 50 rpm. Neat polymer was first melted, and then lignin or additives added. All components were mixed during 3 minutes, and total residence time of polymers was 6 minutes.

Materials used for the first part of the screening (see Chapter IV, section 1, p143) were prepared by mixer. Polymers (PP: 190 °C, TPU : 195 °C, PS : 210 °C, ABS : 200 °C, PLA : 185 °C) where mixed

with Kraft lignin in the weight ratio 70:30. Materials of used in chapter V (ABS with LIG and P-LIG) were prepared in the same conditions.

1.4.2.2.   Compounding by microcompounder

DSM Xplore Micro15 twin screws micro-extruder (15 cm^3 capacity) was used to prepare the materials used in the second part of the screening commented in Chapter IV. Each compounding was 15 g batch. Processing temperatures were set at 185 °C and 200 °C for PLA and ABS respectively. The screws speed was set at 50 rpm. Polymers were first molten, and then powder mixture of lignin with or without other additives added. The residence time was 5 minutes.

1.4.2.3.   Plates and barrels samples

Plates and barrels samples used for testing were prepared with a Sogema press. The temperature was set at the processing temperature of the polymeric matrix (detailed in the previous parts). The pressure was set at 20kN for 2 min and then increased at 40 kN for 8 min. Materials were pressed to make barrels of 100 x 10 x 3 mm^3 (LOI samples), 127 x 12,7 x 3.2 mm^3 (UL-94 samples) and plates of 100 x 100 x 3mm^3 (MLC samples), 50 x 50 x 3 mm^3 (reduced MLC samples) and 60 x 60 x 1.2 mm^3 (Glow Wire samples).

1.4.2.4.   Powder samples

For several analysis like TGA or PCFC, composites were ground in liquid nitrogen to avoid degradation at 10 000 rpm using a high speed rotor mill Retsch – Ultra Centrifugal mill ZM 200. Powders were stored in dessicant to remove residual moisture before any tests.

2. Materials characterization

This section is divided in four parts. The first one is dedicated to the physico-chemical properties of the materials, and the second one describes the evaluation of the fire properties of the formulations. The third and fourth present the techniques the techniques used to characterize gas and condensed phase respectively.

2.1. Physico-chemical and thermal analysis

2.1.1. Color changes measurements

The color changes and reflectance of LIG and P-LIG were evaluated using a Datacolor CHECK 3 portable spectrophotometer from Datacolor Industry. The CIE L*a*b color system was considered for measuring the color. This system is commonly used in textile characterization [149]. The three coordinates presented in Figure 31 represent (i) the lightness of color (L* = 0 corresponds to black and L* = 100 corresponds to diffuse white; specular white may be higher), (ii) its position between red/magenta and green (negative values of a* indicate green and positive values indicate magenta), and (iii) its position between yellow and blue (negative values of b* indicating blue and positive values indicating yellow).
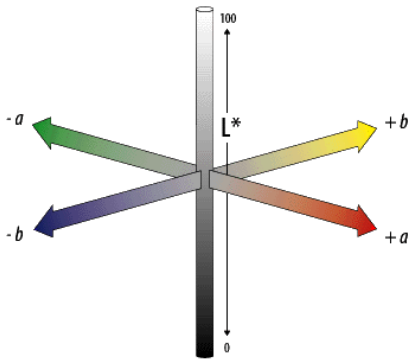
Figure 31. Color characterization in CIE Lab system coordinates

The difference between LIG and P-LIG (ΔE) was calculated according to Equation 3 in which ΔL* represents the lightness difference; Δa* and Δb*, the differences in a and b values.

$$\Delta E = \sqrt{(\Delta L *)^2 + (\Delta a *)^2 + (\Delta b *)^2} \qquad \text{Equation 3}$$

The a* and b* coordinates are close to zero for neutral colors (white and gray) and increase in magnitude for more saturated or intense colors. The advantage of CIE Lab system is that color differences can be expressed in units that can be related to visual perception [150]. Three

reflectance measurements were made on each sample; the samples were rotated 90° before each measurement.

2.1.2. Differential scanning calorimetry

Differential scanning calorimetry, performed on DSC Q100, from TA Instrument, was used to study the behavior of polymers when exposed to a temperature gradient (rise and / or decrease of the temperature at a controlled rate) under inert atmosphere. The samples in sealed crucibles were put in the oven in which the nitrogen flow was set 50 mL/min. An isotherm of 3 minutes at 40 °C was performed to allow temperature homogeneity of the samples. The sample were heated at 10 °C/min up to 160 °C, followed by an isotherm of 3 minutes. Then, the samples were cooled to 40 °C at 10 °C/min. This cycle was repeated a second time to evaluate the possible impact of thermal history of the materials on the heat flow. Each sample was tested two times to ensure repeatability of the obtained results.

2.1.3. Thermogravimetric analysis

TGA measurements were carried out on a Setaram TG92-16. Argon was chosen as protective gas for the furnace. Samples were contained in silica crucibles robed with gold sheet to prevent reactions between phosphorus and silica. Samples were ground into powder using a cryo-grinder (500 µm filter). Sample flow rate was set at 100 mL/min and nitrogen or air zero were chosen depending if the experiment was performed under pyrolysis or thermo-oxidative conditions. Samples of 8 ± 1 mg were submitted to an isotherm at 50 °C for 20 minutes for thermal homogeneity then followed by a heating ramp up to 800 °C. The heating ramps are detailed in the text depending on the experiment. Each sample was tested two times to ensure repeatability of the obtained results.

TG curves allow determining characteristic points. The derivative of the TG curve (DTG) permits finding the mass loss rate at given temperature and ramp, and so identify the main steps of the decomposition. DTG_{max} is the DTG value for each step (maximum), and the related temperature may also be considered (T_{MAX}). Another characteristic point is the onset temperature of degradation ($T_{2\%}$), which corresponds to the temperature when 2 wt.% weight loss is observed. Finally, the amount of residue obtained at 800 °C is called residue (Res).

Differential weight loss curves were calculated (Equation 4) in order to determine potential interactions which could occur between the polymeric matrix and the additives. These represent the difference between the experimental TGA curve for the mixture (w_{exp}(T)) and the linear combination of TGA curves (w_{the}(T)) for the neat components (Equation 5).

$$\Delta w(T) = w_{exp}(T) - w_{theo}(T) \qquad \text{Equation 4}$$

$$w_{theo}(T) = 0,7 \times w_{POL}(T) - 0,3 \times w_{LIG}(T) \qquad \text{Equation 5}$$

Where w_{POL}(T) and w_{LIG}(T) are the experimental TGA curves of the polymeric matrix and LIG respectively. The main objective of this technique is to point out if the addition of the FR additives will stabilize or destabilize the system. When $\Delta w<0$, the weight loss is higher than theoretical one, showing that the reactivity and/or interaction of the polymer with the additives leads to a thermal destabilization of the material. On the opposite, when $\Delta w>0$, the system is thermally stabilized.

2.1.4. Simultaneous Thermal Analysis

A simultaneous measurement of thermogravimetry (TGA) and Differential Scanning Calorimetry (DSC) were conducted using a Netzsch 449 F1 Jupiter simultaneous thermal analysis device (STA). Samples were put in platinum/rhodium pans with lids. The lids had a small orifice (0.25 mm in diameter) for gas escape. This container configuration was used to maximize the thermal contact between a degrading sample and heat flow sensing thermocouples located underneath the pan. Before each experiments, a blank with empty crucibles was performed and subtracted to the experiments so both mass and heat flow signal were independent of the crucibles. Samples were tested at a heating rate of 10 K/min from 50 to 1000 °C.

2.2. Fire testings

2.2.1. Mass Loss Cone

Mass loss calorimeter (MLC) is a bench-scale reaction to fire test which provides a combustion scenario that is typical of developing or developed fires. The measurements were carried out on a Fire Testing Technology (FTT) mass loss calorimeter device (ISO 13927 [184], ASTM E906 [185]).

The schematic representation of the device is shown in Figure 32. The procedure involved exposing plates (100 x 100 x 3 mm^3) in horizontal orientation with heating elements. Samples were wrapped in aluminum foil leaving the upper surface exposed to the heater (external heat flux of 35 kW/m^2, mild fire scenario) and placed on a ceramic backing board at a distance of 35 mm from the cone base. All measurements were repeated at least 3 times to ensure repeatability of the results.
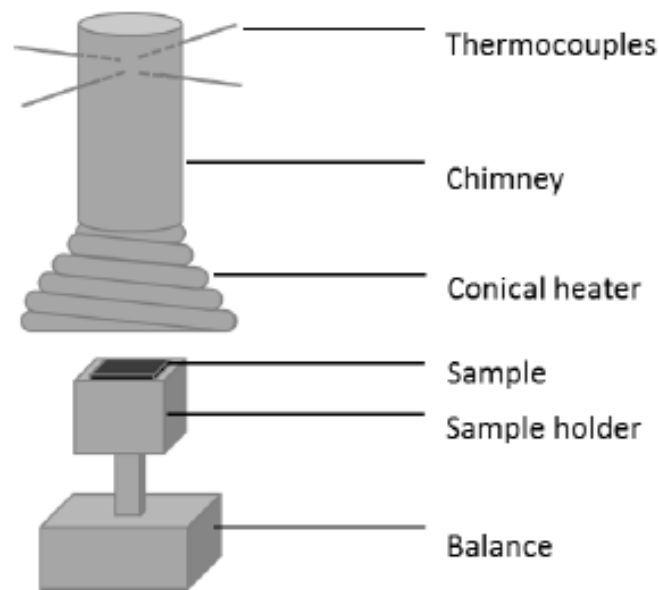
Figure 32. Schematic of the Mass Loss Cone

The mass loss calorimeter measures the temperature of the evolved gases using a thermopile located at the top of the chimney while the mass loss is recorded with a balance. The calibration of the heat release rate (HRR) is performed with methane. A methane flow of 0 to 6.7 mL.min^{-1} is burnt above the sample holder to obtain a calibration curve of the heat release as a function of temperature.

The values measured by mass loss calorimeter are: the heat release rate (HRR), the peak of heat release rate (pHRR), the total heat release (THR), the time to ignition (TTI) and the mass loss of the sample during combustion (ML). All measurements were performed at least twice. The presented curves are the worst case of repeatable results. The acceptable error of measurement is estimated at 10 % for all values.

2.2.2. "Reduced" Mass Loss Cone

In this study, a large screening of materials is performed based on MLC testing mostly (see Chapter IV). MLC testing is material consuming since at least 3 plates of 100 x 100 x 3 mm^3 for each formulation are necessary. Some products, like phosphorylated lignin, are only available in small quantity which is not sufficient to provide enough amount for performing MLC testing. Therefore, reduction of the sample's size was undertaken. Sample holder of 50 x 50 x 3 mm^3 were designed and made at the laboratory. Such dimensions allow to decrease by 4 the amount of material required for one sample. Accordingly, a calibration holder with the same dimensions was also developed. Figure 33 shows that geometry of both sample and calibration holders is very similar to that of standard MLC.
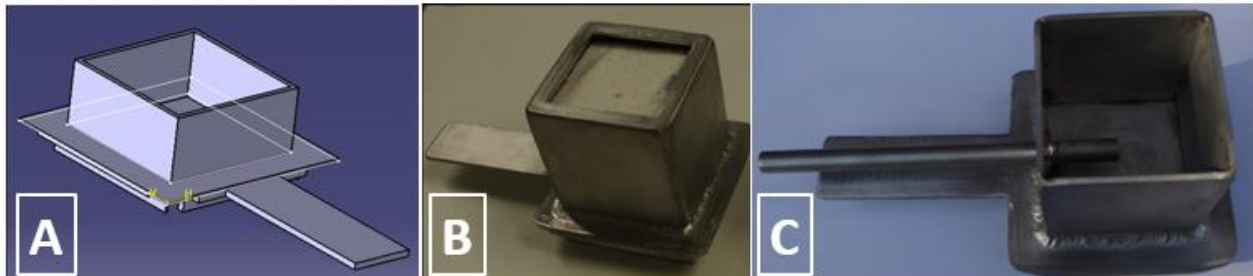
Figure 33. Reduced MLC: schematic of sample holder (A), picture of sample holder (B), picture of calibration holder (C)

Lindohlm *et al.* investigated the influence on calorimeter size results [151]. It was concluded downscaling of cone calorimeter sample size is possible for slow burning materials, although correlations are not trivial. However, fast burning materials such as PP wax exhibit not the similar behavior and so downscaling appeared to be not possible. In this study, it is not intend to correlate "standard" (10 x 10 cm²) and "reduced" MLC (5 x 5 cm²), but only consider the trend in terms of relative pHRR and THR increase or decrease. Therefore, experiments with both standard and reduced MLC were undertaken on two materials of reference of the lab in order to confirm that similar trends are observed.

Two kinds of materials were tested: intumescent and ceramic systems. The aim was to validate the reduced MLC for two types of protective barriers since a scale's reduction could change the mass and heat transfer. The intumescent material is a polyurethane (PU) flame retarded either

with APP or APP/MgO (magnesium oxide). These materials were prepared and fully investigated by Müller *et al.* [152]. The ceramic material is an ethylene-vinyl-acetate (EVA) flame retarded with aluminium trihydroxide (ATH). These last materials were produced at the laboratory from the study of Girardin *et al.* [153]. Absolute values of HRR were different by comparing 10 x 10 or 5 x 5 MLC, however, the reductions of the main parameters, pHRR and THR, were comparable from standard to reduced MLC. The results are detailed in Appendix 2, p258. Amount of residues and chars morphology were also very similar. Reduced MLC was therefore validated, since the same trends in pHRR and THR's reductions than that of standard MLC were noticed.

In the frame of this work, ABS/lignin composites are investigated in detail (see Chapter V), and so results of both reduced and standard MLC are commented in Chapter III and V respectively. Therefore, comparison between standard and reduced MLC testing ABS with LIG or P-LIG is discussed. The curves are presented in Figure 34 and the data in Table 12. The curves of both tests exhibit a similar bimodal behavior typical of charring materials. TTI is slightly delayed in the case of reduced MLC. This change may be attributed to the longer time needed to reach the critical concentration of combustible causing ignition. Indeed, 5 x 5 samples contain 4 times less materials than those of 10 x 10, and so the ratio O_2/fuel may be lower at the surface in the case 5 x 5 MLC. In the same time, longer times of flaming are noticed in the case of reduced MLC. Therefore, THR is higher for reduced MLC than that of standard MLC. To conclude, even if the absolute values of HRR are not comparable, similar reductions in pHRR in THR (less than 10% of difference) are obtained with standard or reduced MLC. In the case of this study, it can be assumed that the trends obtained with reduced MLC will be similar than those with standard MLC. So, reduced MLC will be used in this work to perform screening of the formulations.
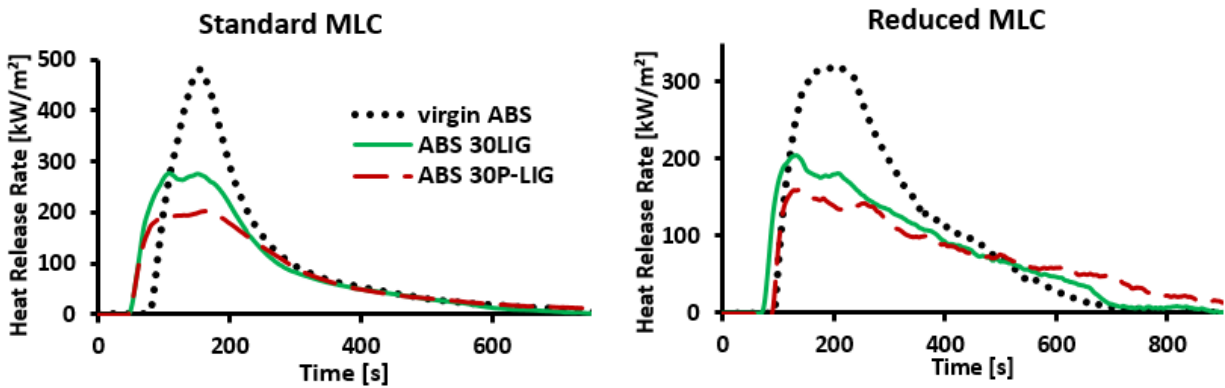
Figure 34. Comparison of FR performance of ABS composites tested with standard (left) and reduced (right) MLC

Table 12. MLC data of the comparison between standard and reduced MLC (ABS composites)

Formulation	TTI [s]		pHRR [kW/m²]		THR [MJ/m²]		Residue [wt.%]	
	10x10*	5x5**	10x10	5x5	10x10	5x5	10x10	5x5
Neat ABS	80	96	482	318	72	84	5	1
ABS_30LIG	49 (-31)	80 (-16)	275 (-43%)	210 (-34 %)	63 (-13%)	70 (-17%)	12	19
ABS_30P-LIG	49 (- 31)	91 (-5)	202 (-58%)	160 (-50 %)	58 (-20%)	64 (-24%)	17	25

* 10 x10 : standard MLC // ** 5 x 5 : reduced MLC

2.2.3. UL-94

The set of UL-94 tests, "Test of Flammability of Plastic Materials for Parts in Devices and Appliances", is an example for small heat-source ignition tests that is approved by the Underwriters Laboratories Inc. The most common and widely used test is the UL-94 V (IEC 60695-11-10) that describes the tendency of a material to extinguish or to spread the flame after ignition of the material. It classifies specimens from NC (not classified), V-2, V-1 to V-0, whereas V-0 is the best rating. The different criteria for the classifications are presented in Table 13. The experimental set-up for the UL-94 test can be seen in Figure 35.

A blue flame with a 20 mm high central cone is applied for 10 s to the bottom edge of the vertical specimen. After 10 s the flame is removed and the afterflame time required to extinguish the

flame is recorded. The flame is reapplied for another 10 s and removed again. After the second burning, the time to extinguish and the afterglow time are noted. It is possible that during the burning the barrels drop and inflame a piece of cotton that is below the specimen. For each material a set of 5 bars was tested. The specimens have a size of 127 x 13 x 1.5 mm³.

Table 13. Classification of materials according to UL-94 V

Criteria	V-0	V-1	V-2
Afterflame time for each individual flaming	≤ 10 s	≤ 30 s	≤ 30 s
Afterflame and glow time for each individual specimen, after second flaming	≤ 30 s	≤ 60 s	≤ 60 s
Total afterflame time for any condition set (5 flamings)	≤ 50 s	≤ 250 s	≤ 250 s
Cotton indicator ignited by flaming drops	No	No	Yes
Afterflame or afterglow of any specimen up to the holding clamp	No	No	No
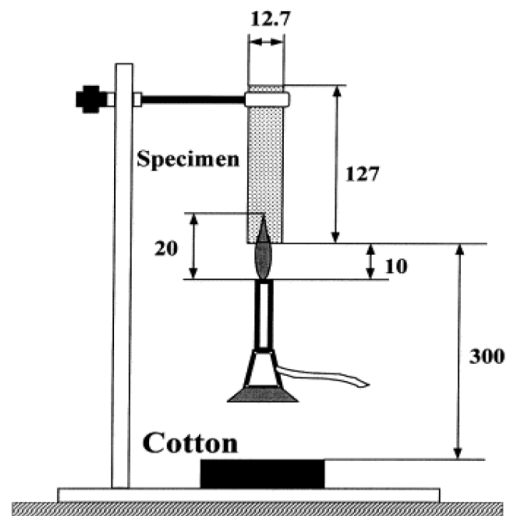
Figure 35. Schematic of UL-94 test

2.2.4. Limiting Oxygen Index

Limiting oxygen index (LOI) (ISO 4589-2) is a small heat source ignition test which evaluates the relative flammability of materials, their ignitability and inflammation. The experimental set-up of the LOI device is shown in Figure 36. LOI measurements are performed on a Fire Testing Technology device with barrels of 100 x 10 x 0.3 mm³ at room temperature. The specimen is

clamped vertically into a glass cylinder in a controlled oxygen-nitrogen mixture atmosphere. The measured LOI value corresponds to the minimal oxygen concentration required to sustain the combustion of a material. It is expressed as the percentage of oxygen in an oxygen-nitrogen mixture, whereas the error of measurement is ± 1 vol%O_2. Materials having a LOI value below 21 vol%O_2 are called combustible, those with a LOI value above 21 vol%O_2 are flame retarded.
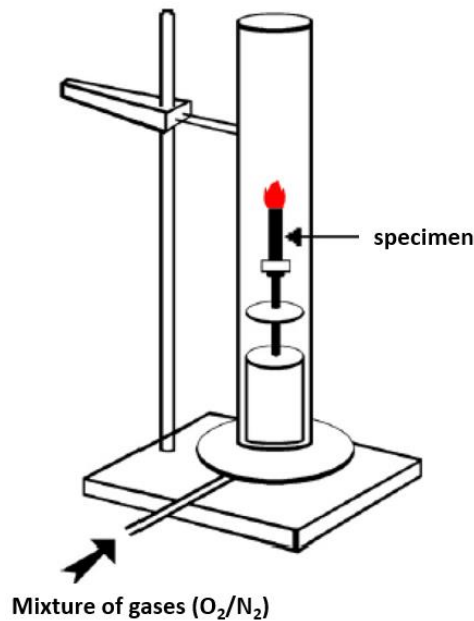
Figure 36. Schematic of LOI apparatus

2.2.5. Glow Wire

Glow wire test (Figure 37), described by IEC 60695-2-12, is widely used to evaluate the flammability of materials used for electrical parts. A sample (60 x 60 x 1.2 mm^3) is fixed vertically on a trolley loaded with a 1N weight. The sample moves towards the glowing wire, settled to a determined temperature (from 550 to 960°C) until they are in contact. After 30 seconds of contact, the trolley goes back to its initial position. The time of ignition (t_i) and the time of extinguishment (t_e) are measured.
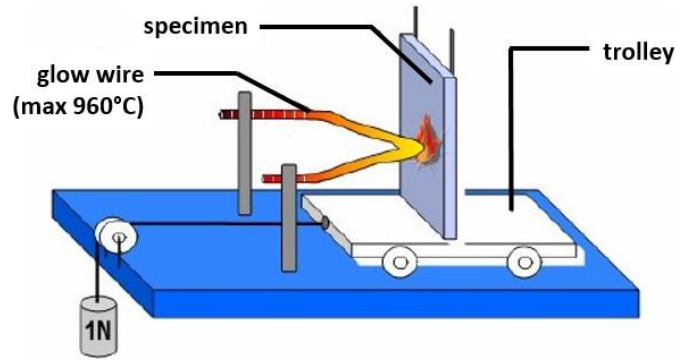
Figure 37. Schematic of Glow Wire apparatus

The test is successful when two conditions are fulfilled simultaneously:

- time of extinguishment must be lower than 30 seconds after the removal of the glow wire,

- cotton placed below the sample must not ignite.

The highest temperature at which the test is successful is called the glow wire flammability index (GWFI). To determine the GWFI, the wire is heated at a temperature ranging from 550°C to 900°C with a 50°C step or to a temperature of 960°C.

The glow wire ignition temperature (GWIT) is the temperature which is 25 °C (30 °C between 900 ° C and 960 ° C) higher than the maximum temperature of the tip of the glow-wire which does not cause ignition of a test specimen of given thickness during three subsequent tests. To evaluate the GWIT, the wire is heated from 550 to 960°C every 25°C.

2.3. Gas phase analysis

2.3.1. MLC coupled with FTIR

Mass loss calorimeter coupled with Fourier Transform Infra-Red (MLC-FTIR) described in Figure 38 is performed in the same conditions as standard MLC (see section 2.2.1, p84), it means 35 kW/m², with a distance between resistance and sample of 35 mm, and using plates of 100 x 100 x 3 mm³.

Gas picking pistol and transfer line are provided by M&C Tech Group. FTIR, Antaris^{TM} Industrial Gas System, is provided by ThermoFisher. The transfer line between MLC and FTIR is 2 m long and

is heated up to 180 °C. Before analyzing the gases by FTIR, soot particles are filtered by two filters (2 and 0.1 µm) made of glass fibers and ceramic respectively. The FTIR gas cell is set to 185 °C and 652 Torr. The optical pathway is 2 m long and the chamber of the spectrometer is filled with dry air. FTIR spectra obtained using MLC-FTIR are treated using OMNIC software. To quantify gases, spectra have to be recorded at different concentrations for targeted gases and a quantification method has to be created using TQ Analyst. Creating a method, representative regions in the spectra of the selected gas have to be chosen and interactions with other gases have to be taken into account. Using MLC-FTIR the following gases can be quantified: water, carbon monoxide, carbon dioxide, nitrogen dioxide and hydrogen cyanide. Quantification is reproducible within 10 %.
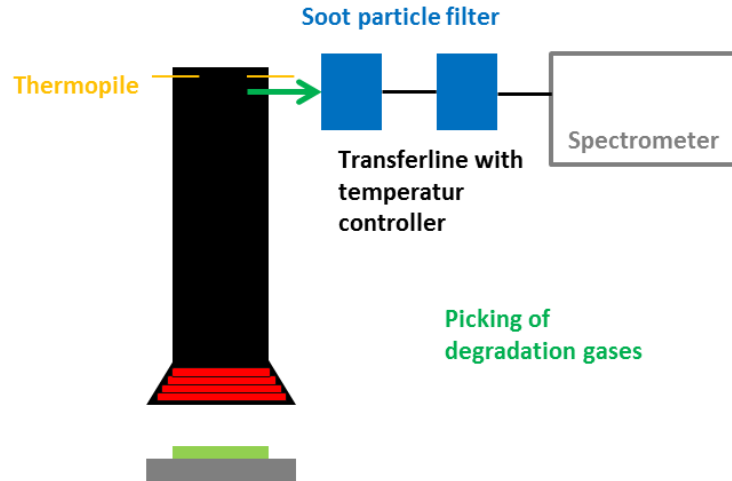
Figure 38. Schematic of MLC coupled with FTIR

2.3.2. TGA coupled with FTIR

Thermogravimetric analysis coupled with Fourier transform infra-red (TGA-FTIR) was performed on a TA Instrument TGA Q5000IR coupled with a Thermo Scientific Nicolet iS10 spectrometer. Analyses were carried out in air or nitrogen in alumina crucibles. Samples weight was 10 ± 1 mg. The balance flow was set to 15 mL/min whereas the purge flow was fixed to 100 mL/min. Samples were heated up from 50 to 800 °C (10 °C/min) after an isothermal of 10 min at 50 °C. Gases evolved during the TGA experiment were detected continuously by the FTIR device. The spectra were recorded every 10 seconds with the OMNIC® software in a range from 600-4000 cm^{-1}. The number of scans was fixed at

8 and the resolution at 4 cm^{-1}. The temperature of the transfer line between the TGA and the FTIR instrument was set to 225 °C to avoid condensation of the evolved gases.

2.3.3. Py-GC/MS

Pyrolysis-gas chromatography-mass spectrometry (Py-GCMS) analyses are performed on a device provided by Shimadzu (Figure 39). The device consists of a micro-furnace pyrolyzer (Frontier Lab PY-2020iD) coupled with a GC/MS (Shimadzu GCMS QP2010 SE). Experiments are performed under inert conditions using helium. Sample size is about 400 µg. In Py-GC/MS, analysis is performed through a flash mode which consists in heating the sample at very high heating rate in the pyrolyzer furnace while heavy evolved gases condensate at the beginning of the GC column and volatile fragments are detected after ionization. After the thermal treatment of the sample at the desired temperature in the pyrolyzer furnace, condensed products are desorbed and separated in the GC column to finally be observed in the mass spectrometer.
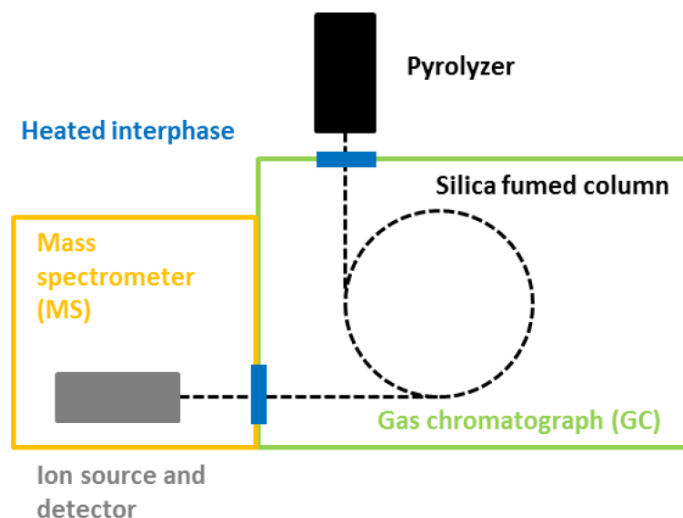
Figure 39. Schematic presentation of the Py-GCMS device

Samples (in a stainless steel cup) are inserted in the pyrolyzer set at a defined temperature during 5 minutes. After the decomposition process evolved gases are introduced into the GC. Released decomposition gases are separated by boiling point using a fused silica capillary column (30 m x 0.25 mm x 0.25 µm film thickness). The temperature of the column is set to 35 °C during the desorption process. The column is then heated up to 320 °C with a heating rate of 10 °C/min

followed by an isotherm at 320 °C for 10 min. The linear velocity of the carrier gas helium is set to 40 cm/s. The separated gases and fragments are then analyzed with the quadrupole mass spectrometer with an Electron-Impact (IE) ionization source. The IE spectra are recorded at 70 eV with a mass scan of 2 scans per second. The interface between the pyrolyzer and the GC is heated up to 320 °C; the interface GC/MS to 280 °C. The temperature of the ion source is set to 230 °C. After the experiments data is analyzed using the GC/MS post-run analysis from Shimadzu and F-Search from Frontier lab, whereas products are identified using NIST database.

To mimic the decomposition of materials obtained by TGA experiments a so called step wise desorption process is used (Figure 40).Materials are degraded at a given heating ramp to their first decomposition step. Then, evolved gases are separated and analyzed by GC/MS. Afterwards the remaining material is heated up to the end temperature of the second decomposition step and the evolved gases are again analyzed. This desorption process is continued until 800 °C following the different decomposition steps.
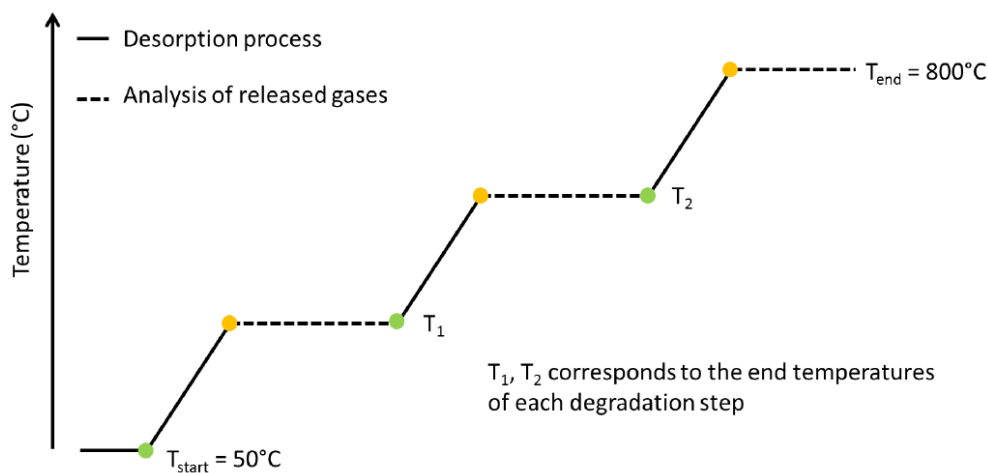
Figure 40. Schematic presentation of step wise desorption process

2.3.4. Pyrolysis Combustion Flow Calorimeter

The combustibility of the gas phase was evaluated with a pyrolysis combustion flow calorimeter (PCFC) supplied by Fire Testing Technology Ltd. PCFC was developed by Lyon [154] from FAA and allows measuring the flammability of small samples. Figure 41 represents the principle of the PCFC device. Samples in the form of powder, were placed in open alumina pans and were

degraded in a nitrogen atmosphere ("pyrolyzer") at a heating rate of 1 °C/s and with a nitrogen flow of 80 cc/min. The decomposition gases were then burnt in a nitrogen/oxygen mixture ("combustor") with 80 cc/min and 20 cc/min flows respectively. The heat release is measured as a function of the temperature using an oxygen analyzer, according to the Huggett relation [155]. Using an heating ramp of 1 °C/s, pHRR value in W/g equals heat release capacity (HRC) in J/(g.K) [154].
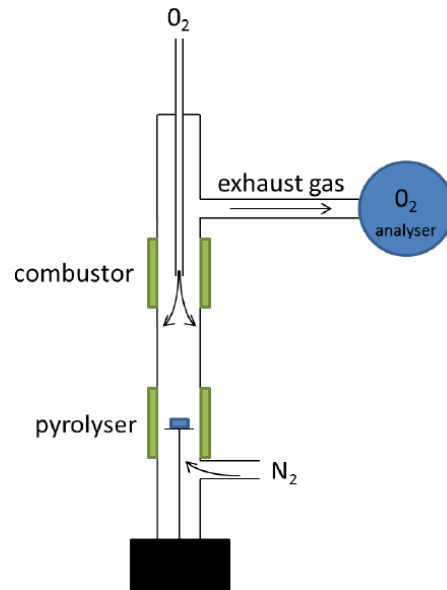
Figure 41. Schematic of Pyrolysis Combustion Flow Calorimeter

In order to get the most repeatable measurements, the maximum oxygen consumption has to reach around 50% of the total O_2 in the mixture. That is to say, starting from a mixture containing 20% of O_2, the peak of consumption as to reach $10\pm3\%$ O_2. Determination of the optimal sample mass (around 5 mg in the case of polymers, 10 mg in the case of lignin) was performed in accordance with this condition. When the decomposition gases are released from the pan, a certain amount of time is needed for them to reach the combustor, and that the oxygen analyzer measure the oxygen depletion. Therefore, a slight shift of temperature is often observed between TGA and PCFC analysis (+ 20°C approximately in PCFC).

2.4. Condensed phase

2.4.1. Thermal treatments

Thermal treatments consist in heating a sample in a furnace (Figure 42) at a defined temperature (Heat Treatment Temperature; HTT). The treatment temperatures were determined according to TGA curves as they correspond to the characteristic degradation steps of the systems. Samples were treated under air or nitrogen flow set at 75 mL.min^{-1} and heated at a heating rate of 10 °C/min (similar to that used for the TGA measurements) from ambient to the HTT followed by an isotherm of 2 hours. The samples were then cooled to ambient temperature before being collected. The residues obtained after thermal treatments were stored in a desiccator to avoid hydrolysis and then analyzed by different techniques such as solid state NMR.
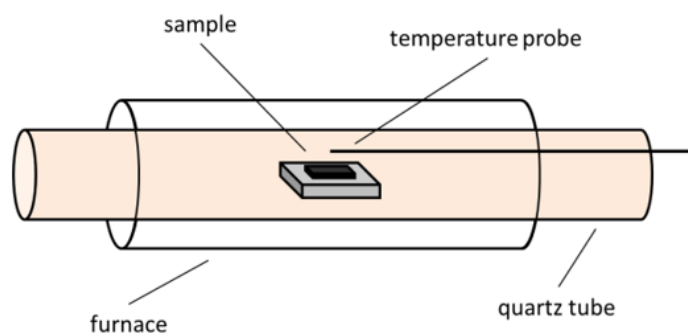
Figure 42. Tubular furnace used for thermal treatments

2.4.2. Apparent particle size

Particle's size distribution of lignin powder was investigated with a Malvern Mastersizer 3000 device. Lignin (LIG or P-LIG) was suspended in water (concentration < 0.1 %) at room temperature, and the particle's size was measured thanks to an optical method.

2.4.3. Size-Exclusion Chromatography

Number average molecular mass (M_n) was determined by size-exclusion chromatography (SEC) in tetrahydrofuran (THF) at 40 °C, with a flow rate of 1 mL/min and a polymer concentration of 2 mg/mL after filtration through a 0.45 mm pore-size membrane. Measurements were performed on a Waters (Separation Module Waters e2695) system equipped with three columns (Styragel HR1, Styr- agel HR3 and Styragel HR4) placed in series and coupled with a differential refractive index (RI) Wyatt detector (WYATT Optilab T-Rex). M_n were calculated using universal calibration reference, i.e. a polystyrene standard. Molar mass of PLA were exactly determined by the

calculation of Equation 6 [156]. Molar mass of ABS formulations was not corrected, so it was considered only an apparent molar mass. Considering the precision of the equipment and all the multiple stages of purification and dissolution of compounds, the error of measurement is estimated at 7%.

$$M_n(PLA) = 0.58 \times M_n(PS)$$
Equation 6

2.4.4. Microscopy

Digital microscopes are a variation of traditional optical microscope that uses optics and a charge-coupled device (CCD) camera to output a digital image to a monitor. In this work, Keyence – VHX-1000 digital microscope was used.

Scanning electron microscopy (SEM) images were taken at various levels of magnification using a Hitachi S4700 SEM at 6 kV. All samples were ultra microtomed with a diamond knife on a Leica UltraCut microtome at cryo temperature (−120 °C) to obtain smooth surfaces.

2.4.5. Electron Probe Micro Analysis

Electron probe microanalysis (EPMA) is an analytical technique that is used to establish the chemical composition of small areas on specimens. A beam of accelerated electrons is focused on the surface of a specimen using a series of electromagnetic lenses, and these energetic electrons produce characteristic X-rays within a small volume (typically 1 to 9 cubic microns) of the specimen. The characteristic X-rays are detected at particular wavelengths, and their intensities are measured to determine concentrations. All elements (except H, He, and Li) can be detected because each element emits at a specific set of X-rays. Additionally, the electron microprobe allows obtaining highly magnified secondary- and backscattered-electron images of a sample. In this work EPMA (Cameca – SX 100) was used to characterize the dispersion of P-LIG in the ABS polymeric matrix. Samples were prepared by pluging samples into an epoxy resin. Once hardened, the resin is polished and leaves cross section of the sample exposed.

2.4.6. X-Ray Diffraction

XRD was carried out with a D8 Advance diffractometer from Bruker, equipped with a LynxEye fast detector and copper radiation. Experiment were performed from 5 to 80°, with a step of 0.02° and 0.5 s. The thermally treated samples were manually grinded before the analysis.

2.4.7. Infrared spectroscopy

FTIR spectra were recorded using powder sample and a Nicolet iS10 ATR spectrophotometer in the range of 4000-500 cm^{-1}. For each spectrum 32 scans with a resolution of 4 cm^{-1} were recorded.

2.4.8. Raman spectroscopy

Raman spectroscopy measurements were performed with a Horiba Jobyn-Yvon Labram infinity instrument, equipped with liquid nitrogen cooled CCD detector. The spectra were recorded at λ=532 nm with a laser power of 0.6 mW. Spectra were recorded in ex-situ mode at room temperature in air.

2.4.9. Liquid NMR spectroscopoy

Liquid NMR was performed using a Bruker Advance II 400 MHz spectrometer. Lignin was dissolved in DMSO-d$_6$. ^{1}H spectra were obtained with 8 scans. ^{31}P spectra were obtained with 1024 scans and a delay of 2 s between each pulse with or without proton decoupling. 2D ^{1}H -^{31}P was performed using HSQC (Heteronuclear Single Quantum Coherence) procedure with 128 time domains and 16 scans and a delay of 1.5 s. Chemical shifts were referenced to DMSO-d$_6$.

Quantitative ^{31}P NMR experiments were carried out following a slightly modified Granata and Argyropoulos method [15] using a Bruker Advance 300 MHz. Lignin (30 mg) was dissolved in 0.5 mL of a CDCl$_3$/pyridine mixture (1:1.6 vol/vol). The internal standard used for quantification, N-hydroxy-6-norbornene-2,3-dicarboximide, was then added (100 mL of 0.1M solution in 1:1.6 v/v CDCl$_3$/pyridine mixture). Followed by 100 mL of 0.014 M solution of chromium(III) acetylacetonate in the same CDCl$_3$/pyridine mixture which was used to complete the solution in order to homogenize and accelerate phosphorus relaxation. Finally, 100 mL of the phosphitylation reagent, 2-chloro-4,4,5,5- tetramethyl-1,3,2-dioxaphospholane, was incorporated in the solution.

A portion of this mixture (0.6 mL) was introduced into a NMR tube. The spectra were recorded with 2 s relaxation time and an average number of 1000 scans. Chemical shifts were relative to the signal of the phospholane hydrolysis product at 132.2 ppm. The integral value of the internal standard was used for the calculations of the absolute amount of each functional group. DMFIT software [157] was used for peaks deconvolution when needed.

2.4.10. Solid state NMR spectroscopy

The solid-state nuclear magnetic resonance (NMR) is an effective tool to analyze the changes in the chemical environment of an atom inside a material. In the solid state (on the contrary to liquid state), the chemical shift anisotropy (anisotropy of magnetic moment, CSA), has a strong effect on the spectra, by broadening peaks. Through a tensorial analysis of the magnetic moments in a molecule, it is possible to demonstrate that it exists a "Magic Angle" with respect to the applied magnetic field at which the spinning of the sample leads to a minimization of absorption line broadening due to CSA. This method of analysis is so called "Magic Angle Spinning" (MAS).

In the case of carbon, the resonance of atoms is only possible in their isotopic form (^{13}C). However their low abundance leads to poor signal. This signal can be overcome by an excitation of protons in the sample and have them resonate at the same frequency than that of targeted atom (Hartman-Hahn condition). This process is called cross-polarization (CP), and the time of polarization is also called contact time. CP leads to a high enhancement of the excitation of studied nuclei. However it exists an interference of the large number of protons on the decay of isolated nuclei, due to weak spin interactions. In this case, the dampening of the signal can be removed with a strong radiofrequency signal which holds the protons in a high resonance state so that they do not absorb resonance from the nuclei. This is called ^{1}H decoupling. All measurements were carried out on a Bruker Advance II 400 (B_0=9.4 T) using a 4 mm standard probe. All NMR data were collected and analyzed at room temperature with the TopSpin software (Bruker).

^{13}C NMR measurements

High power ^{1}H decoupling and ^{1}H-^{13}C CP (with a contact time of 1 ms and a recycle delay of 5 s) were used. 1024 scans were performed. Glycine was used as a reference.

Spectra obtained for lignin characterization (LIG and P-LIG, see Chapter III) were measured at a rotation speed of 15 kHz with an accumulation of 20 000 scans.

Chars NMR analysis were performed at a rotation speed of 12.5 kHz and an accumulation of 1024 scans.

^{31}P NMR measurements

^{1}H decoupling was used because of the high relaxation time of phosphorus nuclei (high powered decoupling - HPDEC method). Accumulation of 512 scans were carried out. A repetition time of 10 s was applied, and H_3PO_4 aqueous solution (85%) was used as reference. The rotation speed was set at 12.5 kHz.

2.4.11. Elementary analysis

Chemical composition of materials, on raw and thermally treated lignin was investigated. Elementary analyzer CHNeO-Rapid (Elementar-Analy-sensysteme GmbH) was used for the elemental analysis of carbon and hydrogen. The amount was determined following the ASTM D 5291-92 standard. Foos-Heraeus elementary analyzer CHNeO- Rapid was used for the elemental analysis of oxygen. The oxygen amount was measured after combustion at 1150 °C. For phosphorus elemental analysis, the amount was determined by photometry (Spectrophotometer CADAS 100) after dissolution of the sample in acid mixture and further reaction with ammonium molybdate.

2.4.12. Rheology

In the case of composites exhibits a charring behavior as the temperature increases, changes in viscosity occurs. The study of the rheology of during the thermal degradation of a charring material is consequently an important parameter to under the charring process. All rheological measurements have been carried out on a parallel plate high temperature rheometer ARES 20A from Rheometric Scientific (Figure 43).
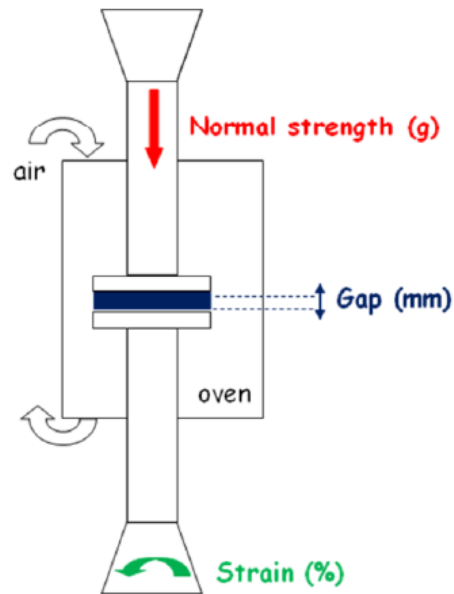
Figure 43. Schematic of the rheometer ARES 20A and the parameters recorded

The sample holder (for the bottom) and the top plates used on the rheometer are shown in Figure 44. The sample holder (a) exhibits a diameter close to that of the top plate (the 25 mm top plate will go inside the 27 mm bottom plate). The aim was to prevent the char to get out by the sides in case of high expansion.

Figure 44. Sample holder (a) and top plate (b) used during rheological measurement

III- **Phosphorylation of lignin**

This chapter is focused on characterization and thermal decomposition of lignin. Lignin exhibits a complex structure which requires to be elucidated before being considered for further studies. This step of characterization is also very important in the context of the valorization of lignin. Indeed, the results presented in this study are dependent of the lignin's structure. A precise knowledge of the chemical structure will permit for further works on this topic to consider similar lignin. As it is the most distributed and available lignin on the market, Kraft lignin (LIG) was chosen. The structure and materials properties are discussed in the first part of this chapter. Because phosphorus is a key element in flame retardancy, it was decided to perform phosphorylation of LIG (P-LIG) to improve its potential fire retardant (FR) efficiency. P-LIG was synthetized in the frame of the PHOENIX project by the Fraunhofer LBF. Elucidation of the structure, which is commented in the second part of this chapter, was done in order to assess if the phosphorylation was successful and to fully characterize the structure of the material. Some materials properties of P-LIG are also presented. Since the thermal decomposition pathway of an FR additive is of interest to investigate its mode of action as FR, the last part is devoted to evaluate the influence of the phosphorylation on lignin's thermal decomposition. Thermal stability, gas phase and the condensed phase were particularly analyzed.

1. Structural characterization of neat lignin (LIG)

This section is devoted to the characterization of LIG, i.e the starting material of this work. As mentioned in Chapter I, lignin's characterization is not easy, according to its complex structure and particular properties (low solubility in organic solvents, impurities, etc …). A complete characterization of LIG is first useful for the valorization of lignin, as the lignin's type will be clearly identified and known for further studies. Then, precise structural information will contribute to understand the mechanisms occurring during thermal degradation. FTIR and NMR spectroscopies were used, since they are known to be the easiest and well accurate to characterize lignin.

1.1. Characterization of LIG by FTIR-ATR

FTIR-ATR is widely used in lignin's analysis since it is a very simple and fast technique [29,31,38]. Databases of lignin's signals can therefore be established. For example, Monteil-Rivera *et al*. [39] proposed an exhaustive list of signal depending on the lignin's type. Referring to these works, LIG was analyzed by FTIR-ATR (Figure 45, Table 14). LIG spectrum exhibits classical patterns described in the literature. Indeed, a wide absorption band centered at 3400 cm^{-1} is observed and attributed to hydroxyl groups from both aliphatic and aromatic chains. It is overlaid by possible residual water, which cannot be avoided during FTIR measurements. The C-H vibrations of CH_3 and CH_2 groups are detected at 2935 and 2840 respectively. Then, many absorption bands are observed below 2000 cm^{-1}, which are presented in Figure 47 and Table 14.
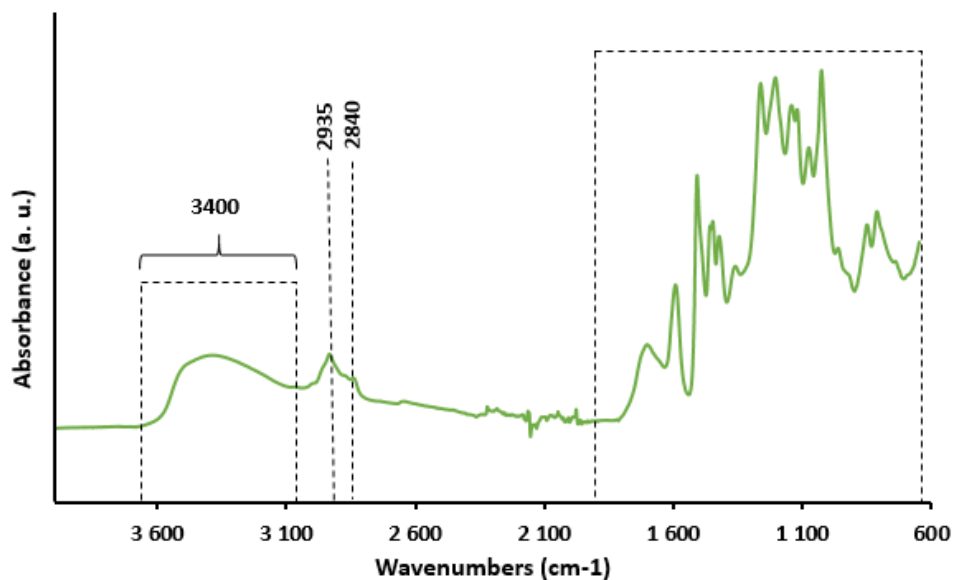
Figure 45. FTIR-ATR spectrum of LIG

Table 14. FTIR signals attributions of LIG [29,31,38,39]

γ: elongation // δ: deformation

Functional group or component	Wave number [cm^{-1}]	Vibration type
O-H	3400	γ
-CH$_3$ (C-H)	2935	γ
-CH$_2$- (C-H)	2840	γ
C=O (unconjugated)	1710	γ
C=O (conjugated)	1653	γ
C=C (S)	1595	Aromatic ring vibration
C=C (G)	1510	
C=C (S+G)	1425	
-CH$_3$, -CH$_2$- (C-H)	1460	δ
O-H (esterified phenol)	1365	δ in plane
C-O (G)	1265	γ
C-O (esterified phenol)	1210	γ
=C-H (S)	1125	δ in plane
=C-H (G)	1030, 1150	
C-O alcohol (II)	1080	δ
C-O alcohol (I)	1030	
=C-H (G)	855,815	δ out of plane

The numerous absorption bands observed in the range 2000 to 600 cm^{-1} reveal the complexity of LIG structure. Depending on the source and the reference, several bands may be attributed to different chemical groups. In order to make an understandable interpretation of the spectrum, attributions for LIG are undertaken first for each lignin's units (S, G, H), and then for specific chemical groups.

S, G and H lignin's units can be identified with FTIR-ATR (structures are available in Figure 5, p23). On LIG spectrum, Syringyl (S) and Guaiacyl (G) units are observed by aromatic skeleton vibrations (C=C) at 1595 for S unit, and 1510 cm^{-1} for G as well at 1425 cm^{-1} for S and G [39,42]. Moreover, aromatic C-H deformation in-plane are detected at 1125 (S) and 1030 cm^{-1} (G). However, breathing of aromatic ring at 1030 cm^{-1}, as well as C-H deformation out-of-plane at 855 and 815 cm^{-1} are only detected for G unit, and not for S [158]. Indeed, expected bands for S unit at 1330 and 832 cm^{-1} respectively were not observed. The same trend is noticed for C-O stretching and C-H in-plane deformation, which absorb only for G units, at 1265 and 1150 cm^{-1} respectively. It seems therefore that LIG contains more G than S units, and probably no H unit.
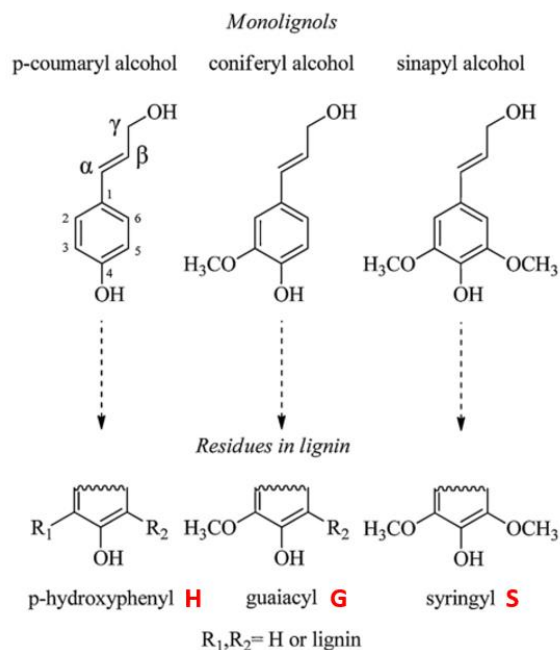
Figure 46. H, G and S units in lignin structure [8]

Typical lignin's chemical groups are also observed in LIG spectrum. The band centered at 1460 cm^{-1}, attributed to C-H deformation of alkyl chains, confirms the presence of CH$_2$ and CH$_3$

groups from aliphatic side-chains previously mentioned. C=O stretching of unconjugated structure is noticed at 1710 cm^{-1}. Because the band is relatively wide, it can be assumed that also conjugated C=O (absorption around 1653 cm^{-1}) may also be part of the structure. As a consequence of the Kraft extraction process, non-esterified phenolic groups are present in LIG structure and absorb at 1365 (O-H in-plane deformation) and 1210 cm^{-1} (C-O stretching) [158]. Finally, secondary and primary alcohols (C-O deformation) are detected at 1080 and 1030 cm^{-1} respectively [29]. It is noteworthy that the band at 1030 cm^{-1} was attributed twice, to breathing of G aromatic group and C-O deformation of secondary alcohol.
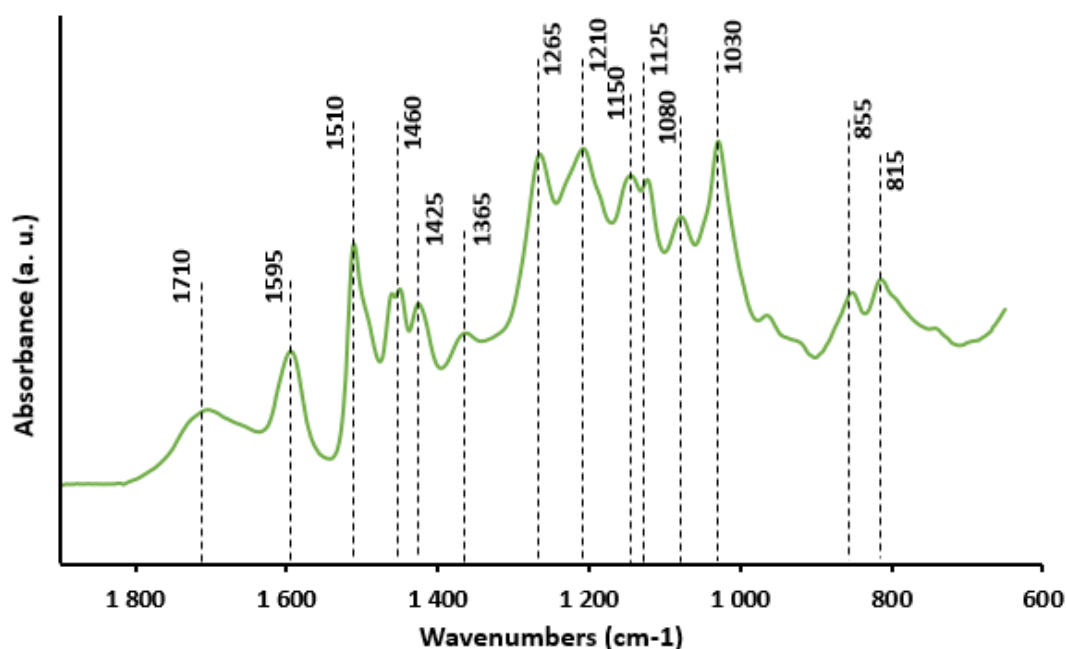
Figure 47. Attribution of signals between 2000 and 600 cm^{-1} of LIG (FTIR-ATR)

In conclusion FTIR-ATR provided information about LIG structure in accordance with the literature. It appears that LIG is mainly composed of G and S units, and probably a few H units. Because some bands of S units are not observed, G is probably the main unit of LIG structure. Moreover, carbonyl and hydroxyl groups were identified in the structure, as well as hydroxyl groups.

1.2. Characterization of LIG by NMR

1.2.1. Liquid state ^{1}H NMR

^{1}H NMR spectrum of LIG (Figure 48) exhibits classical lignin patterns with aliphatic, methoxy, aromatic and phenolic protons [42]. Signals attributed to CH_2 and CH_3 (and possibly residual fatty acids) were found in aliphatic region (0.8 – 1.8 ppm), while proton of methoxy group and lignin side chains were located in the range 3.0 – 6.0 ppm. Water is observed at 3.3 ppm expected from lignin. Finally, aromatic protons of structural units were detected in the range 6.0 – 8.0 ppm, and phenolic group between 8.0 and 9.0 ppm. From this spectra, it can be assumed that LIG is quite pure, as it contains only traces of residual polysaccharides and fatty acids (3.0 – 6.0 and 0.8-3.0 ppm regions respectively).
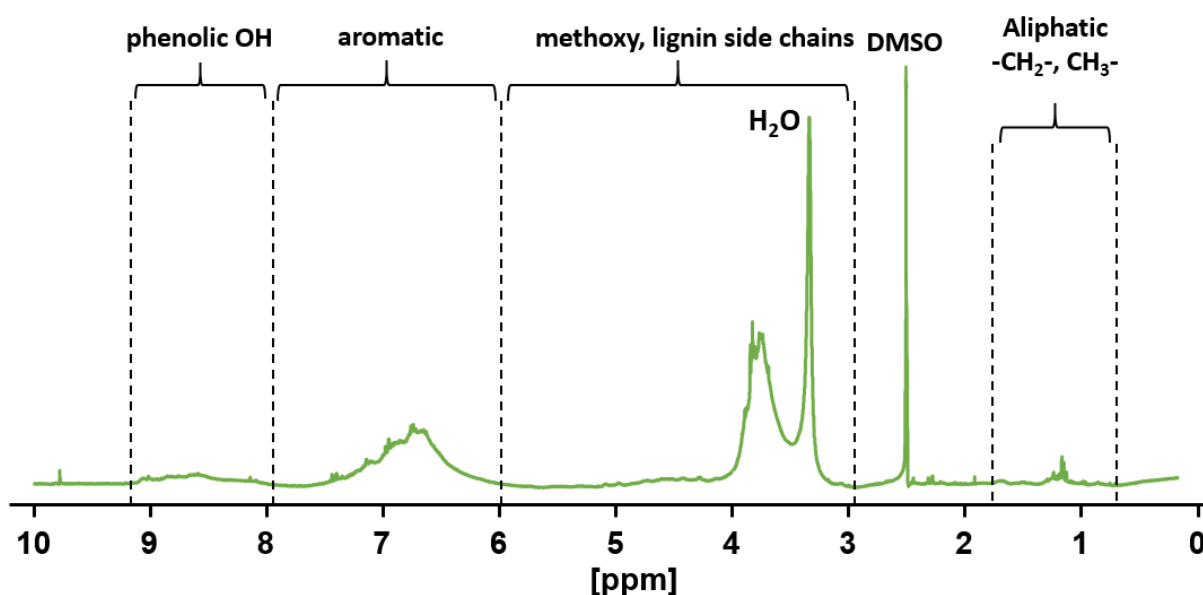
Figure 48. ^{1}H NMR spectra of LIG (DMSO-d$_6$)

1.2.2. Solid-state ^{13}C NMR

As Kraft lignin is hardly soluble in organic solvent, only ^{1}H liquid state NMR was undertaken. Liquid state ^{13}C NMR of lignin is indeed very time consuming. Therefore, it was decided to perform solid state ^{13}C NMR. Even if the resolution is lower in comparison to liquid state NMR, several information about LIG structure can be obtained. In order to get a higher signal/noise ratio, ^{1}H cross polarization was undertaken. The Figure 49 shows the ^{13}C ssNMR spectrum of LIG and the attirbutions are listed in Table 15.

As the rotation speed was set at 15 kHz, the bands between 160 and 220 ppm are attributed to the spinning side band of the signals observed between 20 and 80 ppm. So exploitable signals of LIG are located between 0 and 160 ppm. First 4 major peaks appears in the region 100 and 160 ppm and are attributed to aromatic carbons. According to the schematic representation of S and G units presented in Figure 49, peak at 152 ppm (shoulder) is attributed to C3, at 146 ppm to C4, 129 ppm to C1, at 122 ppm to C6 and at 114 ppm to both C2 and C5 [51]. Then, aliphatic carbon signals are observed from 0 to 90 ppm. Abundant linkage β-O-4 and α-O-4 bonds are both detected at ≈ 84 ($C_β$-OR) and 73 ppm ($C_α$-OR) respectively. Furthermore, the high peak at 55 ppm corresponds to the carbon of aromatic methoxy group. Finally, the broad signal centered at 36 ppm is attributed to alkyl CH_2, while both terminal CH_3 of lignin and CH_3 of potential residual hemicellulose may be detected in the large shoulder around 18 ppm [159].
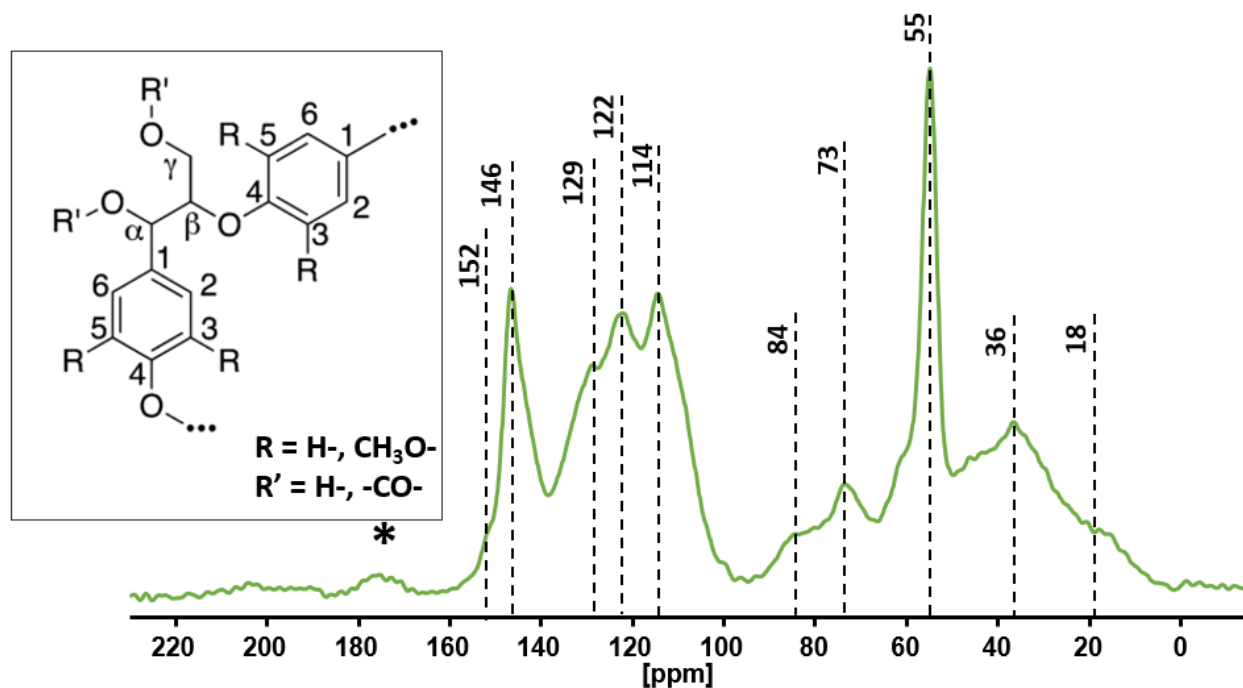
Figure 49. ^{13}C CPMAS NMR spectrum of LIG (*: spinning side band)

(lignin structure from [42])

Table 15. Chemical shift assignment of LIG [51]*, considering R and R' for G units*

C5: R= H- and C3 R=CH₃O-

Type of carbon	Chemical shift [ppm]
Aromatic =C-O (C3)	152
Aromatic =C-O (C4)	146
Aromatic -C=C (C1)	129
Aromatic =CH- (C6)	122
Aromatic =CH- (C2,C5)	114
C_β-OR (β-O-4)	84
C_α-OR (α-O-4)	73
O-CH₃	55
CH₂	33
CH₃	18

Solid state ^{13}C NMR allowed to further confirm that LIG is highly condensed according to the intense area of aromatic carbons in comparison to the aliphatic one, which is a consequence of the Kraft extraction process (see chapter I, section 1.1.2.2, p27). Expected signals, such as aromatic methoxy groups or β-O-4 and α-O-4 bonds, were also detected. It confirms that aliphatic chains, with ether bonds, form bridges between the aromatic units. Moreover, it seems that LIG is relatively neat lignin, since no intense signals of carbohydrates (expected at 104, 74, 71, 64 and 62 ppm) from hemicellulose are observed [160]. However, both liquid state ^{1}H and solid state ^{13}C NMR analysis did not permit to evaluate the ratios of G, S and H units, neither to quantify hydroxyl groups, which are considered as reactive groups for the phosphorylation.

1.2.3. Quantification of hydroxyl groups by liquid state ^{31}P NMR

As the phosphorylation consists in grafting phosphorus moieties onto lignin by reaction of free hydroxyl groups of lignin with P_2O_5 (see Chapter II, 1.4.1, p79), it is important to identify and quantify OH groups in LIG. LIG was therefore characterized using the Argyropoulos ^{31}P NMR method [47], which also determines the S/G/H ratio. This technique is widely used in the lignin field since it is precise and reproducible. It consists in the derivatization of the lignin with a phospholane agent by a phosphitylation reaction. This agent reacts with lignin free hydroxyl

groups. According to a standard, the phosphitylated groups are then quantified. The level of phosphitylation is directly related to the concentration of hydroxyl groups. The results are presented in Table 16 and the ^{31}P NMR spectrum in Figure 50.

The concentration of free hydroxyl groups in LIG is 6.3 mmol/g, divided into three types: 67% of phenolic, 27% of aliphatic and 6% of carboxylic acid. This quantification permitted to set some reaction parameters for the reaction of phosphorylation performed by Fraunhofer LBF. Thanks to deconvolution of S, G and H signals area, it results that LIG is a G-type lignin, confirming that LIG is originated from softwood species. These results are in accordance with the observations made by FTIR-ATR.

Table 16. Hydroxyl groups quantification and monomers ratios in LIG's structure

Sample	OH content [mmol/g]			Monomers ratio [%]		
	Phenolic	**Aliphatic**	**Carboxylic**	**S**	**G**	**H**
LIG	4.2 ± 0.3	1.7 ± 0.3	0.4 ± 0.3	13 ± 5	84 ± 5	3 ± 5
	(67 %)	*(27 %)*	*(6 %)*			
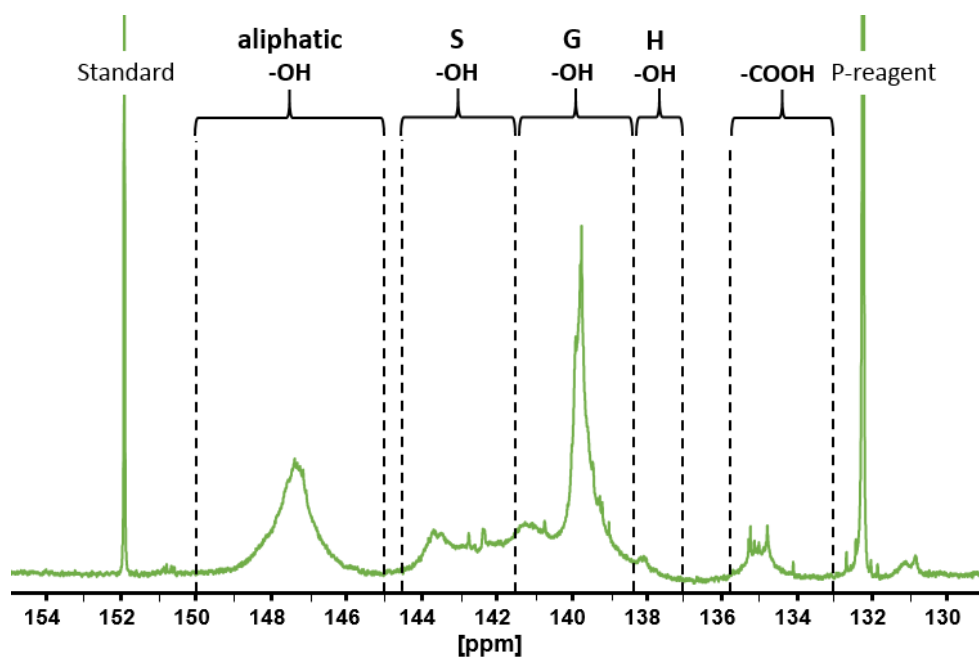
Figure 50. ^{31}P liquid NMR spectrum for quantification of LIG's OH groups (Argyropoulos method)

1.3. Conclusion

Structure of LIG was studied by FTIR-ATR, liquid and solid state NMR. Expected chemical groups of lignin were observed, such as aromatic moieties from monomeric units, ether linkages between the units of hydroxyl groups. It appeared that LIG exhibits a highly condensed structure with the presence of phenolic groups, as a consequence of the Kraft extraction process. It was also confirmed that LIG originates from softwood as it is a G-type lignin. Indeed, LIG contains 84 % of G units, 13 % of S and 3 % of H. Finally, OH groups were quantified and estimated at 6.3 mmol/g. Two third of these hydroxyls are aromatic, one third aliphatic and only few are carboxylic. So these groups are available reactive sites for the phosphorylation. As LIG is now characterized, influence of the phosphorylation on the structure of lignin is investigated in the next section.

2. Characterization of phosphorylated lignin (P-LIG)

Since lignin is expected to be used as flame retardant, and also that phosphorus is known for its FR properties, phosphorylation of LIG was undertaken. Prior to be tested as flame retardant for polymers, the resulting phosphorylated lignin P-LIG is characterized in the following section. The chemical structure is firstly studied. Morphologies of the particles properties are then compared to LIG. This section will be useful in the further sections in order to understand the difference of behaviors between both LIG and P-LIG.

2.1. Phosphorylated lignin: structure investigation

2.1.1. Characterization of P-LIG by FTIR-ATR

The characterization of P-LIG was undertaken firstly by FTIR-ATR and its spectrum is compared to that of LIG in Figure 51. It was shown that phosphorylation process did not degrade the lignin's structure. Indeed, similar bands attributed to aromatic units (mainly G), hydroxyl and carbonyl groups (see bands attributions in section 1.1, p103) were observed. However, P-LIG exhibits some differences compared to LIG. The major change is the large and intense band centered at 1000 cm^{-1} attributed to the absorption of PO-R ester linkages present in phosphate groups [161]. The R group could be lignin, but further analysis must be performed to confirm this assumption.

Stretching of P=O (1200 cm^{-1}) is also detected as the signals ratio 1210/1265 in P-LIG is higher than that of LIG. Moreover, a slight enlargement of the band centered at 3400 cm^{-1} in the region 3100-3300 cm^{-1} reveals a possible increase of the hydroxyl groups' amount which may be attributed to those of phosphate groups itself. Another possibility could be a structural effect, so it remains to be confirmed. In conclusion, phosphates are observed in P-LIG, and may be bonded to the lignin's structure with ester linkages. NMR spectroscopy is undertaken in the following part to confirm this assumption.
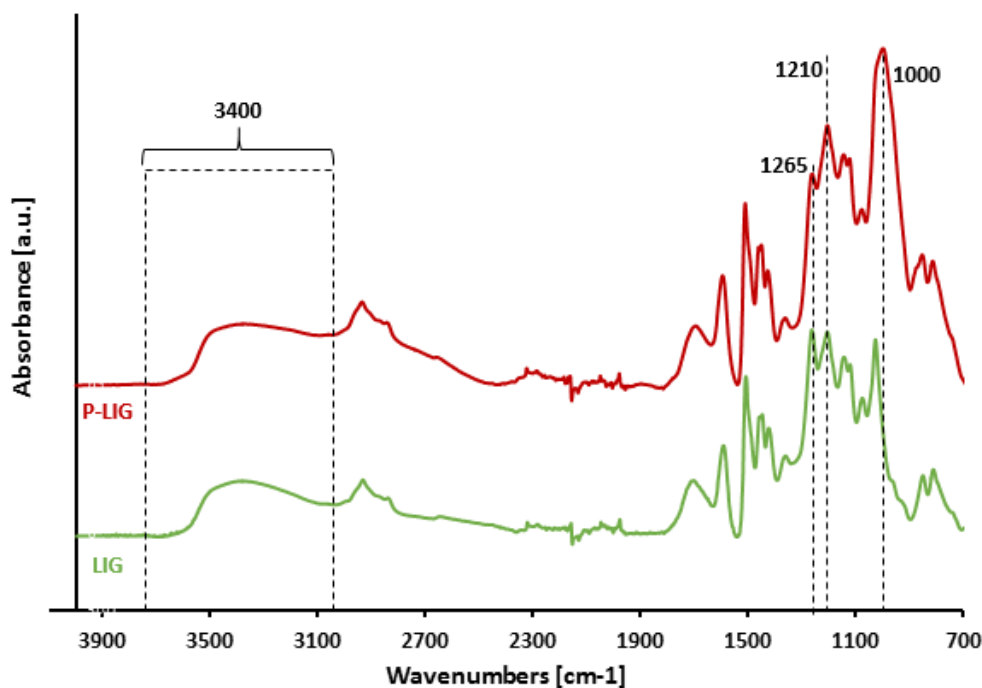
Figure 51. Comparison of FTIR-ATR spectra of LIG and P-LIG

2.1.2. Characterization of P-LIG by NMR

2.1.2.1.   Comparison of LIG and P-LIG skeleton

^{13}C solid state NMR was undertaken to compare the skeleton's structure of P-LIG to the LIG one (Figure 52). As for FTIR-ATR analysis, it appears that the lignin's structure was slightly affected by the phosphorylation's reaction. Indeed, both spectra exhibit very similar signals which indicates that the carbon structures of LIG and P-LIG are very close. Aromatic units (100 − 160 ppm), methoxy groups (55 ppm) and alkyl chains (0 − 90 ppm) are still part of P-LIG structure and similar to LIG ones. Especially the presence of β-O-4 and α-O-4 bonds in P-LIG (84 and 73 ppm) proves

that ether bridges between aromatic units were not significantly cleaved. Unexpected peaks at 67.4 and 25.2 ppm were attributed to residual THF, which is the solvent used to perform the phosphorylation.
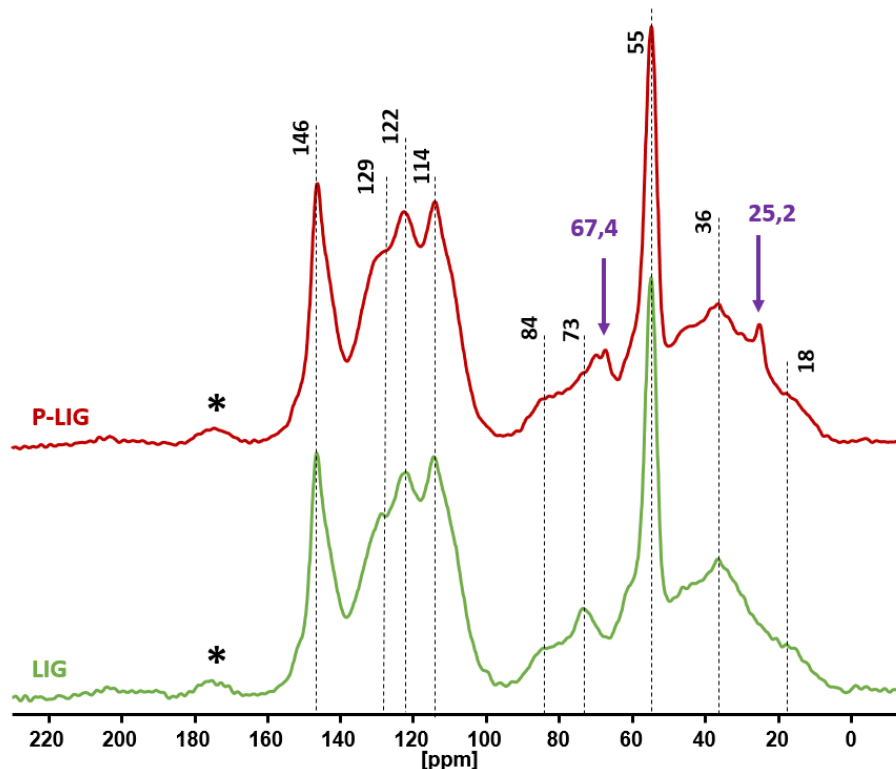
Figure 52. ^{13}C CPMAS NMR of LIG and P-LIG

2.1.2.2.   *Characterization of phosphorus groups in P-LIG*

Liquid state ^{1}H and ^{31}P NMR were undertaken in order to find out if the phosphorylation was successful. It is noteworthy that P-LIG was only partially soluble in DMSO-d$_6$, so conclusion about P-LIG structure must be carefully taken. In the case of ^{1}H NMR, no change was noticed, only the peak of water decreased significantly in P-LIG (not observed). ^{31}P NMR without ^{1}H decoupling revealed three peaks at -1.11 (peak 1), -1.17 (peak 2) and -1.22 ppm (peak 3) (Figure 53). The comparison with H$_3$PO$_4$ (0.32 ppm) clearly shows that there is no remaining phosphoric acid in the lignin. Looking at the H$_3$PO$_4$ spectrum, no coupling ^{31}P-^{1}H is observed as there is only one relatively wide peak. This larger width is due the high lability of the protons, and so the coupling intensity is very low. Chemical shifts of the P-LIG peaks are very close to the phosphoric acid one, thus indicating that the environments of the phosphorus nuclei are comparable for all of them.

As expected, this suggests that the substitution of one P-O-H bond by a P-O-R (R=LIG) shifts the multiplet towards higher field.
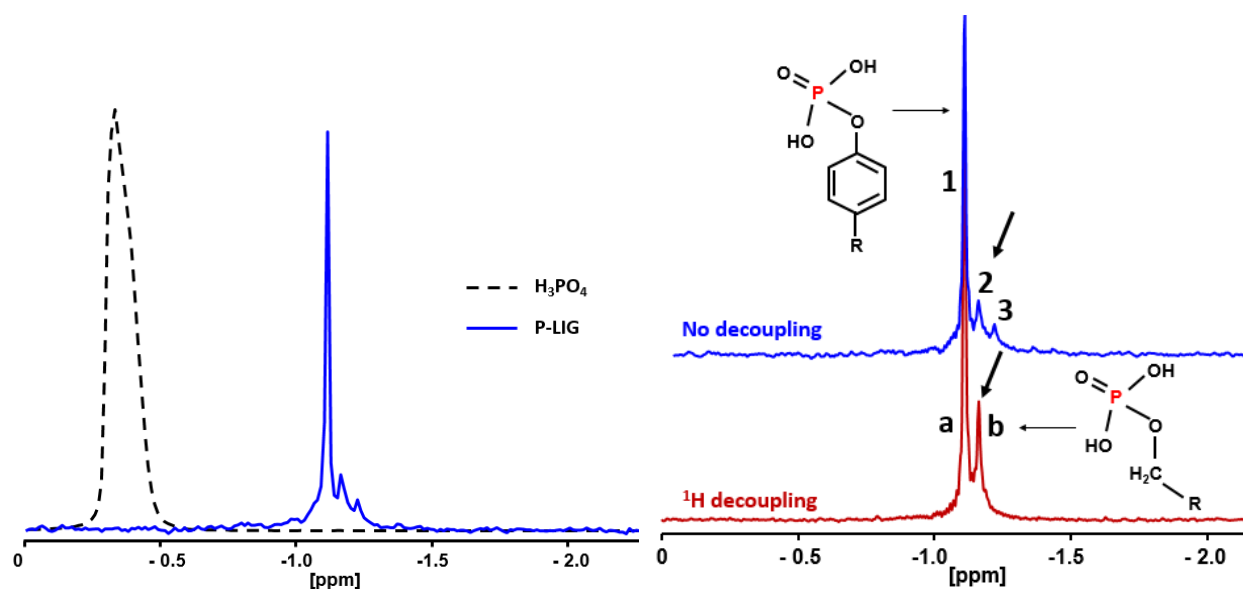
Figure 53. ^{31}P NMR of Phosphoric acid and P-LIG (left) and comparison with or without ^{1}H decoupling (right)

Experiment with ^{1}H decoupling was also undertaken (Figure 53). Two peaks (a and b) are observed, this indicates the presence of two different types of phosphorus. Peak 2 increases significantly (arrows) while the smallest peak (3) disappears. By looking closer, a little shoulder is observed, and the highest peak decreases slightly when using ^{1}H decoupling. So a triplet can be distinguished without ^{1}H decoupling, the third peak (mirror of 3) being overlapped by peak 1. A coupling constant of 7.5 Hz was measured in the triplet. This suggests that the phosphorus is coupled with two protons (J_{3P-H} = 7.5 Hz), which are attributed to a CH_2 group of the alkyl chain of lignin. Moreover, 2D ^{31}P-^{1}H HSQC NMR on P-LIG (Figure 54) shows that phosphorus signal at 1.17 ppm correlates with the aliphatic side chain protons at 3.78 and 3.83 ppm. Regarding the phosphorus signal numbered (1) no coupling with the proton is observed. This peak (1) can therefore be attributed to P-O-R' phosphate where R' is an aryl group of the lignin (J_{4P-H} is too low to be observed). This was confirmed with on spectrum with decoupling, it appears that there are more phosphates bonded to phenolic group than to aliphatic chains (peak ratio = 2:1). This may be due to the amount of aromatic hydroxyl which is higher (4.2 mmol/g) than aliphatic (1.7 mmol/g) hydroxyl groups (see OH quantification of section 1.2.3, p109).
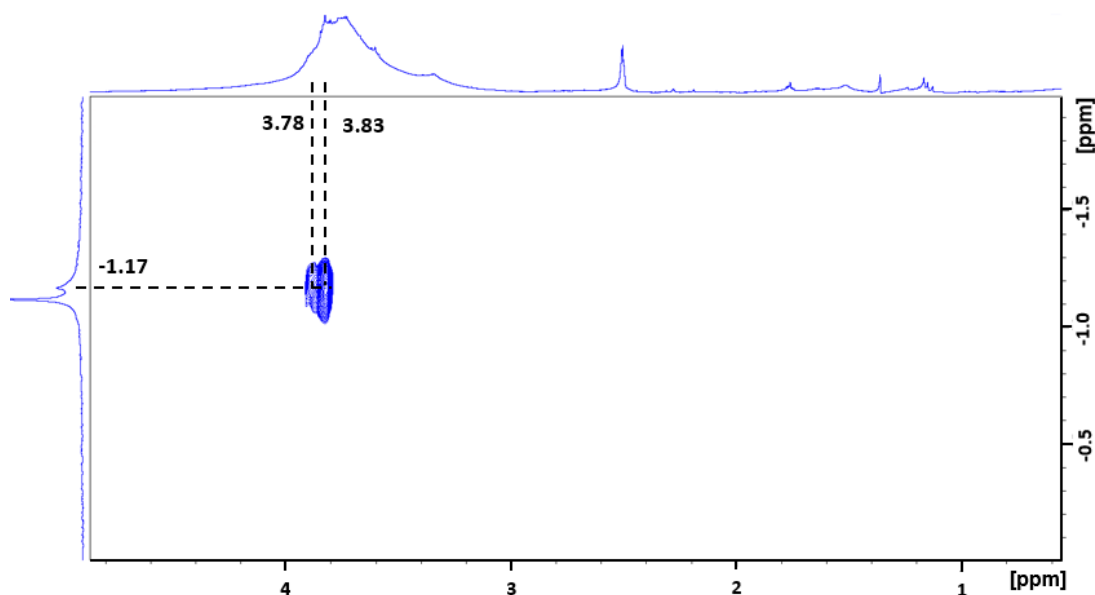
Figure 54. 2D ^{31}P-^{1}H HSQC spectrum of P-LIG

In conclusion, NMR analyzes confirm that Kraft lignin was successfully phosphorylated and that phosphate groups are linked to both phenolic and aliphatic groups. Elementary analysis on P-LIG was performed, and phosphorus content was evaluated to 3.0 % (g/g). However, it was not possible to quantify the yield of phosphorylation by the Argyropoulos method, because P-LIG was only partially soluble in the DMSO/Pyridine mixture used for this technique, so quantification of free hydroxyls remaining in P-LIG was not possible.

2.2. Morphology's comparison of LIG and P-LIG

2.2.1. Color and particles size

As the structure of P-LIG was slightly modified in comparison to LIG, macroproperties may be impacted. The most obvious was the change of color: LIG is light camel as P-LIG is dark brown. This was confirmed by CIE Lab analysis (Table 17). The diminution of L from 38.1 for LIG to 28.7 for P-LIG reveals that lignin got darker after phosphorylation. This change of color was quantified with a ΔE of 14.8 which corresponds to a mild evolution.

Table 17. Differences in CIE Lab measurements between LIG and P-LIG

Samples	Lab values			
	L	a	b	ΔE
LIG	38.1	12.8	24.1	-
P-LIG	28.7 *(-9.4)*	6.6 *(-6.2)*	14.5 *(-12.7)*	14.8

Particle's size distribution was also investigated (Table 18). Two diameters are presented. D [4,3] is an average of the particles' distribution in volume. It appears that P-LIG particles are 5 times bigger thant those of LIG. $D_v(90)$ is the diameter, for which 90 % of the particle's population are smaller or equal. As for D [4,3], it increases from 104 µm for LIG to 686 µm for P-LIG. So P-LIG particles are much bigger than those of LIG. This increase may be due to the phosphorylation process.

Table 18. Particles size of LIG and P-LIG

Samples	Apparent particles diameter [µm]	
	D [4,3]*	D_v (90)**
LIG	46	104
P-LIG	272	686

* D [4,3] – Average diameter in volume // ** Dv(90) – Diameter of 90% of particles below this value

2.2.2. Microscopy analysis of lignin's particles

Morphology of lignin's particles were observed by scanning electron microscopy (SEM). Imaging shown in Figure 55 compared LIG and P-LIG particles of similar sizes. LIG particle appears to be made of small spherical particles (about 1-2 µm) which agglomerates together. It results a homogenous agglomerate with a smooth surface. In the case P-LIG, the particle is not an agglomerate, but looks as one-chunk. Many holes can be distinguished all over the particles which exhibits a porous surface. Bigger particles of P-LIG are probably agglomerates made of the particle shown on the imaging (B). In order to investigate the distribution of phosphorus in P-LIG, EPMA ^{31}P mapping was also undertaken (Figure 56). It shows that phosphorus is present on lignin's particles (light blue spot) and is well distributed on/in lignin.
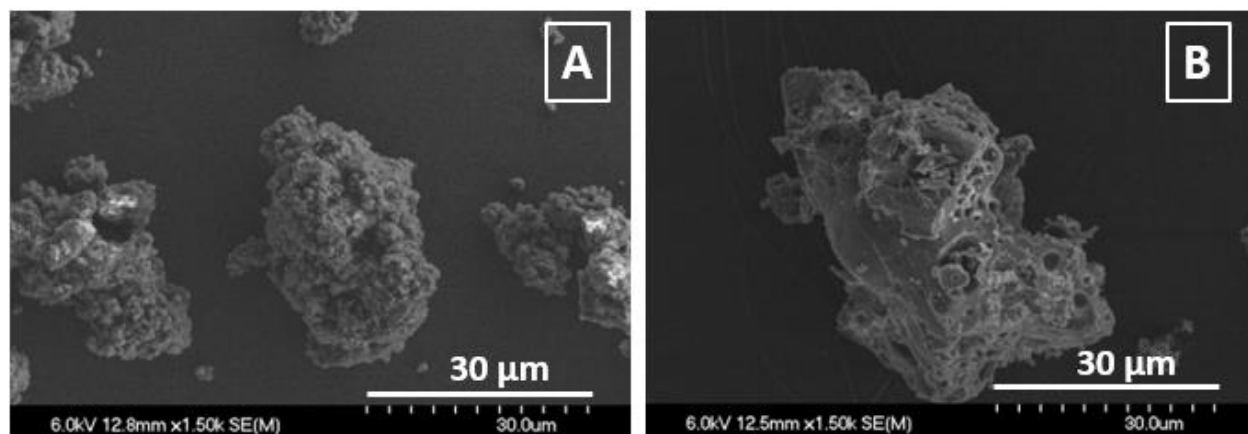
Figure 55. SEM imaging (SE) of LIG and P-LIG particles
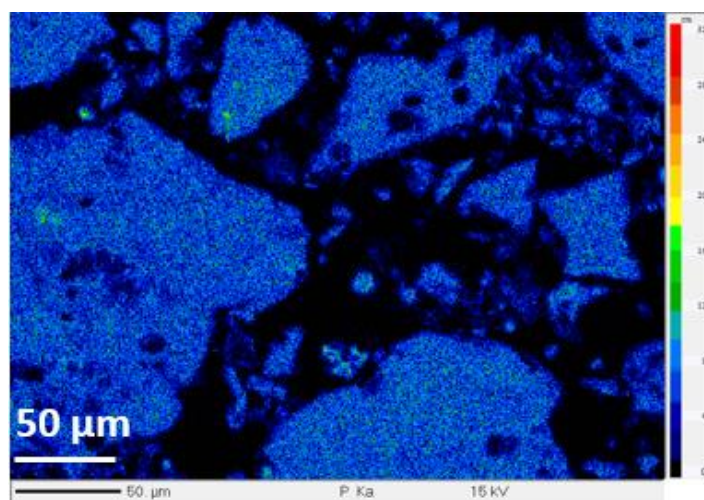
Figure 56. EPMA ^{31}P mapping of P-LIG particles

Legend – Phosphorus presence probability: dark blue-low, light green-high

2.2.3. Crystallinity

Crystallinity of LIG and P-LIG was investigated by XRD. Figure 57 shows that LIG is mostly an amorphous material as a typical amorphous halo pattern is observed at 2Θ = 21.2°, which may be attributed to more or less organized stacking structure of aromatic layers [162]. This peak is broader than that of synthetic amorphous polymers such as polystyrene and which suggests that inter-molecular distance between molecular chains is distributed in a wide range. Peaks observed at 31.6° and 33.1° reveal that residual cellulose or cellobiose are still part of LIG's structure [163] which is in accordance with the conclusions of the ^{1}H NMR study (see Figure 48, p107). These

peaks disappear on P-LIG spectra, which suggests that these compounds were removed during the phosphorylation process. Besides this, it appears that phosphorylation did not change the amorphous behavior of lignin.
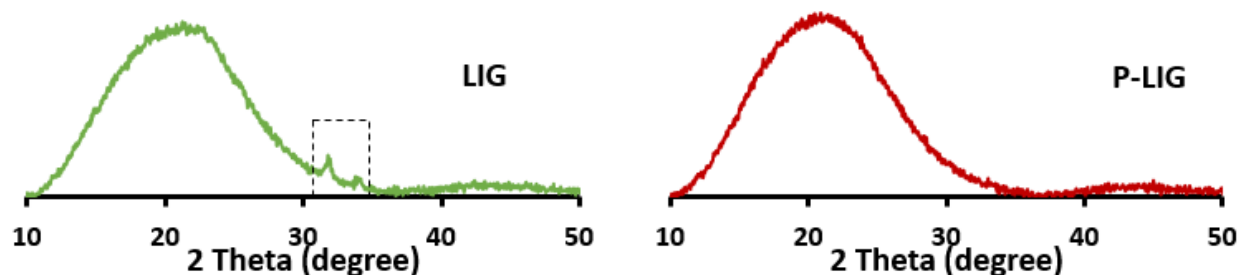
Figure 57. XRD patterns of LIG and P-LIG

2.3. Conclusion

LIG was phosphorylated by the Fraunhofer LBF (partner of the PHOENIX project) and named as P-LIG. Thanks to spectroscopic analysis such as FTIR and NMR, it was concluded that the phosphorylation was successful. Indeed, phosphate groups were proved to be bonded to the lignin's structure, however their quantification was not possible due to low solubility of P-LIG. At least, elementary analysis evaluated that P-LIG contains 3.0 % of phosphorus, which is evenly distributed in/on the particles. Moreover, the initial structure of LIG was not degraded during this transformation. The phosphorylation induced a darkening of the color as well as an increase of the particle's size (5 times bigger). Morphology of the particles turned from smooth and regular (LIG) to porous (P-LIG). As LIG and P-LIG will be used as FR in polymeric matrices in the next part of the study, the following section deals with the investigation of their thermal stability.

3. Influence of phosphorylation on lignin's thermal decomposition

LIG and P-LIG were chemically characterized in the last sections. In this work, both are intended to be used as FR additive in polymeric materials. In this context, their thermal stability is studied firstly to ensure that they are thermally stable enough to be processed in polymers. Secondly, since the strategy is to consider lignin as char former in FR systems for polymers, their charring ability is also examined. Then, the influence of the phosphorylation on lignin's thermal decomposition is analyzed. In order to investigate potential changes in the decomposition

pathway, gas and condensed phase were particularly studied. Finally the influence of the heating rate and the atmosphere are commented.

3.1. Thermal stability of LIG and P-LIG

Thermo-oxidative and pyrolytic decomposition of LIG and P-LIG are presented in Figure 58 in Table 19. For both samples no clear separate decomposition step can be observed, as has already been reported in the literature (see Chapter I, section 1.2.3, p38). The complexity of lignin's structure indeed induces many decomposition steps, several of them overlapping with each other. LIG starts to decompose at 210 °C ($T_{2\%}$) under both thermo-oxidative and inert atmospheres, and maxima of mass loss rate (DTG_{MAX}) are reached at 410 and 370 °C respectively. The first steps in pyrolytic conditions at 250 and 370 °C are very similar to those observed in thermo-oxidative conditions. The first "apparent" step of degradation is therefore not influenced by the atmosphere. But another significant step appears at 410 °C in the presence of oxygen. No residue is left at 800°C under air, while 45 wt.% remained under pyrolysis conditions. LIG is therefore a charring material. The formed char is oxidized at high temperature as usual charred materials are.

P-LIG starts to decompose in the same range of temperature as that of LIG ($T_{2\%} \approx 210$ °C). However, the first step occurs 30 °C lower compared to LIG (220 versus 250 °C), whereas the second step is shifted towards higher temperature, i.e 40 °C under N_2 and 65 °C under air. Above 220 °C, the mass loss rate (MLR) decreases in comparison to that for LIG leading to a stabilization. DTG_{MAX} is indeed reduced from 1.8 to 0.5 wt.%/°C and from 0.3 to 0.2 wt.%/°C under thermo-oxidative and pyrolytic conditions respectively. At high temperature under nitrogen, the residue amount increases from 45 wt.% for LIG to 53 wt.% for P-LIG.
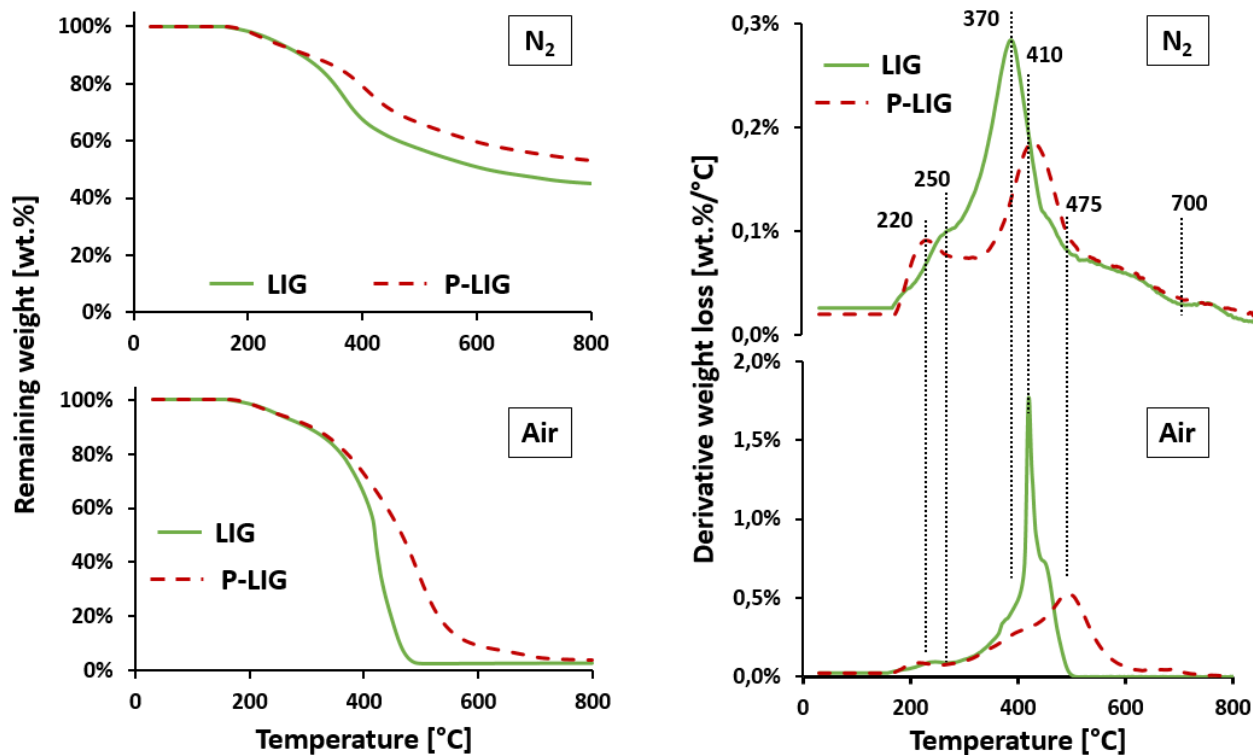
Figure 58. Thermal stability of LIG and P-LIG under air and N₂ atmospheres (10 K/min)

Table 19. Thermogravimetric data of LIG and P-LIG

	Thermo-oxidative atmosphere				Inert atmosphere			
	$T_{2\%}$ [°C]	T_{MAX} [°C]	DTG_{MAX} [%/°C]	Res [%]	$T_{2\%}$ [°C]	T_{MAX} [°C]	DTG_{MAX} [%/°C]	Res [%]
LIG	207	410	1.8	1	208	370	0.3	45
P-LIG	206	475	0.5	4	204	409	0.2	53

It appears that the phosphorylation induces a slight thermal destabilization in the first step of decomposition (210-260°C). Indeed it is known that phosphoric acid-based molecules, such as phosphates (present in the P-LIG structure), catalyzes dehydration of bio-based products such as starch [164]. Even if the LIG chemical structure differs from starch, especially regarding aromatic sites of LIG, some analogy can be established considering hydroxyl and ester groups with respect to dehydration potential. So dehydration of P-LIG could be promoted because activated and catalyzed by P-species.

Above 300 °C a significant thermal stabilization as a consequence of the phosphorylation occurs. First, a higher DTG_{MAX} reduction in the presence of oxygen may be attributed to the phosphorus which is known to prevent oxidation of the char [165]. Moreover, the stabilization observed in inert conditions also demonstrates that the presence of phosphorus increases the char formation probably due to condensed phase interactions. Therefore, the phosphorylation enhances the thermal stability of LIG at high temperature. These significant improvements are obtained with 3.0 % of phosphorus only in the lignin's structure. So mode of actions of phosphorus will be investigated in the next sections to explain these changes.

3.2. Gas phase analysis

3.2.1. Composition of the gas phase released during the thermal degradation

The identification of the decomposition gases, released during pyrolysis, was done using TGA coupled with FTIR (TGA-FTIR). This technique permits to assess the chemical functions of the evolving gas during the thermal degradation. Figure 59 shows spectra of gases released during pyrolysis of LIG and P-LIG at different temperatures. Characteristic temperatures were selected according to main steps of degradation (first step, second step, end of degradation) observed on the TG curves previously presented in Figure 58. Temperatures of 250, 370 and 600 °C were chosen for LIG, 250, 410 and 600 °C for P-LIG. Attribution of bands is summarized in Table 20. At 250 °C, LIG starts to release a low amount of water (3600 and 1500 cm^{-1}), carbon dioxide (2306 cm^{-1}), few compounds with carbonyl functions (1750 cm^{-1}) and some gases containing aliphatic groups (3000 – 2600 cm^{-1}). When the temperature increases to the maximum of degradation at 370 °C (T_{MAX}), many gaseous products evolve in addition to the previously cited gases. CO (2250-2000 cm^{-1}), methane (3015 cm^{-1}) as well as aromatic (3044 and 1035 cm^{-1}) and phenolic (3590 cm^{-1}) compounds are the major degradation gases. Moreover, the presence of compounds containing C-O-C bonds (1270 and 1086 cm^{-1}) shows that large fragments of lignin compounds come off suggesting an advanced degradation. At the end of the degradation (600 °C), water, CO, CO_2, methane and the few hydrocarbons are the main gases released. No significant change is observed regarding the nature of the evolving gases between LIG and P-LIG spectra. However, profiles of gases as a function of temperature appear to be different and is discussed after.
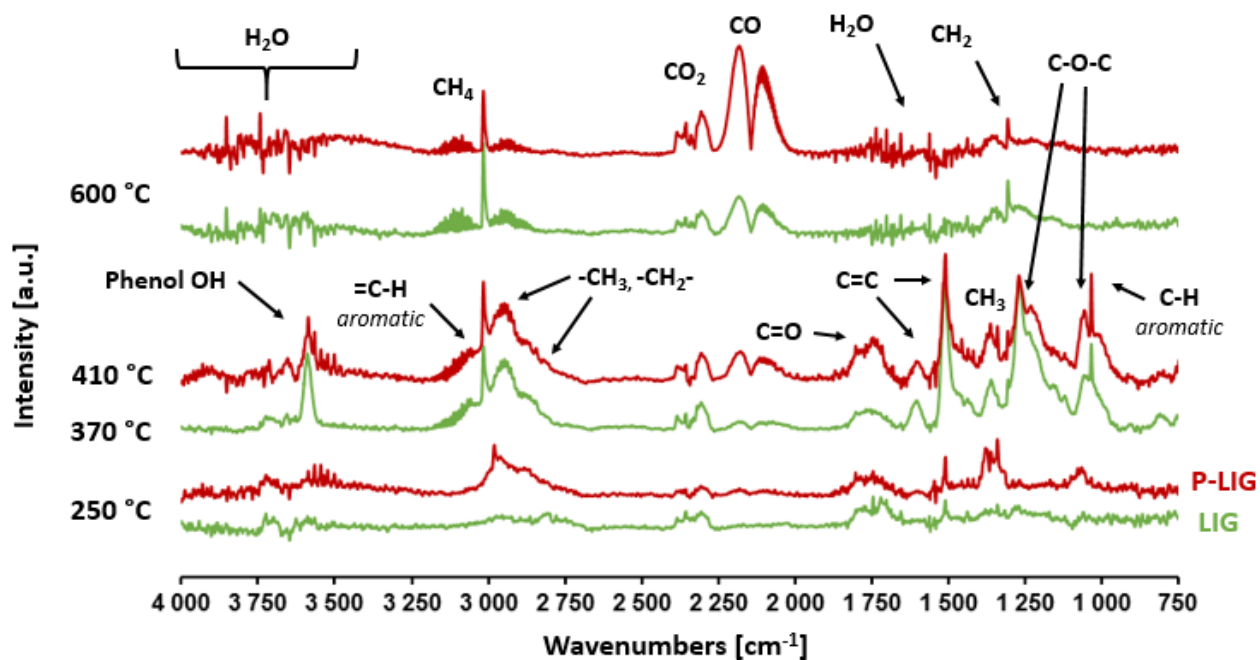
Figure 59. FTIR spectra of the gases evolved during pyrolysis of LIG at different temperatures

Table 20. IR peaks assignment for LIG and P-LIG [166–168]

γ – stretching / δ - deformation

Functional group or component	Wave number [cm^{-1}]	Vibration type
C-H aromatic	1035	δ in plane
C-O-C	1086	δ
	1270	γ
CH$_2$	1036	δ
CH$_3$	1360	δ
C=C	1510	Aromatic ring
	1600	vibrations
C=O	1760	γ
CO	2185 and 2105	γ
CO$_2$	2306 and 2382	γ
CH$_2$	2873	δ
CH$_3$	2970	δ
CH$_4$	3015	γ
=C-H aromatic	3044	γ
O-H phenol	3590	γ
H$_2$O	1700-1400	δ
	3900-3400	γ

Profiles of gases of interest are shown in Figure 60. With the FTIR apparatus used in this study, quantification is not possible. However, since the profiles are normalized by the Gram-Schmidt, it is possible to make comparisons of the two different profiles. Water, CO_2 and CO were selected because they are good indicators of the degradation of lignin's chemical functions (hydroxyls, carbonyl, etc…). Alkenes of aromatic groups and C-H of aliphatic chain were plotted as they represents the structural units of lignin (see Figure 61). They evolve when lignin backbone structure degrades. Methane is finally released in case of advanced degradation step of lignin.
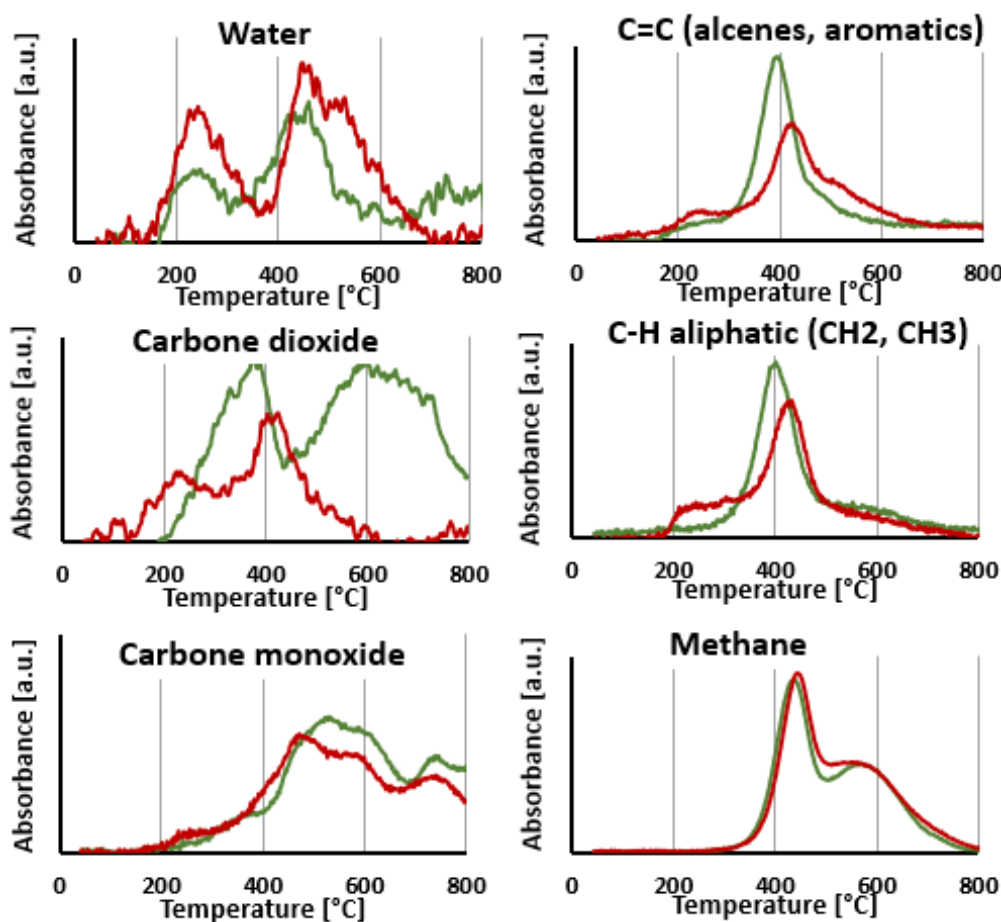
Figure 60. Gases profiles obtained from TGA-FTIR analysis (green: LIG / red: P-LIG)

As release of water and carbon dioxide is observed between 180 and 250 °C, the first apparent step of degradation of LIG (see Figure 58, p120) is attributed to aliphatic OH dehydration and decarboxylation [63] (see Figure 14, p42). From 300 °C, a second release of water is noticed, attributed to the dehydration of phenolic hydroxyl groups [71]. Evolution of CO is due to the weakly bound oxygen groups such as aldehyde groups while CO_2 is related to remaining carboxyl

groups. Aromatic compounds start to evolve from 300°C as the aryl-ether bonds begin to be cleaved. The ether linkages have indeed different pyrolytic cleavage mechanisms, as depending on the side-chain structure of lignin (aliphatic bridges between aromatic units, see Figure 61), and therefore release of aromatic compounds occurs over a wide range of temperature until 700 °C [67]. Finally, methane is released from 300 to 800 °C and is generated from the weakly bond to more stable bond methoxy groups. So the second apparent degradation step, starting around 300 °C is actually composed of many reactions overlapping with each other's.
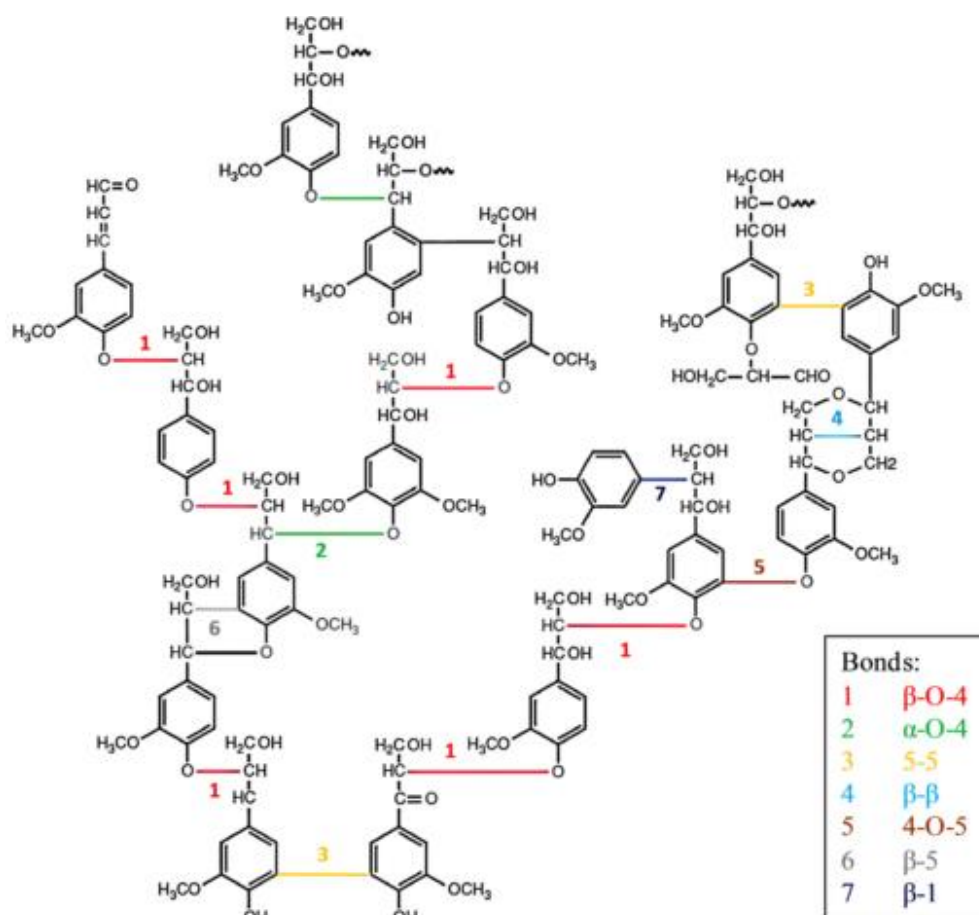
Figure 61. Chemical structure of lignin [8]

Profiles of degradation gases of P-LIG were then compared to those of LIG. Figure 60 shows that CO_2 is released from 170°C which is 30 °C lower than LIG. So decarboxylation is promoted in P-LIG. Moreover, CO_2 release, attributed to degradation of carboxylic groups, is divided in two peaks, showing that the decarboxylation of one type of carboxylic groups is promoted. Besides CO_2, the evolution of water during the first degradation step is more significant for P-LIG than

that of LIG. It indicates that phosphorus promotes dehydration of lignin structure. It is also noticed an increase of the release of aliphatic compounds, which occurs at 75 °C lower than that of LIG (200 versus 275 °C). So phosphorylation appears to induce the degradation of the aliphatic side chain at lower temperature. As a consequence of the degraded structure, a slight increase of the release of aromatic compounds is observed for P-LIG. An assumption could be that phosphorus groups induce the cleavage of the weakest ether linkages at lower temperature. Above 300 °C, less aromatic compounds are released than in LIG. This decrease could be consequence of the reactions promoted by phosphorylation at low temperature, thus resulting in a more thermally stable aromatic structure. This is confirmed by the decrease of CO_2 release after 500 °C, showing less advanced degradation in P-LIG than in LIG [63]. Finally, the phosphorylation does not impact the degradation of methoxy groups as the methane release is comparable to that of LIG.

Phosphorylation of lignin induces change in the thermal degradation behavior. From the TGA-FTIR, it appears that phosphorylation promotes dehydration as well as accelerates decarboxylation of lignin. Aliphatic side-chains cleavage is also favored. It results a much stable aromatic structure a high temperature since globally, less aromatic compounds are released. So according to TGA-FTIR, the gas composition of LIG and P-LIG is similar, however the amounts of the different gases and the temperature at which they are released are different. In order to assess if the changes in the gas phase has an influence on the combustibility of lignin, PCFC study was undertaken.

3.2.2. Combustibility of the gas phase

As LIG and P-LIG are considered as flame retardant additives for polymers, their combustibility was investigated by micro-calorimetry with a Pyrolysis Combustion Flow Calorimeter (PCFC). The results are presented in Figure 62 and Table 21. As PCFC testing involves a pyrolysis at 60 °C/min to degrade the sample (prior to burn the degradation gases), TGA data of LIG and P-LIG in similar pyrolysis conditions are also listed in Table 21 to provide information about lignin degradation. Similar behaviors can indeed be observed between PCFC and TGA [169].

LIG releases combustible gases over a wide range of temperature, i.e. from 225 to 550°C. The HRR reaches 128.7 W/g at 401 °C. The THR is about 14.2 kJ/g. These results correlates with the data

of TGA, as T_{MAX} is only slightly shifted towards higher temperature (+ 20 °C due to PCFC apparatus, see Chapter II) and the residues are comparable. So PCFC results confirms the release of combustible gases from LIG. According to the previous TGA/FTIR analysis, even if any comparison should be done carefully as the pyrolysis heating rate was different, these combustible gases are composed of compounds made of aromatic and aliphatic groups, carbon monoxide and CH_4 mostly. Moreover, no combustion is noticed between 180 and 250 °C although some products evolves (T_{ONSET} =176 °C in TGA). This shows that the decomposition products between 180 and 250 °C are not combustible in those conditions. This observation is in good agreement with that below 250 °C, dehydration and decarboxylation are the main reactions occurring (release of water and carbon dioxide).

In the case of P-LIG, combustible gases release ranges from 180 to 550 °C which exhibits a HRR of 84.6 W/g occurring at 410 °C. The THR is decreased to 12.1 kJ/g. Onset temperatures of PCFC and TGA are comparable, which shows that combustible gases are released when P-LIG starts to degrade. Aliphatic compounds as well as a few aromatic compounds are indeed released in this range of temperature, as it was evidenced by TGA/FTIR analysis in Figure 60. This observation is in good agreement with the previous conclusion, which reveals that the phosphorylation promotes also the cleavage of the aliphatic side chains. T_{MAX} occurs at 410°C although it was expected at 430 °C from the TGA analysis. Moreover, the full width at half maximum is larger in the case of LIG than that of P-LIG. So it can be assumed from this observation, in the case of P-LIG, that less combustible evolves at higher temperature than 410 °C (T_{MAX} in TGA). This is in good agreement with the THR reduction of 15 % in comparison to that of LIG. Release of high molar mass compounds from the charring residue may be an explanation of this limited combustibility [170]. Indeed, it seems that the phosphorylation promotes the charring, and so the formation of high molecular and condensed compounds.
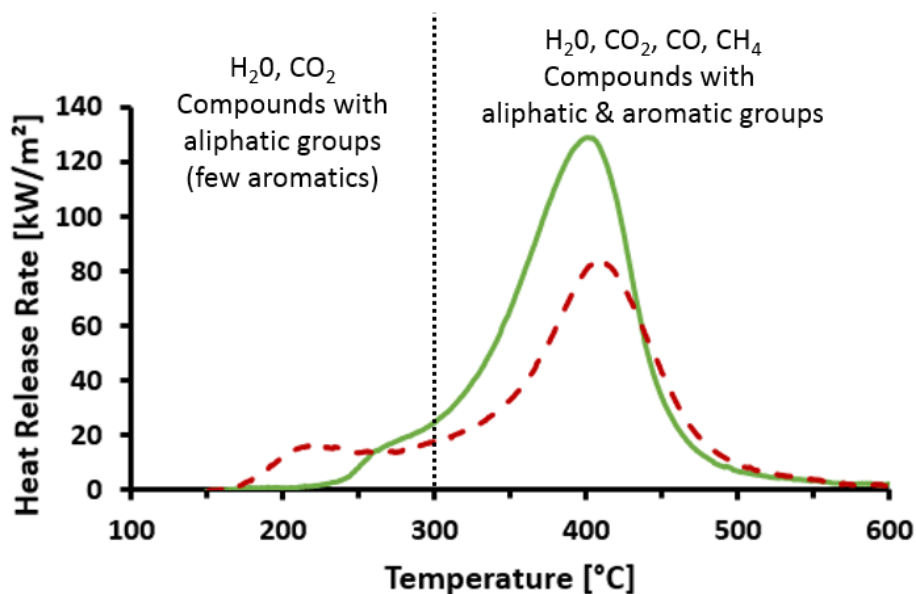
Figure 62. PCFC curves of LIG (green) and P-LIG (red) to assess combustibility

(Gases were identified according to TGA/FTIR at 10 K/min)

Table 21. PCFC data of LIG and P-LIG

	PCFC results					TGA (60 °C/min)		
	T_{onset} [°C]	T_{MAX} [°C]	pHRR [W/g]	THR [kJ/g]	Res [%]	T_{onset} [°C]	T_{MAX} [°C]	Res [%]
LIG	225	401	128.7	14.2	41	176	381	45
P-LIG	180	410	84.6	12.1	50	180	430	52
			-35%	-15%				

3.2.3. Conclusion about the gas phase analysis

Gas phase analysis of LIG decomposition reveals mainly releases of water, CO_2, CO, aromatics and hydrocarbons compounds as expected according to this work and the literature. Such mixture is combustible and could contribute to feed the flame, but in a relatively low contribution in comparison to energy of combustion of polymers ($pHRR_{ABS}$ = 602.3 W/g is 5 times higher than that of LIG, and THR_{ABS} = 37.7 kJ/g is 2.5 times higher). The gas phase analysis of P-LIG showed that phosphorus has an influence on the gas distribution. It appears indeed that dehydration, decarboxylation and degradation of aliphatic side chains are promoted, while the release of

aromatic and hydrocarbons compounds at high temperature is reduced in comparison to LIG. The combustibility was therefore reduced by 15 % in comparison to that of LIG. In order to investigate changes in LIG and P-LIG structures, characterization of the condensed phase is undertaken in the next section.

3.3. Condensed phase

3.3.1. Elementary composition of the condensed phase

Elementary analysis of LIG and P-LIG as a function of the temperature and in pyrolysis conditions was undertaken in order to evaluate the evolution of their chemical composition (see Chapter II for thermal treatment procedure). Evolutions of carbon, oxygen, and hydrogen content in LIG are presented in Figure 63. Nitrogen content was below 0.1 % and therefore it was not considered. During the first step of degradation (until 250 °C), significant decrease of oxygen content (%O) is observed as well as a slight decrease of hydrogen content (%H). This indicates that compounds containing oxygen and hydrogen are released. This is in good agreement with the gas phase analysis, and confirms that dehydration and decarboxylation are the main reactions occurring at this step. From 250 to 700 °C, carbon content (%C) slightly increases, as %O remains stable and %H almost reaches 0 %. The decrease of H/C ratio is explained mainly by the release of methane occurring above 350 °C (from the methoxy groups). So the residue produced by lignin is a carbonaceous material, which contains some oxidized carbons (>10%). The presence of oxygen in the condensed phase at high temperature is relative to the initial composition of lignin. Polyphenols and other derivatives containing groups are indeed part of the polyaromatic structure of the char. Even if degradation compounds containing oxygen are released, there is still some oxygen in the structure of the final residue.
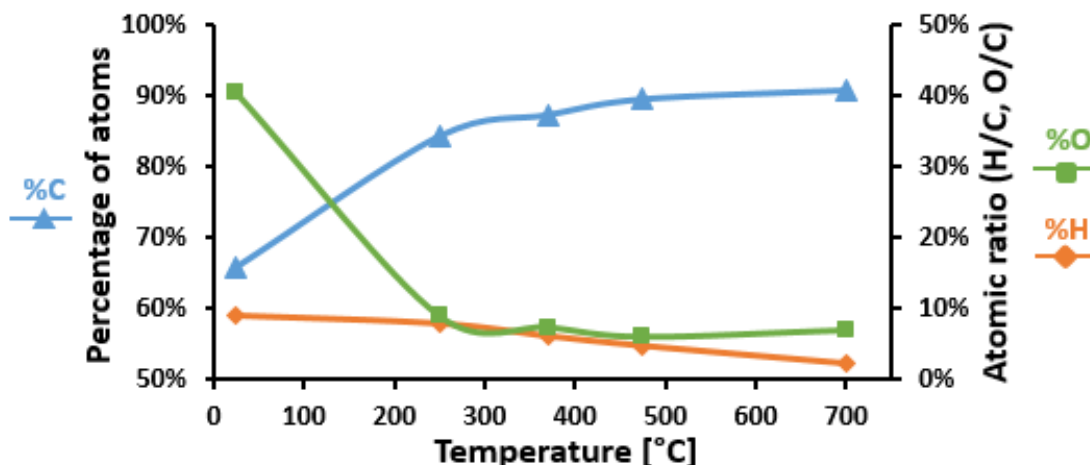
Figure 63. Chemical composition of LIG degraded at different temperatures (pyrolysis)

The evolution of the chemical composition of P-LIG is very similar to that of LIG. However, %P/%C ratio as a function of the temperature is presented in Figure 64 to investigate if phosphorus remains in the condensed phase. At 250 °C, around half of the initial amount of phosphorus remains in the condensed phase, so around 1.5 % of phosphorus is therefore released in the gas phase below 250 °C. Above 250 °C, %P remains constant at 1.5 % until 700 °C. Until 250 °C, phosphorus species are released in the gas phase, and an inhibition effect may be expected [171]. However, it is hard to measure according to PCFC since only a very low HRR is noticed at this temperature. Above 250 °C, it can be assumed that the phosphorus acts only in the condensed phase of lignin during its thermal degradation.
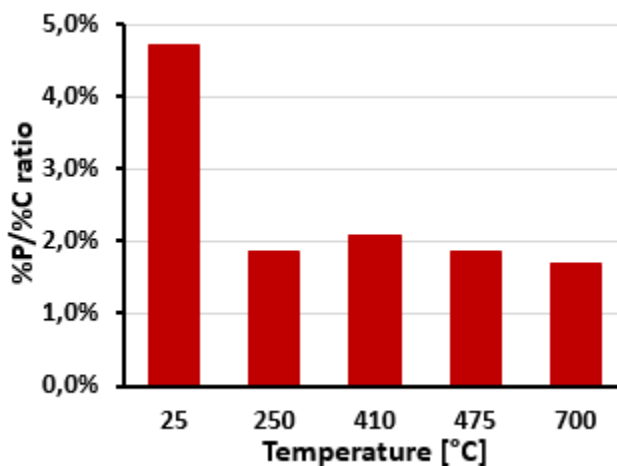
Figure 64. Evolution of %P in P-LIG structure at different temperatures (pyrolysis)

3.3.2. Calorimetry analysis of LIG and P-LIG's thermal degradation

Thermal degradation of lignin was assessed by TGA/DSC in order to measure the enthalpies of degradation in pyrolysis conditions (Figure 65). LIG degrades from 180 to 900 °C and releases energy since an exotherm is observed between 150 and 800 °C. It is assumed that many reactions occur during the degradation of LIG, therefore the heat flow measured is the average of all the enthalpies of reaction. As chemical bonds generally requires energy to be cleaved, endothermic events were expected [172]. Moreover, in absence of oxygen (pyrolysis), oxidation due to atmosphere cannot occur. However, successive exothermic reactions occur. They were attributed to scission of aliphatic groups which initiates the carbonization at the surface, scission of aromatic parts which increases the carbonization and the condensation of the carbon in the char into graphite like structure [173].

In order to compare LIG with P-LIG heat flows, the degradation was decomposed in to three steps. As LIG exhibits a slight exothermic event in step 1 (beginning of aliphatic groups cleavage), P-LIG shows "apparent" endothermic event. So endothermic reactions occur and balances the aliphatic group's scission. Dehydration, which is an endothermic reaction [174], is probably contributing in this way. This would be in good agreement with the analysis of the gas phase, which showed that the phosphorylation promote the dehydration of lignin. During step 2, LIG and P-LIG exhibit the same exotherm's maximum of - 0,4 mW/g, even if the mass loss rate of P-LIG is much lower than that of LIG. It can be concluded that in this range of temperature too, phosphorus changes the degradation pathway of lignin by promoting more exothermic reactions. Higher rate of carbonization, promoted by the phosphorus, may be an explanation. Finally, heat flow of P-LIG is much more stable than that of LIG in step 3, which seems to turn to an endothermic event from 750-800 °C. In conclusion, the presence of phosphorus in lignin modifies the chemical reactions occurring during its thermal decomposition. The assumption that the phosphorylation of lignin promotes the dehydration and then carbonization reactions was proposed, which is in good agreement with the previous results. To evaluate changes in the chemical structure of LIG and P-LIG, solid state NMR was undertaken.
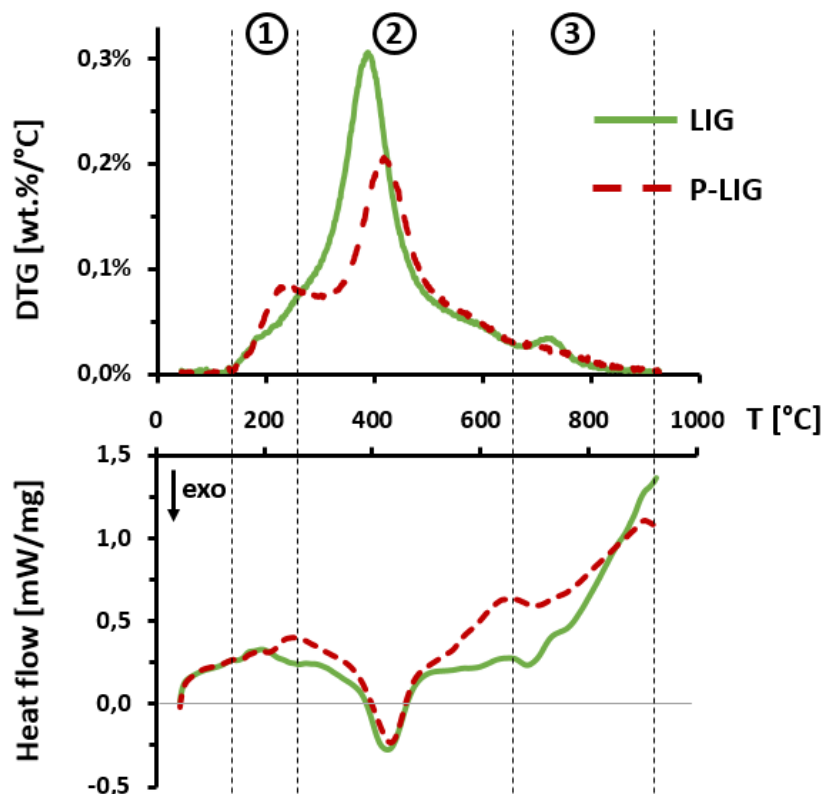
Figure 65. DTG and heat flow signals of LIG and P-LIG during pyrolysis (10 °C/min)

3.3.3. Changes in structure during thermal degradation

Condensed phase was analyzed by ^{13}C and ^{31}P solid state NMR in order to investigate the evolution of the structure of LIG or P-LIG during thermal degradation. Samples were treated in tubular furnace under pyrolysis conditions at selected temperatures from the TGA analysis (see Figure 58, p120). ^{13}C CPMAS NMR (Figure 66) permits to analyze the evolution of the lignin's backbone. By increasing the temperature from 25 °C to 475 °C, the aromatic character of LIG's chars becomes more important while lignin's substructures (aliphatic side chains) decrease. No significant changes are noticed between the initial step and 250°C as only dehydration and decarboxylation occur (carboxylic carbon non observable because it overlaps with spinning side band). A slight decrease of the α,β,γ carbons from ether linkages demonstrates that bonds between aromatic units begins to be cleaved. Then, at the DTG$_{MAX}$ temperature (370 °C), aromatic, methoxyl, hydromethoxyl and aliphatic carbons as well as ether bonds progressively disappear to form an aromatic char with still many phenolic groups (142 ppm) and few methoxy groups (55 ppm). Finally, the last step at 475 °C shows a lignin which exhibits a full aromatic

structure (centered at 125 ppm) with a few oxidized carbons in C-O-C configuration (152 ppm). These changes occurring in LIG structure were expected from the literature [131,175,176].
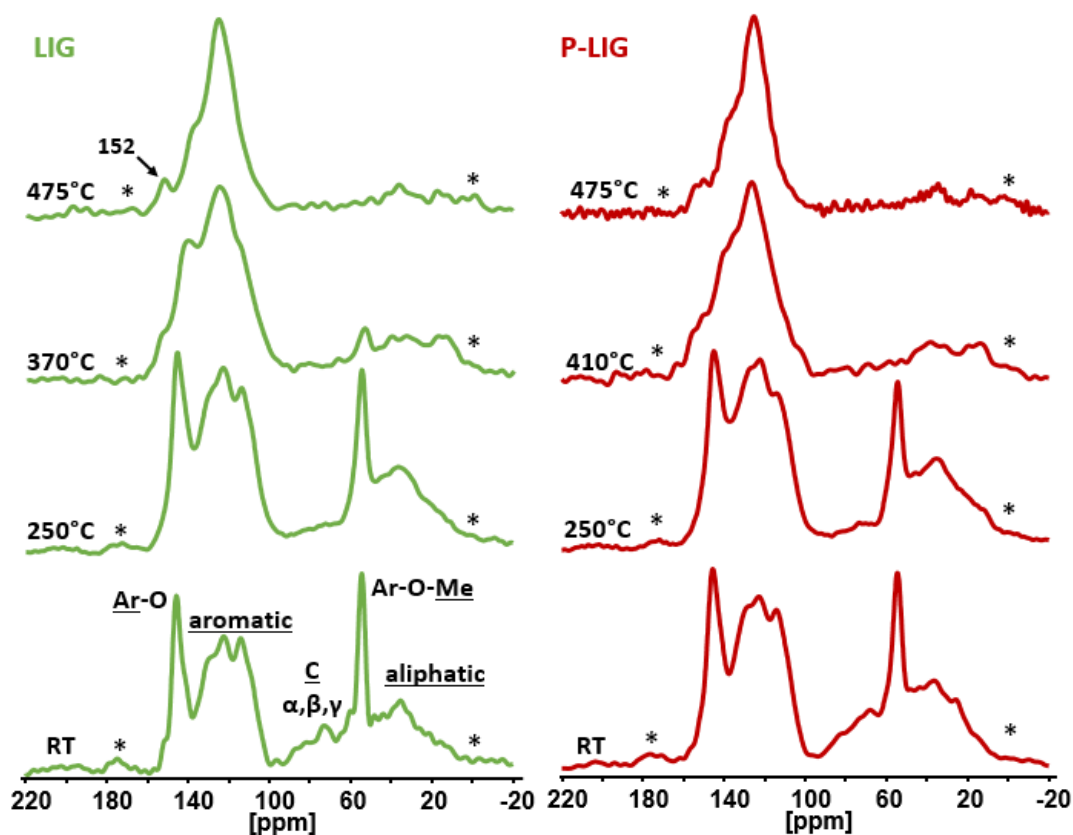
Figure 66. ^{13}C CPMAS NMR of LIG and P-LIG treated at different temperatures (pyrolysis conditions, rotation speed: 12.5 kHz)

The comparison of LIG and P-LIG chars in Figure 66 shows that very similar spectra at comparable degradation step are observed. Only the structure at T_{MAX} (370 °C for LIG, 410 °C for P-LIG) differs slightly, as P-LIG exhibits a more significant decrease of the peak at 146 ppm (C-O involves in the aliphatic bridge between aromatic parts) than LIG. This slight difference shows that the phosphorylation slightly promotes the cleavage of the aliphatic chain, which is in good agreement with the previous analysis (gas phase, DSC/TGA). In conclusion no significant changes occurred in the degradation patterns of the lignin's carbon structure after the phosphorylation. It means that by increasing the temperature, structural backbone on lignin degrades to form a residue made of aromatic species.

Chemical environment of phosphorus in P-LIG at different degradation steps (250, 410, 475 and 700 °C) was also investigated by ^{31}P HPDEC NMR (Figure 67). As solid state NMR induces significant signals broadening, a single peak is observed at -0.7 ppm in P-LIG, the two peaks noticed in liquid state were too close to be distinguished in solid state. At 250 °C, significant broadening of the peaks is noticed because of disordered structure (amorphization and dissymmetric/disordered phosphates). It is in good agreement with the fact that the structure of P-LIG starts to degrade, as previously seen by ^{13}C NMR. Moreover, an additional signal indeed arises at 12.3 ppm (shifting to 5.7 ppm at 475 °C) and may be attributed to $(RO)_2P-OH$, ie phosphonate structures [177]. So phosphorus exhibits a new chemical environment, and therefore appears to interact with lignin. Reduction of phosphates (+V) in phosphonates (+III) is possible and well documented in the literature [178,179], however it requires strong basic media and specific conditions, which are not fulfilled in this system. Considering the lignin's structure, oxido-reduction reaction with phenols could lead to formation of phosphonates and quinones may occur. Further investigation would be required to verify this assumption.

When the temperature increases to 410 °C, shifting of the signals towards lower chemical shift is noticed. Formation of aromatic orthophosphates [180] and pyrophosphates [181] (0 – -11 ppm) occurred between 250 and 410 °C, which partially lead to polyphosphates (- 25 ppm) [124] at 475 °C. At advanced degradation state (700°C), a large signal ranges from 50 to -30 ppm is observed. The broadening of the peaks shows that the char is disordered and so phosphorus exhibits many different chemical environments. Except the degradation of polyphosphates chains as the peak at -25 disappeared, all species previously observed are still present in the char and the appearance of peaks at 29 and 22 ppm show that phosphonate and phosphonic acid are formed [177]. Their presence suggests that a reductive phenomenon occurred at high temperature and in presence of lignin's degradation products [182]. Under air conditions, pyro- (-5 ppm) and polyphosphates (- 13.2 ppm) are formed at 315 °C, as phosphoric acid is noticed at 0 ppm. Then, at higher temperature, the pyrophosphates are converted in polyphosphates, which are stable. So phosphorus strongly interacts with the lignin structure during the degradation by forming different types of species, which enhances the thermal stability of the char. Polyphosphate chains are especially known for forming bridges between the different aromatic species [183]. Moreover, phosphorus is known to prevent aromatic structures from oxidation [184].
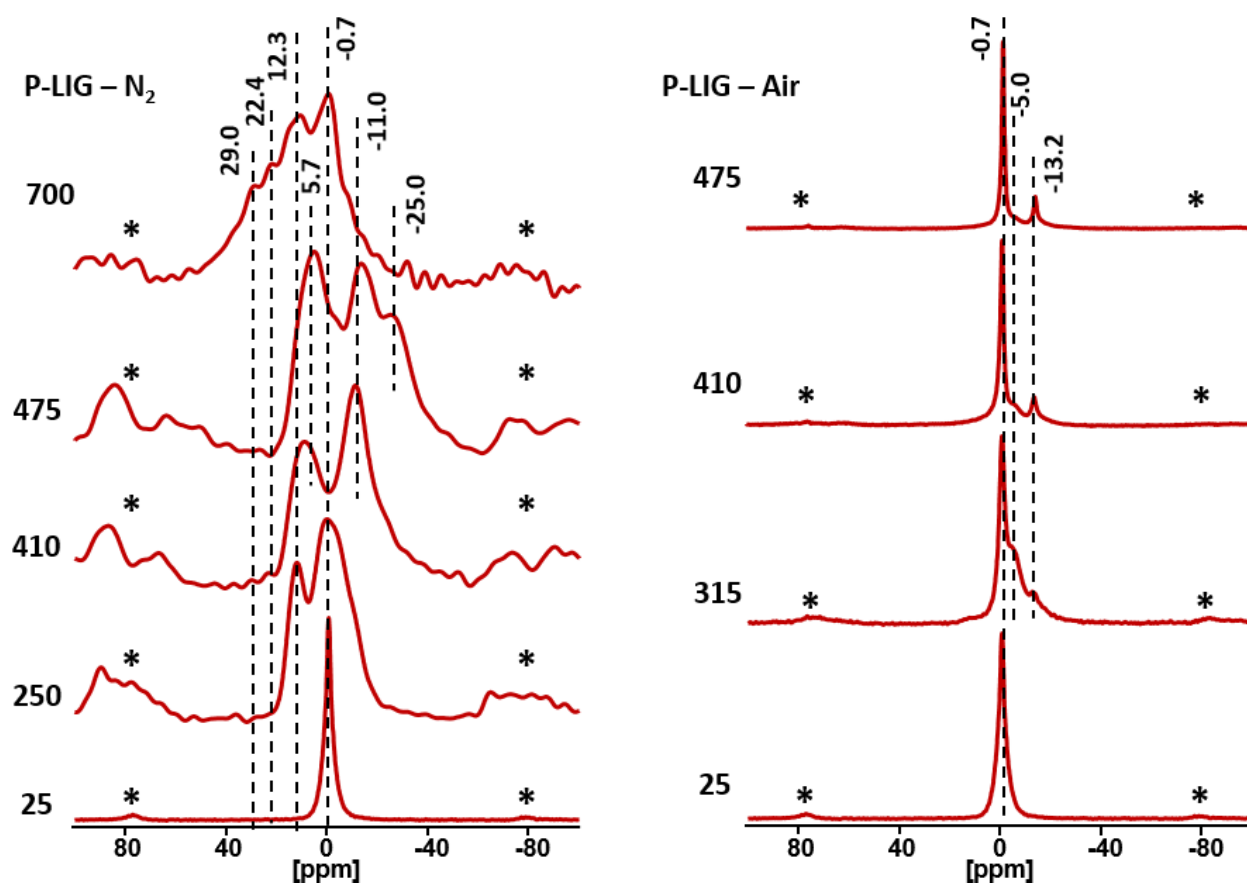
Figure 67. ^{31}P HPDEC NMR of P-LIG chars and signals attributions (rotation speed: 12.5 kHz)

Table 22. Attribution of chemical shifts in ^{31}P solid state NMR

Type of phosphorus	Chemical shift [ppm]
phosphonic acid	22.4 - 29.0
phosphonates	5.7 - 22.4
phosphates	-0.7
ortho- and pyrophosphates	-0.7 – -11.0
polyphosphates	-25.0

3.3.4. Changes in morphology during thermal degradation

As a carbonaceous char is formed during thermal degradation of lignin, XRD and Raman were undertaken in order to evaluate changes in morphology along with the temperature. XRD patterns of LIG and P-LIG are presented in Figure 68. The typical amorphous halo pattern (2Θ = 21.2°) is observed at each temperature for both lignin. The increase of the temperature makes

this wide peak slightly shift from 21.2° (initial state) to 23.7° (700 °C). This indicates that aromatic microstructures may partially reorganize into ordered layers stacking [162]. The fact that the halo pattern becomes sharper with increasing the temperature confirms that the structure gets more ordered at higher temperature. Finally, peaks observed at 22.9° (1), 25.2° (2), 31.6° and 33.1° (3) for LIG reveals that residual cellulose or cellobiose [163] are still part of LIG's structure, but disappeared at 700 °C. In conclusion, it appears that the phosphorylation of lignin does not change the crystallinity of lignin's char.
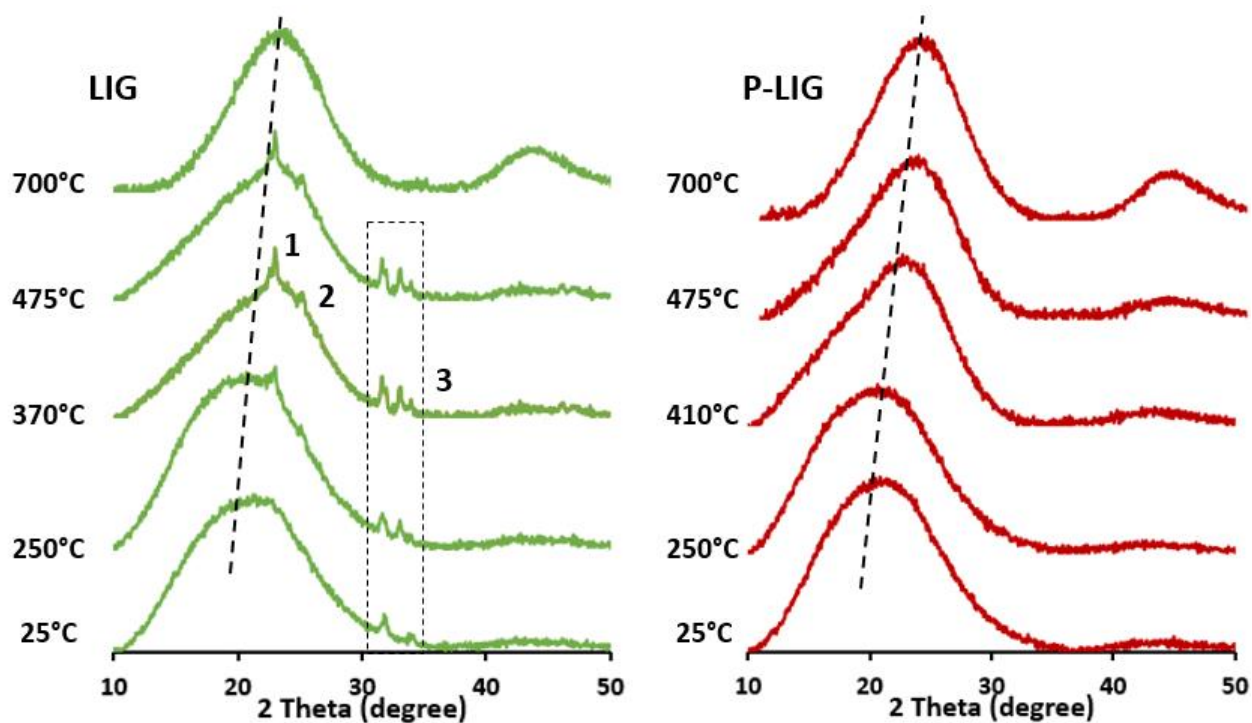
Figure 68. XRD patterns of LIG and P-LIG treated at different temperatures (pyrolysis)

Graphitization evolution in the lignin's structures was analyzed by Raman spectroscopy. Figure 69 shows that similar spectra were obtained for LIG and P-LIG, which exhibit two bands at 1595 (G band) and 1350 cm^{-1} (D band). At 250 °C, fluorescence phenomenon occurred during the analysis for both samples, which makes impossible the interpretation of the results. G-band may be assigned to the E_{2g} vibrational mode of "organized" carbon, whereas D-band, also called defect band, is associated with A_{1g} vibrational mode of carbon atoms with dangling bonds in the plane terminations of disordered graphite or glass carbons [185]. Before degradation, none of these bands are noticed. Therefore appearance of these bands when increasing the temperature proves

that a "turbostratic carbon" is formed during the degradation [185], in other words, a local structure of carbon species which is arranged in polyaromatic layers. At 370 and 410 °C, it appears that I_D/I_G ratio is higher for P-LIG than that of LIG. This means that the lignin's char is more disordered because of the phosphorylation during its formation. Such difference may have a role in the char development, as a high ordered structure is more exposed to constraints and therefore possible cracks. Then, I_D/I_G ratios are increasing along the degradation, thus showing that the carbonaceous structure becomes locally more disordered as lignin degrades. However, it was shown with XRD analysis that it does not negatively impact the organization the high-order structure. As P-LIG exhibits the same behavior than LIG, and that intensity ratios I_D/I_G are very close, it can be concluded that grafting of phosphorus (at 3 %g/g) on lignin does slightly influence its graphitization process when the char is developing, but does not modify the char's behavior at high temperature [186].
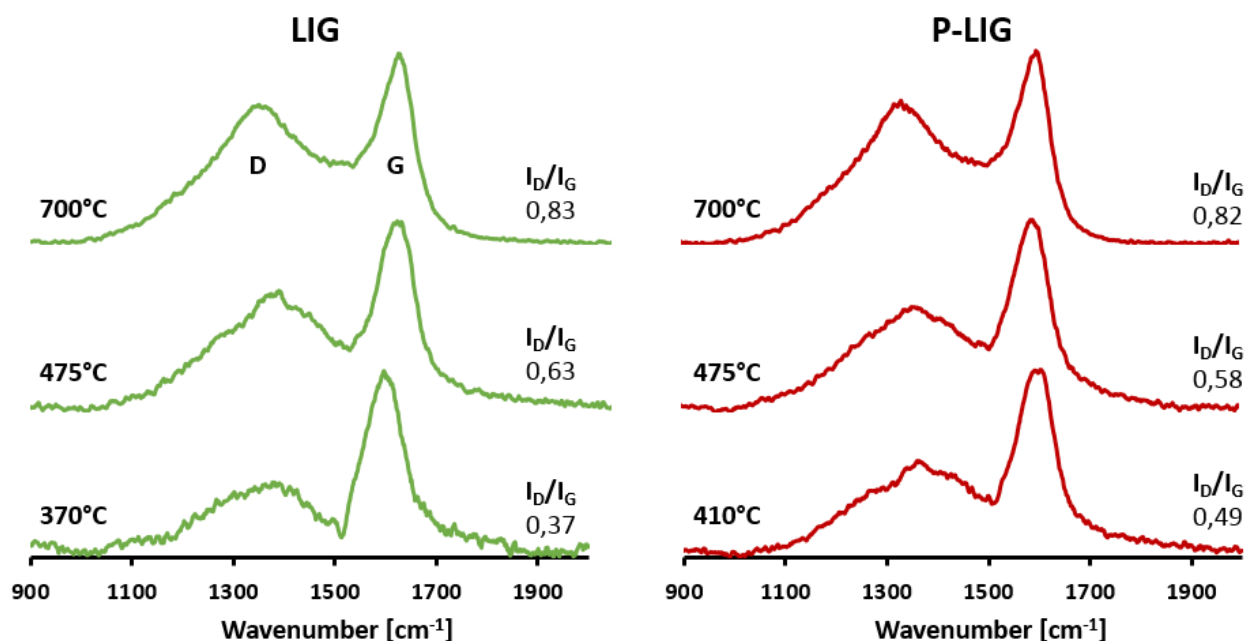
Figure 69. Raman spectra of LIG and P-LIG's treated at different temperatures (pyrolysis)

3.3.5. Conclusion about the condensed phase analysis

Analysis of the condensed phase during thermal degradation of LIG showed that decomposition starts first with disappearance of hydroxyl and other organic functions such as carbonyl groups (dehydration and decarboxylation), then with aliphatic side chains and at higher temperature

inter-units ether bonds. During this decomposition, exothermic events are noticed which indicates that lignin decomposes by carbonization. It leads to a stable carbonaceous residue under pyrolytic conditions. The phosphorylation clearly has an influence on the decomposition pathway. Half of the phosphorus remains in the condensed phase and reacts with the char's structure, which is more thermally stable in comparison to that of LIG. As the thermal degradation of lignin was investigated with techniques using different heating rate, the influence of the heating rate is commented in the next part.

3.4. Influence of heating rate

The influence of the phosphorus on the thermal degradation of lignin was also investigated, at different heating rates and under inert and thermo-oxidative atmosphere. The aim is to evaluate the influence of kinetic on the role of phosphorus shown in the last sections. The quantification of stabilization (or destabilization) was achieved by plotting in Figure 70 the TG difference between P-LIG and LIG according to Equation 7.

In pyrolysis condition, similar behavior is observed at 5, 10, 20 and 60 °C/min. A first destabilization, due to promoted dehydration and decarboxylation, is slightly favored with increasing the heating rate, reaching - 2.% at 60 °C/min. Then, a significant stabilization occurred above 300 °C which appears to be only slightly dependent of the heating rate as a plateau at ≈ 10 % is reached above 500 °C. The heating rate slightly shifts the maximum of stabilization, from 390 to 440 °C at 5 and 60 °C/min respectively. This stabilization occurring in pyrolysis conditions shows that phosphorus acts as char promoter in lignin's structure [187], even at high heating rates. However this effect is limited at 1°C/min as the stabilization is only increased by 5 wt.%, so probably reactions have time to take place (potentially rearrangement in the lignin'structure) and are competitive to those occurring with phosphorus at higher heating rate.

$$TG_{DIFF} = TG_{P-LIG} - TG_{LIG} \qquad Equation\ 7$$

with TG = remaining weight (TGA curve)

In thermo-oxidative condition, a slight destabilization occurs between 180 and 300 °C (depending on the heating rate) and is slightly favored as the heating rate increases. It can be concluded that dehydration and decarboxylation reactions are intrinsic to the phosphorylated lignin material and

are not influenced by the atmosphere. Again, no destabilization is noticed at 1 °C/min. Then, a significant stabilization is observed from 300 to 700 °C for every heating rate, except for 1 °C/min where it ranges from 150 to 600 °C. This stabilization shows that phosphorus prevents oxidation of the char produced during thermal decomposition of lignin [165]. Moreover, this effect is kinetically dependent as shown in Figure 71. It is observed that the maxima of TG_{DIFF} falls from 55 to 14 % at 1 and 60 °C/min respectively. So the higher the heating rate, the lower the protection of phosphorus. The maximum stabilization is also shifted towards higher temperature, from 380 to 570 °C at 1 and 60 °C/min respectively.
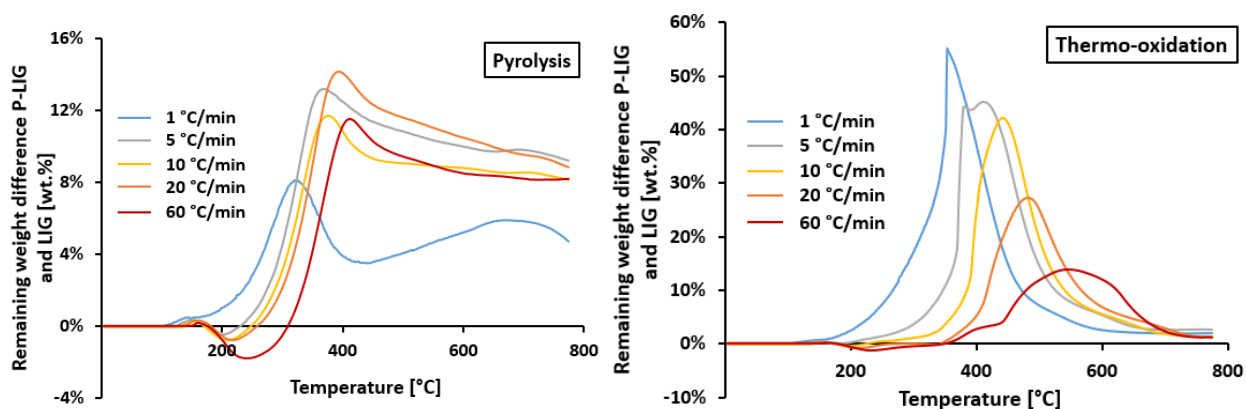
Figure 70. TGA difference of P-LIG and LIG at different heating rates (N₂ and air atmospheres)
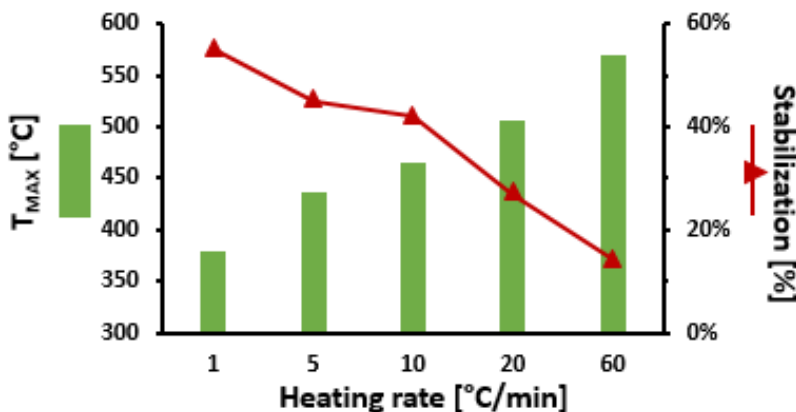
Figure 71. Stabilization as a function of the heating rate (thermo-oxidation)

In pyrolysis condition, it was established that phosphorus increases the charring of lignin by promoting dehydration and decarboxylation. It appears that this phenomenon is not dependent of the heating rate, except at low heating rate. The prevention against oxidation of the char by

phosphorus is less efficient as the heating rate increases. However, in any conditions, P-LIG exhibits superior thermal stability in comparison to LIG.

3.5. Conclusion

Thermal decomposition of LIG and P-LIG was investigated in this section. LIG starts to decompose around 200 °C by releasing water and CO_2 (dehydration and decarboxylation reactions). As the temperature increases, side chains are cleaved, followed by inter-units ether bonds. Under pyrolytic conditions, a carbonaceous residue of 45 wt.% is obtained, which is totally oxidized under thermo-oxidation. It was also shown that the decomposition gases may react with the char as the lignin degrades. The gas phase, mainly composed of water, CO_2, CO, aromatic and hydrocarbon compounds is slightly combustible. The phosphorylation of LIG permits to improve its thermal stability. First degradation reactions such as dehydration, decarboxylation and side chains cleavage are promoted, thus inducing a higher char yield at higher temperature. Phosphorus acts mainly in the condensed phase by forming pyrophosphates, polyphosphates and phosphonates structures which provides an enhanced thermal stability to the char. Besides acting as char promoter, phosphorus also prevents oxidation of the char under thermo-oxidation. Combustibility of the gas mixture released by P-LIG during thermal decomposition is 30 % less combustible than that of LIG with only 3 % of phosphorus in the structure.

4. Conclusion and discussion

As this work intends to valorize lignin as flame retardant additive, Kraft lignin (LIG), which is one of the most available lignin on the market, was chosen for this study. FTIR and NMR analysis showed that this G-type lignin contains 6.3 mmol/g of free hydroxyl groups which are available for phosphorylation. Phosphorylation of lignin (P-LIG) was proven to be successful. FTIR and liquid state NMR analysis indeed showed that phosphate groups were grafted to the lignin's structure as P-O-C were observed. Solid state NMR and XRD also proved that the phosphorylation did not degrade the initial structure of lignin. Quantification of P-O-C bonds was not possible using Argyropoulos method, however elementary analysis revealed that 3.0 % of phosphorus was part of the P-LIG's structure. Finally, SEM analysis revealed that P-LIG tends to agglomerate probably

because of affinity between phosphates with each other's and free remaining hydroxyls. It resulted that P-LIG particles or agglomerates are 5 time bigger than those of LIG.

Phosphorylation of LIG led to enhanced thermal stability of lignin. Indeed, char yield was increased, and the degradation rate lowered. Analysis of the gas phase by TGA coupled with FTIR showed that the presence of phosphorus promoted the dehydration and decarboxylation reactions, as well that the cleavage of the aliphatic side chains, thus promoting the charring. This was confirmed by solid state NMR, TGA/DSC and elementary analysis. As a consequence, release of aromatic compounds and hydrocarbons was decreased, thus lowering the combustibility of P-LIG by 30 % in comparison to that of LIG according to PCFC. It was also shown that phosphorus mostly acts in the condensed phase by forming ortho-, pyro- and polyphosphates as well as phosphonates which stabilizes the char's structure. Additionally, TGA under thermo-oxidative conditions demonstrated that phosphorus prevented oxidation of the carbonaceous residue, but that the protection's efficiency decreases as the heating rate increases.

During this study, LIG appeared to be a promising candidate as FR additives in polymers. Indeed, it produces a significant char under thermal decomposition, which could act as physical barrier preventing the polymer matrix from burning. Additionally, phosphorylation of lignin was proven to be successful since phosphates were covalently bonded to the structure, and P-LIG exhibited enhanced properties. Indeed, 3 % of phosphorus in the lignin's structure permits to improve its thermal stability by promoting the charring and to decrease its combustibility. As phosphorus was proven to be active in the condensed phase, interactions with degrading polymeric matrices may be expected when using P-LIG as FR. Finally, phosphorus was found to prevent the char from oxidation, which may be an asset to avoid the protective barrier to collapse after long time of exposure to heat in presence of oxygen. As a consequence, the next chapter will thus focus on evaluating LIG and P-LIG as FR additives in different polymers and different formulations.

IV- **Material screening**

This chapter deals with the development of new polymeric materials containing lignin as flame retardant additive. Lignin belonging to the family of polyphenols (full aromatic structure) could indeed develop a char under fire conditions. The first part of the screening consisted on finding a polymer in which polymer neat lignin provides promising FR performance. Most of the time, it is impossible to compare effectiveness of lignin as FR in plastics from the literature since the source of lignin is never the same. The originality of this work is to consider a unique source of lignin, i.e. Kraft lignin, and to draw conclusion about it FR properties in different polymers. To do so, Kraft lignin was incorporated in several types of polymers such as polyolefines, styrenics, thermoplastic polyurethane and bio-based matrices and the fire performance of each composite was evaluated. Then, innovative systems were developed in the selected polymers in order to further improve the FR properties. Depending on the polymeric matrix, different strategies were selected. Phosphorylated lignin, co-additives and synergists were considered to elaborate such FR systems. Because P-LIG is not available in large quantities, a "reduced" MLC was validated in the laboratory (see Chapter II, section 2.2.2, p86) allowing to perform more experiments. Thus all formulations were screened using "reduced" MLC. At the end of this chapter, the most promising material was selected and its fire retardant mechanism is analyzed in Chapter V.

1. Neat lignin as FR additive in several polymers

This section intends to select the polymers in which Kraft lignin exhibits the most promising FR performance. The approach consists in using neat lignin as additive in order to evaluate its intrinsic FR properties in several plastics. Because fire retardancy mechanisms may involve interactions between FR additives and polymeric matrix, thermoplastics based on different monomers were considered. The polymers selected for the screening are the polypropylene (PP), thermoplastic polyurethane (TPU), polystyrene (PS), acrylonitrile-butadiene-styrene (ABS) and polylactic acid (PLA). PP was chosen since lignin exhibits interesting FR properties in polyolefines. In the case of polyurethane, lignin is mainly used as macromonomer in such materials. Therefore, the innovative approach is to consider lignin in TPU as FR additive. Then, PS and ABS were chosen because lignin exhibits an interesting compatibility in the styrenics and thus could lead to enhanced FR performance [93]. Finally, PLA was selected to be representative of biobased polymers, since it is the most used in the green plastics market. The aim would be to develop a green PLA composite flame retarded with renewable FR additive [143,144].

In the first part of this screening, different fire testings are considered to evaluate the FR properties of the materials. Limiting Oxygen Index (LOI), UL-94 and Mass Loss Cone (MLC) assess different features such as the flammability or the heat released during the combustion. According to the literature, lignin is more efficient as FR additive at high loading (Chapter I, 2.3, p62). In order to observe significant effect and discriminate the formulations, lignin's loading was set at 30 wt.%.

1.1. Limiting Oxygen Index (LOI)

LOI is a common test used for evaluating the flammability of a material. This test has no link with the reality of a fire, but the idea is to measure the limit percentage value of oxygen in the atmosphere which is required to ignite a material with a standard flame. A material presents some FR properties when the LOI is higher than 20 %, and a concrete interest for flame retardancy if higher than 30 %. Like for the other FR testing, the behavior of the materials under the flame is very important and will be considered.

The results of LOI testing are presented in the Figure 72. The majority of the neat polymers are very flammable as they all start burning between 18 (PP, PS and ABS) and 19 O_2vol% (TPU and PLA) of oxygen. Since none of these polymers are char formers, no char was noticed during the combustion. When lignin is incorporated in the polymers, no significant improvement of the flammability occurs. Indeed, LOI's values are increased only by 1 O_2vol% in the case of PP, PS, ABS and PLA and 2 O_2vol% for TPU. Since the margin of error of this testing is ± 0.5 O_2vol%, it is concluded that lignin used alone has no significant effect on the flammability, which is consistent with other studies in PP or in PLA [88,141].

Moreover, in the presence of lignin, char was formed at the top of the composites barrels, but it was not efficient enough to extinguish the samples. However, different behaviors were observed depending on the plastics. PP and PLA make chars, but it falls off because of the low viscosity of the underlying polymer. For PS and ABS, cohesive but no expanded char was formed. Finally, the char produced with TPU expands. However, during combustion of the sample, decomposition gases evolve, thus inducing bubbling. These gases therefore feed the flame which cannot extinguish rapidly.
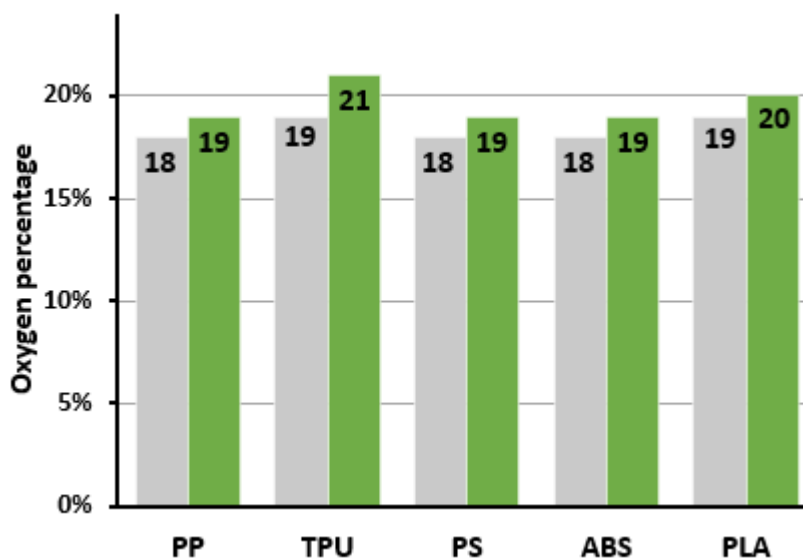
Figure 72. LOI values of neat polymers (grey) and composites with 30 wt.% of Kraft lignin (green)

Incorporation of lignin in these polymers has no positive effect on the flammability of the plastics. However, different behaviors of charring were observed, and will be particularly considered in the other testing.

1.2. UL-94 Classification

Like LOI, UL-94 testing is used to evaluate mainly the flammability of a material, but in ambient atmosphere. Moreover, the sample is ignited at its top in LOI, and at the bottom in UL-94. In this test, besides the flammability, the flame spread along the sample can also be measured. The behavior of the samples during burning, such as char formation, gives precious information about the modes of action of the FR additive.

The ranking and observations are listed in Table 23. Except TPU which shows V2-rating, other polymers are not classified. During the combustion, the majority of the polymers drips, and ignites the cotton. Only ABS does not drip, but burns to the clamps. The addition of lignin in the polymers did not permit to improve the UL-94 rating, since TPU_30LIG remains V2 and the others are NC.

However, some differences of behavior were noticed for several polymers. TPU ignites and burns while small flaming drops fall on the cotton. After a certain time, the dripping leads to the extinction of the flame. But when TPU_30LIG is burning, no dripping is observed. Actually, the sample extinguishes immediately when a big flaming part of the barrel falls. In the case of PS, the sample drips, ignites the cotton and burns to the clamps. Even if PS_30LIG also burns to the clamps, no dripping occurred. On the contrary, neat ABS is not dripping whereas ABS_30LIG drips and ignites the cotton. Both burn to the clamps. Finally, PLA burns while flaming drops ignite the cotton. The addition of lignin significantly reduces the amount of dripping, but not enough to stop the combustion and to reach V2.

Table 23. UL-94 (3.2 mm) results of neat polymers and composites with 30 wt.% of Kraft lignin

Samples	Dripping*	Cotton**	Comments	Classification
PP	Y	Y	Flaming drops	NC
PP 30LIG	Y	Y	Flaming drops	NC
TPU	Y	Y	Flaming drops	V2
TPU 30LIG	Y	Y	Only one big flaming drop	V2
PS	Y	Y	Flaming drops	NC
PS 30LIG	N	N	Burns to the clamps	NC
ABS	N	N	Burns to the clamps	NC
ABS 30LIG	Y	Y	Flaming drops	NC
PLA	Y	Y	Flaming drops	NC
PLA 30LIG	Y	Y	Much less flaming drops	NC

*Dripping: if the sample drips during the test // **Cotton: if the cotton is ignited by the drops

The addition of lignin in the polymers did not increase the UL-94 rating of the composites. Nonetheless, differences in the behavior under the flame between neat polymers and composites were noticed. Particular attention is paid for PLA as lignin permits to drastically reduce the dripping. It also induces a dripping when blended in ABS, which could be interesting for the sample to extinguish and potentially improve NC ranking to V2. So lignin may have an influence on the flame retardancy of these polymers.

1.3. Mass Loss Cone (MLC)

The mass loss cone is a FR testing representative of a fire scenario. It measures many quantitative data such as the time required for a sample to ignite or the heat released during the combustion. Moreover, the development of a char may also significantly influence the results. Since lignin produces char during the combustion, MLC appears to be a powerful tool to evaluate the influence of lignin on the combustion of polymers [13,133].

The neat polymers as well as the composites were tested in the conditions of a mild fire scenario (35 kW/m²). The numerical results are listed in Table 24. PP starts burning after 67 s exposure time and releases 99 MJ/m² of heat, with a peak of heat release rate of 654 kW/m². The residue after combustion is unstructured and fragile ashes. The addition of lignin significantly shortens the TTI by 36 s, which was already observed at 20 wt.% lignin's loading in the work of Gallina *et*

al. [133]. But in the same time both THR and pHRR are interestingly reduced by 39 and 48 %. These reductions are different from the work of Gallina and it could be explained by the sample's thickness. Gallina worked with 6 mm thickness, while the results of this study are generated from 3 mm thick sample. Changes of heat and mass transfer are not comparable [134], especially in the case of the formation of a carbonaceous shield, and could explain the differences. These results are also hard to compare with the work of Yu [13] since the testing was done at 25 mm from the heat source (here 35 mm) and with only 20 wt.% loading.

The FR performances of lignin-composites based on the other polymers are similar to PP. Indeed, the TTI is always dramatically shortened (around 50 %). The worst example is PS, since the composite ignites after only 23 s exposure time while neat PS requires more than 60 s. The change in absorptivity of the sample induced by the addition of lignin in the polymers may be one cause of these short TTI's [188]. Then, pHRR is significantly reduced, by 34 % for the PLA or 45 % for TPU. In the case of THR, broad dispersion of the results is observed. The worst reduction is about 9 % and achieved in TPU. The PS exhibits the best improvement since THR is decreased by 22 %. The results obtained for ABS are in accordance with the previous work of Song *et al.* [94]. No sources were found in the literature to make comparison in the case of the other composites. The types of residue obtained after combustion can be clustered into 3 categories: unstructured ashes (PP, PS, ABS), collapsed char (TPU) and cohesive char (PLA).

Table 24. MLC data and pictures of the residue of the formulations

Formulations	TTI [s]	pHRR [kW/m²]	THR [MJ/m²]	Residue
PP	67	654	99	
PP_30LIG	31 (- 36)	342 (- 48 %)	60 (- 39 %)	
TPU	64	366	55	
TPU_30LIG	25 (- 39)	201 (- 45 %)	50 (- 9 %)	
PS	66	416	70	
PS_30LIG	23 (- 43)	257 (- 38 %)	55 (- 22 %)	
ABS	80	482	72	
ABS_30LIG	49 (- 31)	275 (- 43 %)	63 (- 13 %)	
PLA	67	316	72	
PLA_30LIG	41 (- 26)	208 (-34 %)	59 (- 18 %)	

In terms of FR performances, lignin is more effective as FR additive in PP. Indeed, both pHRR and THR are significantly reduced. However, no cohesive char is obtained after combustion. The curves of the test are presented in Figure 73. It is agreed that a bimodal curve is typical of char formation, as the second peak is generated when the char collapses [134]. All composites make char during MLC testing, which then collapses. Surprisingly, no bimodal curve is observed in the case of PP_30LIG. For the other composites, such remarkable curve is clearly noticed. Three behaviors can be considered. First, a sharp and intense peak (pHRR) demonstrates a strong combustion in the case of TPU and PS composites. HRR then decreases slowly, which corresponds

to the protection effect of the char. Finally HRR falls when the flame extinguishes. The second behavior is observed with ABS composite. The difference with the first one regards the larger and smoother peak (pHRR), which shows slighter combustion, attributed to rapid formation of the char. Moreover, there is no gradual decrease of the HRR, showing a less effective protection of the char. After a second pHRR, HRR decreases dramatically. Finally, the third behavior was obtained with PLA composite. It combines both previous behaviors, with the smooth pHRR (observed with ABS) followed by a slow decrease of the HRR (observed with TPU and PS). So lignin acts differently from a polymer to another, mainly because of the formation of chars with diverse properties. The formation of char is a complex process, which is, in this case, mainly attributed to lignin degradation. However, interactions between lignin and polymeric matrix could also contribute to char formation. According to this, a special attention is paid for ABS and PLA composites since a rapid formation of the char was observed. Moreover, the PLA composite exhibits a cohesive char as residue.
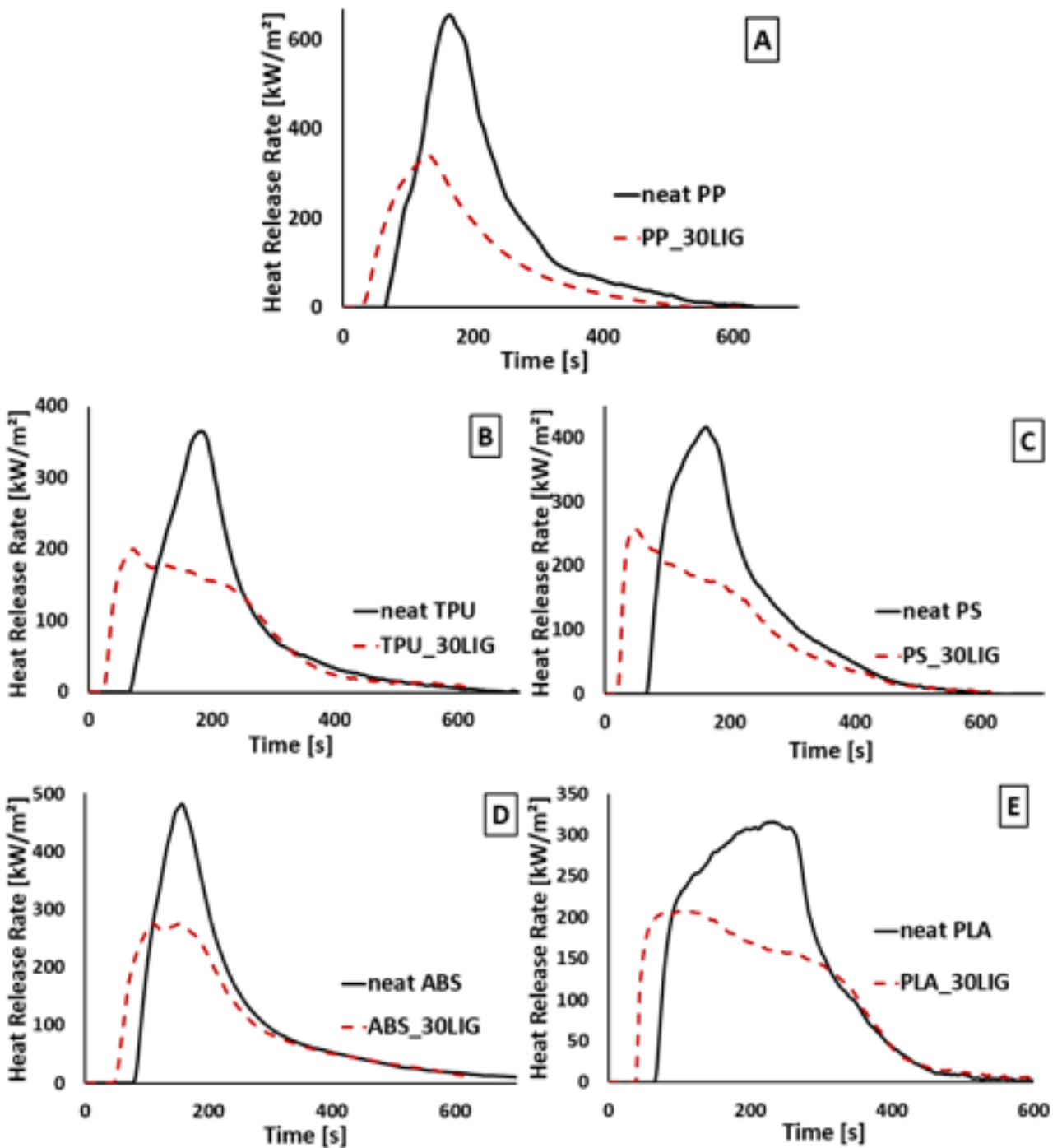
Figure 73. MLC curves of neat polymers and composites with lignin

(A) – PP / (B) – TPU / (C) – PS / (D) – ABS / (E) – PLA

1.4. Conclusion

The aim of this first part of the screening was to point out Kraft lignin FR properties in five different polymers: PP, TPU, PS, ABS and PLA. To do this, FR performances of neat polymers were compared to those of composites with 30 wt.% loading of neat lignin. The flammability was first studied with LOI testing. Composites did not exhibit higher LOI (around 19-20 %), so lignin had no positive influence according to this test. Then UL-94 was considered in order to also evaluate the flammability of the composites, but also to investigate their behavior under a flame. Even if no improvement of the rating was noticed (all composites are NC, except for TPU which is V2), differences of burning behavior induced by lignin were noticed. The last fire testing undertaken was the MLC which represents a real fire scenario. It showed that lignin permits to reduce pHRR as well as THR in a significant way by forming a char, but its presence clearly led to shortened TTI.

In conclusion, lignin exhibits interesting FR properties in these polymers. PLA and ABS composites especially caught attention because of their interesting behavior in UL-94 and MLC testing. Therefore, these two polymers were chosen to go further with the screening. In the following, phosphorylated lignin as well as coadditives will be used in order to develop FR systems based on lignin. From this first step of the screening, MLC testing appears to be a good tool for screening and will be used in the next parts. First, the systems developed in PLA are presented and commented, the last part is devoted for ABS.

2. FR lignin systems for PLA

The incorporation of lignin as additive leads to an improvement of the FR properties of PLA. Indeed, the behavior of this polymer changes with lignin in UL-94 and MLC testing. Moreover, the formation of a carbonaceous protective barrier seems to be the main cause of the improvement in MLC. Therefore, the development of FR systems based on lignin in PLA was undertaken. First, lignin was replaced by phosphorylated lignin P-LIG (see chapter III) in order to evaluate the influence of the phosphorylation on the FR performance of PLA. Then, it was decided to develop a char forming system because of the charring ability of lignin. To do so, synthetic and bio-based acid sources were combined with lignin in PLA. Finally, the promising combination of lignin with

ammonium polyphosphate (APP) was optimized. The FR properties of all the formulations are evaluated with the reduced MLC.

2.1. Phosphorylated lignin

Phosphorylated lignin was characterized in chapter III and used in this study. As a consequence of the phosphorylation, the thermal stability of P-LIG was considerably improved, and the analysis with PCFC showed that P-LIG releases non-combustible compounds during thermal decomposition. Moreover, the presence of phosphorus could be interesting in the charring process occurring during the combustion of the PLA/LIG composite. Therefore, P-LIG was incorporated in PLA at 30 wt.%.

The curves of R-MLC testing are shown in Figure 74 and the data in

Table 25. The incorporation of LIG or P-LIG induces a shorter time to ignition. The composites ignite around 30 s faster than neat PLA. As expected from the screening, PLA_30LIG exhibits a reduction of pHRR by 34 % and of THR by -26 % in comparison to that of neat PLA. In the case of P-LIG, a further improvement of the FR performance is noticed. Indeed, compared to neat PLA, pHRR of PLA_30P-LIG is reduced by 49 %, and THR by 41 %. The residue obtained with P-LIG seems to be more cohesive than that obtained with LIG, but it was less expanded. This observation is supported with the higher amount of P-LIG residue obtained after combustion.
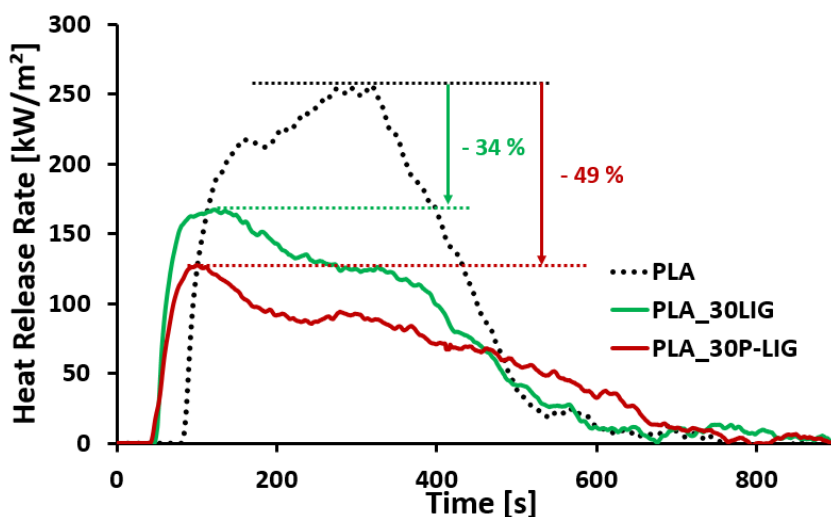
Figure 74. R-MLC curves of PLA-based composites with LIG or P-LIG

Table 25. R-MLC data of PLA-based composites with LIG or P-LIG

Formulation	TTI [s]	pHRR [kW/m²]	THR [MJ/m²]	Residue [wt.%]
Neat PLA	85	257	80	1
PLA_30LIG	52 (- 33)	170 (- 34 %)	59 (- 26 %)	9
PLA_30P-LIG	50 (- 35)	130 (- 49 %)	47 (- 41 %)	17

The polymer's molar mass (M_n) may have an influence on several FR properties. Indeed, M_n is representative of the polymer chain's length. In case of degradation, chains may be shortened and M_n decreases. In terms of FR properties, shorter chains induce lower viscosity, change in the mass distribution and potentially in the nature of the degradation gases. Therefore, FR properties may be affected. PLA is known to be sensible to moisture and temperature, so it seems important to control the molar mass of the pure polymer and the FR formulations in order to evaluate the influence of the additive on the polymeric matrix and before assuming any conclusions about FR performance. The molar masses of the neat PLA and the composites with lignin were measured and are presented in Figure 75. While addition of LIG in PLA does not affect the polymeric matrix by keeping M_n in the range of 55 000 – 60 000 g.mol^{-1}, the incorporation of P-LIG clearly decreases the molar mass of PLA which falls to 45 000 g.mol^{-1}. Because PLA is known to be sensible to hydrolysis, blending it with P-LIG (which is relatively acid) may lead to polymer's chains degradation during the process [189]. Therefore, it was decided to not use P-LIG in PLA, and to focus the development of FR formulations based only on LIG.
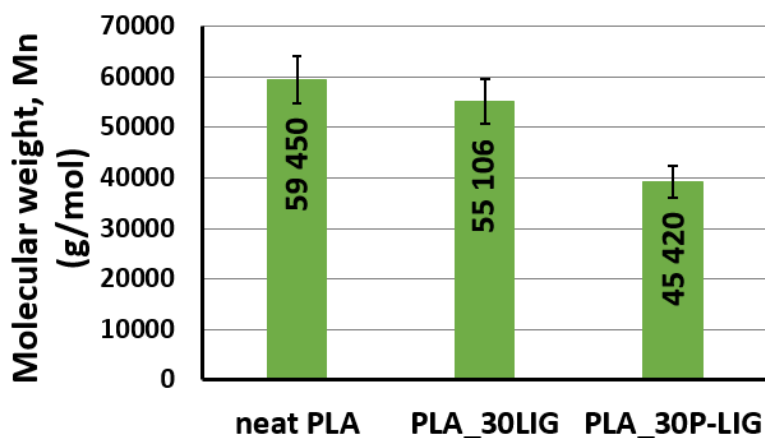
Figure 75. Molar mass of PLA composites with LIG or P-LIG

2.2. Combination of lignin with different acid sources

In the previous section, lignin was considered as promising FR additive in PLA since it develops a char under fire conditions. In this context, the development of intumescent systems (IS) based on lignin appears to be a viable solution to flame retard PLA. Intumescence was indeed widely studied in PLA [140]. To create an intumescent system, three main components are required: an acid source, a carbon source and a blowing agent (see section 2.1.4, p56). Réti *et al.* [141] investigated systems combining ammonium polyphosphates (APP), acting as both acid source and blowing agent, with a mixture of lignin and starch. Considering that the char produced by lignin alone in PLA expended well, it was therefore decided to combine it with only an acid source. Following a "green" approach, bio-based acid sources were chosen in order to develop a 100 % green FR PLA. Phytic acid was considered since it exhibits some FR properties in PLA [190]. Following this idea, succinic acid was also tested. In such systems, the ratio lignin/acid is commonly set at 1:3 [141]. In the context of lignin's valorization, the ratio of lignin and acid source was set at 3:1 and the total loading at 30 wt.% to be comparable with PLA_30LIG.

The formulations were tested with R-MLC. The curves are shown in Figure 76, and the data listed in Table 26. Besides a slight increase of the TTI, the IS systems exhibit different behavior depending on the acid source. In the case of APP, significant reductions of pHRR and THR are noticed, 47 % and 46 % respectively. The combination of LIG with phytic acid leads to the same FR performance than that of ABS_30LIG. For both formulations an expanded char is produced

during the combustion, which seems more cohesive with the acid source than that of LIG. Moreover, the amount of char is increased in comparison to that of PLA_30LIG. Finally, the use of succinic acid induces antagonism effect on the FR properties. PHRR is indeed increased by 26 % in comparison to that of PLA_30LIG. The char does not expand, and a low amount of residue is left after the combustion. A degradation of the PLA matrix due to interactions with succinic acid could have occurred during the processing.
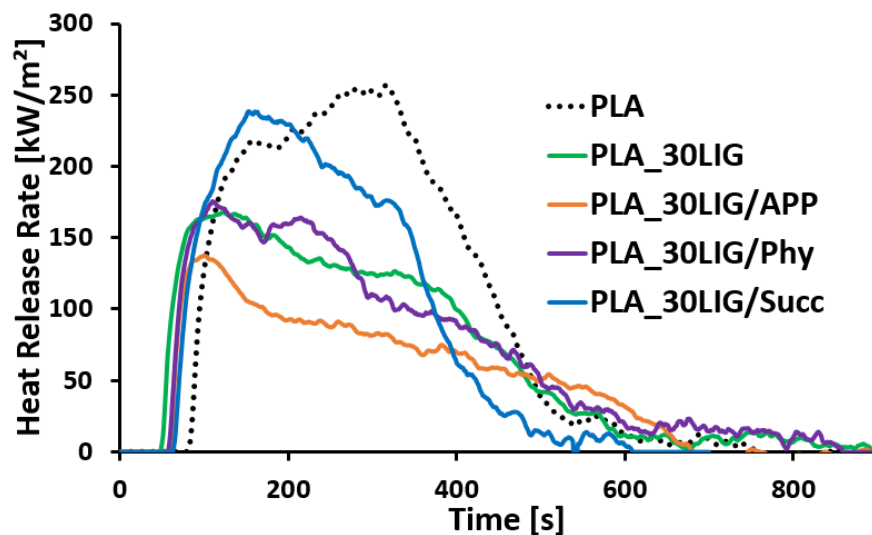
Figure 76. R-MLC curves of PLA flame retarded with IS-lignin systems

Table 26. R-MLC data of PLA flame retarded with IS-lignin systems

Formulation	TTI [s]	pHRR [kW/m²]	THR [MJ/m²]	Residue [wt.%]
Neat PLA	85	257	80	1
PLA_30LIG	52 (- 33)	170 (- 34 %)	59 (- 26 %)	9
PLA_30LIG/APP	62 (- 24)	137 (- 47 %)	43 (- 46 %)	22
PLA_30LIG/Phy	56 (- 29)	188 (- 27 %)	61 (- 24 %)	16
PLA_30LIG/Succ	65 (- 20)	238 (- 8 %)	64 (- 20 %)	6

In conclusion, only the IS system combining lignin with APP permits to improve the FR performance of PLA_30LIG. The use of phytic acid leads to the same FR performance than PLA_30LIG, while the succinic acid induces antagonism effect with lower FR performance. The role as both acid source and blowing agent of APP in comparison to others acid sources may be the reason of improved FR performance. Therefore, the ratio LIG/APP was optimized, and the results are presented in the next section.

2.3. Optimization of the system PLA/LIG/APP

The intumescent system based on lignin and APP exhibits the best FR performance in comparison to the other formulations of the screening. In comparison to another study on the similar system [141], lignin is the main component of the IS and the total loading is reduced to 30 wt.%. In order to optimize the formulations and to better understand the mode of action of this IS, composites with LIG/APP ratios of 1:1 and 1:3 were developed. A formulation with 30 wt.% of APP was prepared as well and considered as a reference with PLA_30LIG.

The R-MLC curves are shown in Figure 77 and the data in Table 27. PHRR is not really affected by the ratio of APP. Indeed, pHRR's reduction ranges from 45 to 50 % for all IS systems, even for PLA_30APP. It is still better than that of PLA_30LIG which is about 34 %. However the ratio clearly influences THR. MLC curves of the composites with the ratios 3:1 and 1:1 are very similar: THR is reduced by 45 % in comparison to neat PLA. When the ratio is set at 1:3, THR is further reduced by 84 %. The behaviors can be gathered in two categories: one is driven by the lignin (comparing curves to PLA_30LIG) and the second by the APP (comparing curves to PLA_30APP). This difference is explained by the fact that the composites extinguish faster when APP is the main FR additive. Since the ratios 3:1 and 1:1 exhibit the same FR performance, it can be assumed that adding of APP below a critical ratio (between 1:1 and 1:3) does not allow to improve the FR performance of the formulation. Finally, the use of APP alone significantly delays the ignition (+ 52 s). On the contrary, lignin leads to shorter TTI, even if APP is added to the system.
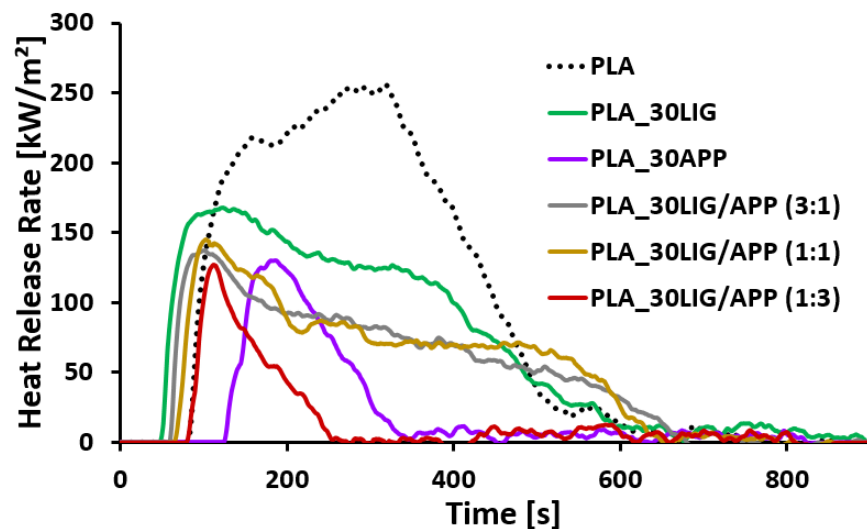
Figure 77. R-MLC curves of PLA flame retarded with LIG and APP at different ratios

Table 27. R-MLC data of PLA flame retarded with LIG and APP at different ratios

Formulation	TTI [s]	pHRR [kW/m²]	THR [MJ/m²]	Residue [wt.%]
Neat PLA	85	257	80	1
PLA_30LIG	52 (- 33)	170 (- 34 %)	59 (- 26 %)	9
PLA_30APP	137 (+ 52)	130 (- 49 %)	18 (- 78 %)	65
PLA_30LIG/APP (3:1)	62 (- 24)	137 (- 47 %)	43 (- 46 %)	22
PLA_30LIG/APP (1:1)	71 (- 15)	145 (- 44 %)	44 (- 45 %)	28
PLA_30LIG/APP (1:3)	74 (- 12)	129 (- 50 %)	13 (- 84 %)	66

The combination of LIG with APP leads to an improvement of the FR properties of PLA. A small amount of APP permits to further reduce THR in comparison to LIG used alone. When APP is considered as the main component of the IS, THR is dramatically decreased. Looking at the char formed during the test, it can be assumed that the main mode of action of these systems is based on condensed phase mechanisms. The amount of residue is significantly increased with higher APP amount (Table 27). Looking at the pictures in Figure 78, it is assumed that the morphology of

the char is clearly influenced by this ratio. PLA_30LIG produces a fragile and porous char. It becomes more and more cohesive as the amount of APP increases in the formulation. This evolution may be one of the explanation of THR's reductions. Nevertheless, in the context of valorization of lignin, it is interesting to observe that an efficient intumescent system for PLA can be developed containing a high amount of LIG (22.5 wt.%) and APP (7.5 wt.%).
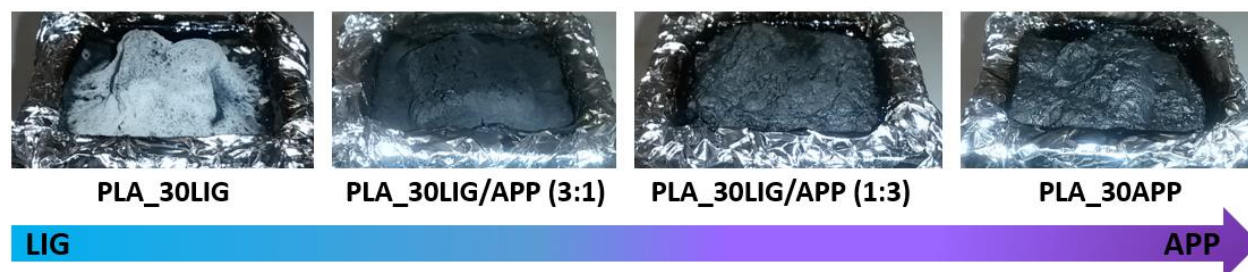
Figure 78. Evolution of the R-MLC residues depending on the ratio LIG/APP

2.4. Conclusion

Based on FR performance induced by the use of LIG in PLA, FR formulations based on lignin were developed. First, P-LIG was considered and led to promising results with MLC testing. However, the PLA matrix was considerably degraded probably during the processing because of the acidity of P-LIG. Therefore, it was not accurate to continue working with PLA_30P-LIG. Then, several acids were combined with LIG in order to develop a more efficient charring protective barrier. APP provided good results, while sodium phytate and succinic acid did not permit to improve the FR performance. In fact, succinic acid clearly showed antagonism effects. Finally, different LIG/APP ratios (3:1, 1:1 and 1:3) were tested. The best FR performance was obtained with a high amount of APP. This result was attributed mostly to the formation of a more efficient protective barrier. Indeed, chars obtained with high APP amount appeared more cohesive. However, PLA_30LIG/APP (3:1) exhibited good FR performance, and which showed that LIG can be valorized as FR additive in an intumescent system to flame retard PLA.

3. FR lignin systems for ABS

Lignin exhibits interesting FR properties when it is used in ABS according to UL-94 and MLC. Even if the FR performance was not significantly improved, the addition of lignin considerably modifies the behavior of ABS when it burns. The formation of a char appears promising, and the development of the formulations is focused on producing an effective protective barrier. Therefore, a second phase of screening was undertaken in order to improve the FR properties of the ABS/lignin system. To do this, lignin was phosphorylated (P-LIG) and blended in ABS. Then, different coadditives were added to the FR system. According to the first phase of the screening, reduced MLC is considered as the most appropriate FR testing to discriminate the formulations.

3.1. Phosphorylated lignin

Lignin was successfully phosphorylated and characterized in the chapter III. As a consequence of the phosphorylation, the thermal stability of P-LIG was considerably improved, and the analysis with PCFC showed that P-LIG released non-combustible compounds. Moreover, the presence of numerous aromatic functions in lignin permits to expect a good compatibility in styrenic polymers. For these reasons, P-LIG was considered as potential flame retardant for ABS. In order to evaluate the influence of the phosphorylation of lignin on the FR properties of ABS, two composites were prepared either with 30 wt.% of LIG or P-LIG.

These composites were submitted to the reduced R-MLC testing, as well as neat ABS as reference. The curves are presented in Figure 79, and the numerical results in Table 28. The incorporation of lignin in ABS induces a slight diminution of the TTI. PHRR and THR are reduced by 34 and 17 % respectively, as expected from the first part of the screening (see section 1.3, p146). When P-LIG is blended with ABS, pHRR is further decreased by 50 %, as is THR by 24 %.

For both LIG and P-LIG formulations, a second pHRR is noticed at 200 s for LIG and at 275 s for P-LIG. It corresponds to the degradation of the char during the combustion [134], thus releasing more combustible to the flame. In the case of P-LIG it seems that the char formed resists longer than that of LIG. Unfortunately, the center of the char collapses around 500 s thus consequently increasing HRR. Moreover, the use of P-LIG induces longer time of combustion (726 s) than that

with LIG (608 s). Both of these observations explain why the THR is only slightly reduced with P-LIG (25 wt.%) in comparison to neat LIG (19 wt.%). However, a larger amount of residue is obtained with P-LIG than with LIG, which is interesting for the action of the char as protective barrier. Pictures of the residues are shown in Figure 80. Even if the char collapsed at its center, the residue obtained with P-LIG appears much more cohesive than the ashes obtained with LIG. The change of color, from grey ashes for LIG to black "islands" for P-LIG, is significant too. So it is obvious that the phosphorylation of lignin involves changes of the degradation process occurring in the condensed phase.
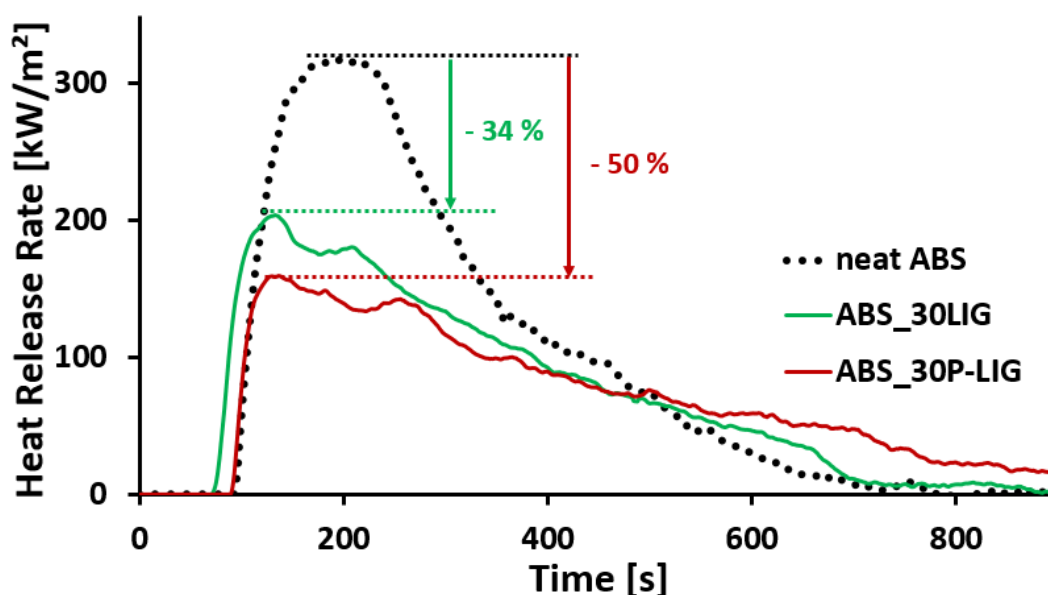
Figure 79. R-MLC curves of ABS formulations with LIG or P-LIG

Table 28. R-MLC data of ABS formulations with LIG of P-LIG

Formulation	TTI [s]	pHRR [kW/m²]	THR [MJ/m²]	Residue [wt.%]
Neat ABS	96	318	84	1
ABS_30LIG	80 (- 16)	210 (- 34 %)	70 (- 17 %)	19
ABS_30P-LIG	91 (- 5)	160 (- 50 %)	64 (- 24 %)	25
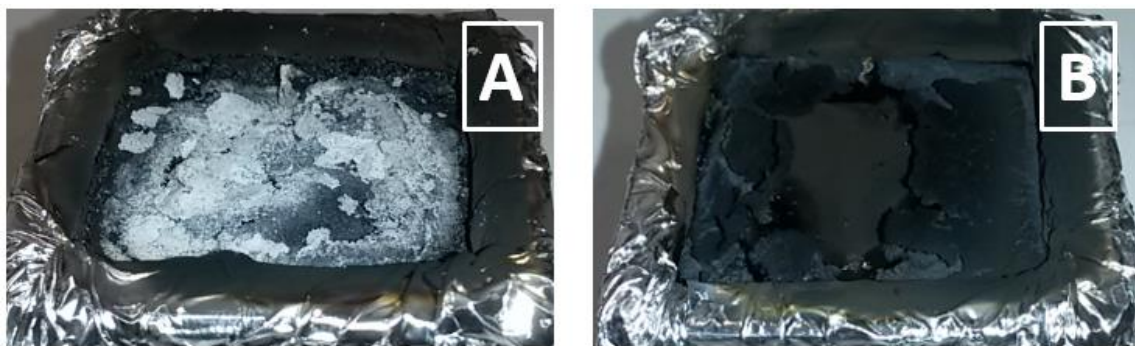
Figure 80. MLC residues of ABS formulations with LIG (A) and P-LIG (B)

Before drawing any conclusion on fire retardancy of a polymer, it is agreed that the additive does not significantly deteriorate the chemical structure of the matrix. As seen before with the case of PLA, P-LIG is relatively acidic and could degrade the polymeric matrix during the process. Therefore, the apparent molar masses of neat ABS and the composites were measured by SEC (Figure 81). It appears clearly that the incorporation of LIG or P-LIG does not degrade the polymeric matrix since the apparent M_n remains stable around 50 000 g.mol^{-1}. Therefore, P-LIG is used with different coadditives in the next steps of the screening. The results are presented in the next sections.
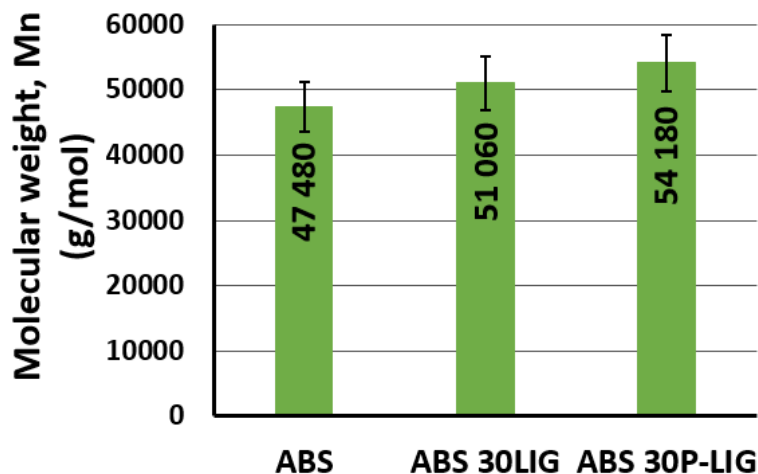
Figure 81. Apparent molar mass of ABS composites with LIG or P-LIG

3.2.   Phosphorus-based-coadditives

In the previous section, the phosphorylation of lignin led to enhanced FR properties of ABS. It was then decided to investigate the influence of phosphorus-based coadditives used in combination with P-LIG, and to evaluate the effect of an increase of the phosphorus amount. The use of phosphorus-based additives to substitute halogenated compounds gained a lot of interest in the field of flame retardancy of styrenics: phosphates and phosphonates [191–193], aromatic phosphates [194], metal salts of alkylphosphonic acids [111,195–197], red phosphorus [198] and ternary (or more) systems included phosphorus based molecules [199–204] are well investigated. In this context, two commercial phosphorus additives which already demonstrated FR performance in ABS, ammonium polyphosphate (APP) [205] and aluminium diethyl phosphinate (OP1230) [206] were considered. Because the aim of this work is to valorize lignin, a LIG/coadditive ratio of 3:1 at a global loading of 30 wt.% in ABS was chosen.

The formulations were tested with R-MLC. The curves are shown in Figure 82, and the numerical data in Table 29. The formulations with both P-LIG and additives ignite slightly faster than P-LIG alone. In terms of pHRR, no significant improvement is observed in comparison to P-LIG. Indeed, reductions of 50, 56 and 54 % are considered similar since the uncertainty of pHRR is about 10 %. However, THR is significantly reduced from 24 % for P-LIG to 40 % and 43 % when P-LIG is combined with OP1230 and APP respectively. This difference is mainly caused by the longer combustion time obtained with P-LIG alone. Indeed, the time to flame out occurs around 530 s for OP1230 and APP, while the sample burns until 817 s for P-LIG. It is noteworthy that the chars did not collapse with OP1230 or APP. Residues look similar, even if a larger weight loss occurred in the case of APP.
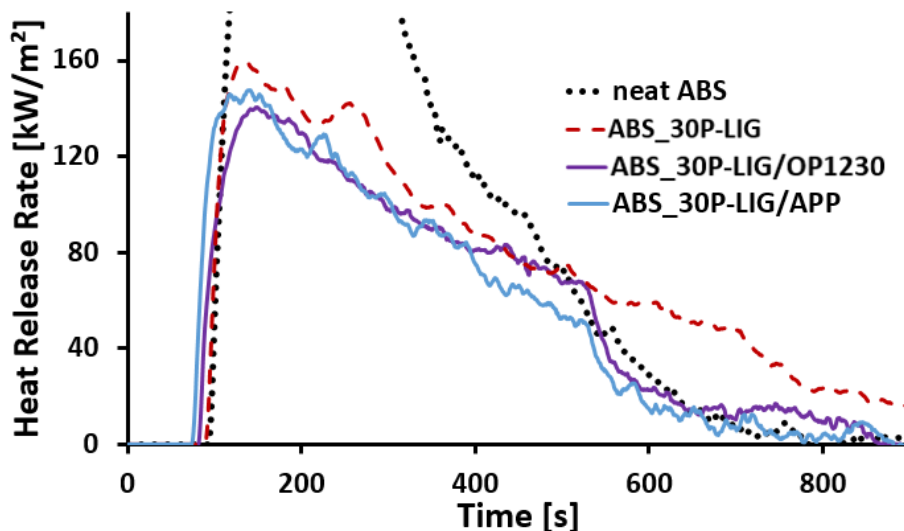
Figure 82. R-MLC curves of formulations with P-LIG and APP or OP1230

Table 29. R-MLC data of formulations with P-LIG and APP or OP1230

Formulation	TTI [s]	pHRR [kW/m²]	THR [MJ/m²]	Residue [wt.%]
Neat ABS	96	318	84	1
ABS_30P-LIG	91 (- 5)	160 (- 50%)	64 (- 24 %)	26
ABS_30P-LIG/OP1230	84 (- 12)	141 (- 56%)	50 (- 40 %)	28
ABS_30P-LIG/APP	76 (- 20)	147 (- 54 %)	48 (- 43 %)	17

The FR performance of ABS composites were slightly improved by combining P-LIG with OP1230 or APP according to the further reduction of THR. These additives are known for their actions mainly in the gas phase for OP1230, and in the condensed phase for APP. Different mechanisms were probably involved, and both led to a faster extinction of the sample.

3.3. Metallic-based additives

Organic or inorganic metallic based additives are often used in the flame retardancy of polymers. For example, they can act as synergist in a FR system when they are incorporated at low loading. Several studies deals with the use of Lewis acid-type transition metal chloride, ie $NiCl_2$, in ABS

[206–208]. Such metallic-based compounds increase the thermal stability of ABS by interacting with cyano groups of ABS thus producing non-volatile char, especially $FeCl_3$ showed an interesting activity [209], Moreover, $FeCl_3$ [69] and metallic acetates [137] shown interaction with lignin, and therefore could be considered as potential FR synergist in ABS. For these reasons, $FeCl_3$ and $NiCl_2$ were incorporated with P-LIG in ABS (ratio 70/29/1). In the frame of this study, Safire® series is a good candidate as it combines melamine with metal polyphosphates [210,211]. Safire® 200 (S200), Safire® 400 (S400) and Safire® 600 (S600) are respectively based on aluminum, zinc and magnesium. Their mode of action was elucidated by previous work of the lab, in epoxy resins [212] or polyamide 66 [213,214]. However, a higher amount is required. Each Safire® was blended with P-LIG in ABS (ratio 70/20/10).

The formulations were tested with R-MLC. The curves are shown in Figure 83 and the data in Table 30. The incorporation of ferric and nickel chlorides induces antagonism effects since the pHRR is increased by 14 %. Despite a shorter combustion time (around 550 s versus 726 s), the incorporation of $FeCl_3$ and $NiCl_2$ at 1 wt.% loading did not permit to improve the FR performance of the ABS/P-LIG composite. The same conclusion can be drawn regarding the formulations with Safire®. A slight antagonism effect is also observed (see the increase of the pHRR) while no further reduction is noticed of THR. Only S200 leads to shorter time of combustion than that with P-LIG alone (566 s versus 726 s).
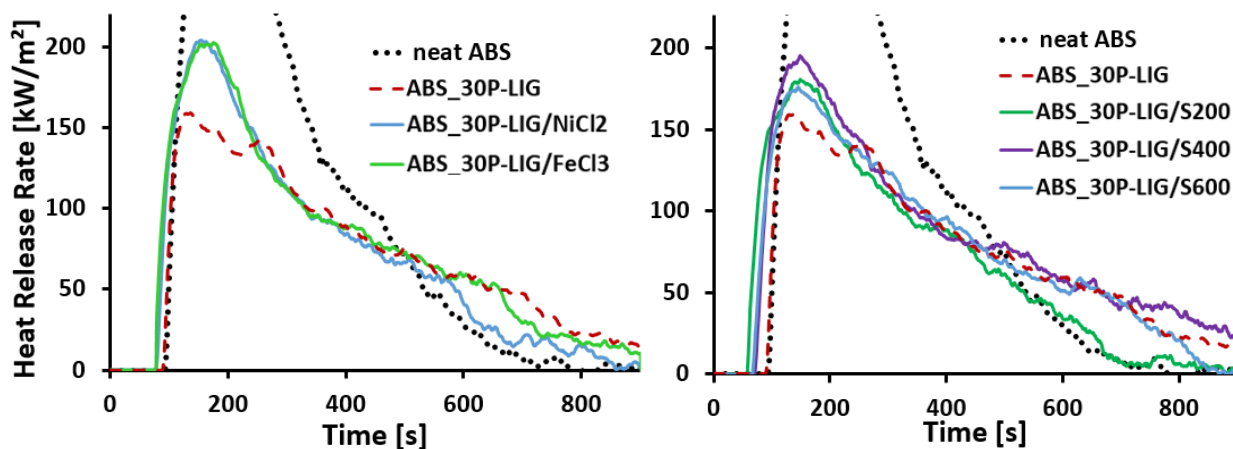
Figure 83. R-MLC curves of ABS formulations with P-LIG in combination with metallic compounds

Table 30. R-MLC data MLC curves of ABS formulations with P-LIG in combination with metallic compounds

Formulation	TTI [s]	pHRR [kW/m²]	THR [MJ/m²]	Residue [wt.%]
Neat ABS	96	318	84	1
ABS_30P-LIG	91 (- 5)	160 (- 50%)	64 (- 24 %)	26
ABS_30P-LIG/NiCl₂ (70/29/1)	81 (- 15)	204 (- 36%)	62 (- 26 %)	19
ABS_30P-LIG/FeCl₃ (70/29/1)	78 (- 18)	202 (- 36 %)	68 (- 19%)	16
ABS_30P-LIG/S200 (70/20/10)	60 (- 36)	180 (- 43 %)	59 (- 30 %)	13
ABS_30P-LIG/S400 (70/20/10)	73 (- 23)	195 (- 39 %)	74 (- 12 %)	12
ABS_30P-LIG/S800 (70/20/10)	69 (- 27)	176 (- 45%)	67 (- 21 %)	19

The use of metallic based additives in combination with P-LIG as synergists or co-additives was unfortunately not successful to further improve the FR performance of ABS according to MLC. Slight antagonism effects were even observed as pHRR was increased. Moreover, the catalysis of the charring process, which was expected, did not occur according to the amount of residue.

3.4. Nanoparticles

Nanoparticles are another alternative to flame retard polymers (see section 2.1.3.2, p53), and many studies were undertaken regarding ABS or its derivatives. For example, mineral hydroxides [215], carbon nanotubes [216] and clays [217,218] were investigated. Because clays exhibit promising FR properties in styrenics, organoclay C30B was incorporated in the composite ABS_30P-LIG (70/29/1). In the same approach, oligomeric silsesquioxane (POSS) can be used as FR nanoadditive, such as in polyethylene terephthalate [219]. So POSS was added to P-LIG in ABS (70/25/5). Changes mainly in the condensed phase behavior were expected by using these nanoadditives.

The results of R-MLC curves are presented in Figure 84 and the data in Table 31. No significant differences were noticed by comparing ABS_30P-LIG, ABS_30P-LIG/C30B or ABS_30P-LIG/POSS.

The slight reductions of pHRR and THR are in the margin of error of MLC, and the residues looked similar. However, the formulation with C30B exhibited a shorter combustion time (548 s) than that with POSS (786 s) or with P-LIG only (726 s).
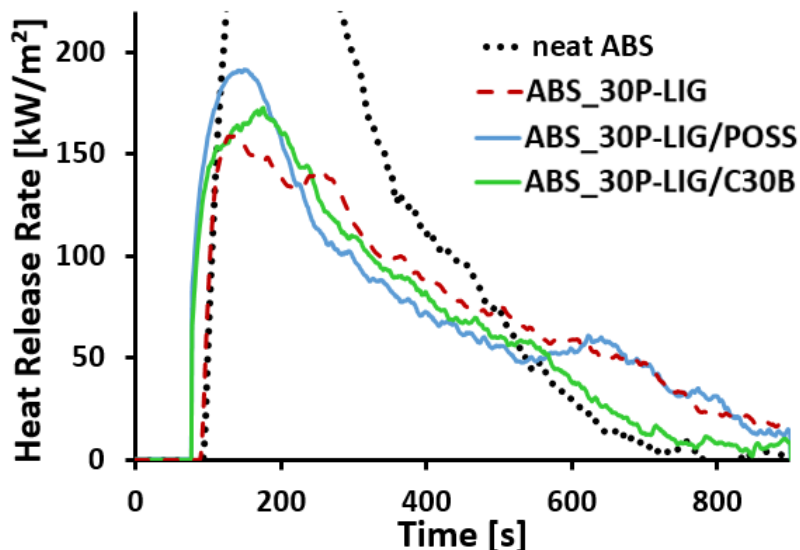
Figure 84. R-MLC curves of ABS formulations with P-LIG in combination with nanoparticles

Table 31. R-MLC curves of ABS formulations with P-LIG in combination with nanoparticles

Formulation	TTI [s]	pHRR [kW/m²]	THR [MJ/m²]	Residue [wt.%]
Neat ABS	96	318	84	1
ABS_30P-LIG	91 (- 5)	160 (- 50%)	64 (- 24 %)	26
ABS_30P-LIG/POSS (70/25/5)	69 (- 27)	191 (- 40%)	64 (- 23 %)	17
ABS_30P-LIG/C30B (70/29/1)	70 (- 26)	173 (- 46 %)	58 (- 31 %)	25

The incorporation of nanoparticles in combination with P-LIG did not permit to further improve the FR performance of the ABS_30P-LIG composite. One reason could be that the total loading of additives is too high. Indeed, nanoparticles require space in order to create exfoliated structure. In this study, the high amount of lignin may disturb the formation of an efficient nanoparticle's network in the char.

3.5. Conclusion

Since ABS composite with neat lignin exhibited promising FR performance, the development of FR formulations based on lignin was undertaken. The reduced MLC was used as FR testing. First, LIG was replaced by P-LIG which permits to improve the FR performance. This enhancement was attributed to the phosphorus grafted to P-LIG. Then, several additives were tried in combination with P-LIG and different strategies were followed. The amount of phosphorus was increased by substituting part of P-LIG with OP1230 or APP. Such formulations exhibited same pHRR than that of ABS with P-LIG, however THR was decreased. Then, metallic based additives were used in order to catalyze the charring process. $FeCl_3$ and $NiCl_2$ were added at low loading (1 wt.%) as synergists while the Safire® series (S200, S400 and S600) were incorporated at higher loading (10 wt.%). The FR performances of the composites were worse than that with P-LIG alone, because of antagonism. Finally, the use of nanoparticles such as nanoclays (C30B, 1 wt.%)) or POSS (5 wt.%) did not permit to improve the FR performance in comparison to P-LIG.

4. Conclusion and discussion

Chapter IV was dedicated to the screening of Kraft lignin as FR additive in different types of polymers and in combination with other FR additives. The first approach consisted in evaluating the influence of neat Kraft lignin, at 30 wt.% on the FR performances of polypropylene, thermoplastic polyurethane, polystyrene, acrylonitrile-butadiene-styrene and polylactide acid. It was that incorporation of lignin in these polymers did not permit to decrease the FR properties of the composites according to LOI and UL-94. However, lignin induces several changes in the behavior of the materials during the combustion with MLC. Interesting behaviors were remarkable especially for PS, ABS and PLA. It appeared that the incorporation of lignin in the polymers leads to the formation of a char and a decrease the heat released by the polymers. However, the composites ignite faster than pure polymers. Because of the influence of LIG in PLA and ABS was particularly remarkable, the next steps of the screening consisted in developing FR systems based on lignin for these both polymers.

The aim of this work is to valorize lignin, so it was considered as the main additive in the formulations. First, several FR systems were tested in PLA. Phosphorylated lignin (see Chapter III)

was incorporated in the polymer but it was shown that it led to degradation of the matrix. Therefore, formulations were developed based only on neat lignin. Several acid sources (APP, sodium phytate and succinic acid) were used in combination with LIG in order to promote the charring. Only APP leads to promising FR performance in PLA. The ratio APP/lignin was then investigated. The larger the amount of APP, the better the FR performance. These results were mostly attributed to the formation of a cohesive char. In the same idea as the screening was conducted for PLA, lignin FR systems were tested in ABS. P-LIG was incorporated in ABS without degrading the matrix, and FR performance were enhanced in comparison to that with LIG. This improvement was attributed to the phosphorylation of LIG. FR coadditives were then combined with P-LIG. Different strategies were adopted. First, phosphorus-based additives, APP and OP1230 exhibited slight improvements of FR performance according to MLC. Then, $FeCl_3$ and $NiCl_2$ (low loading) and Safire® compounds (higher loading) were added as synergists. Catalysis of the charring process was expected. But no further enhancement of the FR performance was noticed. Finally, nanoparticles were tested as potential synergistic agents reinforcing the char. C30B and POSS were tested, but as for the metallic-based additives, the use of nanoparticles in combination with P-LIG was unsuccessful.

According to this screening, some interesting results emerged. Indeed, lignin exhibits promising properties to be valorized as FR additives in polymers. A system combining lignin with a low amount of APP permits to significantly reduce the flammability of PLA. However, phosphorylated lignin cannot be processed in PLA since it leads to a partial degradation of the polymeric matrix. More interestingly, phosphorylated lignin, without other additives, clearly enhanced the FR performance of ABS. The development of this ABS/P-LIG system is promising, and the next step thus consists in investigating the flame retardant mechanisms of phosphorylated lignin in ABS. The next chapter is therefore devoted to an advanced study of the ABS_30P-LIG to find out the mode of action of P-LIG in ABS.

V- Neat and phosphorylated lignin as flame retardant additives in ABS

According to Chapter IV, FR performance of ABS was improved by incorporating 30 wt.% of neat Kraft lignin (LIG). Furthermore, it was shown that these FR properties were enhanced when phosphorylated lignin was used (P-LIG). Based on the thermal decomposition of LIG and P-LIG studied in chapter III, this chapter intends to investigate the mode of action of neat and phosphorylated lignin as FR additive in ABS, and to understand the role of the phosphorus in such FR system. First, ABS/lignin composites are characterized. Potential degradation of the polymeric matrix due to lignin's incorporation and the dispersion of lignin are particularly discussed. Then, FR properties are studied in detail according to MLC, Glow Wire and UL-94. Finally, the last section is devoted to the elucidation of the FR mode of action where thermal stability as well as gas and condensed phases are deeply investigated. To conclude, mode of action of LIG and P-LIG in ABS are proposed.

1. Material properties of ABS/lignin composites

1.1. Incorporation of lignin in ABS: influence on ABS properties?

1.1.1. Chemical structure

Acrylonitrile butadiene styrene (ABS) is a styrene-acrylonitrile copolymer (SAN) in which rubber particles of polybutadiene (PBD) are dispersed. The chemical structure of the monomeric units, butadiene, styrene and acrylonitrile, are shown in Figure 85. Depending on the rubber particles, butadiene exhibits two different types of carbon double bond, $CH=CH_2$ (1,2-butadiene) or $HC=CH$ (1,4-butadiene, configurations cis or trans). Acronyms (in blue in Figure 85) were attributed for each unit and are used in the following. S represents styrene, A acrylonitrile while V means 1,2-butadiene and B 1,4-butadiene (cis or trans).
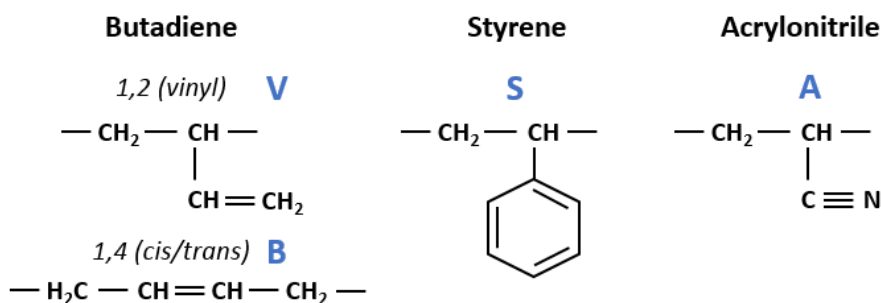
Figure 85. Monomeric units of ABS and corresponding acronyms (in blue)

This section aims to compare the structure of neat ABS with those of ABS/lignin composites and investigate if some degradation occurs during the process. The chemical structure of ABS composites was characterized by ^{13}C solid state NMR (Figure 86 and Table 32). The spectrum of neat ABS is comparable with those reported in the literature [220]. Aromatic carbons are observed between 115 and 160 ppm, including –CH= of 1,2-butadiene and styrene units (143.0 ppm) as well as double bond of butadiene and styrene units (peak centered at 128.3 ppm). Aliphatic carbons of alkyl chains in butadiene, styrene and acrylonitrile are attributed in the range 15 – 60 ppm.

Similar bands are also detected for ABS/lignin composites, which indicates that the carbon skeleton of ABS chains did not change after incorporation of LIG of P-LIG. For both composites, an additional peak at 55.7 ppm appeared, and enlargement of the peak at 143.0 ppm as well as a shoulder in the peak at 128.3 ppm were observed. These changes are attributed to the classical lignin's patterns, since methoxy groups are expected at around 55.0 ppm, double bonds between 100 and 135 ppm, and =C-O around 145 ppm (see Chapter III, section 1.2.2, p107). So it appears that for both ABS and lignin structures no significant changes are detected by ^{13}C NMR after the mixing process.
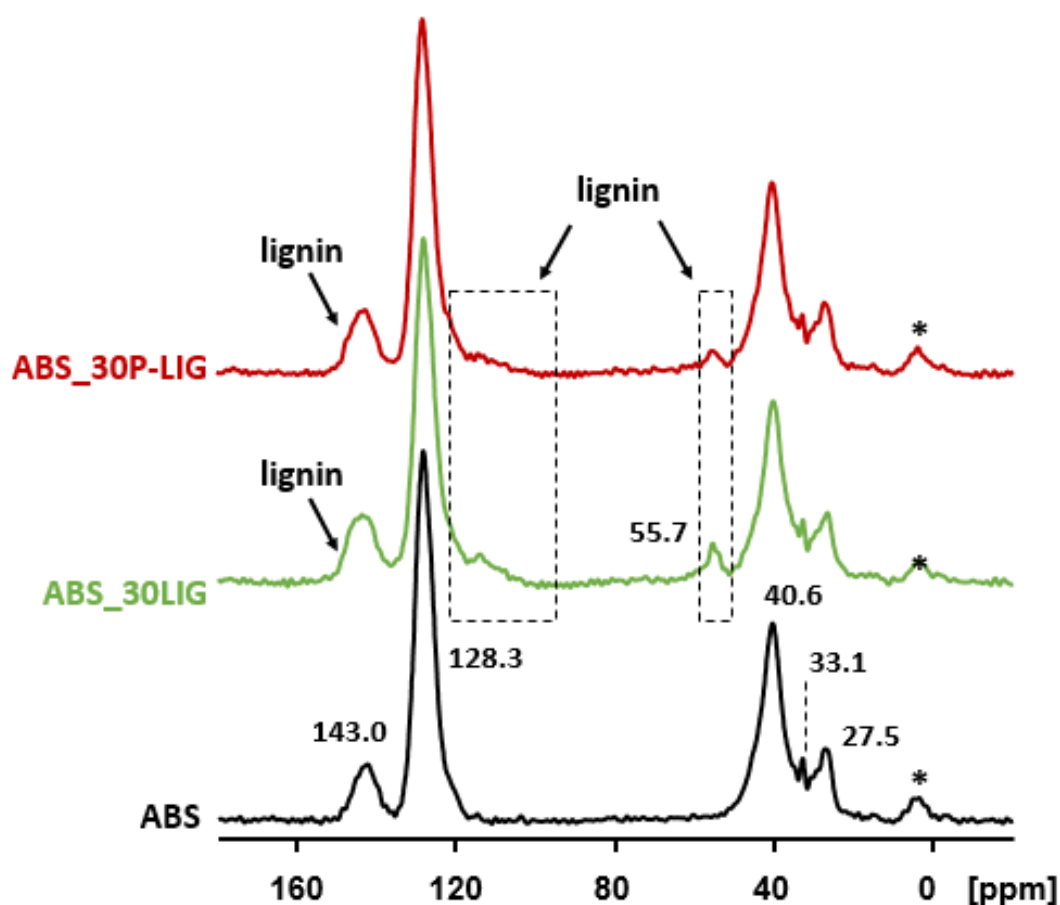
Figure 86. ^{13}C CPMAS NMR of ABS – pure, with LIG and with P-LIG (* = spinning side bands)

Table 32. Chemical shift attributions of ABS pure or with lignin

Type of carbon	Chemical shift [ppm]
Pure ABS [220]	
-CH= (V, S)	143.0
C=C (B, A , S)	128.3
-CH-, -CH$_2$- (A, S)	40.6
-CH-, -CH$_2$- (B, A, V, S)	36-20
Lignin (see Chapter III, section 1.2.2, p107)	
Aromatic C-O	≈146 (shoulder)
Aromatic C-H	125 - 100
O-CH$_3$	55.7

1.1.2. Molar mass

Another way to evaluate if the incorporation of lignin induced a degradation of the ABS polymeric chains is to measure their molar masses. Apparent molar mass were determined by SEC (Table 33, already presented in Chapter IV, see section 3.1, p159). As the uncertainty of this technique is about 10 %, it appears that the apparent molar mass remains constant; between 47480 (neat ABS) and 54180 g.mol^{-1} (ABS_30P-LIG). No decrease was observed, so it can be concluded that the ABS polymeric chains were not degraded with the addition of lignin and the processing.

Table 33. Reminder of apparent molar mass of ABS composites

Formulation	Apparent molar mass [g.mol^{-1}]
ABS	47 480 ± 3 798
ABS_30LIG	51 060 ± 4 085
ABS_30P-LIG	54 180 ± 4 334

1.1.3. Glass transition temperature

The glass transition temperature (T$_g$) is an important property of polymers as it reveals many information about the behavior of the molecular chains in the polymeric matrix. DSC was undertaken to measure the T$_g$ of neat ABS and the ABS/lignin composites (Table 34). Neat ABS

exhibits a T_g of 107.9 °C, which was expected from the supplied technical data. T_g's of ABS_30LIG and ABS_30P-LIG were only slightly reduced, by 3.0 and 2.7 °C respectively. This reduction of T_g may be due to shortened molecular chains [221] or a plasticization effect due to lignin [222]. However it was shown that no degradation of the ABS polymeric matrix occurs. It can be concluded that lignin induces a slight plasticization effect in ABS, which is still observed when lignin is phosphorylated.

Table 34. Glass transition temperatures of neat ABS and ABS/lignin composites

Formulation	T_g [°C]
ABS	107.9 ± 1
ABS_30LIG	104.9 ± 1
ABS_30P-LIG	105.2 ± 1

1.2. Dispersion of LIG and P-LIG in ABS

1.2.1. Dispersion and Interface

The dispersion state of the FR additive may have an influence on the FR performance of the composites. For example, it was shown that in ABS, the better the dispersion of LIG, the higher the FR performance of ABS [94]. Therefore, dispersion of LIG and P-LIG in ABS was investigated by SEM. Figure 87 shows SEM imaging at low magnification obtained with backscattered electrons (BSE), i.e. differentiation between polymeric matrix and particles was achieved by chemical contrast.

LIG is uniformly dispersed in ABS, and exhibits a narrow distribution of particle's size, which ranges from 5 µm for the biggest to less than 1 µm for the smallest particles. Agglomerate's size of LIG is therefore decreased after being processed in ABS. Indeed, average diameter of LIG was assessed around 46 µm (see Table 18, p116). As LIG was not degraded during the process, it can be concluded that agglomerates of LIG were mechanically broken, thus leading to smallest LIG particles dispersed in the polymer. In the case of P-LIG, reduction of particle's size was also noticed when it was processed in ABS, however much bigger agglomerates remained (> 50 µm). P-LIG is also uniformly dispersed, but the size distribution is much wider because of the

agglomerates of different sizes (consequence of the chemical modification). So both lignins are well dispersed in ABS, however P-LIG exhibits much larger particles probably because of agglomerates which were not broken during the process. Shear strength occurring in the material during the mixing, due to the rotor speed and the viscosity, was probably not high enough to break these agglomerates.
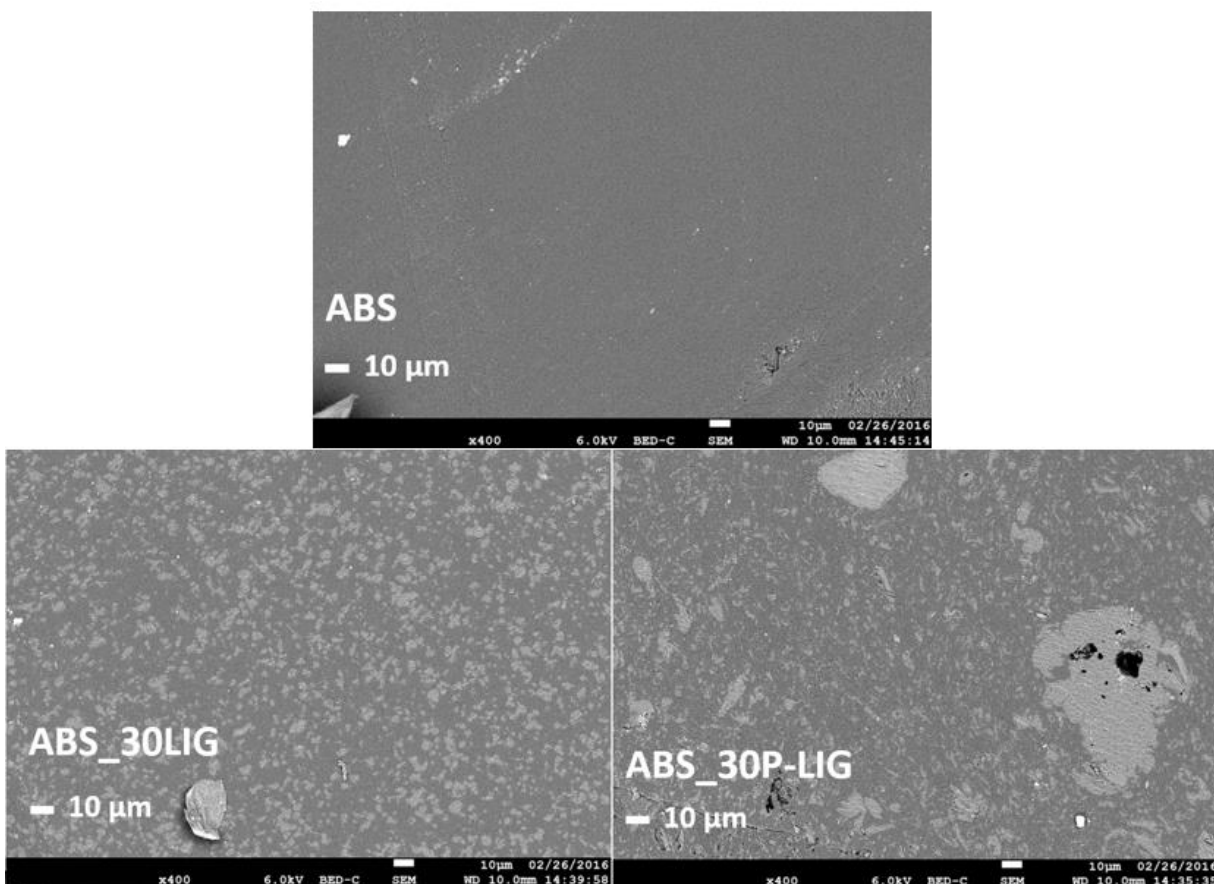
Figure 87. SEM imaging of neat ABS, ABS_30LIG, and ABS_30P-LIG (backscattered electrons)

Figure 88 shows SEM imaging at high magnification of interfaces between ABS and LIG and P-LIG in both ABS_30LIG and ABS_30P-LIG composites respectively. Secondary electrons (SE) mode was selected in order to obtain information about local topography. In both formulations, no cracks or defects were noticed (except streaks due to ultramicrotome cut) indicating a good interfacial compatibility between the ABS and lignin, even if this one was phosphorylated. This was expected as both ABS (due to large amount of styrenic units) and lignin (branched polyphenol) exhibits a

high aromatic character. This is noteworthy to point out that the phosphorylation of lignin does not perturb the compatibility with ABS, but only the particle's size.
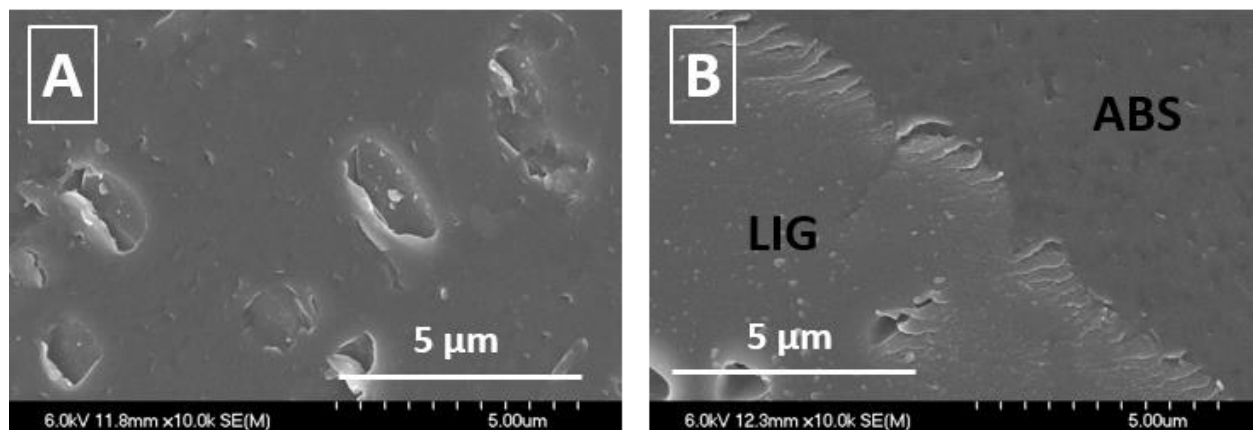
Figure 88. SEM imaging of interfaces between ABS and lignin in ABS_30LIG (A) and ABS_30P-LIG (B) (secondary electrons)

1.2.2. Phosphorus dispersion in the composites

In the case of ABS_30P-LIG, additional SEM imaging (backscattered electron - BSE) and EPMA ^{31}P mapping presented in Figure 89 were conducted to evaluate the phosphorus distribution in the composite. On such mapping, the warmer the color (warm=red), the higher the probability of finding the phosphorus element. The mapping shows that phosphorus is present on the lignin particles. This confirms that phosphorus groups are bonded to the lignin's structure as they remain on the lignin's particles after being processed in ABS. Indeed, the mixing process involved severe conditions, such as high temperature (200 °C) and shear stress (rotors), and "free" phosphorus would have spread everywhere in the composites if not intimately bonded to lignin. So phosphorus is homogenously dispersed on lignin, and it was shown that P-LIG was also well distributed in the ABS matrix. Therefore, phosphorus is homogenously distributed in the composite.
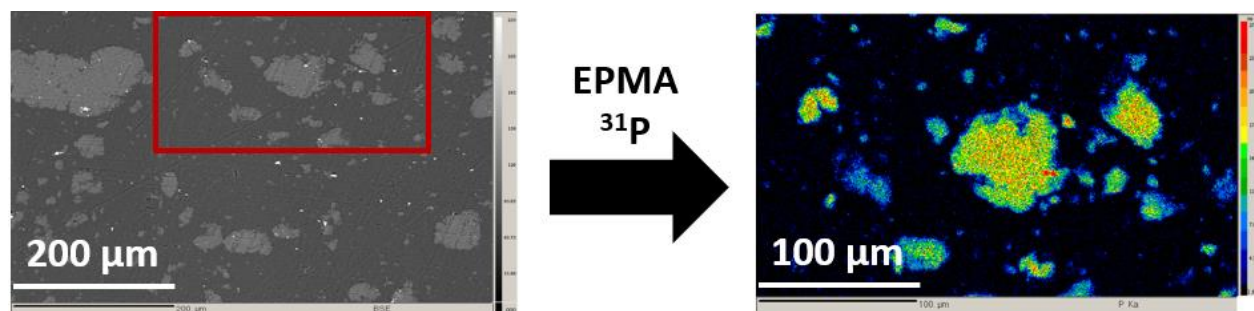
Figure 89. SEM and ^{31}P EPMA mapping of ABS_30P-LIG

Legend – Phosphorus presence probability: dark blue-low, red-high

1.3. Conclusion

In this section, it was found that incorporation of lignin, phosphorylated or not, did not degrade the chemical structure of ABS according to solid state NMR. Moreover, SEC and DSC analysis exhibited that apparent molar masses and glass transition temperatures of the formulations were not significantly changed, thus demonstrating that polymeric chains were not affected. Finally, SEM analysis revealed that LIG was uniformly dispersed in the ABS matrix and formed a homogeneous composite. P-LIG was also well distributed, even if much bigger particles were found (due to the chemical modification process). Moreover, ^{31}P EPMA mapping confirmed that phosphorus remains bonded on P-LIG particles after the process.

2. Fire performance of ABS/lignin composites

The screening presented in Chapter IV on ABS composites was achieved using reduced MLC as fire testing. This section intends to deeply investigate the FR properties of ABS_30LIG and ABS_30P-LIG. The composites are first tested with standard MLC, i.e. the samples size is increased to 10 x 10 x 0.3 cm^3 (in comparison to that of reduced MLC, see Chapter IV). Besides referring to the standard, the sample's size increase also allows a better precision of the FTIR measurements realized during the MLC testing. ABS being widely used in the E&E sector, glow wire testing and UL-94 were performed as these tests are often required for materials used in such applications. Moreover, from the point of view of understanding mode of action, such tests involve different fire behavior than MLC.

2.1. Mass loss calorimetry

2.1.1. Investigation of the heat release rates and weight losses

Mass loss calorimeter (MLC) testing was undertaken on ABS, ABS_30LIG and ABS_30P-LIG with a heat flux of 35 kW/m² in order to simulate a mild fire scenario. The distance between the cone heating element and the sample was set at 35 mm to prevent the char from touching the resistance, if expanding. The curves are presented Figure 90, the data in Table 35 and pictures of the residue in Figure 91.

Virgin ABS exhibits a strong combustion starting after 80 seconds exposure to the heating cone element. The HRR peak reaches 480 kW/m², the total heat released is about 70 MJ/m² and only few ash residue remained (5 wt.%). Addition of 30 wt.% LIG leads to a faster ignition since the TTI is only 50 seconds compared to 80 seconds, but the pHRR is decreased by 43%, the THR is decreased by 13 %. Ash residue of 12 wt.% remains. When LIG is substituted by P-LIG, no further decrease of TTI is noticed while pHRR is interestingly reduced by 58 % and THR by 20 % in comparison to the corresponding values for neat ABS. A bimodal curve is recorded similarly to that of ABS_30LIG. Moreover, the residue is increased by 17 wt.% and seems more cohesive than that obtained with LIG composite. The grey ashes from ABS_30LIG turns into black ordered chunks with P-LIG. These results are in good agreement with those of the Chapter IV.
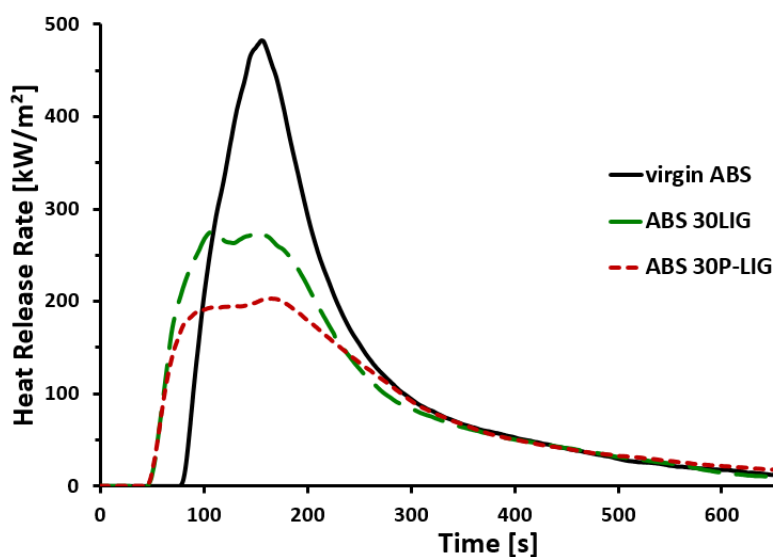
Figure 90. MLC curves of neat ABS and ABS/lignin composites (35 kW/m², 35 mm)

Table 35. MLC data of neat ABS and ABS/lignin composites (35 kW/m², 35 mm)

Formulation	TTI [s]	pHRR [kW/m²]	THR [MJ/m²]	Residue [wt.%]
Neat ABS	80	482	72	5
ABS_30LIG	49 (- 31 %)	275 (- 43 %)	63 (- 13 %)	12
ABS_30P-LIG	49 (- 31 %)	202 (- 58 %)	58 (- 20 %)	17
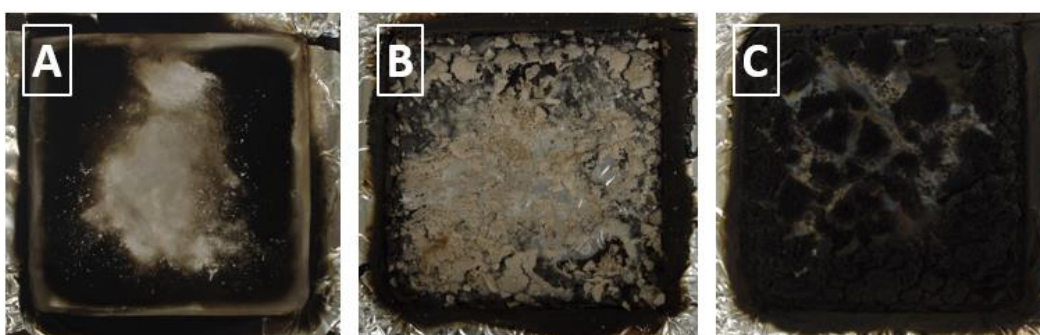
Figure 91. MLC residues of neat ABS (A), ABS_30LIG (B) and ABS_30P-LIG (C)

The combustion of the sample is governed by the fuel release in the flame, and so the curves of the remaining weight were measured as a function of time during the MLC (Figure 92). As expected, neat ABS starts to significantly lose weight around 90 s, in the same time that ignition occurs. The ignition occurs at a critical fuel flux of 0,064 kg/s/m². The mass loss rate is significant until 200 s, and then starts to progressively decrease until 500 s when the residue is close to 5 wt.%. It is in good agreement with the HRR curve, which exhibits a time to pHRR of 170 s. ABS_30-LIG and ABS_30P-LIG start to lose weight at 50 s (in accordance with the TTI of 49 s). The critical fuel fluxes causing the ignition are 0,110 and 0,106 kg/s/m² respectively. Then the MLR is significantly reduced in comparison to neat ABS, as does the ABS_30P-LIG. As for neat ABS, the MLR's begin to decrease around 200 s, just after the pHRR on HRR curves. In the case of P-LIG, the MLR is further reduced in comparison to ABS_30LIG.
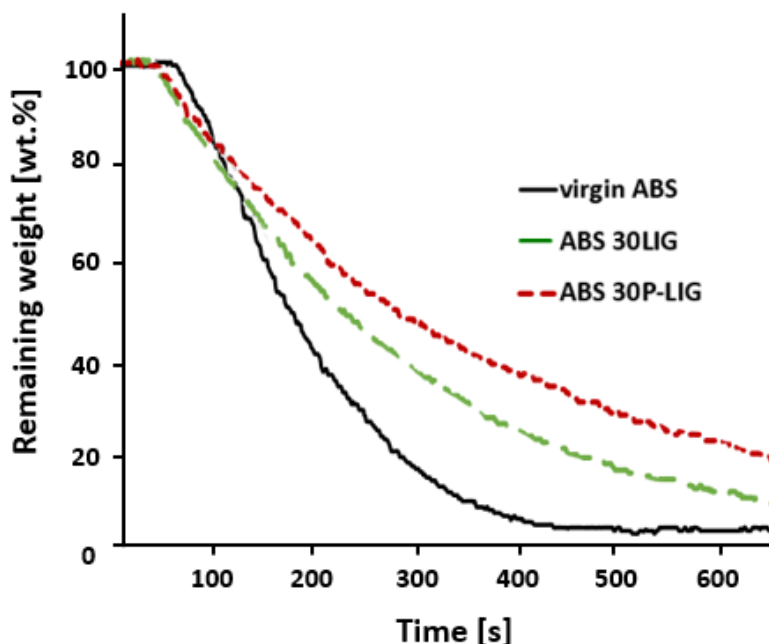
Figure 92. Weight loss of ABS and ABS/lignin composites during recorded during MLC experiment

Incorporation of LIG or P-LIG induces a faster ignition. First, it was seen that the critical fuel fluxes measured at the ignition of the sample was increased with the presence of lignin. So it appears that the composites with lignin degrades faster than neat ABS. One reason could be an increase of the thermal conductivity of the material, which may be expected by the incorporation of aromatic full structures induced by lignin. Higher thermal conductivity means high heat diffusion through the sample: one the one hand, the heat may be evacuated faster, but on the other hand, a higher rise of temperature in the sample may potentially lead to faster degradation of the material. The thermal stability will be therefore investigated in the following in order to evaluate the influence of lignin on the thermal stability of ABS. Moreover, incorporation of lignin in ABS causes change in the sample color from white/beige (neat ABS) to dark brown (ABS_30LIG or P-LIG). Optical properties were changed in the visible wavelength range, and this suggests that optical properties were possibility modified in IR or UV ranges also. Since the samples are submitted to radiative heat in the MLC testing (IR wavelength range), these changes may have an influence on the emissivity and absorptivity of the material. Therefore an increase of the temperature in the sample could occur due to an increased absorption of the radiative heat from the cone. This would imply a higher temperature rise at the surface of the sample and so, the

temperature of ignition is reached sooner. The investigation of all these parameters is complex and may be considered in another study, which could focused on elucidating the optical and thermal properties of the ABS/lignin composites. In this study, because the TTI of ABS is shortened and the critical heat flux increased in the presence of lignin, it is assumed that higher heat absorption coupled with lower thermal stability are the two most predominant phenomena explaining the shorter TTI.

Despite a shorter TTI, significant reductions of pHRR are observed, especially in the case of P-LIG. According to the HRR curves, average mass loss rates (MLR) of the samples were measured for three different time periods (Table 36). The first period, from TTI to 150 s is related to the formation of the char layer at the top of the sample's surface. The average MLR is 0.5 wt.%/°C for neat ABS, and decreased to 0.34 and 0.27 wt.%/°C in the presence of LIG and P-LIG respectively. Since no layer is formed in the case of ABS, a high MLR is noticed. But with lignin, the char layer physically limits the release of fuel, thus explaining the lower MLR's and as a consequence the lower HRR's. The physical barrier appears to be more efficient with P-LIG, as the fuel release is further reduced. Between 150 and 300 s, average MLR of ABS is 0.34 wt.%/°C. Along the combustion, less fuel is available since the amount of unburnt ABS decreased, thus explaining this decrease of MLR. In the case of LIG and P-LIG, the MLR is further reduced, again because of the char layer. However, no significant difference is noticed between both lignins. So when well established, the char layers exhibit the same performance. During the last time period (300 – 600 s), small and localized flames are observed on the samples. It means that possibly, oxygen may reach the surface of the materials, and may induce oxidation of the residues [154]. The oxidation will be commented in the next sections. Because a large part of fuel is already consumed at S3, the MLR is very low (not a lot of material to degrade). Furthermore, no difference is noticed between LIG and P-LIG. However, the amount of residue of ABS/LIG decreases from 41 to 16 wt.% during this time period, which represents 61 % weight loss and in the case of P-LIG, this decrease is about 50 %. So the char residue of P-LIG appears to be more resistant to high exposure time degradation than that of LIG. The higher resistance of the ABS_30P-LIG char may be related to the presence of P, which may prevent the char's oxidation. It would be in good agreement with the conclusion about P-LIG in the chapter III, which proved that phosphorus was preventing the lignin's char from oxidation (section 3.5, p139).

Table 36. Average MLR values between 90 and 200 s of the formulations during MLC experiment

Formulation	MLR (TTI – 150 s) [wt.%/s]	MLR (200 – 400 s) [wt.%/s]	MLR (400 – 600 s) [wt.%/s]
Neat ABS	0.5	0.34	0.05
ABS_30LIG	0.34	0.23	0.09
ABS_30P-LIG	0.27	0.19	0.08

Finally, THR reductions are also noticed, however less impressive than those of pHRR. Indeed, during the combustion, the char starts to crack and collapse, thus allowing further heat release. This is the reason for the second peak of the bimodal curve [134], causing an increase of the THR. Furthermore, the low amount of residue reveals that a large part of the composites was burnt, thus leading to high value of THR.

The enhanced FR performance were attributed to the formation of a char layer which limits the fuel release in the flame, thus reducing the HRR. Moreover, it was found that this layer was more effective with phosphorylated lignin. This conclusion was achieved by analyzing only the condensed phase during MLC. In the following, the gas phase is investigated.

2.1.2. Gas phase analysis: MLC coupled FTIR

The MLC coupled FTIR test is entirely different from the TGA coupled FTIR or PCFC since it is undertaken in fire conditions. Parameters such as the presence of the flame, the mass and heat transfers, the sample size as well as the atmosphere are responsible for these differences. With this technique, the analyzed gases are released from the flame (when combustion occurs). In order to evaluate the combustion, water, CO and CO_2 were quantified. HCN and NO (only a small amount of NO_2 was detected at the limit of spectrometer's sensibility) were also observed as typical ABS degradation gases from the acrylonitrile units (AN). Gases evolution curves of ABS, ABS_30LIG and ABS_30P-LIG are presented in Figure 93 and the data in Table 37.

Released gases of the three formulations are first compared. For both composites, all gases start to evolve 20 seconds earlier than for neat ABS, in accordance with the TTI. ABS_30LIG releases the same amount of water than ABS while 8% diminution of CO_2 evolution is observed. Both NO

and HCN releases are decreased by 17%. In the case of ABS_30P-LIG, the water is released at a similar amount. Carbon dioxide evolution is further reduced by 23%, and NO by 29%. On the contrary, an increase of 17% of the hydrogen cyanide release is observed.

As expected, the shape of the curves mimics the bimodal MLC HRR curves. For both ABS_30LIG and ABS_30P-LIG, as the pHRR's were reduced in MLC, similar reductions in the release of water, CO_2, CO and NO are observed. Reduction of water is less significant since lignin combustion also produces water (see chapter III, section 3.2, p121). Peaks due to the total release of water, CO_2 and CO decreases more for ABS_30P-LIG, meaning that less fuel was burnt. It is noteworthy that the total amount of CO_2 is particularly reduced. On the contrary, CO evolution is not further decreased, so the CO/CO_2 ratio is increased for ABS_30P-LIG. This means that the combustion is more incomplete. Inhibition process in the flame, change in the composition of decomposition gases or a less energetic flame may be the causes of an incomplete combustion.

In addition, an increase in gas concentration of HCN release is measured. Less HCN was burnt (since it is detected at the top of the chimney), so the oxidative power of the flame was probably decreased. Furthermore, NO release is also further reduced by 29% in comparison to that of ABS_30LIG. This gas being directly related to ABS decomposition (oxidation of nitrogen-based compounds), this suggests that some ABS degradation reactions in the condensed phase may have been changed, thus resulting in a reduction of ABS nitrogen-containing decomposition products. Interactions of P-LIG with ABS matrix will be investigated in the following. Changes in the decomposition pathways or reactions between degradation products and FR may also be considered. In order to explain these results and either confirm or not these assumptions, gas and condensed phase analysis are required. This will be undertaken in the following, but before, further FR tests are presented to continue with the investigation of the FR properties of these composites.
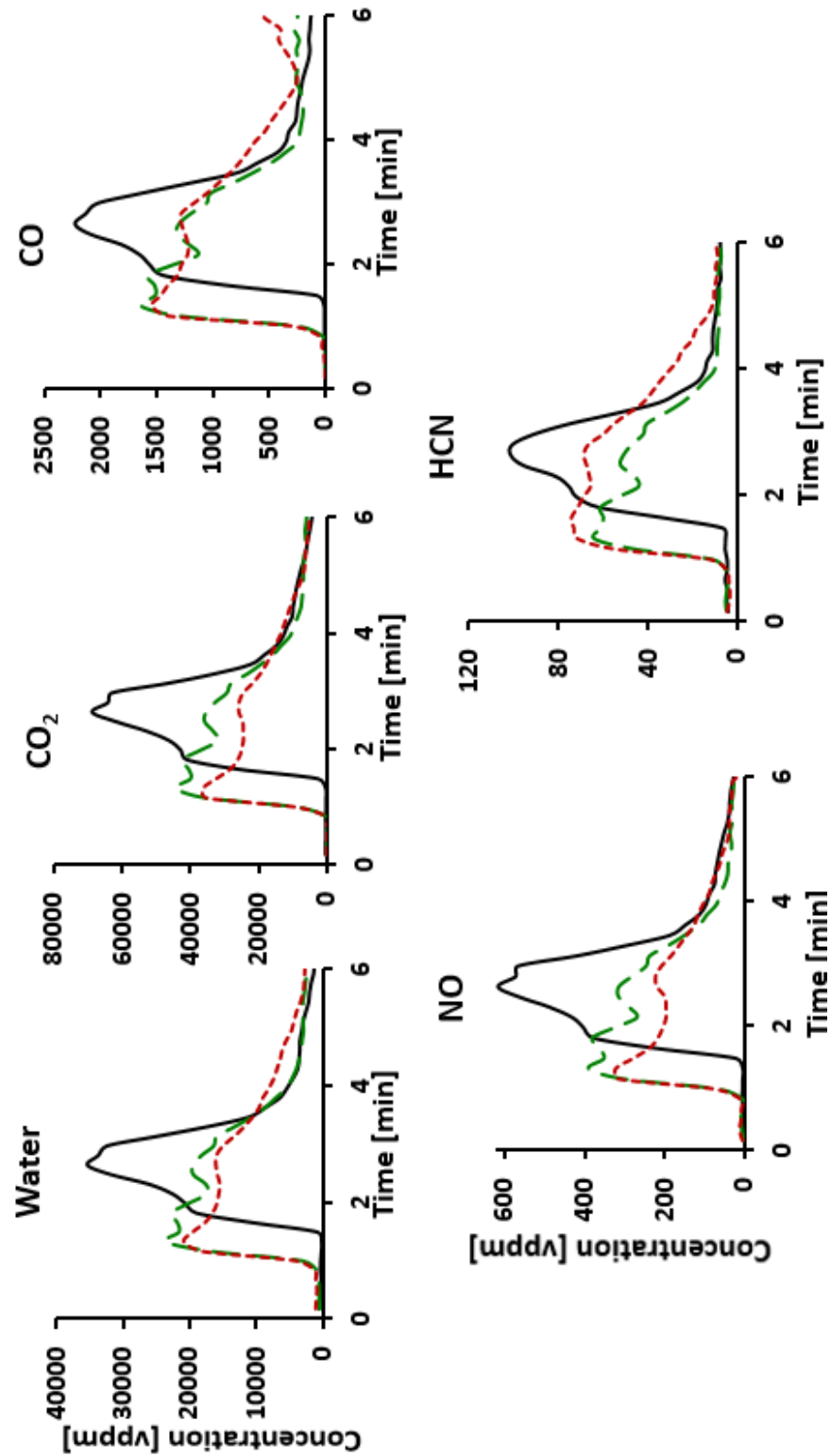
Figure 93. Profiles of selected gases released during MLC test of ABS and ABS/lignin composites

Table 37. Quantification data of the gases released during MLC test of ABS and ABS/lignin composites

	Peak of gases release [ppm]				
	H_2O	CO_2	CO	NO	HCN
ABS	35249	68746	2233	615	101
ABS 30LIG	23685	44477	1642	388	64
	(-23%)	*(-35%)*	*(-26%)*	*(-37%)*	*(-37%)*
ABS 30P-LIG	20818	36260	1565	324	74
	(-41%)	*(-47%)*	*(-30%)*	*(-47%)*	*(-27%)*
	Quantification of gases [ppm]				
	H_2O	CO_2	CO	NO	HCN
ABS	346032	713528	26412	6310	1107
ABS 30LIG	344293	657549	23181	5216	920
	(-1%)	*(-8%)*	*(-12%)*	*(-17%)*	*(-17%)*
ABS 30P-LIG	334239	550762	26644	4450	1297
	(-1%)	*(-23%)*	*(-0%)*	*(-29%)*	*(+17%)*

From these results it appears that the presence of phosphorus in the lignin's structure enhances the FR properties of the ABS composite according to MLC. It has to be mentioned that only 1.0 % (g/g) phosphorus is part of the composite. As seen in chapter III, 3.0 % (g/g) of phosphorus is indeed found in the lignin and the loading of P-LIG in the composite is set at 30 wt.%. Even with low phosphorus content, a positive effect on FR performances is achieved. So phosphorylation of lignin seems to be very promising in terms of flame retardancy. Glow wire and UL-94 tests were performed to complete the MLC results, and are discussed in the next part.

2.2. Glow Wire and UL-94 testing

The experimental conditions differ completely from the MLC which is a radiative test. In the case of glow wire, physical contact is established between the sample and a metal wire heated at high temperature. In UL-94, the sample is directly submitted to a flame. Different phenomena are therefore occurring, and so the measured properties can induce different and complementary conclusions than those of MLC. The results of both glow wire and UL-94 tests are presented in Table 38.

Neat ABS exhibits a GWT of 675 °C, and a GWFI of 700 °C. Incorporation of LIG in ABS did not permit to enhance the GWT, which remains stable at 675 °C. Moreover, it led to a diminution of the flammability index, from 700 °C to 650 °C. The use of P-LIG instead of LIG induced better performance. Indeed GWT, as well as GWFI, were increased both at 725 °C. So incorporation of phosphorylated lignin permits to improve the performance of ABS according to Glow Wire. This improvement was due to the phosphorylation of lignin, since neat lignin was not efficient. The phosphorus, which was shown to be evenly distributed in the composite, may prevent the composite to ignite by acting either in the gas or the condensed phase, or both. Indeed, gas phase can delay ignition by releasing phosphorus-based compounds which exhibit radicals scavenging action. It would results in less exothermic radicals' reactions, and therefore a delay of the flame formation. In this test, the condensed phase action is attributed to char formation, which limits contact between the polymer (the fuel) and the hot wire.

Table 38. Glow wire and UL-94 results of neat ABS and ABS/lignin composites

Formulation	GWT* [°C]	GWFI** [°C]	UL-94 (3.2 mm)
Neat ABS	675	700	N.C
ABS_30LIG	675	650	N.C
ABS_30P-LIG	725	725	N.C

* GWT – Glow Wire Temperature //** GWFI – Glow Wire Flammability Index

UL-94 revealed that neat ABS is not classified. It starts burning from the first flame application. A large amount of dark smoke is noticed, and the flame spreads up to the clamps. Strong flaming occurs, and ABS burns totally but no drops are observed. When LIG or P-LIG is incorporated in ABS, no significant change occurs. Samples exhibited more and increased amount of char, however it was not enough to stop the combustion. This also proves that if a gas phase action takes place with P-LIG, it is not significant enough to prevent the composite from burning. The composites exhibit the same behavior than neat ABS, and are therefore also not classified.

Although the addition of neat lignin in ABS decreased the FR performance of the composite according to glow wire, a significant improvement was observed when phosphorylated lignin was used. However, no improvement was noticed at UL-94, as neat ABS and ABS/lignin composites

were not classified and all exhibited the same behavior. In all cases, a charring phenomenon was observed, suggesting some condensed phase actions. A gas phase action may still be considered, but further tests are required to confirm this assumption.

2.3. Conclusion

FR performance of neat ABS and ABS/lignin composites were evaluated by three different FR tests. Mass loss calorimeter, glow wire and UL-94 were considered as they induce different conditions. MLC is exposing the sample to heat by radiation, while glow wire involves physical contact with a high temperature metallic wire and UL-94 with a flame. Incorporation of LIG permitted to improve FR performance of ABS in MLC, and further enhancement was noticed with P-LIG. The formation of a char layer and a less intense flame were observed and may be responsible for these improvements. In glow wire, only P-LIG led to enhanced performance as GWT and GWFI were the highest for ABS_30P-LIG formulations. So phosphorus appeared to play an important role. Finally, no change was noticed with UL-94, and neat ABS as well as ABS/lignin composites were not classified. These results show that FR performances are induced by complex mode of action of LIG or P-LIG, in condensed phase for sure, and maybe in gas phase too. The next section is devoted to investigate how LIG and P-LIG act as FR additives in ABS.

3. Comprehension of the mode of action

In order to explain the results obtained in the FR tests and also how lignin acts as flame retardant, the modes of action of LIG and P-LIG in ABS were investigated with different techniques. At this point of the study, it seems that the formation of a char layer in the condensed phase is the predominant phenomenon responsible for these promising FR performance. The aim is now to explain the formation of the char, if any gas phase action occurs, and why P-LIG is a better FR additive than LIG in ABS. Before ignition and after flame extinction, the material is exposed to a heat source and degrades in thermo-oxidative conditions. Then, during the combustion of a polymeric material, it is assumed that when the flame is intense enough, all the oxygen is consumed and so the material is considered to degrade in pyrolytic conditions [154]. However, when the combustion is decreasing, localized flames are observed, and oxygen may reach the material and induce oxidation. It is therefore noteworthy to study how a material behaves under

thermo-oxidative and pyrolysis conditions. Thermal stability was studied with TGA. The gas phase was analyzed thanks to TGA-FTIR, Py-GC/MS, and the combustibility by PCFC. Finally solid state NMR and rheometer were used to characterize the condensed phase.

3.1. Investigation of the thermal stability

3.1.1. Thermo-oxidation of ABS and ABS/lignin composites

The thermal stability of neat ABS and ABS composites in thermo-oxidative conditions was investigated by TGA (Figure 94 and Table 39). The decomposition of ABS involves an apparent two-steps process. The first step ranges from 291 to 376 °C with a weight loss of 75 wt.%. This step is attributed to degradation of PBD and depolymerization of the SAN structure [223]. The second step is the formation of a transient char commonly observed in styrenics [224], occurring from 425 to 570°C which then decomposes entirely (25 wt.%) such that no residue is left.

A similar two steps decomposition process is observed for ABS_30LIG. But the decomposition starts 28°C lower when 30 wt.% LIG is incorporated in ABS. Then LIG enhances the thermal stability of ABS for the first step of decomposition by reducing the MLR from 1.0 to 0.7 wt.%/°C. It results that the amount of the transient char is increased by 40 wt.% instead of 25 wt.% for ABS. However, at higher temperatures, LIG destabilizes the transient char, i.e T_{MAX} (2) is 26 °C lower than that of neat ABS, and an increase of the MLR maximum from 0.4 to 1.3 wt.%/°C is observed. Considering P-LIG, it leads to comparable thermal stabilization of the first step as with LIG, by increasing even more the transient char amount to 47 wt.%. But the second step is also stabilized. The MLR maximum is indeed only slightly increased by 0.2 %/°C, while the temperature range is significantly enlarged as the degradation ends at 625 °C instead of 570 °C for neat ABS. In conclusion, the phosphorylated lignin permits to significantly enhance the thermal stability of ABS under air atmosphere.
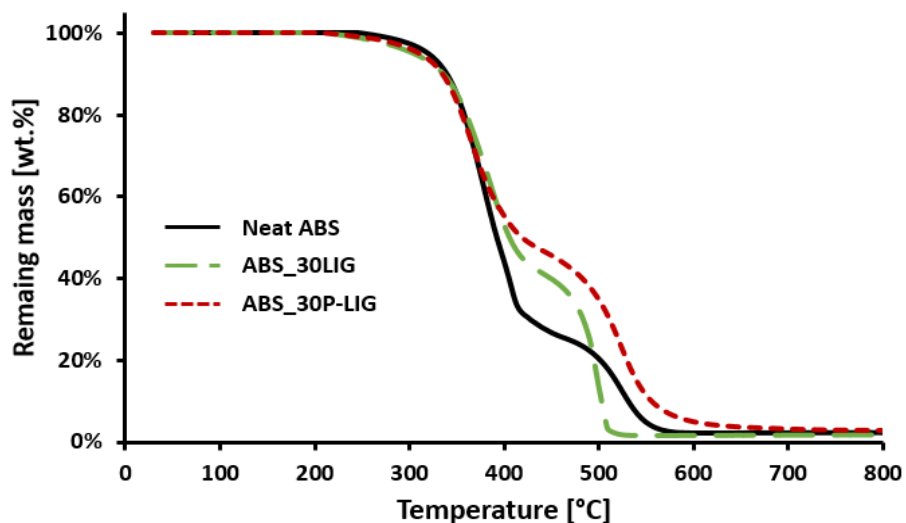
Figure 94. Thermo-oxidative degradation of ABS, ABS_30LIG and ABS_30P-LIG (Air, 10 °C/min)

Table 39. TGA data of neat ABS and ABS/lignin (Air, 10 °C/min)

	Thermo-oxidative atmosphere					
	$T_{2\%}$ [°C]	T_{MAX} (1) [°C]	DTG_{MAX} (1) [%/°C]	T_{MAX} (2) [°C]	DTG_{MAX} (2) [%/°C]	Res [%]
Neat ABS	291	376	1.0	523	0.4	1.0
ABS_30LIG	263	384	0.7	497	1.3	1.8
ABS_30P-LIG	273	364	0.7	521	0.6	2.7

(1) – First step of degradation   (2) – Second step of degradation

In Figure 95, differential TG curves (see Chapter II, section 2.1.3, p83) were plotted for both ABS_30LIG and ABS_30P-LIG in order to investigate potential interactions between ABS and lignin in thermo-oxidative conditions. ABS_30LIG exhibits a significant stabilization between 350 and 500 °C, followed by an intense destabilization between 500 and 550 °C. It confirms that LIG stabilizes significantly the formulations until 500 °C, however interactions occurring above 500 °C leads to a destabilization of the transient char. Slight destabilization of the formulation occurs between 275 and 390 °C when P-LIG is incorporated in ABS, which then leads to a significant stabilization of the transient char. This stabilization at high temperature (> 500 °C) may be due to oxidation prevention of the transient char thanks to the phosphorus, according to the conclusion of Chapter III. In any case, this suggests that LIG and P-LIG obviously interact with the ABS matrix, each in a different way. These interactions obviously play a role in the charring process.
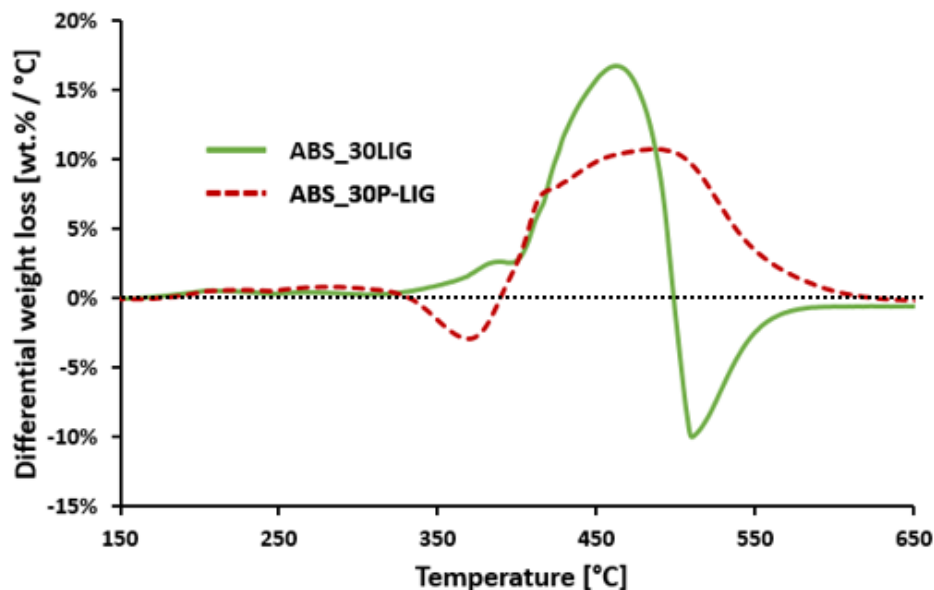
Figure 95. Differential TGA of ABS_30LIG and ABS_30P-LIG (Air, 10°C/min)

3.1.2. Pyrolysis of ABS and ABS/lignin composites

The thermal stability of neat ABS and ABS composites in pyrolytic conditions was also investigated by TGA (Figure 96 and Table 40). ABS exhibits a one-step decomposition process. This step is attributed to depolymerization of the SAN structure and degradation of PBD [223,225,226]. The polymer degrades completely from 347 to 490 °C, with a maximal MLR of 1.8 %.°C occurring at 426 °C. The incorporation of LIG promotes the beginning of the degradation as $T_{2\%}$ is lowered by 81 °C in comparison to neat ABS. Moreover, the maximum MLR is reduced to 1.2 %/°C, and a final residue of 12.8 wt.% remains at 800 °C attributed to the formation of char. Overall behavior is similar with P-LIG, except that T_{MAX} is shifted 10°C higher and the char amount is increased to 15 wt.%. In both cases, it appears that ABS is potentially destabilized.
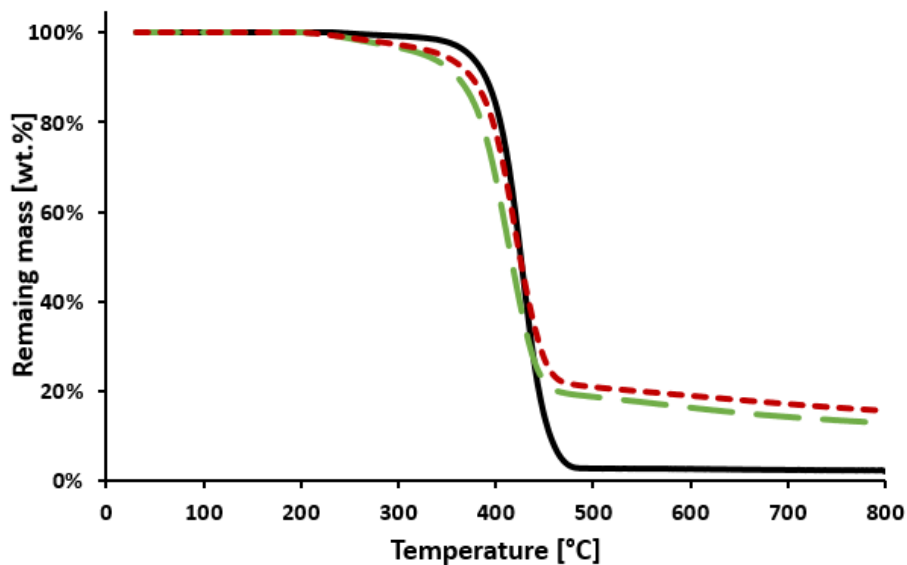
Figure 96. Pyrolytic degradation of ABS, ABS_30LIG and ABS_30P-LIG (N₂, 10 °C/min)

Table 40. TGA data of neat ABS and ABS/lignin (N₂, 10 °C/min)

	Pyrolytic atmosphere			
	$T_{2\%}$ [°C]	T_{MAX} [°C]	DTG_{MAX} [%/°C]	Res [%]
Neat ABS	347	426	1.8	2.2
ABS_30LIG	266	408	1.2	12.8
ABS_30P-LIG	275	416	1.2	15.4

In Figure 97, differential TG curves (see Chapter II, section 2.1.3, p83) were plotted for both ABS_30LIG and ABS_30P-LIG in order to investigate potential interactions between ABS and lignin in pyrolytic conditions. ABS_30LIG exhibits a significant destabilization occurring between 350 and 475 °C. The range of temperature suggests that LIG promotes the depolymerization of the SAN matrix. In the case of ABS_30P-LIG, similar behavior was observed, although ABS was destabilized in a small extent in comparison to ABS_30LIG. It appears therefore that the presence of phosphorus in lignin modifies the interactions between the ABS and lignin in pyrolytic condition by limiting the thermal destabilization of the SAN matrix of ABS.
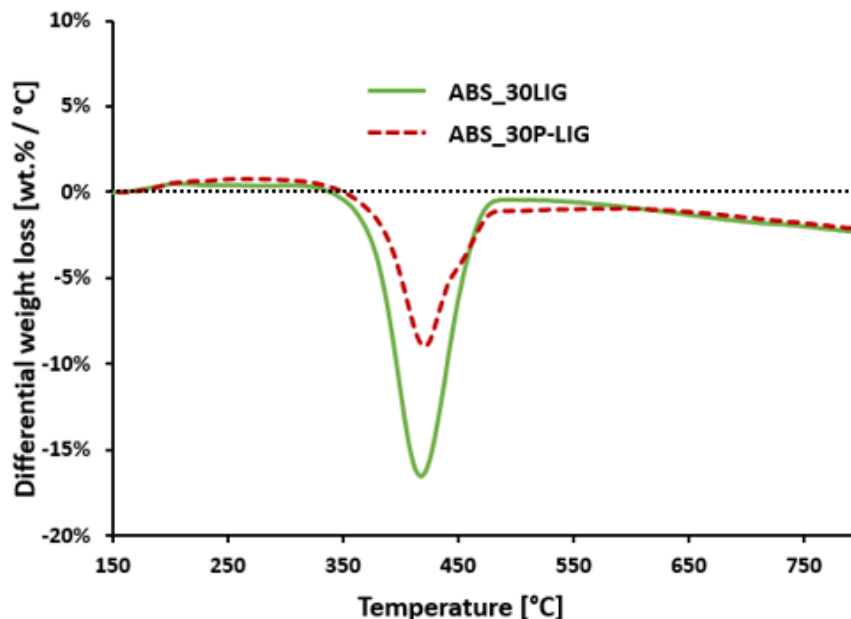
Figure 97. Differential TGA of ABS_30LIG and ABS_30P-LIG (N$_2$, 10°C/min)

3.1.3. Influence of the heating rate on the interactions between ABS and lignin

The thermal stability was firstly studied at a heating rate set at 10 °C/min. In order to investigate the influence of the heating rate on the thermal stability of these composites, TGA were also performed at 1, 5, 20 and 60 °C/min under both inert and oxidative atmospheres. Differential TG curves were therefore calculated and permit to assess the interactions between either LIG or P-LIG with ABS matrix as a function of the heating rate (see Chapter II, p 83). To simplify the charts, only 3 heating rates were plotted: 1 °C/min (the lowest), 10 °C/min (reference) and 60 °C/min (the highest). In pyrolytic conditions (Figure 98) the higher the heating rate, the lower the thermal destabilization induced by LIG. Because the destabilization is less significant, P-LIG permits to limit the destabilization in comparison to LIG, and that at each heating rate. Moreover, it seems that this limitation is more significant as the heating rate increases. However, as a one-step destabilization is observed whatever the heating rage, it appears that no significant changes of interactions occurred in pyrolytic conditions.
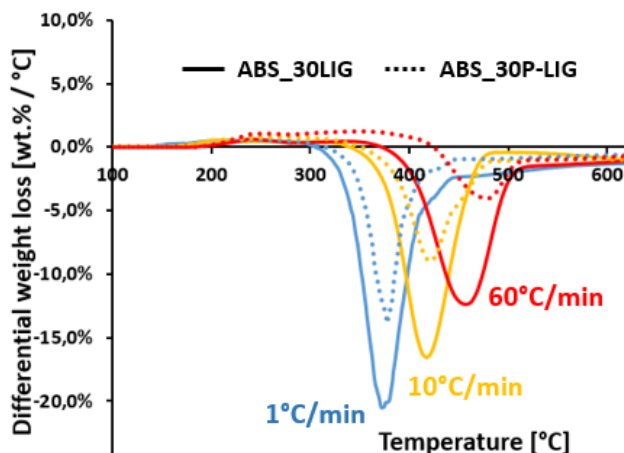
Figure 98. Differential TGA of ABS/lignin formulations at different heating rates in pyrolytic conditions

In thermo-oxidation conditions (Figure 99), interactions are completely different depending on the heating rate. Indeed, the curves significantly change if 1, 10 and 60 °C/min as heating rate is considered. Since the interactions are very similar at 5, 10 and 20 °C/min, only the curves at 10 °C/min are shown. ABS_30LIG exhibits two significant destabilization steps at 1 °C/min, whereas one major stabilization step followed by a destabilization one are observed at 10 °C/min, and almost no interactions occurred at 60 °C/min. In the case of P-LIG, stabilizations take place at 1 °C/min, a significant stabilization is observed at 10 °C, and mainly destabilizations happen at 60 °C. So this reveals that numerous and complex interactions are occurring between ABS and lignin under air. Moreover, the phosphorylation of lignin clearly induces some changes to these interactions. For both LIG and P-LIG, they strongly depend on the heating rate.
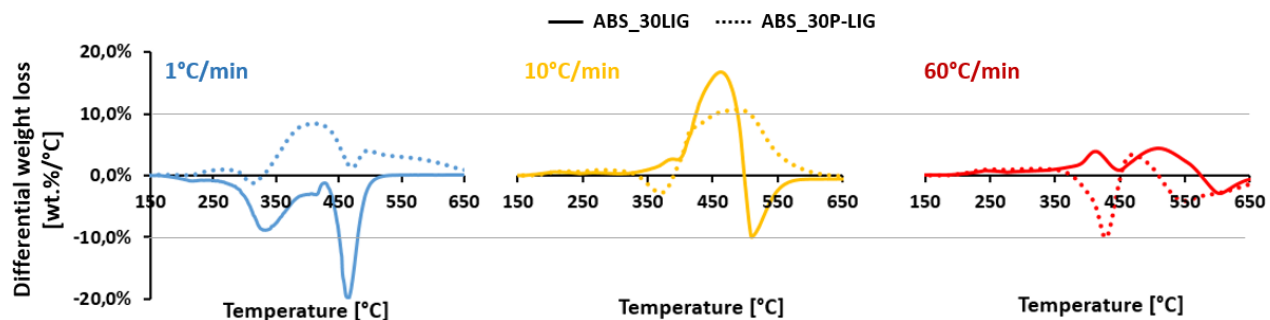
Figure 99. Differential TGA of ABS/lignin formulations at different heating rates in thermo-oxidative conditions

As a conclusion, it appears that interactions are less distinguishable when the heating rate increases. Even if correlations of TGA results with behavior under fire conditions should be done carefully, these results evidence that lignin and ABS interact together during their thermal degradation, and that these interactions are governed by the heating rate (kinetic) in the material. By considering that the more significant interactions occur at a heating rate of 10 °C/min, the following analyses of both gas and condensed phases will be undertaken at this heating rate, when applicable.

3.1.4. Conclusion about thermal stability

In conclusion ABS thermal decomposition undergoes by depolymerization of the SAN chains which overlaps the degradation of PBD particles. It decomposes therefore in a one step process in pyrolytic conditions. In thermo-oxidative condition, an apparent two-step process is observed, as a transient char is formed, which is then totally oxidized at high temperature. It appeared that incorporation of lignin thermally destabilizes ABS, and more specifically the SAN matrix. In pyrolysis conditions, incorporation of LIG and P-LIG permits to limit the MLR and to increase the amount of residue attributed to the formation of char. In thermo-oxidative conditions, both lignins promote the transient char formation. However only P-LIG limits its degradation at high temperature, while LIG destabilizes it in comparison to that of neat ABS. Finally, it was found that in both conditions, ABS and lignin interact together. Moreover, these interactions are governed by the heating rate.

This part revealed that ABS depolymerization was first promoted by incorporating lignin, however these composites were char former materials at high temperatures. These conclusions are in good agreement with the observations of FR testing. The lower thermal stability may indeed explain the shortened TTI of ABS/lignin composites, and their charring behavior responsible of the char layer formation occurring during the combustion. In the next sections, gas and condensed phases of the composites will be further investigated in order to elucidate the mode of formation of the char and the nature of the interactions taking place between ABS and lignins.

3.2. Gas phase analysis

3.2.1. Gas phase generated under thermo-oxidation

TGA coupled with FTIR was used to study the gas phase. The FTIR spectra of the gases released to the characteristic degradation temperatures during thermo-oxidation of ABS and ABS_30LIG are shown in Figure 100. As ABS_30LIG and ABS_30P-LIG spectra were very similar, so those of ABS_30P-LIG are not presented in order to simplify the figure. The spectra are available in Appendix 3, p259. Characteristic temperatures were selected according to the main steps of degradation (beginning, T_{MAX1}, T_{MAX2}) observed on the TG curves previously presented in Figure 94. Temperatures of 300, 376 and 523 °C were chosen for neat ABS and 300, 384 and 497 °C for ABS_30LIG. Some of the species released by ABS are similar to those of lignin, i.e. aromatic species and FTIR does not allow to separate. So interpretations may be complex in certain signals region. Attributions were done according Table 20, p122. Nitrile groups, specific to ABS, were noticed at 2235 cm^{-1} [226]. Because many peaks are overlapping between 2000 and 500 cm^{-1} and hard to distinguish if originating from ABS, lignin or CO_2, the region 2000 and 500 cm^{-1} was not attributed on the chart.

At 300 °C, peaks of water, CO_2 and CO are observed for ABS. CO and CO_2 originates from the air which is the atmosphere gas used in this experiment, while ABS is known to exhibit a high water uptake and so water was probably adsorbed by ABS before the experiment [227]. So it appears that the neat polymer does not degrade at this temperature, as expected. On ABS_30LIG spectrum, an additional signal is noticed around 1700 cm^{-1} attributed to aldehyde and ketone groups of LIG. At 376 °C (T_{MAX1}), the main degradation products of ABS are aromatic compounds (3075 cm^{-1}) and nitrile (2235 cm^{-1}) [226,228]. Similar spectrum is observed for ABS_30LIG at 384 °C with less intense nitrile bands. At 523 °C (T_{MAX2}) which corresponds to the oxidation of the transient char, main gases released are CO_2 and CO meaning that the char structure is oxidized. The similarity between the spectra of ABS and ABS_30LIG were expected as both ABS and LIG release similar compounds (aromatic mostly), which cannot be separated by FTIR in an efficient way.
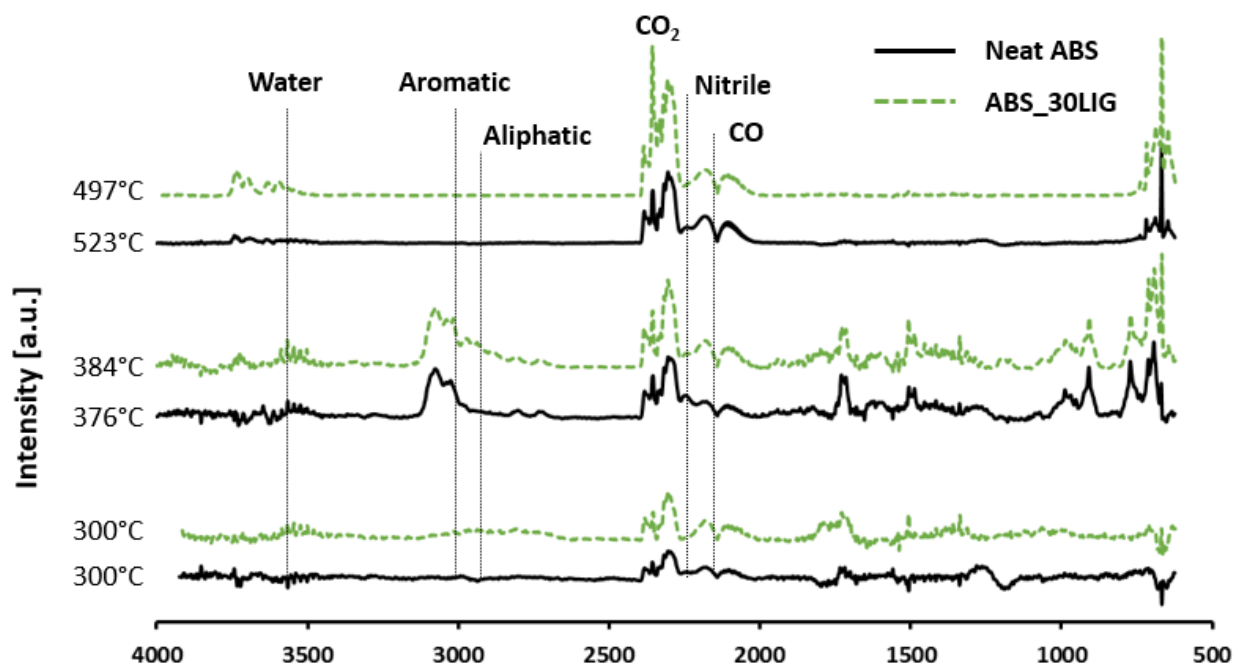
Figure 100. FTIR spectra of the gases evolved during the thermo-oxidative degradation of ABS and ABS_30LIG at characteristic temperatures (10 °C/min)

Since nitrile groups' (CN) evolution (2235 cm^{-1}) is a specific degradation product of ABS, produced by the degradation of acrylonitrile units, it is of interest to follow its evolution as a function of temperature for ABS and ABS/lignin composites (Figure 101). For ABS, nitrile groups are released in two steps and in the same proportion (peaks area). The first peak was attributed to depolymerization of SAN, and the second to acrylonitrile units which were part of the transient char according to TGA analysis. When LIG is incorporated, the first step of decomposition begins at higher temperature (+ 50 °C), while the second step shifts to lower temperature (destabilization of around 50 °C). It is noteworthy that P-LIG leads to a destabilization of only 20 °C. Moreover, ABS_30LIG releases less nitrile than neat ABS during the first step, but more during the second (peaks area ratio). With P-LIG, nitrile evolution is further reduced in the first step, and the second is in-between ABS and ABS_30LIG. These observations show that incorporation of lignin does change the distribution of the release of nitriles species, which confirms that the degradation patterns of ABS (and especially SAN matrix) are modified, which is in accordance with the conclusion of the thermal stability analysis.
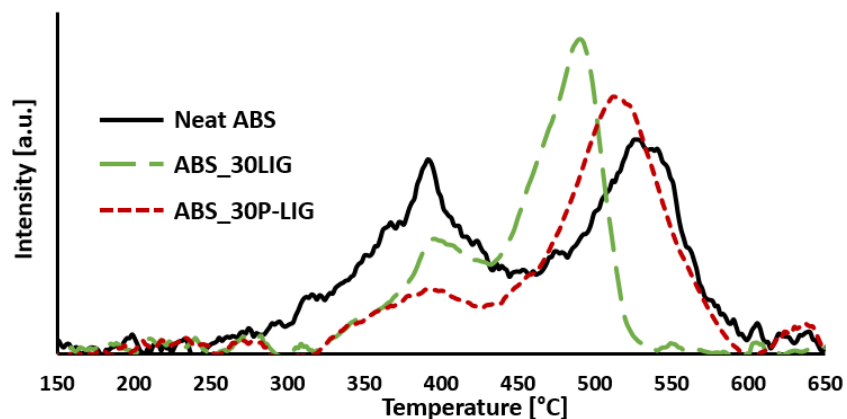
Figure 101. Nitrile groups (2235 cm^{-1}) evolution during the thermal degradation of ABS and ABS/lignin composites (air, 10 °C/min)

According to these results, a hypothesis can be suggested. In the presence of lignin, less nitrile groups are released in the gas phase during the first step of decomposition, attributed to SAN depolymerization. This means that more nitrile groups remains in the condensed phase (according to the fact that no release of NO is observed). It can therefore be concluded that during the depolymerization step of SAN, some nitrile groups interacts with the condensed phase, probably with lignin, under thermo-oxidative atmosphere. But these interactions are influencing the second step, the oxidation of the transient char. Indeed, these interactions with LIG induce a destabilization of the transient char at higher temperature (promotion of the degradation), whereas P-LIG significantly limits this destabilization. A reasonable assumption can be that presence of phosphorus and nitrogen in the condensed leads to a more stable char [200]. So the gas phase analysis allows to indirectly suggest some phenomena occurring in the condensed phase. This must be further investigated in the following.

3.2.2. Gas phase generated under pyrolysis

3.2.2.1. TGA-FTIR under inert atmosphere

In order to characterize the gas released during pyrolysis, FTIR spectra were recorded at characteristic temperatures (Figure 102). These temperatures were selected according to main step of degradation: 375 °C (beginning), 460 °C (end), as well as 426 and 408 °C for the maximum of degradation (T_{MAX}) of ABS and ABS_30LIG respectively (see Figure 96, p191). As previously

mentioned, ABS_30P-LIG spectra are not presented since they are similar to those of ABS_30LIG, in order to simplify the figure. The spectra are available in Appendix 3 p259.

On the spectra recorded at 375 °C, peaks of water, nitriles, aromatic and aliphatic compounds are observed for ABS. Water was probably adsorbed by ABS before the experiment because of ABS water uptake [227]. ABS_30LIG exhibits a very similar spectrum at this temperature. At T_{MAX}, the main degradation products of ABS are aromatic compounds (3075 cm^{-1}), and less significantly aliphatic compounds. Nitrile groups were only slightly observed. As the intensity is relatively low in comparison to styrenics, it is reasonable to conclude that this grade of ABS contains a low amount of acrylonitrile units in comparison to styrene units [226]. Similar spectrum is observed for ABS_30LIG, except that aromatic and aliphatic are released at the same intensity. Methane, originated from lignin (see Chapter III), was noticed at 3015 cm^{-1}. At the end of the degradation step (460 °C), inversion of the ratio aromatic/aliphatic is noticed for ABS where more aliphatic compounds are released. This suggests that the decomposition of PBD lasts longer than the styrene part [226]. The same observation as for neat ABS was done for ABS_30LIG. Because of the similarity between the degradation compounds, FTIR spectra of ABS and ABS/LIG are very similar in pyrolysis conditions.
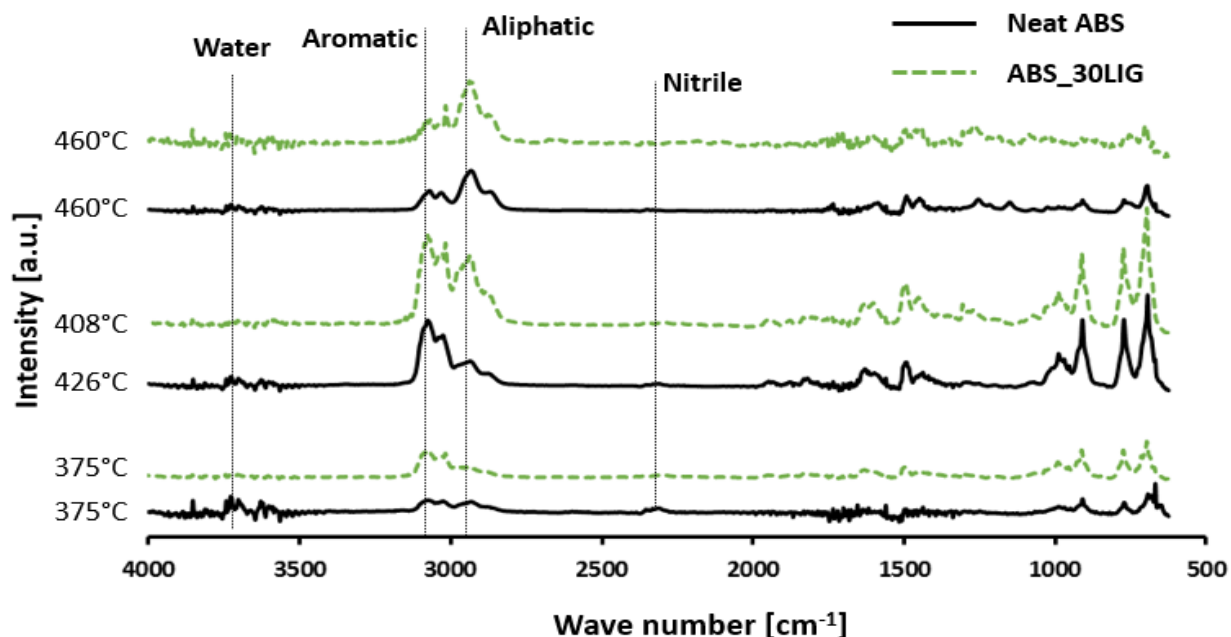
Figure 102. FTIR spectra of the gases evolved during the pyrolytic degradation of ABS and ABS_30LIG at characteristic temperatures (10 °C/min)

3.2.2.2.   Py-GC/MS

Py-GC/MS is commonly used in polymer science to identify polymer's nature or their degradation products [229]. On one hand, Py-GC/MS permits to separate the decomposition products of the gas phase, and elucidate their structures. On the other hand, it is not possible to plot the profiles of gases as a function of the degradation progress (as with TGA-FTIR). Having this drawback in mind, a temperature step approach was considered (see chapter II, section 2.3.3, p93). The aim is to identify each products evolving at each step of the degradation. Neat ABS and ABS/lignin were treated at 350 °C (onset of the main step of degradation), 425 °C (maximum rate of degradation) and 475 °C (end of the degradation step) according to thermal stability analysis previously done (see section 3.1.2, p190).

At 350 °C, degradation products additives of ABS are noticed, as well as some ABS decomposition products, mostly butadiene, styrene derivatives and SAN trimers. This confirms that the ABS matrix starts to degrade at this temperature by PBD and SAN depolymerization (Figure 103). In the case of ABS/lignin composites, additional peaks are observed between 12 and 18 min elution time, attributed to lignin degradation products. Moreover, some additional peaks related to ABS decomposition products (20.5 min) as well as peaks ratios of some ABS decomposition products are changed in comparison to neat ABS. Therefore, it appears that both LIG and P-LIG influences the thermal decomposition pathways of ABS. Differences between the spectra are most obvious at 425 °C, and are therefore commented more in details in the following.
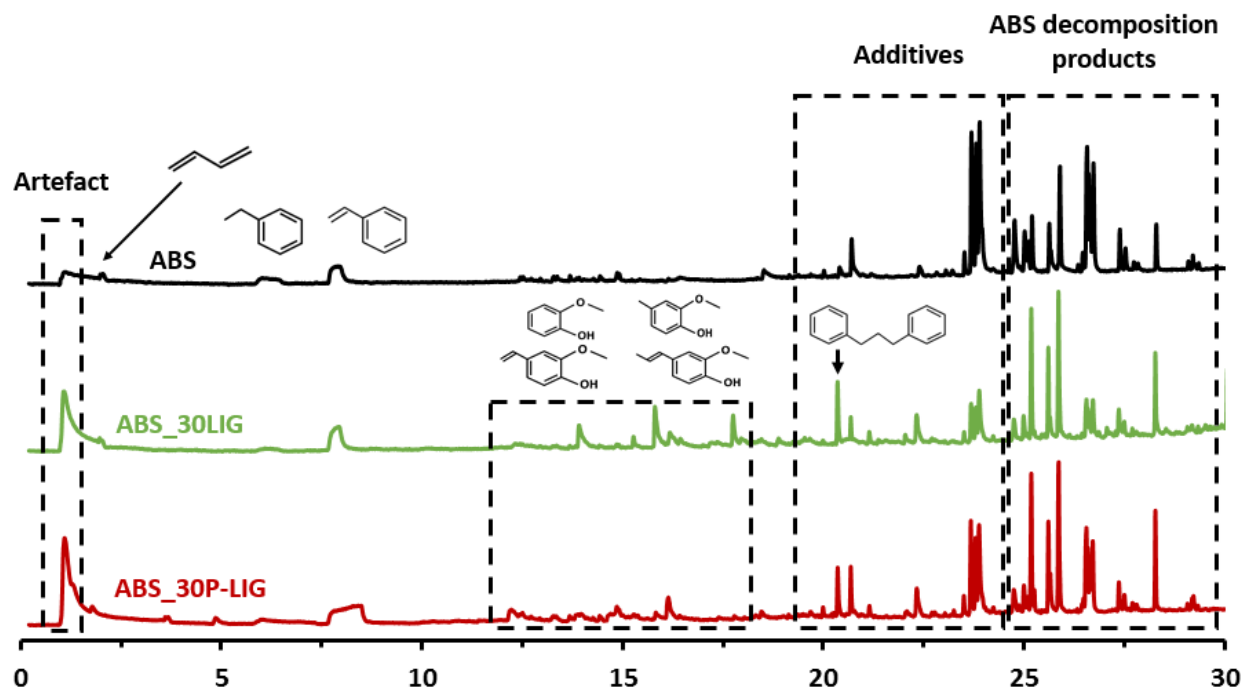
Figure 103. Comparison of ABS, ABS/lignin composites chromatograms obtained at 350 °C

The chromatograms obtained at 425 °C are presented in Figure 104. Each numerated peak was then analyzed in mass spectrometry and the related compounds are presented in Table 41. Spectra of neat ABS is first commented. Compounds from SAN depolymerization such as acrylonitrile (1), toluene (2) and α-methylstyrene (4) are first observed, in a lower amount than styrene (3). These are the monomeric units of SAN matrix. When the temperature of the column increases, dimers (5) or trimers (6) of acrylonitrile-styrene units are released. At higher temperature, dimers (7,8) of styrenic units , trimers of acrylonitrile-styrene units (9, 10, 11) and compounds originated from recombination of S units (12) are observed. Finally, other trimers of acrylonitrile-styrene units (13, 14, 15) and styrene (16) units are observed at longer retention time. These decomposition products were observed in good agreement with other studies [230,231]. Because monomers, dimers and trimers of SAN matrix are the main products released, it confirms that ABS thermal decomposes by depolymerization of the SAN matrix [223,226]. Because no significant change was observed between the formulations at 475 °C, the spectra are shown in Appendix 4, p259.
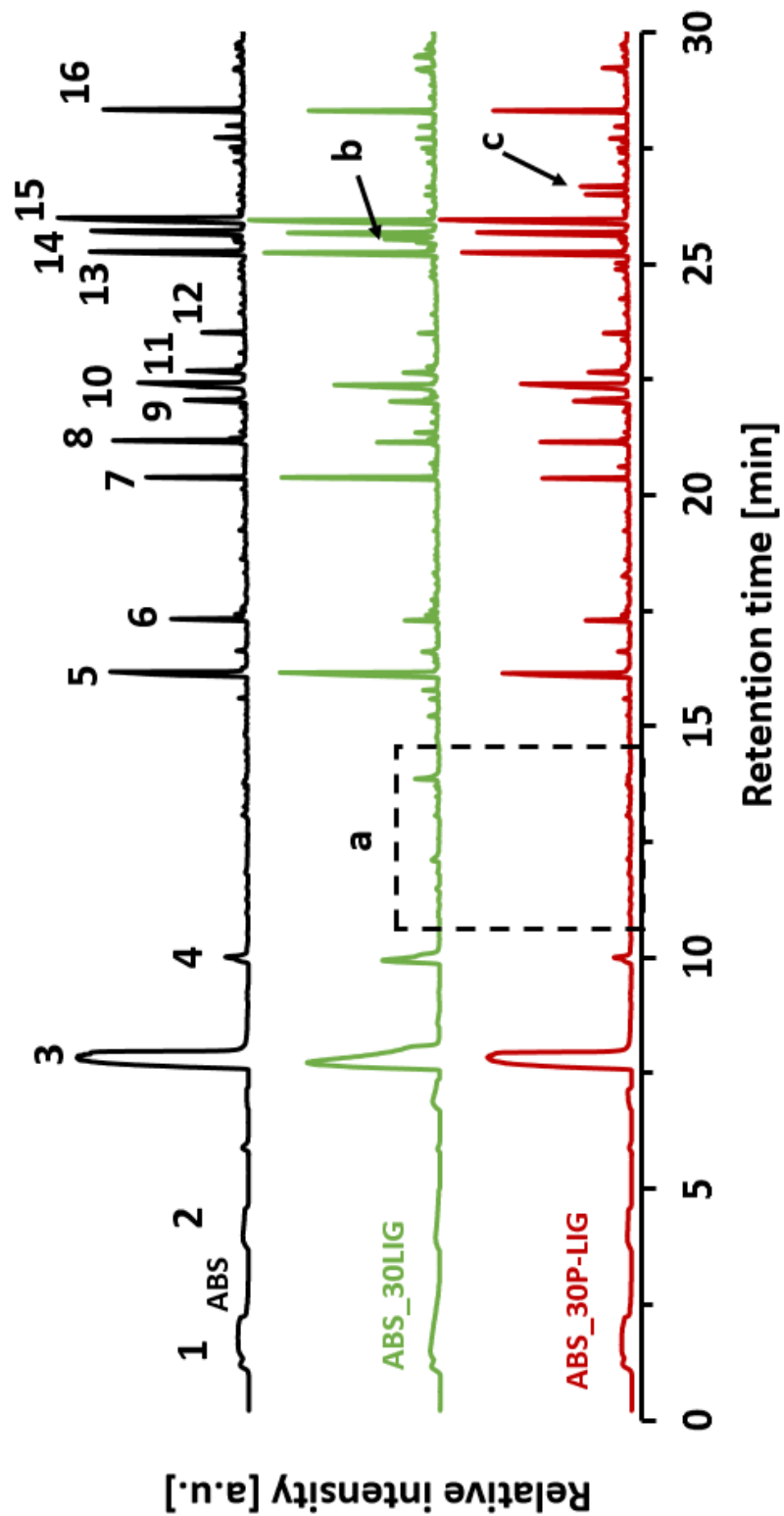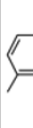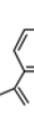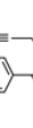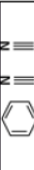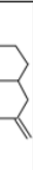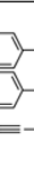
Figure 104. Comparison of ABS, ABS/lignin composites chromatograms obtained 425 °C

	Retention time [min]	M_w [g/mol]	Molecule
1	1.6	53	
2	3.8	92	
3	7.8	104	
4	10.0	118	
5	16.2	157	
6	17.3	157	
7	20.4	196	
8	21.2	208	
9	22.0	210	
10	22.4	210	

	Retention time [min]	M_w [g/mol]	Molecule
11	22.7	210	
12	23.5	236	
13	25.3	261	
14	25.7	261	
15	26.0	261	
16	28.3	312	
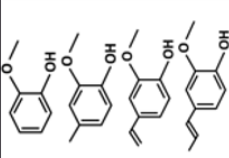
	Retention time [min]	M_w [g/mol]	Molecule
a	10.5-14.5	126	
		138	
		150	
		164	
b	25.9	261	ABS trimer
c	26.7	281	ABS trimer

Table 41. Identification of the main decomposition products of ABS at 425 °C

Decomposition products of ABS_30LIG and ABS_30P-LIG were compared to those of neat ABS in order to evaluate the influence of lignin on ABS thermal decomposition (Figure 104, Table 41). At

first glance, only few differences are noticed between ABS and ABS/lignin chromatograms. All peaks related to ABS decomposition products are still observed, however few additional peaks appear. In the range 11.0-14.5 min (a), decomposition products of lignin are identified. This was expected since LIG and P-LIG are still degrading at 425 °C [26,59]. Then, an additional peak is noticed for ABS_30LIG at 25.5 min (b) identified as another trimer combination of acrylonitrile-styrene units originated from SAN matrix. Another additional peak (c) is also appearing on ABS_30P-LIG chromatogram and is also attributed to another form of trimer from SAN matrix.

Furthermore, changes in area ratios of several peaks occurred in presence of lignin. These were calculated as indicators and shown in Table 42. Such experiment is only semi-quantitative, the approach is only to point out differences (increase or decrease). Ratios of peaks 3 and 4, 5 and 6 as well as 7 and 8 were calculated as example. The compounds related to these peaks are degradation products of the SAN matrix. For example, incorporation of LIG induces an increase of the 6:5 ratio from 0.39 to 4.74. This shows that the dimer 6 is released in larger amount than 5. So changes in ratios reveal that the degradation pathways of the SAN matrix are modified. Moreover, they are more significant in the presence of LIG than those with P-LIG. This confirms that P-LIG limits the destabilization of the SAN matrix in comparison to LIG.

Table 42. Area ratios of selected peaks of ABS, ABS_30LIG and ABS_30P-LIG chromatograms

	Peaks area ratios		
	4 : 3	6 : 5	8 : 7
Neat ABS	0.04	0.39	1.71
ABS_30LIG	0.19	4.74	0.42
ABS_30P-LIG	0.04	0.30	1.17

In conclusion, Py-GC/MS analysis allows to confirm that LIG and P-LIG influences the decomposition pathways of ABS, and especially of SAN matrix. In the previous thermal stability study, it was shown that LIG promotes the degradation of ABS (T_{MAX} is decreased by 18 °C), and P-LIG also but in a smaller extent (- 10 °C). Combining both studies, a reasonable assumption could be that LIG promotes the SAN depolymerization. When P-LIG is considered instead of LIG, the destabilization is limited. Condensed phase analysis is required and will be then undertaken in

order to understand why LIG and P-LIG does not interact in the same way with ABS. But before, since changes occurred in the gas phase composition, combustibility of the composites will be evaluated.

3.2.2.3.   *PCFC*

In order to assess if the changes in the gas phase composition influence the ABS combustion, combustibility of the gas phase was assessed with PCFC (Figure 105 and Table 43). Since the material is pyrolyzed at 60 °C/min in PCFC experiment, the data of pyrolytic TGA are also presented in order to have information about the behavior of the thermal degradation at this heating rate. ABS exhibits single peak starting at 340 °C and centered at 470 °C. The pHRR reaches 602.6 W/g and the THR is 37.7 W/g. When LIG is incorporated, the HRR onset temperature is slightly reduced by 7 °C, and the pHRR occurs 9 °C lower, which is in good agreement with TGA analysis. Reduction of pHRR and THR are 20.2 and 9.6 % respectively. ABS_30P-LIG starts to release combustible compounds at 340 °C, and the peak is centered at 471 °C. In terms of pHRR, the reductions are similar than that of ABS_30LIG considering the margin of error related to the experiment. The residues obtained for both ABS/lignin composites are in accordance with those measured by TGA at 60 °C in pyrolytic conditions.

The neat ABS releases combustible gases when it degrades. Therefore, it is assumed that it will contribute to feed the flame during its decomposition. It is observed that for ABS/lignin composites, HRR and THR are reduced. As the sample is considered thermally thin in PCFC, no limitation of mass transfer can occur (with the formation of a char layer for example) even if charring material is tested. Considering this, it can be concluded that incorporation of LIG slightly reduces the combustibility of ABS. An acceptable assumption could be that decomposition products of ABS reacts with decomposing lignin, thus leading to char formation and a diminution of the combustibles release. Differential TGA investigation confirms this idea, and TGA-FTIR as well as Py-GC/MS analyses revealed that interactions were occurring between the SAN matrix and lignin. Nitrile groups were particularly suspected to be involved in such interactions. Finally, no further reduction of the combustibility was noticed by using P-LIG. Although flame inhibition may have been expected since it is one possible mode of action of phosphorus [171], the phosphorus, according to several analysis, does not act in the gas phase. Nonetheless, P-LIG shifted the peak

of combustion towards higher temperature, as it was shown that it limits the thermal destabilization of the SAN matrix in comparison to ABS_30LIG, probably by acting in the condensed phase, thus influencing the gas phase (see section 3.1, p119).
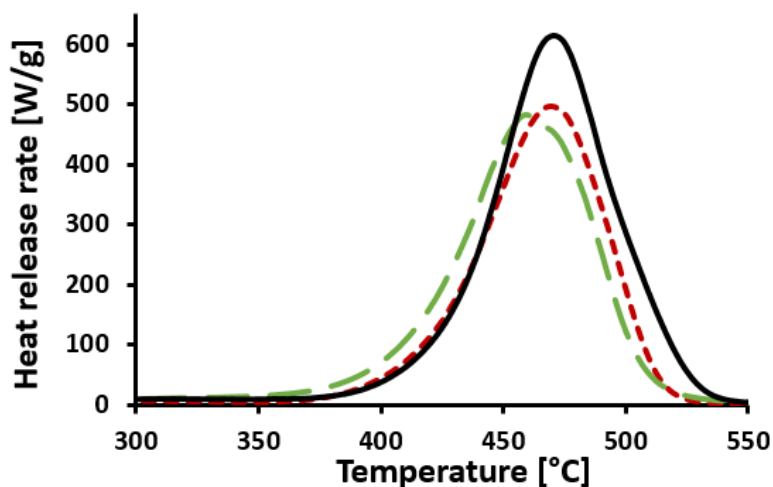
Figure 105. Heat release rates in PCFC of ABS and ABS/lignin composites

Table 43. PCFC data of ABS, ABS_30LIG and ABS_30P-LIG

	PCFC results					TGA (60 °C/min)		
	T_{onset} [°C]	T_{MAX} [°C]	pHRR [W/g]	THR [kJ/g]	Res [%]	$T_{2\%}$ [°C]	T_{MAX} [°C]	Res [%]
Neat ABS	340	470	602.6	37.7	1	360	453	2
ABS_30LIG	333	461	481.0 (-20.2%)	34.1 (-9.6%)	13	297	440	12
ABS_30P-LIG	340	471	498.2 (-17.4%)	33.0 (-12.5%)	18	305	450	17

3.2.3. Conclusion

The gas phase generated during the thermal decomposition of ABS and ABS/lignin composites was investigated. In thermo-oxidative conditions, it was shown by TGA-FTIR that LIG interacts with the SAN matrix of ABS. As a consequence, transient char formation was promoted, which was even more significant when using P-LIG. This transient char was more stable towards oxidation in the presence of P-LIG. In pyrolysis condition, TGA-FTIR and Py-GC/MS allowed to

identify that lignin were interacting with the SAN matrix by slightly promoting its depolymerization. It was also found that P-LIG limits this destabilization in comparison to LIG. Finally, the combustibility of ABS was slightly reduced when lignin was incorporated (PCFC). A reasonable assumption is that this improvement is due to reaction of some combustible decomposition products of ABS with LIG or P-LIG in the condensed phase, which therefore do not evolve in the gas phase.

So the gas phase was modified by the incorporation of lignin in ABS. However, these changes are caused indirectly because lignin's actions in the condensed phase. Several assumptions emerged, such as interactions between nitrile groups of ABS and lignin. In order to either confirm or deny these assumptions, the condensed phase is investigated in the following.

3.3. Condensed phase analysis

3.3.1. Generation of the residues

The characterization of the condensed phase was performed on residues generated in fire conditions with MLC. MLC shutter experiments were undertaken at characteristic times (S1, S2, S3 and char) in order to study residues representative of the burning composites at different steps of degradation (Figure 106). It therefore permits to follow how the condensed phase behaves as the combustion goes on. Thus S1 (90 s) is the time when the char layer starts to develop in ABS/lignin composites. Residues obtained at S2 (115 s) represent the condensed phase when the HRR of ABS/lignin reaches a plateau: the combustion is intense, and the char layer is submitted to severe conditions. S3 was chosen to study the residues when the combustion is significantly reduced to assess the structure. Finally, the final residues (called char), were collected after the flame extinction in order to characterize the residual materials.
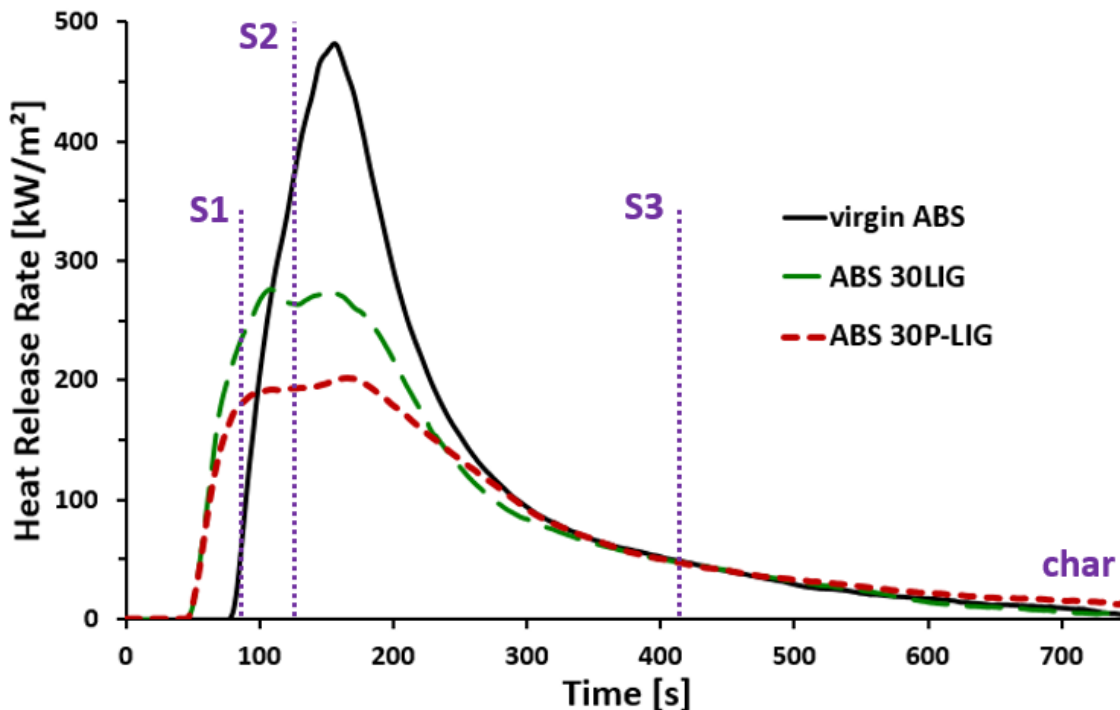
Figure 106. MLC shutter experiment: S1, S2, S3 and char positions on the MLC curves

3.3.2. Char morphology

Pictures of the chars generated at the different characteristic times are shown in Figure 107. From the ignition to the pHRR, neat ABS releases gases and a bubbles formation is observed on the top of the sample. The polymer indeed melts, but the viscosity remained apparently relatively high since surface of S1 samples appears porous. This bubbling effect was noticed also for both ABS/lignin composites, however the bubbles were much smaller. Indeed, a thin solid layer was formed at the surface attributed to the beginning of the formation of the char. It only partially covers the center of the sample, as burning polymer is still noticed on the edges: a grey "island" (char) in a dark "see" (burning polymer). HRR continues to increase since the flame is fed by the burning polymer on the edges, because the surface of the sample is not fully covered.
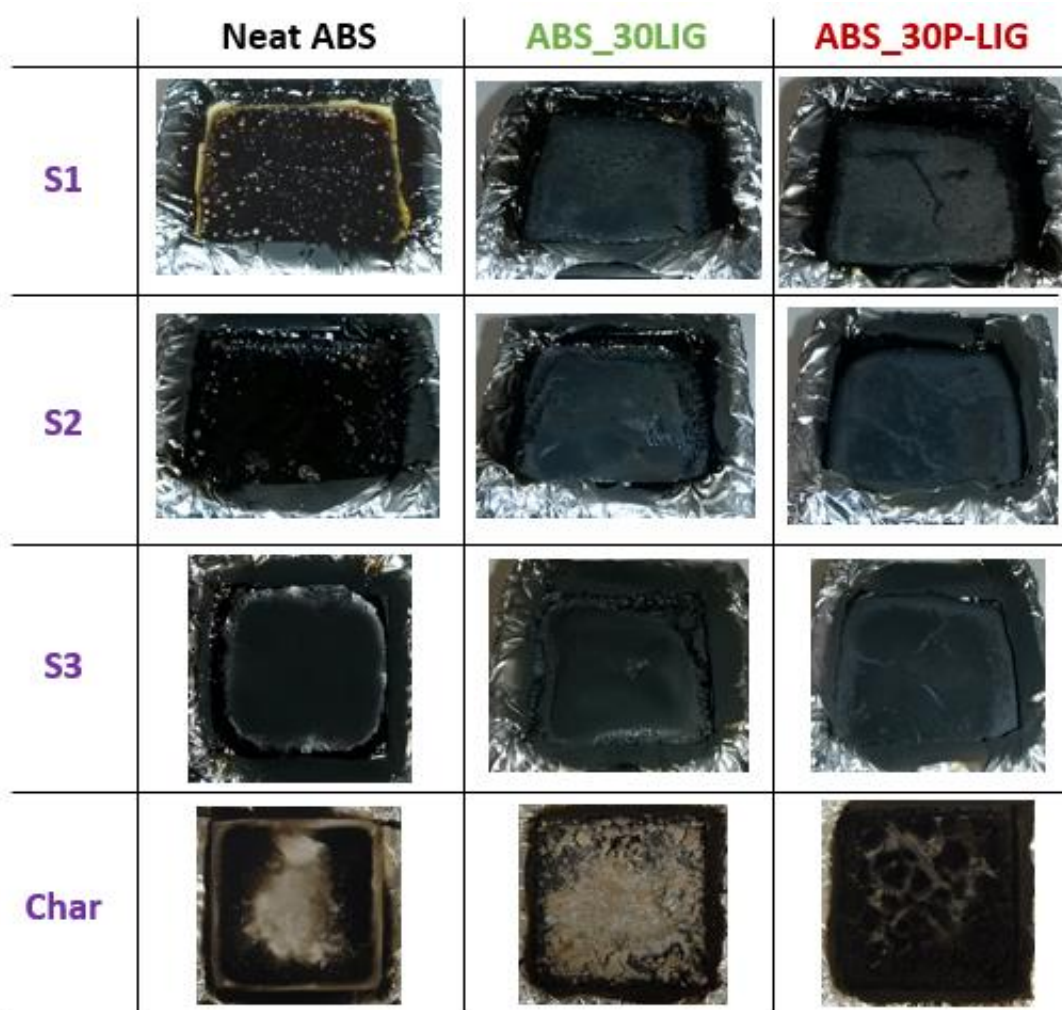
Figure 107. Pictures of the residues generated during MLC shutter experiments

S2 is the time corresponding to a significant combustion of neat ABS (just before the pHRR). At this time, half of the material is already burnt. The condensed phase is a dark high viscous melt, which continues to bubble. In the case of ABS/lignin composites, bubbling stops at the beginning of the plateau. However, a porous surface is still noticed, which allows decomposition products of the underlying polymer to reach the flame and continue to feed it, thus explaining the HRR plateau [134]. It is noteworthy that ABS_30P-LIG char's layer covers all the surface sample, whereas ABS_30LIG exhibits ashes on the edges. It shows that the layer produced did not permit to protect all the surface of the sample exposed to the cone.

At the end of combustion (S3), localized flames are still observed on the edges of the sample holder because fed by residual melt. Only few ashes are left in the center of the sample holder,

which do not contribute to the flame in the case of neat ABS. In the case of ABS/lignin composites, very small blue flames are localized above the char (center of the sample holder). That shows that fuel is still released by polymer, going through the porous char layer. At this long time of exposure, ABS_30LIG char begins to collapse (cracks and big holes appear), while the ABS_30P-LIG char remains intact.

Finally, pictures of the final residues show that no residue is left for neat ABS. When the flame is close to extinguish, the char layer observed for ABS_30LIG turns to degrade in grey ashes. In the case of ABS_30P-LIG, many cracks appear on the layer, and some big aggregates constitute the final residue. For both ABS/lignin composites, the exposition to oxygen may be a reason of the high degradation state of the final residue. Indeed, when the flame becomes less intense or extinguishes, the oxygen can reach the surface of the sample and therefore induces oxidation of the char which degrades.

Residues amounts at characteristic times of each formulation are shown in Figure 108. At S1, neat ABS exhibits the highest residue (97 wt.%) in comparison to the ABS/lignin composites (≈ 91 wt.%). This difference is explained by the fact that ABS/lignin composites had been burning for 40 s, against only for 10 s for neat ABS. At S2, residue amounts decrease as the combustion progresses. However, ABS_30P-LIG amount is higher (77 wt.%) than that of ABS_30LIG (71 wt.%). This evolution is more obvious at S3, the residue weight 36 and 23 wt.% respectively. At the same time, the residue of ABS drastically falls down to 7 wt.%. The final residue is further reduced, as no residue is noticed of ABS, 12 and 17 wt.% for ABS_30LIG and ABS_30P-LIG.
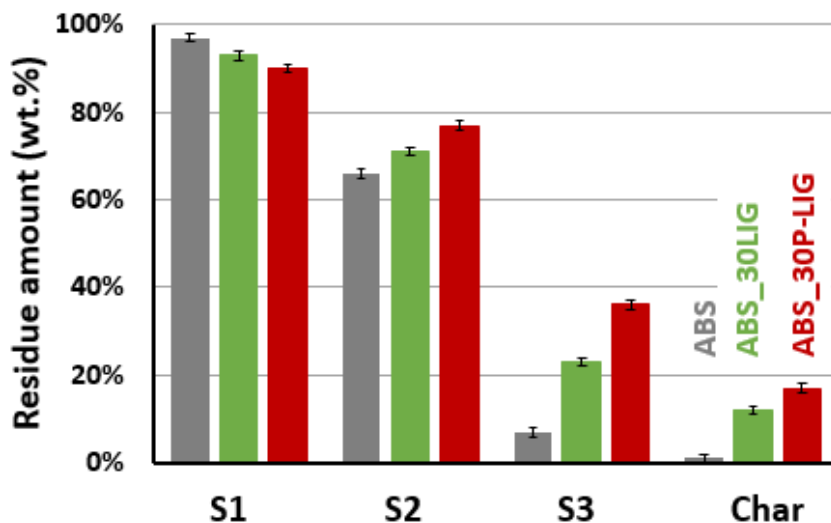
Figure 108. Residue amount of each formulation at the different characteristic times

These observations show the action of the char layer. In the case of neat ABS, no char layer is formed, and therefore all the polymer burns. When the char layer is formed, the amount of residue decreases in a less extent than that of neat ABS. In the case of P-LIG, the amount of residue is higher than that of ABS_30LIG, which allows to confirm that the char layer is more effective when the lignin is phosphorylated. However, since the amount of residue continues to decrease, even with LIG or P-LIG, that proves that the char layer is not performant enough to preserve the underlying polymer from burning. The formulation can still be optimized.

From these results, it can be concluded that during the combustion, the improvement observed in FR performance of ABS are mainly due to the formation of a char layer, and that this improvement is more significant in the case of P-LIG. But how does act this char layer? At this point, different modes of action may be considered:

- The formed layer is thermally insulating the underlying polymers, thus limiting its degradation. Indeed, thermal insulation effect may be observed with well expended char, meaning high swelling [232] or particular char composition [233]. In the case of lignin, the char composition is standard and no swelling is noticed. So the char layer is too thin to be efficient in that way (1 to 2 mm). This mode of action cannot be considered.

- The pores of the layer are small enough to limit the mass transfers between the flame and the polymer. However experimental assessment of the porosity was not possible because the char layer is thin and very fragile. But this mode of action may be considered.

- The char layer of P-LIG is formed faster than that of LIG, and so the mass transfer is limited faster too. This assumption will be evaluated by rheology in the following.

- Change in the degradation pathways of the condensed phase leads to a reduction of the combustible which are released. The thermal stability and gas phase studies suggested indeed that interactions were occurring between the SAN matrix and the lignin. This assumption will be investigated by chemical characterizations of the condensed phase.

3.3.3. Characterization of the char formation by rheology

Rheology analysis of the condensed phase as a function of temperature is a powerful tool in order to assess the formation of a char in a polymeric material [234,235] and its mechanical strength [234]. In the last section, the char's layer of ABS_30P-LIG was observed to be formed faster than that of ABS_30LIG in MLC. Therefore this technique was undertaken to investigate if the charring process occurs at the same temperature in ABS_30LIG and ABS_30P-LIG composites (Figure 109).

Neat ABS was investigated as a reference. A decrease of the viscosity is noticed from 200 to 250 °C. As the producer mentioned a melting temperature range of 230-260 °C, it is attributed to the softening of the polymer. The viscosity reaches a plateau between 250 and 440 °C until the polymer degrades. This is in good agreement with the bubbling noticed in the melt during MLC experiment. Then, a significant increase is observed around 440 °C which is attributed to the formation of the transient char as this test is performed in thermo-oxidative conditions (formation of the transient char assessed at 450 °C for neat ABS with TGA at 20 °C/min under air). Between 200 and 300 °C, viscosity profiles of both ABS/lignin are comparable to that of neat ABS showing that the composites soften before the degradation occurs. However, an increase of the viscosity occurs at 320 and 350 °C for ABS_30P-LIG and ABS_30LIG respectively. This is explained by the formation of the char's layers. So it appears that the charring process occurs at lower temperatures with P-LIG than with LIG in ABS. Chemical characterization of the residues was therefore undertaken in order to explain these differences and is presented in the next part.
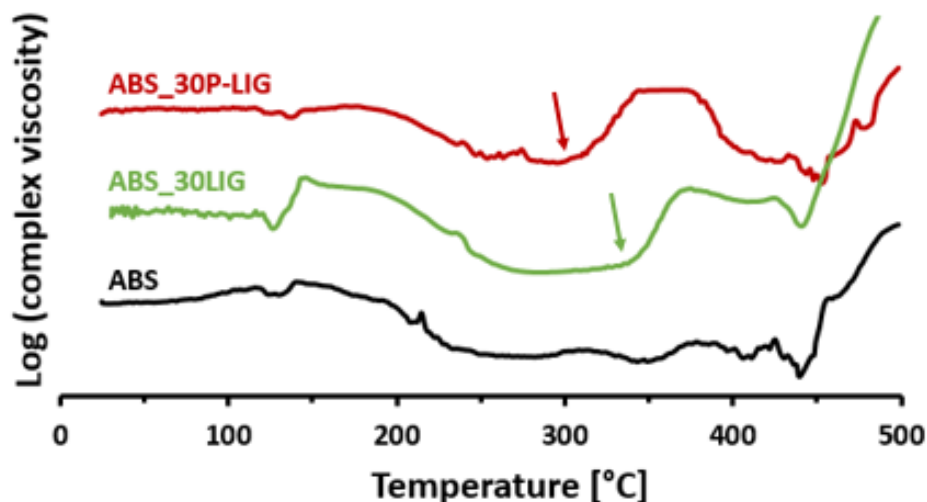
Figure 109. Evolution of the viscosity of the condensed phase depending on the temperature

3.3.4. Chemical characterization of the char's layer

Thermogravimetric and gas phase analyses revealed that different interactions where occurring between the ABS matrix and lignin, whether LIG or P-LIG is used (Figure 95 p190 and Figure 97 p192). Moreover, charring process appeared at lower temperature with P-LIG than with LIG in ABS. Therefore, chemical analysis of the char's layer which is produced during the MLC shutter was undertaken.

The first approach consists in characterizing the carbonaceous residue by ^{13}C solid state NMR (Figure 110). Attribution of the signals of unburnt materials is available Table 32, p173. The spectra obtained from the S1 residues shows that ABS matrix starts to be degraded in both composites. The bands in the aliphatic region broadens suggesting that the structure is more disordered. This observation becomes more obvious in S2 residues spectra. Moreover, the aromatic region also broadens, confirming that the structure gets disordered. This is in good agreement with the formed char's layer observed on the pictures. After a long time of combustion (S3), ABS_30LIG residue exhibits only a large peak centered at 130 ppm revealing that ABS as well as LIG turn completely in a structure made of aromatic carbons and some oxidized aromatic carbons (shoulder at 140 ppm), typically observed in a disorganized char [182]. The spectra of the final residues are very comparable to those of S3, exhibiting disorganized char structure. This disorganized structure was confirmed by Raman spectroscopy. Indeed, two bands at 1595 (G

band, "organized" carbon) and 1350 cm^{-1} (D band, "disordered carbon) are noticed. The height ratio I_D/I_G, evaluated at 0.72, indicates that a large part of the char is composed of disordered carbon [183]. In the case of P-LIG, similar ^{13}C NMR and Raman spectra than those of LIG are noticed. The char structure is similar to that obtained with ABS_30LIG.
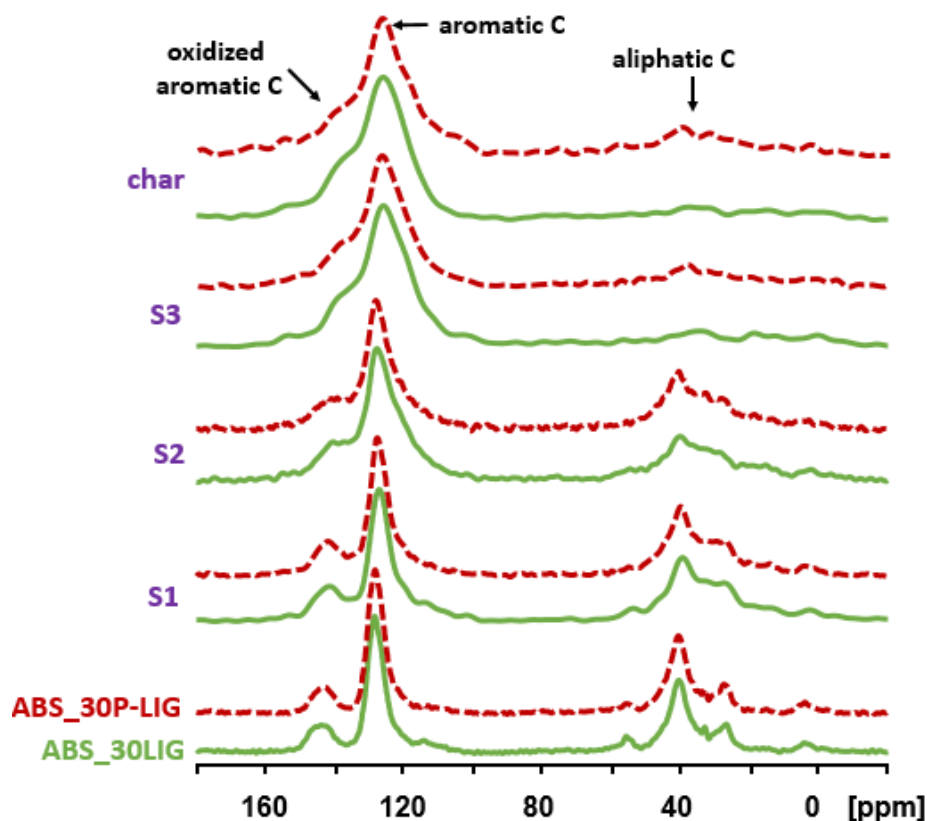
Figure 110. ^{13}C CPMAS NMR of the residues generated from the MLC shutter experiments
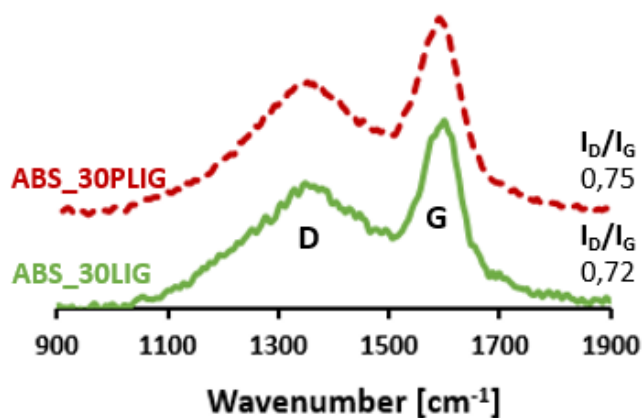
Figure 111. Raman spectra of ABS_30LIG and ABS_30P-LIG residues

It was shown in Chapter III (section 3.3.3, p131) that P-LIG thermal decomposition was influenced by phosphorus which reacts in the condensed phase according to ^{31}P NMR (Figure 67, p134). Similar ^{31}P HPEC NMR was undertaken on ABS_30P-LIG residues, in order to assess the chemical environment of phosphorus, and therefore try to elucidate how it acts in the condensed phase in fire conditions (Figure 112). In S1 and S2, phosphates signals (- 5 ppm) broadens showing disordered structure (amorphization and dissymmetric phosphates), as the phosphates reacts with the decomposing lignin and polymeric matrix [200]. This is also due to progressive apparition of pyro- (-12 ppm) and condensed phosphates (-25 ppm). These changes of phosphorus structures in a carbonaceous material with increasing the temperature is well known and was fully discussed in previous works [183]. Moreover, phosphonate structures are noticed (10 ppm) attributed to partial reduction of phosphates. This phenomenon was also happening during the thermal degradation of P-LIG alone, and was commented in Chapter III (see section 3.3.3, p131). This transformation was unexpected and further investigation is required to understand its origin. It was suggested that oxido-reduction between phenols and phosphates may occur. Since phosphonates arise in P-LIG either alone or in the ABS matrix, it appears that this phenomenon is independent of the presence of ABS and strictly related to interactions between phosphate groups and lignin.

S1 and S2 spectra are similar with that of P-LIG under inert conditions. This is consistent with the fact that the oxygen in consumed in the flame as the combustion is significant at S1 and S2 times. Therefore the condensed phase degradation can be assumed to occur in pyrolytic conditions. Spectrum of S3 char shows similar patterns, however phosphonate species progressively disappear, probably beginning to be oxidized. As localized flames are close to extinguish at S3, oxygen may reach the surface and starts to oxidize the char. This assumption is confirmed by the spectra of the final residue. It is very similar to that of P-LIG after degradation under thermo-oxidation, with the presence of phosphoric acid (0 ppm), ortho- (- 5 ppm) and pyrophosphates (-12 ppm), as well as residual phosphonates (10 ppm) and condensed phosphates (-25 ppm). So S3 and char spectra demonstrate that oxygen progressively reaches the surface of the sample.
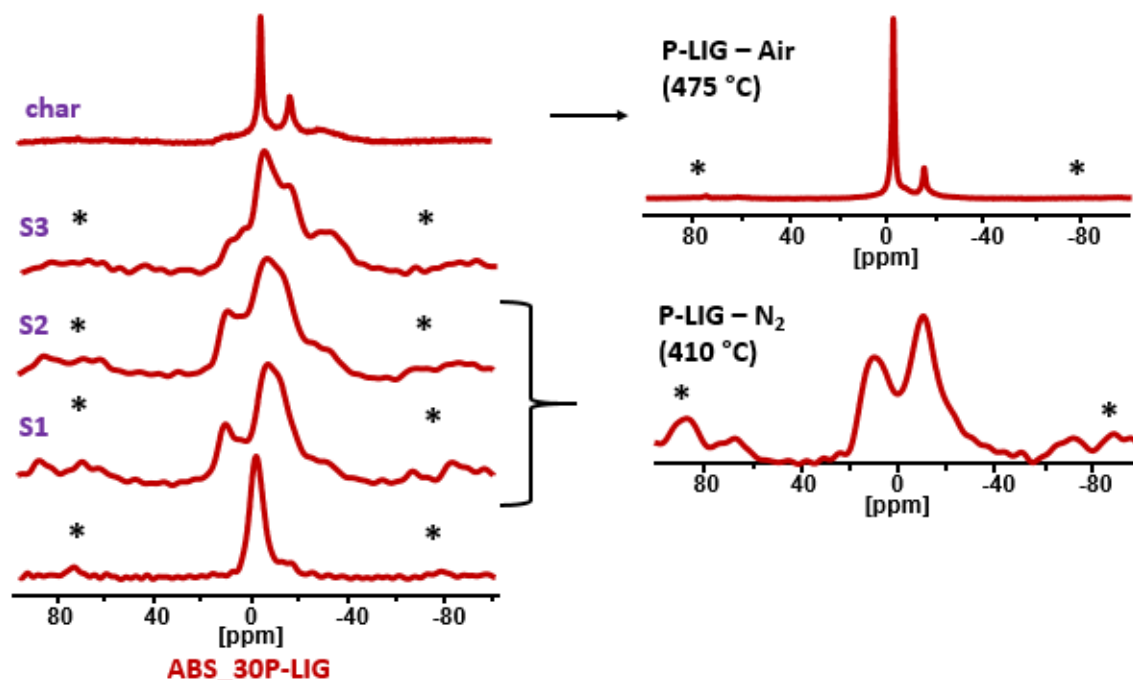
Figure 112. ^{31}P HPDEC NMR of the residues generated from the MLC shutter experiments

So phosphorus in P-LIG exhibits the same mode of action than that proposed in Chapter III. When the flame is intense, it promotes the charring by reacting with lignin and ABS structures in pyrolytic conditions which induce the formation phosphonates, and ortho-, pyro- and polyphosphates. Oxido-reduction reactions with phenolic compounds in lignin may be responsible of the reduction of phosphates to phosphonates. When the combustion decreases, the flame is less intense and oxidation at the surface of the sample is possible. This is confirmed by the oxidation of phosphonates which only occurs in the presence of oxygen according to NMR investigation of Chapter III. Therefore, phosphonates structures contribute to prevent the oxidation of the char [184]. So these results permits to confirm that when an intense flame occurs, the degradation of the underlying materials can be considered to take place in pyrolytic conditions as the oxygen is consumed by the flame [154] (presence of phosphonates). However, when the combustion decreases, oxidation at the surface of the material can occur (oxidation of phosphonates). Unfortunately, it was not possible to identify if phosphorus interacts with nitrogen (from AN units). This is probably due to the low concentration of the compounds resulting from these interactions.

3.3.5. Conclusion

The condensed phase of neat ABS and ABS/lignin composites was investigated in order to characterize the char formation and the interactions occurring between the components during the degradation. The condensed phase was prepared in fire conditions thanks to MLC shutter experiments. Residues were generated at different states of degradation (just after ignition, during the HRR plateau, after a long time of combustion and the final residue) in order to observe the change that happens while the material burns.

Morphologies of the residues showed that ABS_30P-LIG generates the char's layer faster than that of ABS_30LIG. It covers the entire surface, and appears to be more efficient. It indeed limits the mass transfer according to weight loss analysis which therefore induces a reduction of the HRR. Viscosity profiles of the composites confirmed that the charring process occurs at lower temperature with P-LIG than with LIG in ABS. ^{13}C and ^{31}P solid state NMR were undertaken to chemically characterize the charring process. It appeared that the phosphorus reacts with lignin and ABS matrix to form ortho-, pyro and polyphosphates which promotes and stabilizes the char. Moreover, phosphonates were also produced as a result of interactions of phosphates with decomposition products. These were further oxidized as the combustion time increased and the flame became less intense, showing preventing action of the phosphorus towards char oxidation.

3.4. Proposed mode of action of lignin as FR additive in ABS

The ABS/lignin system was studied in detail, so the mode of action of lignin as FR additive in ABS may be proposed. The cartoon presented in Figure 113 presents the mode of action in the MLC test. Only neat ABS and ABS_30P-LIG are drawn, and differences with ABS_30LIG will be commented in the text. At the beginning (step 1), the material is submitted to an external heat source leading to its thermo-oxidative degradation. The composite evolves decomposition products such as hydrocarbons (PBD), aliphatic and aromatic compounds (SAN, and lignin for the composites) which forms a combustible mixture. The degradation is promoted by the thermal destabilization of the SAN matrix combined with potentially change in the optical properties of ABS, due to the presence of lignin, , which allows to reach faster the critical fuel flux required for

ignition. It results that ABS/lignin composites ignite faster than neat ABS. The phosphorylation does not influence the step 1.

In the second step, the materials are burning, and the presence of a flame induces a degradation under pyrolytic conditions. In the case of ABS, no char is formed and the polymer strongly burns. In the presence of lignin, a thin char layer is formed. This charring process involves the lignin and phosphorus, which were found to interact with ABS (especially acrylonitrile groups). As a consequence, this physical barrier permits to limit the mass transfer between the decomposing polymer (fuel source) and the flame. The combustion is consequently reduced in comparison to that of neat ABS. Moreover, some combustible from ABS is "trapped" in the condensed phase by being involved in the charring, and thus do not contribute to feed the flame. These interactions are different when lignin is phosphorylated, and accelerate the formation of the char layer. As a consequence, mass transfer is limited faster and the combustion is further decreased. It is noteworthy that no significant changes of the gas phase composition were induced by the presence of LIG and P-LIG, and also that expected inhibition from phosphorus species does not occur. But obviously, phosphorus plays an important role in the charring process.

When the combustion decreases (step 3), localized flames remain at the surface of the degraded material. Oxidation of the char of ABS/lignin composite occurs as oxygen can reach the surface. It results that cracks appear, which allows the residual underlying ABS to burn. With phosphorylated lignin, the char exhibits much less cracks. The presence of phosphorus species in its structure makes the char more cohesive, and also more resistant towards oxidation. It results different final residues: complete disorganized ashes with LIG, and cohesive chunks with P-LIG.
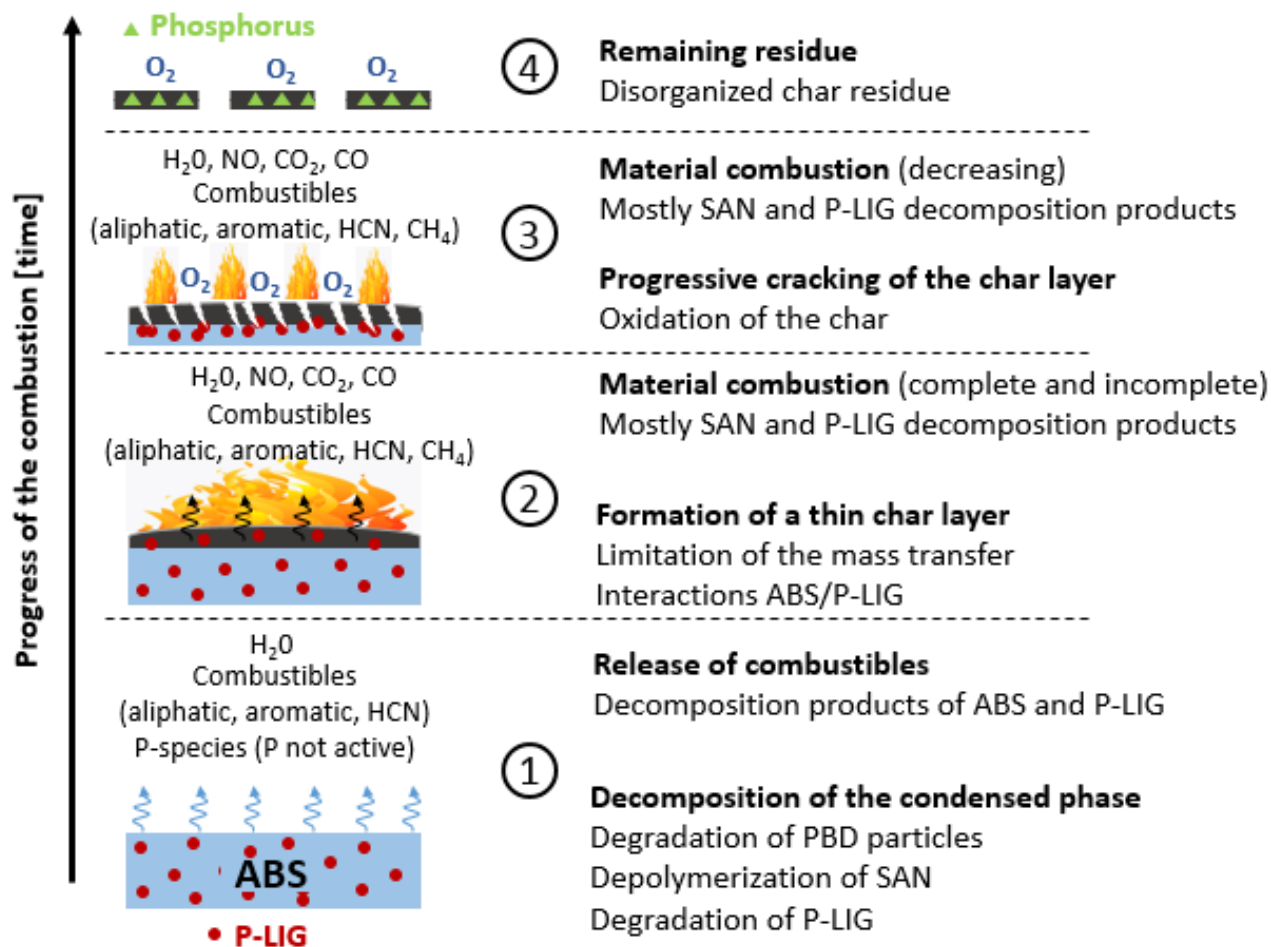
Figure 113. Schematic of the mode of action of lignin as FR in ABS (in MLC)

The mode of action was illustrated with the example of MLC. In the case of Glow Wire, as the phosphorus was found to be uniformly distributed in the composite, an efficient char is formed as soon as the hot wire touches the sample, which delays its inflammation. The better results with P-LIG may be due to the faster formation of the char and its higher resistance towards oxidation in comparison to that with LIG. However, this char is not performant enough to improve the UL classification. One assumption could be that the char is not expanding enough in order to prevent the flames to lick the upper part of the barrel. It results that the flame is continually fed with fuel from the composite.

4. Conclusion and discussion

In this chapter, the fire behaviors of the formulations based on a promising system, ABS containing 30 wt.% of neat (LIG) and phosphorylated lignin (P-LIG), were investigated. It was first shown that incorporation lignin did not degrade the ABS polymeric matrix. Lignin was uniformly dispersed in ABS. This was attributed to the high aromaticity of both phases. Interestingly, the phosphorylation of lignin did not influence the dispersion, only the particles size was larger (inherent to process). The phosphorus was therefore uniformly distributed, ensuring that homogenous composites were prepared.

In the second part, fire testing was undertaken. MLC results showed a decrease of peak of heat release rate and total heat release with LIG, which was more significant with P-LIG (by 58 and 20 % respectively). Glow wire experiments indicates that LIG lead to worst FR performance than that of neat ABS, although P-LIG did enhance GWT and GWFI. Finally, no improvement was noticed at UL-94 as all the formulations were not classified. So the phosphorylation of lignin allowed to improve the FR performance of ABS, and the mode of action were investigated.

The mode of action was mainly based on condensed phase actions. For all fire testing conditions, charring was indeed observed. Investigation of the thermal stability, and both gas and condensed phases revealed that the presence of lignin was thermally destabilizing ABS. However, this destabilization due to interactions between the polymer and lignin promotes the char formation. It results limited mass transfer between the flame and the polymer, which induce a reduction in the release of combustible. Moreover, some combustible of ABS is "trapped" in the char. It was also found that the use of P-LIG leads to a more performant char. Because of the presence of phosphorus, it is formed faster and appears to be more resistant towards oxidation in comparison to that of LIG. As a consequence, FR performance are further enhanced with P-LIG.

In conclusion, it is noteworthy that phosphorylation of lignin leads to much better FR performance, with only 1.0 % of phosphorus in the composite. This chapter provided a better understanding of the mode of action, it is a solid basis to continue developing lignin based systems as flame retardant for ABS, or further for other polymers. However, some parts of the understanding are still unclear or were indirectly demonstrated, and some assumptions need to

be confirmed. Some further work needs to be achieved. In this context, outlook will be proposed at the end of this work.

General conclusion

This study was dedicated to the valorization of lignin, a byproduct of the pulping industry, as flame retardant additive for polymeric materials. Literature review showed that this material exhibits interesting FR properties, especially because of its charring ability. Moreover, specific properties of lignin can be tuned by chemical modifications. In this context, a screening using Kraft lignin, an abundant and commercially available lignin, revealed that promising FR performances were achieved in polylactic acid and acrylonitrile-butadiene-styrene (ABS). The phosphorylation of lignin was also undertaken, and allowed to further improve the FR performances of ABS by forming a more efficient charring barrier.

The goal was to prove the FR potential of Kraft lignin, first by developing effective FR systems based on lignin, and then by understanding its mode of action. The screening generated reliable and comparable data about the FR performance of Kraft lignin in several thermoplastic polymers. Moreover, it revealed that two approaches may be followed to design efficient FR systems with lignin: the use of coadditives (and/or synergists), or the chemical modifications of the lignin's structure. In this study, phosphorylated lignin was produced with a simple protocol. The influence of the phosphorus on the thermal degradation of Kraft lignin was investigated and elucidated. The presence of phosphorus led to the promotion of the dehydration and decarboxylation of lignin, thus increasing the char yield and forming a more cohesive char, also resistant towards oxidation. It resulted that the combustibility of the phosphorylated lignin was reduced. When considered as FR additive, it appeared that the FR performance of ABS was improved using neat lignin, and further enhanced when phosphorylated lignin was considered, according to Glow Wire and Mass Loss Cone. Obviously, the formation of a carbonaceous barrier due to the presence of lignin was found to be the main mode of action as FR additive. Mass transfers were especially decreased, thus limiting the feeding of the flame. Considering phosphorylated lignin, the formation of this barrier occurred faster, and the char was more resistant towards oxidation. These improvements were attributed to the role of the phosphorus on lignin's thermal degradation inducing specific interactions with the ABS matrix.

In summary, this work confirms that lignin may be valorized as flame retardant for polymers and offers the possibility of developing green flame retardants. Indeed, the possibility to tune the lignin's properties with simple chemical reactions is an interesting possibility for increasing its FR potential. The phosphorylation of lignin is especially promising. More than developing efficient FR lignin, this study also established its mode of action as FR retardant. The influence of the phosphorylation on the lignin's properties, especially the thermal degradation and the formation of a char, was deeply investigated as well. So this work can be used as basis for further work, aiming the valorization of lignin by the development of new FR systems based on lignin for polymers.

Outlook

This PhD confirms that lignin could be a promising flame retardant for polymers. It also demonstrates that phosphorylation allows to further enhance its FR performance, especially in ABS. Many efforts have been undertaken to elucidate the mode of action of lignin in this polymer and several experiments could lead to a better understanding. For example, it was indirectly assumed that interactions occur between P-LIG and the SAN matrix, especially the acrylonitrile units. Therefore, investigation of this system in ABS with different amount of acrylonitrile could be the first approach. Another possibility is to use a similar approach which was used by Suzuki and Wilkie [226] to investigate the thermal stability of ABS. The effect of lignin of the FR performance of each the constituent parts of that polymer separately such as polystyrene, acrylonitrile, styrene-acrylonitrile copolymer and polybutadiene. It would show with which constituent lignin interacts the most and elucidate the mechanism involved.

This work was achieved aiming to propose a mode of action of lignin as FR additive, in order to develop strategies for developing new FR system based on lignin. A critical property of lignin is its ability to make char. It was found that the char yield is increased by the promotion of dehydration and decarboxylation reactions. In this context, it would be interesting to evaluate the charring ability of different neat lignins with different amount of hydroxyls and carbonyl groups, different hydroxyls ratio (aliphatic/aromatic) or changing S,G,H ratios [31,34]. Such study would lead to a better understanding of the charring process in lignin and the identification of the governing factors. Moreover, the phosphorylation of lignin was found to be very efficient to improve its FR performance by increasing its charring ability. It would be interesting to investigate the influence of an increase of the amount of phosphorus (higher than 3 %) on the lignin's properties. This could be achieved by using a lignin grade with higher amount of free hydroxyl groups, or optimizing the reaction, for example by using others phosphorus reactive than P_2O_5.

Considering the example of the phosphorylation, chemical modifications appears to be a promising way to tune lignin's properties [8]. It opens a wide range of possibility, and therefore accurate strategies in the domain of flame retardancy require to be established. FR performance of lignin may be directly improved by specific modifications, such as hybrid phosphorus-nitrogen

groups, which already showed promising FR performance in polymers [138,139,236]. Other heteroatoms worth to be consider, such as boron or sulfur, and researches should be continuing in this direction [237]. Another opportunity is to increase the charring potential of lignin, one way would be by preparing macro-lignin based polyol [76]. This modified lignin could be used as charring agent (similarly to synthetic polyols such as pentaerythritol) in an intumescent system, for example in combination with ammonium polyphosphate. Finally, another perspective is to modify the lignin's structure to improve the compatibility in a polymeric matrix. For example, in polyolefines, alkyl non polar chains could be considered. In conclusion, tuning lignin's properties, based on a strategy established as a function of the host polymer and the expected FR mode of action, appears to be a very promising way to valorize lignin as flame retardant additive for plastics.

List of tables, figures, and equations

List of tables

List of figures

List of equations

References

1. Luong, N. D.; Binh, N. T. T.; Duong, L. D.; Kim, D. O.; Kim, D. S.; Lee, S. H.; Kim, B. J.; Lee, Y. S.; Nam, J. Do An eco-friendly and efficient route of lignin extraction from black liquor and a lignin-based copolyester synthesis. *Polym. Bull.* **2012**, *68*, 879–890.

2. Wertz, J. L. *La lignine - Note de synthèse*; 2010.

3. Lin, S.; Dence, C. W. *Methods in lignin chemistry*; Berlin : S.; 1998.

4. Gregorová, A.; Cibulková, Z.; Košíková, B.; Šimon, P. Stabilization effect of lignin in polypropylene and recycled polypropylene. *Polym. Degrad. Stab.* **2005**, *89*, 553–558.

5. Lora, J. H.; Glasser, W. G. Recent industrial applications of lignins : a sustainable alternative to nonrenewable materials. *J. Polym. Environ.* **2002**, *10*, 39–48.

6. Gosselink, R. J. a.; de Jong, E.; Guran, B.; Abächerli, a. Co-ordination network for lignin—standardisation, production and applications adapted to market requirements (EUROLIGNIN). *Ind. Crops Prod.* **2004**, *20*, 121–129.

7. Holladay, J. E.; White, J. F.; Bozell, J. J.; Johnson, D. *Results of Screening for Potential Candidates from Biorefinery Lignin*; 2007.

8. Laurichesse, S.; Averous, L. Chemical modification of lignins: Towards biobased polymers. *Prog. Polym. Sci.* **2014**, *39*, 1266–1290.

9. Plasticseurope An analysis of European plastics production demand and waste data http://www.plasticseurope.org/cust/documentrequest.aspx?DocID=59108.

10. Association, N. F. P. Fires in the US http://www.nfpa.org/research/reports-and-statistics/fires-in-the-us.

11. Levchik, S. V.; Weil, E. D. Flame retardancy of thermoplastic polyesters - a review of the recent literature. *Polym. Int.* **2005**, *54*, 11–35.

12. Online, F. R. Flame retardants market http://www.flameretardants-online.com.

13. Yu, Y.; Fu, S.; Song, P.; Luo, X.; Jin, Y.; Lu, F.; Wu, Q.; Ye, J. Functionalized lignin by grafting phosphorus-nitrogen improves the thermal stability and flame retardancy of polypropylene. *Polym. Degrad. Stab.* **2012**, *97*, 541–546.

14. Ferry, L.; Dorez, G.; Taguet, A.; Otazaghine, B. Chemical modification of lignin by phosphorus molecules to improve the fi re behavior of polybutylene succinate. *Polym. Degrad. Stab.* **2015**, *113*, 135–143.

15. Sudip, S. Lignin Market is Expected to Reach US$ 985.5 Mn in 2023 http://www.transparencymarketresearch.com/pressrelease/lignin-market.htm (accessed Mar 7, 2016).

16. Saake, B.; Lehnen, R. *Lignin*; Weinheim, 2007.

17. Freudenberg, K.; Neish, A. C. Constitution of lignin. *Mol. Biol. Biochem. Biophys.* **1968**, *2*, 47–122.

18. Sjöström, E. *Wood Chemistry Fundamentals and Applications (2nd edition)*; Academci P.; San Diego, 1993.

19. Whetten, R. W.; MacKay, J. J.; Sederoff, R. R. Recent advances in understanding lignin biosynthesis. *Plant Physiol. Plant Mol. Biol.* **1998**, *49*, 585–609.

20. Windeisen, E.; Wegener, G. Lignin as building unit for polymers. In *Polymer Science: a comprehensive reference*; Elsevier, Ed.; Amsterdam, 2012; pp. 255–65.

21. Dence, C. W.; Lin, S. Y. *Methods Lignin Chem.* 1992, pp. 3–19.

22. Sarkanen, K. V.; Ludwig, C. H. *Lignins: Occurrence and Formation, Structure, Chemical and Macromolecular Properties, and Utilization*; Interscience, New York, 1971.

23. Dorrestijn, E.; Laarhoven, L. J. J.; Arends, I. W. C. E.; Mulder, P. The occurrence and reactivity of phenoxyl linkages in lignin and low rank coal. *J. Anal. Appl. Pyrolysis* **2000**, *54*, 153–192.

24. Watkins, D.; Nuruddin, M.; Hosur, M.; Tcherbi-Narteh, A.; Jeelani, S. Extraction and characterization of lignin from different biomass resources. *J. Mater. Res. Technol.* **2014**, 1–7.

25. Calvo-Flores, F. G.; Dobado, J. a Lignin as renewable raw material. *ChemSusChem* **2010**, *3*, 1227–35.

26. Kim, J.-Y.; Oh, S.; Hwang, H.; Kim, U.-J.; Choi, J. W. Structural features and thermal degradation properties of various lignin macromolecules obtained from poplar wood (Populus albaglandulosa). *Polym. Degrad. Stab.* **2013**, *98*, 1671–1678.

27. Björkman, A. Extraction of lignin with neutral solvents. In *Studies on finely divided wood*; 1956; Vol. 5, pp. 59–485.

28. Yasuda, S.; Fukushima, K.; Kakehi, A. Formation and chemical structures of acid-soluble lignin I: sulfuric acid treatment time and acid-soluble lignin content of hardwood. *J. Wood Sci.* **2001**, *47*, 69–72.

29. Bykov, I. Characterization of Natural and Technical Lignins, Lulea University of Technology, 2008.

30. Mäule, C. M. *Beitr. Wiss. Botanik*; 1900.

31. Schorr, D.; Diouf, P. N.; Stevanovic, T. Evaluation of industrial lignins for biocomposites production. *Ind. Crops Prod.* **2014**, *52*, 65–73.

32. Mousavioun, P.; Doherty, W. O. S. Chemical and thermal properties of fractionated bagasse soda lignin. *Ind. Crops Prod.* **2010**, *31*, 52–58.

33. Sarwar Jahan, M.; Liu, Z.; Wang, H.; Saeed, A.; Ni, Y. Isolation and characterization of lignin from prehydrolysis liquor of kraft-based dissolving pulp production. *Cellul. Chem. Technol.* **2012**, *46*, 261–267.

34. Gosselink, R. J. a.; Abächerli, a.; Semke, H.; Malherbe, R.; Käuper, P.; Nadif, a.; van Dam, J. E. G. Analytical protocols for characterisation of sulphur-free lignin. *Ind. Crops Prod.* **2004**, *19*, 271–281.

35. Gärtner, A.; Gellerstedt, G.; Tamminen, T. Determination of phenolic hydroxyl groups in residual lignin using a modified UV-method. *Nord. Pulp&Paper Res.* **1999**, *14*, 163–170.

36. Liitiä, T.; Tamminen, T. Direct method for the determination of phenolic hydroxyl groups in pulp. *Holzforschung* **2007**, *61*, 623–627.

37. El Hage, R.; Brosse, N.; Chrusciel, L.; Sanchez, C.; Sannigrahi, P.; Ragauskas, A. Characterization of milled wood lignin and ethanol organosolv lignin from miscanthus. *Polym. Degrad. Stab.* **2009**, *94*, 1632–1638.

38. El Mansouri, N.-E.; Salvadó, J. Analytical methods for determining functional groups in various technical lignins. *Ind. Crops Prod.* **2007**, *26*, 116–124.

39. Monteil-Rivera, F.; Phuong, M.; Ye, M.; Halasz, A.; Hawari, J. Isolation and characterization of herbaceous lignins for applications in biomaterials. *Ind. Crops Prod.* **2013**, *41*, 356–364.

40. Bardet, M.; Lundquist, K.; Park, J.; Robert, D.; Unge, S. Von Spectral Assignments and

Reference Data. **2006**, 976–979.

41. Kim, H.; Ralph, J.; Akiyama, T. Solution-state 2D NMR of Ball-milled Plant Cell Wall Gels in DMSO-d 6. *BioEnergy Res.* **2008**, *1*, 56–66.

42. Fradet, A. Structural Analysis of Alfa Grass (Stipa tenacissima L.) Lignin Obtained by Acetic Acid/Formic Acid Delignification. **2011**.

43. Zhang, L. Quantitative 2D HSQC NMR determination of polymer structures by selecting suitable internal standard. **2007**, 37–45.

44. Capanema, E.; Balakshin, M.; Kadla, J. A Comprehensive Approach for Quantitative Lignin Characterization by NMR Spectroscopy. *J. Agric. Food Chemisitry* **2004**, *52*, 1850–1860.

45. Liitia, T.; Maunu, S.; Hortling, B.; Toikka, M.; Kilpeläinen, I. Analysis of Technical Lignins by Two- and Three-Dimensional NMR Spectroscopy. *J. Agric. Food Chemisitry* **2003**, *51*, 16–18.

46. Mbotchak, L.; Le Morvan, C.; Duong, K. L.; Rousseau, B.; Tessier, M.; Fradet, A. Purification, structural characterization, and modification of organosolv wheat straw lignin. *J. Agric. Food Chem.* **2015**, *63*, 5178–88.

47. Granata, A.; Argyropoulos, D. S. a Reagent for the Accurate Determination of the Uncondensed and Condensed Phenolic Moieties in Lignins. *J. Agric. Food Chemisitry* **1995**, 1538–1544.

48. Baccile, N.; Falco, C.; Titirici, M. Characterization of biomass and its derived char using 13C-solid state nuclear magnetic resonance. **2014**, 4839–4869.

49. Mao, J.; Holtman, K. M.; Scott, J. T.; Kadla, J. F.; Schmidt-Rohr, K. Differences between Lignin in Unprocessed Wood , Milled Wood , Mutant Wood , and Extracted Lignin Detected by 13 C Solid-State NMR. *J. Agric. Food Chemisitry* **2006**, *54*, 9677–9686.

50. Dou-Yong, M.; Waters Smith, S.; Hou-Min, C.; Hasan, J. com Influence of Isolation Condition on Structure of Milled Wood Lignin Characterized by Quantitative 13 C Nuclear Magnetic Resonance Spectroscopy. *Bioresources* **2013**, *8*, 1790–1800.

51. Holtman, K. M.; Chen, N.; Chappell, M. a; Kadla, J. F.; Xu, L.; Mao, J. Chemical structure and heterogeneity differences of two lignins from loblolly pine as investigated by advanced solid-state NMR spectroscopy. *J. Agric. Food Chem.* **2010**, *58*, 9882–92.

52. Zakzeski, J.; Bruijnincx, P. C. a; Jongerius, A. L.; Weckhuysen, B. M. The catalytic valorization of lignin for the production of renewable chemicals. *Chem. Rev.* **2010**, *110*, 3552–99.

53. Akim, L. G.; Al., E. Holzforschung. *Holzforschung* **2001**, *55*, 386.

54. Lu, F.; Ralph, J. DFRC Method for Lignin Analysis . 1 . New Method for -Aryl Ether Cleavage : Lignin Model Studies. **1997**, 4655–4660.

55. Brebu, M.; Spiridon, I. Co-pyrolysis of LignoBoost® lignin with synthetic polymers. *Polym. Degrad. Stab.* **2012**, *97*, 2104–2109.

56. Hakakeyama, H.; Hatakeyama, T. Advances in Polymer Science Editorial Board : *Adv. Polym. Sci.* **2010**, *232*, 1–63.

57. Mansouri, N.-E. El; Salvadó, J. Structural characterization of technical lignins for the production of adhesives: Application to lignosulfonate, kraft, soda-anthraquinone, organosolv and ethanol process lignins. *Ind. Crops Prod.* **2006**, *24*, 8–16.

58. Zhang, M.; Resende, F. L. P.; Moutsoglou, A.; Raynie, D. E. Pyrolysis of lignin extracted from prairie cordgrass, aspen, and Kraft lignin by Py-GC/MS and TGA/FTIR. *J. Anal. Appl. Pyrolysis*

2012, *98*, 65–71.

59. Nunes, C. a; Lima, C. F.; Barbosa, L. C. a; Colodette, J. L.; Gouveia, a F. G.; Silvério, F. O. Determination of Eucalyptus spp lignin S/G ratio: a comparison between methods. *Bioresour. Technol.* **2010**, *101*, 4056–61.

60. Amen-chen, C.; Pakdel, H.; Roy, C. Production of monomeric phenols by thermochemical conversion of biomass : a review. *Biotresource Technol.* **2001**, *79*, 277–299.

61. Mckendry, P. Energy production from biomass (part 2): conversion technologies. *Bioresour. Technol.* **2002**, *83*, 47–54.

62. Faravelli, T.; Frassoldati, a.; Migliavacca, G.; Ranzi, E. Detailed kinetic modeling of the thermal degradation of lignins. *Biomass and Bioenergy* **2010**, *34*, 290–301.

63. Brebu, M.; Tamminen, T.; Spiridon, I. Thermal degradation of various lignins by TG-MS/FTIR and Py-GC-MS. *J. Anal. Appl. Pyrolysis* **2013**, *104*, 531–539.

64. Koufopanosi, C. A.; Maschio, G. Kinetic Modelling of the Pyrolysis of Biomass and Biomass Components. *Can. J. Chem. Eng.* **1989**, *67*, 75–84.

65. Caballero, J. A.; Font, R.; Marcilla, A. Study of the primary pyrolysis of Kraft lignin at high heating rates : yields and kinetics. *J. Anal. Appl. Pyrolysis* **1996**, *36*, 159–178.

66. Caballero, J. A.; Font, R.; Marcilla, A.; Garcia, A. N. Flash pyrolysis of Klason lignin in a Pyroprobe. *J. Anal. Appl. Pyrolysis* **1993**, *27*, 221–244.

67. Brebu, M.; Vasile, C. Thermal degradation of lignin - a review. **2010**, *44*, 353–363.

68. Adam, M.; Mohammad, J.; Berruti, F.; Briens, C. Kinetic Investigations of Kraft Lignin Pyrolysis. *Ind. Eng. Chem. Res.* **2013**, *52*, 8645–8654.

69. Afifi, A. I.; Hindermann, J. P.; Chornet, E.; Overendt, R. P. The cleavage of the aryl-0-CH , anisole as a model compound. *Fuels* **1989**, *68*, 498–504.

70. Awal, A.; Sain, M. Spectroscopic Studies and Evaluation of Thermorheological Properties of Softwood and Hardwood Lignin. **2011**.

71. Avni, E.; Coughlin, R. W.; Solomont, P. R.; King, H. H. Mathematical modelling of lignin pyrolysis. *Fuels* **1985**, *64*, 1495–1501.

72. Nimz, H. H. Lignin-based wood adhesives. *Wood Adhes. Chem. Technol.* **1983**, 247–88.

73. Matsushita, Y.; Yasuda, S. Reactivity of a condensed – type lignin model compound in the Mannich reaction and preparation of cationic surfactant from sulfuric acid lignin. *Wood Sci.* **2003**, 166–171.

74. Du, X.; Li, J.; Lindström, M. E. Modification of industrial softwood kraft lignin using Mannich reaction with and without phenolation pretreatment. *Ind. Crops Prod.* **2014**, *52*, 729–735.

75. Gandini, A.; Belgacem, M. N.; Guo, Z.; Montanari, S. Lignin as Macromonomers for Polyesters and Polyurethanes. In *Chemical modification, Properties, and Usage of Lignin*; 2002; pp. 57–80.

76. Laurichesse, S.; Huillet, C.; Avérous, L. fatty acids : new bio-based building blocks for. *Green* **2014**, *16*, 3958–3970.

77. Effendi, a.; Gerhauser, H.; Bridgwater, a. V. Production of renewable phenolic resins by thermochemical conversion of biomass: A review. *Renew. Sustain. Energy Rev.* **2008**, *12*, 2092–2116.

78. Zhang, L.; Huang, J. I. N. Effects of Nitrolignin on Mechanical Properties of Polyurethane –

Nitrolignin Films. **2001**, 1213–1219.

79. Jesionowski, T.; Klapiszewski, Ł.; Milczarek, G. Kraft lignin and silica as precursors of advanced composite materials and electroactive blends. *J. Mater. Sci.* **2013**, *49*, 1376–1385.

80. Pan, X.; Saddler, J. N. Effect of replacing polyol by organosolv and kraft lignin on the property and structure of rigid polyurethane foam. *Biotechnol. biofuels* **2013**, *6*, 1–10.

81. Sun, G.; Sun, H.; Liu, Y.; Zhao, B.; Zhu, N.; Hu, K. Comparative study on the curing kinetics and mechanism of a lignin-based-epoxy/anhydride resin system. *Polymer (Guildf).* **2007**, *48*, 330–337.

82. Valkonen, S.; Biesalski, M.; Klein, R.; Miehlhase, S.; Baaske, M.; Suetsch, M.; Ringena, O.; Rehahn, M. WO2014184446A1 Method for producing a curing agent 2014.

83. Pouteau, C.; Dole, P.; Cathala, B.; Averous, L.; Boquillon, N. Antioxidant properties of lignin in pp. *Polym. Degrad. Stab.* **2003**, *81*, 9–18.

84. G.Alexy, P.; Kosikova, B.; Podstranska The effect of blending lignin with polyethylene and polypropylene on physical properties. *Polymer (Guildf).* **2000**, *41*, 4901–4908.

85. Kadla, J. F.; Kubo, S. Lignin-based polymer blends: analysis of intermolecular interactions in lignin–synthetic polymer blends. *Compos. Part A Appl. Sci. Manuf.* **2004**, *35*, 395–400.

86. Canetti, M.; Chirico, A. De; Audisio, G. Morphology , Crystallization and Melting Properties of Isotactic Polypropylene Blended with Lignin. **2003**.

87. Sailaja, R. R. N.; Deepthi, M. V. Mechanical and thermal properties of compatibilized composites of polyethylene and esterified lignin. *Mater. Des.* **2010**, *31*, 4369–4379.

88. Chen, F.; Dai, H.; Dong, X.; Yang, J.; Zhong, M. Physical Properties of Lignin-Based Polypropylene Blends. **2011**.

89. Pineda, Â.; Corradini, Ã.; Go, E. A.; Adelina, A.; Hechenleitner, W. Lignin-poly (vinyl alcohol) blends studied by thermal analysis. **1999**, *66*, 199–208.

90. Fernandes, D. M.; Hechenleitner, A. A. W.; Job, A. E. Thermal and photochemical stability of poly (vinyl alcohol)/ modified lignin blends. **2006**, *91*, 1192–1201.

91. Fernandes, D. M.; Hechenleitner, a. a. W.; Pineda, E. a. G. Kinetic study of the thermal decomposition of poly(vinyl alcohol)/kraft lignin derivative blends. *Thermochim. Acta* **2006**, *441*, 101–109.

92. Kubo, S.; Kadla, J. F. Poly(Ethylene Oxide)/Organosolv Lignin Blends: Relationship between Thermal Properties, Chemical Structure, and Blend Behavior. *Macromolecules* **2004**, *37*, 6904–6911.

93. Pouteau, C.; Baumberger, S.; Cathala, B.; Dole, P. Lignin–polymer blends: evaluation of compatibility by image analysis. *C. R. Biol.* **2004**, *327*, 935–943.

94. Song, P.; Cao, Z.; Fu, S.; Fang, Z.; Wu, Q.; Ye, J. Thermal degradation and flame retardancy properties of ABS / lignin : Effects of lignin content and reactive compatibilization. *Thermochim. Acta* **2011**, *518*, 59–65.

95. Qin, J.; Woloctt, M.; Zhang, J. Use of Polycarboxylic Acid Derived from Partially Depolymerized Lignin As a Curing Agent for Epoxy Application. *ACS Sustain. Chem. Eng.* **2014**, *2*, 188–193.

96. Kaewtatip, K.; Thongmee, J. Effect of kraft lignin and esterified lignin on the properties of thermoplastic starch. *Mater. Des.* **2013**, *49*, 701–704.

97. Gordobil, O.; Egüés, I.; Llano-Ponte, R.; Labidi, J. Physicochemical properties of PLA lignin blends. *Polym. Degrad. Stab.* **2014**, 1–9.

98. Domenek, S.; Louaifi, A.; Guinault, A.; Baumberger, S. Potential of Lignins as Antioxidant Additive in Active Biodegradable Packaging Materials. *J. Polym. Environ.* **2013**, *21*, 692–701.

99. Gordobil, O.; Delucis, R.; Egüés, I.; Labidi, J. Kraft lignin as filler in PLA to improve ductility and thermal properties. *Ind. Crops Prod.* **2015**, *72*, 46–53.

100. Yang, W.; Dominici, F.; Fortunati, E.; Kenny, J. M.; Puglia, D. Effect of lignin nanoparticles and masterbatch procedures on the final properties of glycidyl methacrylate-g-poly (lactic acid) films before and after accelerated UV weathering. *Ind. Crops Prod.* **2015**, *77*, 833–844.

101. Ionic Flame Retardant Inc - Flame Retardants Applications and Markets http://ionicflameretardant.com/flame-retardant/.

102. Laoutid, F.; Bonnaud, L.; Alexandre, M.; Lopez-Cuesta, J.-M.; Dubois, P. New prospects in flame retardant polymer materials: From fundamentals to nanocomposites. *Mater. Sci. Eng. R Reports* **2009**, *63*, 100–125.

103. Price, D.; Anthony, G.; Carty, P. Introduction: polymer combustion, condensed phase pyrolysis and smoke formation. In *Fire Retardant Materials*; 2001.

104. Morgan, A. B.; Wilkie, C. A. *Fire retardancy of polymeric Materials*; Group, T. & F., Ed.; CRC Press.; 2010.

105. Bocchini, S.; Camino, G. Chapter 4: Halogen-Containing Flame Retardants. In *Fire Retardancy of Polymeric Materials*; Wilkie, C. A.; Morgan, A. B., Eds.; CRC Press, 2010; pp. 75–106.

106. Hornsby, P. R. Chapter 7: Fire-Retardant Fillers. In *Fire Retardancy of Polymeric Materials*; Wilkie, C. A.; Morgan, A. B., Eds.; CRC Press, 2010; pp. 163–182.

107. Hull, T. R.; Witkowski, A.; Hollingbery, L. Fire retardant action of mineral fillers. *Polym. Degrad. Stab.* **2011**, *96*, 1462–1469.

108. Joseph, P.; Edbon, J. R. Chapter 5: Phoshorus-based flame retardants. In *Fire Retardancy of Polymeric Materials*; Wilkie, C. A.; Morgan, A. B., Eds.; CRC Press, 2010; pp. 107–128.

109. Nguyen, C.; Lee, M.; Kim, J. Relationship between structures of phosphorus compounds and flame retardancies of the mixtures with acrylonitrile-butadiene-styrene and ethylene-vinyl acetate copolymer. *Polym. Adv. Technol.* **2011**, *22*, 512–519.

110. van der Veen, I.; de Boer, J. Phosphorus flame retardants: properties, production, environmental occurrence, toxicity and analysis. *Chemosphere* **2012**, *88*, 1119–53.

111. Jenewein, E.; Kleiner, W. .; Budzinsky, W. US6365071 Synergistic flame protection agent combination for thermoplastic polymers 2002.

112. Awad, W. H. Chapter 8: Recent Developments in Silicon-Based Flame Retardants. In *Fire Retardancy of Polymeric Materials*; Wilkie, C. A.; Morgan, A. B., Eds.; CRC Press, 2010; pp. 187–203.

113. Bourbigot, S.; Gardelle, B.; Vandereecken, P. WO2013150121 A1 Protecting substrates against damage fire 2013.

114. Shen, K.; S., K.; Jouffret, F. Chapter 9: Boron-based Flame Retardants and Flame Retardancy. In *Fire Retardancy of Polymeric Materials*; Wilkie, C. A.; Morgan, A. B., Eds.; CRC Press, 2010; pp. 207–228.

115. Fina, A.; Bocchini, S.; Camino, G. Chapter 2: Thermal Behavior of Nanocomposites and Fire Testing Performance. In *Fire and Polymers V - Materials and Concepts for Fire Retardancy*; Wilkie, C. A.; Morgan, A. B.; Nelson, G. L., Eds.; American Chemical Society, 2013; pp. 10–24.

116. NPCS Board of Consultants & Engineers Phosphorus Compounds. In *Handbook on Textile Auxiliaries, Dyes and Dye Intermediates Technology*; 2009; p. 53.

117. Vandersall, H. . Intumescent coating systems, their development and chemistry. *J. Fire Flammabl.* **1971**, *2*, 197–140.

118. Ballistreri, A.; Montaudo, G.; Puglisi, C.; Scamporrino, E.; Vitalini, D. Intumescent flame retardants for polymers. I. The poly(acrylonitrile)-ammonium polyphosphate-hexabromocyclododecane system. *J. Appl. Polym. Sci.* **1983**, *28*, 1743–1750.

119. Montaudo, G.; Scamporrino, E.; Vitalini, D. Intumescent Flame Retardants for Polymers. II. The Polypropylene -Ammonium Polyphosphate-Polyurea System. *J. Appl. Polym. Sci.* **1983**, *21*, 3361–3371.

120. Camino, G.; Costa, L.; Trossarelli, L. Study of the Mechanism of Intumescence in Fire Retardant Polymers : Part IV - Evidence of Ester Formation in Ammonium Polyphosphate-Pentaerythritoi Mixtures. *Polym. Degrad. Stab.* **1984**, *8*, 13–22.

121. Camino, G.; Costa, L.; Trossarelli, L. Study of the Mechanism of Intumescence in Fire Retardant Polymers : Part III- Effect of Urea on the Ammonium Polyphosphate-Pentaerythritol System. *Polym. Degrad. Stab.* **1984**, *7*, 221–229.

122. Camino, G.; Costa, L.; Trossarelli, L. Study of the Mechanism of Intumescence in Fire Retardant Polymers : Part II - Mechanism of Action in Pentaerythritol Mixtures. *Polym. Degrad. Stab.* **1984**, *7*, 25–31.

123. Camino, G.; Costa, L.; Trossarelli, L. Study of the Mechanism of Intumescence in Fire Retardant Polymers : Part I - Thermal Degradation of Ammonium Polyphosphate-Pentaerythritol Mixtures. *Polym. Degrad. Stab.* **1984**, *6*, 243–252.

124. Jimenez, M.; Duquesne, S.; Bourbigot, S. Intumescent fire protective coating: Toward a better understanding of their mechanism of action. *Thermochim. Acta* **2006**, *449*, 16–26.

125. Bourbigot, S.; Duquesne, S. Chapter 6 : Intumescence-based fire retardants. In *Fire Retardancy of Polymeric Materials*; Wilkie, C. .; Morgan, A. B., Eds.; CRC Press, 2010; pp. 129–162.

126. Lawson, J.; Srivastava, D. Formation and structure of amorphous carbon char from polymer materials. *Phys. Rev. B* **2008**, *77*, 144209.

127. Duquesne, S.; Bourbigot, S. Chapter 10: Char Formation and Characterization. In *Fire Retardancy of Polymeric Materials*; Wilkie, C. A.; Morgan, A. B., Eds.; CRC Press, 2009; pp. 239–259.

128. Lu, L.; Kong, C.; Sahajwalla, V.; Harris, D. Char structural ordering during pyrolysis and combustion and its influence on char reactivity. *Fuel* **2002**, *81*, 1215–1225.

129. Li, J.; Li, B.; Zhang, X.; Su, R. The study of flame retardants on thermal degradation and charring process of manchurian ash lignin in the condensed phase. **2001**, *72*, 493–498.

130. Wang, J.; Camino, G.; Bras, M.; Bourbigot, S.; Delobel, R. The use of intumescence. In *The use of intumescence*; 1998; pp. 159–172.

131. Sharma, R. K.; Wooten, J. B.; Baliga, V. L.; Lin, X.; Geoffrey Chan, W.; Hajaligol, M. R. Characterization of chars from pyrolysis of lignin. *Fuel* **2004**, *83*, 1469–1482.

132. Li, J.; Li, B.; Zhang, X. Comparative studies of thermal degradation between larch lignin and manchurian ash lignin. *Polym. Degrad. Stab.* **2002**, *78*, 279–285.

133. Gallina, G.; Bravin, E.; Badalucco, C.; Audisio, G.; Armanini, M.; Chirico, A. De; Provasoli, F. Application of Cone Calorimeter for the Assessment of Class of Flame Retardants for Polypropylene. **1998**, *22*, 18–21.

134. Schartel, B.; Hull, T. R. Development of fire-retarded materials — Interpretation of cone calorimeter data. *Fire Mater.* **2007**, *31*, 327–354.

135. De Chirico, A.; Armanini, M.; Chini, P.; Cioccolo, G.; Provasoli, F.; Audisio, G. Flame retardants for polypropylene based on lignin. *Polym. Degrad. Stab.* **2003**, *79*, 139–145.

136. Canetti, M.; De Chirico, A.; Fabio, B.; Guido, A. Thermal degradation behaviour of isotactic pp blended with lignin. *Polym. Degrad. Stab.* **2006**.

137. Yu, Y.; Jin, C.; Fu, S.; Zhao, L.; Wu, Q.; Ye, J. Catalytic E ff ects of Nickel (Cobalt or Zinc) Acetates on Thermal and Flammability Properties of Polypropylene-Modi fi ed Lignin Composites. **2012**.

138. Gao, L.; Zheng, G.; Zhou, Y.; Hu, L.; Feng, G. Improved mechanical property, thermal performance, flame retardancy and fire behavior of lignin-based rigid polyurethane foam nanocomposite. *J. Therm. Anal. Calorim.* **2015**, *120*, 1311–1325.

139. Zhu, H.; Peng, Z.; Chen, Y.; Li, G.; Wang, L.; Tang, Y.; Pang, R.; Khan, Z. U. H.; Wan, P. Preparation and characterization of flame retardant polyurethane foams containing phosphorus–nitrogen-functionalized lignin. *RSC Adv.* **2014**, *4*, 55271–55279.

140. Bourbigot, S.; Fontaine, G. Flame retardancy of polylactide: an overview. *Polym. Chem.* **2010**, *1*, 1413.

141. Réti, C.; Casetta, M.; Duquesne, S.; Bourbigot, S.; Delobel, R. Flammability properties of intumescent PLA including starch and lignin. *Polym. adv* **2008**, *19*, 628–635.

142. Reti, C.; Casetta, M.; Duquesne, S.; Delobel, R.; Soulestin, J.; Bourbigot, S. Intumescent Biobased-Polylactide Films to Flame Retard Nonwovens. **2009**, *4*, 33–39.

143. Zhang, R.; Xiao, X.; Tai, Q.; Huang, H.; Yang, J.; Hu, Y. Preparation of lignin-silica hybrids and its application in intumescent flame-retardant poly(lactic acid) system. *High Perform. Polym.* **2012**, *24*, 738–746.

144. Zhang, R.; Xiao, X.; Tai, Q.; Huang, H.; Hu, Y. Modification of Lignin and Its Application as Char Agent in Intumescent Flame-Retardant Poly(lactic acid). *Polym. Eng. Sci.* **2012**, 2620–2626.

145. Zhang, R.; Xiao, X.; Tai, Q.; Huang, H.; Yang, J.; Hu, Y. The effect of different organic modified montmorillonites (OMMTs) on the thermal properties and flammability of PLA/MCAPP/lignin systems. *J. Appl. Polym. Sci.* **2013**, *127*, 4967–4973.

146. Alalykin, A. A.; Vesnin, R. L.; Kozulin, D. A. Preparation of modified hydrolysis lignin and its use for filling epoxy polymers and enhancing their flame resistance. *Russ. J. Appl. Chem.* **2011**, *84*, 1616–1622.

147. Zhang, J.; Chen, Y.; Sewell, P.; Brook, M. a. Utilization of softwood lignin as both crosslinker and reinforcing agent in silicone elastomers. *Green Chem.* **2015**, *17*, 1811–1819.

148. Zhang, J.; Fleury, E.; Chen, Y.; Brook, M. A. Flame retardant lignin-based silicone composites. *RSC Adv.* **2015**, *5*, 103907–103914.

149. Ghoreishian, S. M.; Badii, K.; Norouzi, M.; Malek, K. Effect of cold plasma pre-treatment

on photocatalytic activity of 3D fabric loaded with nano-photocatalysts: Response surface methodology. *Appl. Surf. Sci.* **2016**, *365*, 252–262.

150. Guo, C.; Zhou, L.; Lv, J. Effects of expandable graphite and modified ammonium polyphosphate on the flame-retardant and mechanical properties of wood flour-polypropylene composites. *Polym. Polym. Compos.* **2013**, *21*, 449–456.

151. Lindholm, J.; Brink, A.; Hupa, M. Influence of decreased sample size on cone calorimeter results. *Fire Mater.* **2012**, 63–73.

152. Muller, M.; Bourbigot, S.; Duquesne, S.; Klein, R.; Giannini, G.; Lindsay, C.; Vlassenbroeck, J. Investigation of the synergy in intumescent polyurethane by 3D computed tomography. *Polym. Degrad. Stab.* **2013**, *98*, 1638–1647.

153. Girardin, B.; Fontaine, G.; Duquesne, S.; Försth, M.; Bourbigot, S. Characterization of thermo-physical properties of EVA/ATH: Application to gasification experiments and pyrolysis modeling. *Materials (Basel).* **2015**, *8*, 7837–7863.

154. Lyon, R. E.; Walters, R. N. Pyrolysis combustion flow calorimetry. *J. Anal. Appl. Pyrolysis* **2004**, *71*, 27–46.

155. Huggett, C. Estimation of rate of heat release by means of oxygen consumption measurements. *Fire Mater.* **1980**, *4*, 61–65.

156. Duda, A.; Penczek, S. Polymerization of ε-caprolactone initiated by aluminum isopropoxide trimer and/or tetramer. *Macromolecules* **1995**, *28*, 5981–5992.

157. Massiot, D.; Fayon, F.; Capron, M.; King, I.; Le Calvé, S.; Alonso, B.; Durand, J. O.; Bujoli, B.; Gan, Z.; Hoatson, G. Modelling one and two-dimensional solid-state NMR spectra. *Magn. Reson. Chem.* **2002**, *40*, 70–76.

158. Tejado, a; Peña, C.; Labidi, J.; Echeverria, J. M.; Mondragon, I. Physico-chemical characterization of lignins from different sources for use in phenol-formaldehyde resin synthesis. *Bioresour. Technol.* **2007**, *98*, 1655–63.

159. Almendros, G.; Martinez, A. T.; Gonziilez, A. E.; Gonziilez-vila, F. J.; Frund, R.; Ludemannll, H. CPMAS 13C NMR Study of Lignin Preparations from Wheat Straw Transformed by Five Lignocellulose-Degrading Fungi. **1992**, 1297–1302.

160. Popescu, C.-M.; Demco, D. E.; Möller, M. Assessment of historic Tilia codrata wood by solid-state 13C CPMAS NMR spectroscopy. *Polym. Degrad. Stab.* **2013**, *98*, 2730–2734.

161. Streck Roman; Barnes, A. J.; Herreboutc, A.; Veken, B. J. Van Der Conformational behaviour of trimethyl phosphate infrared spectroscopy '. *J. Mol. Struct.* **1996**, *376*, 277–287.

162. Hu, J.; Shen, D.; Wu, S.; Zhang, H.; Xiao, R. Effect of temperature on structure evolution in char from hydrothermal degradation of lignin. *J. Anal. Appl. Pyrolysis* **2014**, *106*, 118–124.

163. Ouyang, X.; Wang, W.; Yuan, Q.; Li, S.; Zhang, Q.; Zhao, P. Improvement of lignin yield and purity from corncob in the presence of steam explosion and liquid hot pressured alcohol. *RSC Adv.* **2015**, *5*, 61650–61656.

164. Dupretz, R.; Fontaine, G.; Bourbigot, S. Fire retardancy of a new polypropylene-grafted starch: Part II: investigation of mechanisms. *J. Fire Sci.* **2013**, *32*, 210–229.

165. Trotta, F.; Zanetti, M.; Camino, G. Thermal degradation of cyclodextrins. **2000**, *69*, 373–379.

166. Jiang, X.; Li, C.; Wang, T.; Liu, B.; Chi, Y.; Yan, J. TG-FTIR study of pyrolysis products evolving from dyestuff production waste. *J. Anal. Appl. Pyrolysis* **2009**, *117*, 296–309.

167. Alén, R.; Kuoppala, E.; Oesch, P. Formation of the main degradation compound groups from wood and its components during pyrolysis. *J. Anal. Appl. Pyrolysis* **1996**, *36*, 137–148.

168. Ma, Z.; Sun, Q.; Ye, J.; QiufangYao; Zhao, C. Study on the thermal degradation behaviors and kinetics of alkali lignin for production of phenolic-rich bio-oil using TGA-FTIR and Py-GC/MS. *J. Anal. Appl. Pyrolysis* **2015**, *117*, 116–124.

169. Schartel, B.; Pawlowski, K. H.; Lyon, R. E. Pyrolysis combustion flow calorimeter: A tool to assess flame retarded PC/ABS materials? *Thermochim. Acta* **2007**, *462*, 1–14.

170. Coquelle, M.; Duquesne, S.; Casetta, M.; Sun, J.; Zhang, S.; Bourbigot, S. Investigation of the decomposition pathway of polyamide 6/ammonium sulfamate fibers. *Polym. Degrad. Stab.* **2014**, 6–13.

171. Schartel, B. Phosphorus-based Flame Retardancy Mechanisms—Old Hat or a Starting Point for Future Development? *Materials (Basel).* **2010**, *3*, 4710–4745.

172. Zhang, H. *Fire-Safe Polymers and Polymer Composites*; 2004; Vol. DOT/FAA/AR.

173. Nassar, M. M.; MacKay, G. D. M. Mechanism of thermal decomposition of lignin. *Wood Fiber Sci.* **1984**, *16*, 441–453.

174. De Klerk, A. 17. Dehydration, Etherification and Hydration. In *Fischer-Tropsch Refining*; 2011; p. 340.

175. Brosse, N.; El Hage, R.; Chaouch, M.; Pétrissans, M.; Dumarçay, S.; Gérardin, P. Investigation of the chemical modifications of beech wood lignin during heat treatment. *Polym. Degrad. Stab.* **2010**, *95*, 1721–1726.

176. Inari, G. N.; Mounguengui, S.; Dumarçay, S.; Pétrissans, M.; Gérardin, P. Evidence of char formation during wood heat treatment by mild pyrolysis. *Polym. Degrad. Stab.* **2007**, *92*, 997–1002.

177. Harris, R.; Merwin, L.; Hägele, G. Solid-state nuclear magnetic resonance study of a series of phosphonic and phosphinic acids. *J. Chem. Soc. …* **1989**, *85*, 1409–1423.

178. Hammerschmidt, F.; Schmidt, S. The Phosphonate-Phosphate and Phosphate-Phosphonate Rearrangement and Their Applications V [1]. On the Reaction of s-Butyllithium / TMEDA with Symmetrical Trialkyl Phosphates. **1997**, *1180*, 1173–1180.

179. Montchamp, J.-L. *Phosphorus Chemistry II: Synthetic Methods*; Montchamp, J.-L., Ed.; Springer, 2015.

180. Bourbigot, S.; Le Bras, M.; Delobel, R.; Trémillon, J.-M. Synergistic effect of zeolite in an intumescence process. Study of the interactions between the polymer and the additives. *J. Chem. Soc. Faraday Trans.* **1996**, *92*, 3435.

181. Prochnow, D.; Grimmer, A. R.; Freude, D. Solid-state NMR studies of 17O-enriched pyrophosphates. *Solid State Nucl. Magn. Reson.* **2006**, *30*, 69–74.

182. Karrasch, A.; Wawrzyn, E.; Schartel, B.; Jäger, C. Solid-state NMR on thermal and fire residues of bisphenol A polycarbonate/silicone acrylate rubber/bisphenol A bis(diphenyl-phosphate)/(PC/ SiR/BDP) and PC/SiR/BDP/zinc borate (PC/SiR/BDP/ZnB) - Part I: PC charring and the impact of BDP and ZnB. *Polym. Degrad. Stab.* **2010**, *95*, 2525–2533.

183. Bourbigot, S.; Bras, M. L. E.; Delobel, R. Carbonization mechanisms resulting from intumescence association with the ammonium polyphosphate-pentaerythritol fire retardant system. *Carbon N. Y.* **1993**, *31*, 1219–1230.

184. McKee, D. W.; Spiro, C. L.; Lamby, E. J. The inhibition of graphite oxidation by phosphorus

additives. *Carbon N. Y.* **1984**, *22*, 285–290.

185. Nakamizo, M.; Kammereck, R.; Walker, P. L. Laser raman studies on carbons. *Carbon N. Y.* **1974**, *12*, 259–267.

186. Tai, F. C.; Lee, S. C.; Wei, C. H.; Tyan, S. L. Correlation between ID∕IG Ratio from Visible Raman Spectra and sp2/sp3 Ratio from XPS Spectra of Annealed Hydrogenated DLC Film. *Mater. Trans.* **2006**, *47*, 1847–1852.

187. Dupretz, R.; Fontaine, G.; Bourbigot, S. Fire retardancy of a new polypropylene-grafted starch: Part II: investigation of mechanisms. *J. Fire Sci.* **2013**, *32*, 210–229.

188. Lindholm, J.; Brink, A.; Hupa, M. Cone calorimeter – a tool for measuring heat release rate. *Finnish-Swedish Flame Days 2009* **2009**, 4B.

189. Lucas, N.; Bienaime, C.; Belloy, C.; Queneudec, M.; Silvestre, F.; Nava-Saucedo, J. E. Polymer biodegradation: Mechanisms and estimation techniques - A review. *Chemosphere* **2008**, *73*, 429–442.

190. Costes, L.; Laoutid, F.; Dumazert, L.; Lopez-cuesta, J.-M.; Brohez, S.; Delvosalle, C.; Dubois, P. Metallic phytates as efficient bio-based phosphorous flame retardant additives for poly(lactic acid). *Polym. Degrad. Stab.* **2015**, *119*, 217–227.

191. Ryu, Y. S.; Hong, S. H.; Ahn, S. H.; Kim, T. U. WO2005017021A1 Flameproof thermoplastic resin composition.

192. Ryu, Y. S.; Hong, S. H.; Ahn, S. H.; Yang, J. H.; Bae, S. H. WO2005012416A1 Flameproof thermoplastic resin composition 2005.

193. Kumar, G.; Worku, A. WO0017268A1 Halogen-free flame retardant thermoplastic polymer compositions 2000.

194. Masato, H.; Matsuyama-shi, E.; Akiyoshi, T.; Tamura, S. EP1055705A1 Flame-retardant composition and molded product formed of the same 2000.

195. Richardson, N.; Dellar, R. J. EP0245207A3 Phosphonsäuresalze enthaltende flammfeste Polymer-Zusammensetzungen 1989.

196. Antonov, Y.; Zubkova, N. S. Decreasing the flammability of polystyrene using phosphonic acid derivatives. *Plast. Massy* **2002**, *9*, 38–40.

197. Inata, H.; Ishida, S.; Kuwaki, T. US6146557 Fire resistant resin composition 2000.

198. Weil, E. D.; Levchik, S. V. Flame Retardants for Polystyrenes in Commercial Use or Development. *J. Fire Sci.* **2007**, *25*, 241–265.

199. Kim, J.; Lee, K.; Lee, K.; Bae, J.; Yang, J.; Hong, S. Studies on the thermal stabilization enhancement of ABS; synergistic effect of triphenyl phosphate nanocomposite, epoxy resin, and silane coupling agent mixtures. *Polym. Degrad. Stab.* **2003**, *79*, 201–207.

200. Weil, D.; Pate, N.; Mukhopadhyay, S. M. A systems approach to flame retardancy and comments on modes of action. *Polym. Degrad. Stab.* **1996**.

201. Matsumoto, H.; Koyama, M.; Yamauchi, K. EP001312644 Flame-retardant resin composition, moldings thereof and flame retardant 2005, *99*.

202. Lee, S.; Lee, C.; Hwang, Y.; Nam, K.; Kim, T. WO03027180A1 2003.

203. Chigwada, G.; Wilkie, C. a Synergy between conventional phosphorus fire retardants and organically-modified clays can lead to fire retardancy of styrenics. *Polym. Degrad. Stab.* **2003**, *81*, 551–557.

204. Noro, M.; Matsusaka, K.; Sumimoto, N. US 6737453 Flame retardant thermoplastic composition 2004, *2*.

205. Wang, J.; Cai, X. Synergistic effect of a novel charring agent with ammonium polyphosphate on flame retardancy and thermal degradation of acrylonitrile-butadiene-styrene copolymer. *Polym. Int.* **2012**, *61*, 703–710.

206. Carpanese, C.; Feng, J.; Fina, A.; Sánchez, A.; Villanueva, S.; Camino, G. *Flame retardant ABS through catalytic charring: comparison of thermal degradation effect of different Lewis acid metal salts*; 2012.

207. Jang, J.; Kim, J.; Bae, J.-Y. Effects of Lewis acid-type transition metal chloride additives on the thermal degradation of ABS. *Polym. Degrad. Stab.* **2005**, *88*, 324–332.

208. Jang, J.; Kim, J.; Bae, J.-Y. Synergistic effect of ferric chloride and silicon mixtures on the thermal stabilization enhancement of ABS. *Polym. Degrad. Stab.* **2005**, *90*, 508–514.

209. Cai, Y.; Hu, Y.; Song, L.; Xuan, S.; Zhang, Y.; Chen, Z.; Fan, W. Catalyzing carbonization function of ferric chloride based on acrylonitrile–butadiene–styrene copolymer/organophilic montmorillonite nanocomposites. *Polym. Degrad. Stab.* **2007**, *92*, 490–496.

210. Dave, T.; Köstler, H.; Wehner, W. DE 102010035103 A1 Flammschutzmittelzusammensetzungen enthaltend Triazin-interkalierte Metall-Phosphate 2010.

211. Dave, T.; Wehner, W. DE 102007036465 A1 Phosphorus-containing triazine compounds as flame retardants 2007.

212. Müller, P.; Schartel, B. Melamine poly(metal phosphates) as flame retardant in epoxy resin: Performance, modes of action, and synergy. *J. Appl. Polym. Sci.* **2016**, *43549*, n/a–n/a.

213. Naik, A. D.; Fontaine, G.; Samyn, F.; Delva, X.; Louisy, J.; Bellayer, S.; Bourgeois, Y.; Bourbigot, S. Outlining the mechanism of flame retardancy in polyamide 66 blended with melamine-poly(zinc phosphate). *Fire Saf. J.* **2014**, *70*, 46–60.

214. Naik, A. D.; Fontaine, G.; Samyn, F.; Delva, X.; Louisy, J.; Bellayer, S.; Bourgeois, Y.; Bourbigot, S. Mapping the multimodal action of melamine-poly(aluminium phosphate) in the flame retardancy of polyamide 66. *RSC Adv.* **2014**, *4*, 18406.

215. Xu, S.; Zhang, L.; Lin, Y.; Li, R.; Zhang, F. Layered double hydroxides used as flame retardant for engineering plastic acrylonitrile–butadiene–styrene (ABS). *J. Phys. Chem. Solids* **2012**, *73*, 1514–1517.

216. Ebadi, M.; Mirdamadian, Z.; Ghanbari, D.; Moradi, L. The Effect of Aminated Carbon Nanotube and Phosphorus Pentoxide on the Thermal Stability and Flame Retardant Properties of the Acrylonitrile–Butadiene–Styrene. *J. Clust. Sci.* **2013**.

217. Bras, M. Le; Wilkie, C. A.; Bourbigot, S. Styrene-acrylonitrile copolymer montmorillonite nanocomposite: processing, characterization and flammability. In *Fire Retardancy of Polymers New Applications of Mineral Fillers*; 2005; pp. 177–186.

218. Morgan, A. B.; Jr, R. H. H.; Kashiwagi, T.; Chyall, L. J.; Gilman, J. W. Flammability of Polystyrene Layered Silicate (Clay) Nanocomposites : Carbonaceous Char Formation. **2002**, *253*, 247–253.

219. Vannier, A.; Duquesne, S.; Bourbigot, S.; Alongi, J.; Camino, G.; Delobel, R. Investigation of the thermal degradation of PET, zinc phosphinate, OMPOSS and their blends—Identification of the formed species. *Thermochim. Acta* **2009**, *495*, 155–166.

220. Munteanu, B. S.; Brebu, M.; Vasile, C. Thermal behaviour of binary and ternary copolymers containing acrylonitrile. *Polym. Degrad. Stab.* **2013**, *98*, 1889–1897.

221. Fox, T. G.; Flory, P. J. The glass temperature and related properties of polystyrene. Influence of molecular weight. *J. Polym. Sci.* **1954**, *14*, 315–319.

222. Andrianova, G. P.; Bakeyev, N. F.; Kozlov, P. V Structural plasticization of polymers. *Polym. sicence U.S.S.R.* **1971**, *13*, 298–309.

223. Di Cortemiglia, L.; Camino, G.; Costa, L.; Gualta, M. Thermal degradation of ABS. *Thermochimica* **1985**, *93*, 187–190.

224. Bourbigot, S.; Gilman, J. W.; Wilkie, C. a. Kinetic analysis of the thermal degradation of polystyrene–montmorillonite nanocomposite. *Polym. Degrad. Stab.* **2004**, *84*, 483–492.

225. Bhaskar, T.; Murai, K.; Matsui, T.; Brebu, M. A.; Muto, A.; Sakata, Y.; Murata, K. Studies on thermal degradation of acrylonitrile Á butadiene Á styrene copolymer (ABS-Br) containing brominated flame retardant. **2003**, *70*, 369–381.

226. Suzuki, M.; Wilkie, C. A. The thermal degradation of acrylonitrile-butadiene-styrene terpolymer as studied by TGA/FTIR. *Polym. Degrad. Stab.* **1995**, *47*, 217–221.

227. Rimdusit, S.; Atthakorn, D.; Damrongsakkul, S.; Saramas, D.; Tiptipakorn, S. Mechanical, Thermal, and Water Uptake Characteristics of Woodflour-Filled Polyvinyl Chloride/Acrylonitrile Butadiene Styrene Blends. *J. Appl. Polym. Sci.* **2012**, *124*, 943–950.

228. Feng, J.; Carpanese, C.; Fina, A. Thermal decomposition investigation of ABS containing Lewis-acid type metal salts. *Polym. Degrad. Stab.* **2016**, *129*, 319–327.

229. Kusch, P. Pyrolysis-Gas Chromatography/Mass Spectrometry of Polymeric Materials. In *Advanced Gas Chromatography - Progress in Agricultural, Biomedical and Industrial Applications*; 2012; p. 470.

230. Kusch, P. Identification of Synthetic Polymers and Copolymers by Analytical Pyrolysis Gas Chromatography/Mass Spectrometry. *J. Chem. Educ.* **2014**, *91*, 1725–1728.

231. Shapi, M. M.; Hesso, A. Gas chromatographic-mass spectrometric analysis of some potential toxicants amongst volatile compounds emitted during large-scale thermal degradation of poly (acrylonitrile- butadiene-styrene) plastic. *J. Chromatogr.* **1991**, *562*, 681–696.

232. Gérard, C.; Fontaine, G.; Bellayer, S.; Bourbigot, S. Reaction to fire of an intumescent epoxy resin: Protection mechanisms and synergy. *Polym. Degrad. Stab.* **2012**, *97*, 1366–1386.

233. Fontaine, G.; Gallos, A.; Bourbigot, S. Role of montmorillonite for enhancing fire retardancy of intumescent PLA. *Fire Saf. Sci.* **2014**, *11*, 808–820.

234. Muller, M.; Bourbigot, S.; Duquesne, S.; Klein, R. a.; Giannini, G.; Lindsay, C. I. Measurement and investigation of intumescent char strength: Application to polyurethanes. *J. Fire Sci.* **2013**, *31*, 293–308.

235. Jimenez, M.; Duquesne, S.; Bourbigot, S. Characterization of the performance of an intumescent fire protective coating. *Surf. Coatings Technol.* **2006**, *201*, 979–987.

236. Liu, L.; Qian, M.; Song, P.; Huang, G.; Yu, Y.; Fu, S. Fabrication of Green Lignin-based Flame Retardants for Enhancing the Thermal and Fire Retardancy Properties of Polypropylene/Wood Composites. *ACS Sustain. Chem. Eng.* **2016**, acssuschemeng.6b00112.

237. Korich, A. L.; Fleming, A. B.; Walker, A. R.; Wang, J.; Tang, C.; Iovine, P. M. Chemical modification of organosolv lignin using boronic acid-containing reagents. *Polymer (Guildf).*

2012, *53*, 87–93.

Appendix

Appendix 1- Technical data sheets of the polymers used in the PhD

Moplen HP401R (PP)

Typical Properties	Method	Value	Unit
Physical			
Density	ISO 1183	0.905	g/cm³
Melt flow rate (MFR) (230°C/2.16Kg)	ISO 1133	25	g/10 min
Melt volume flow rate (230°C/2.16Kg)	ISO 1133	34	cm³/10min
Mechanical			
Tensile Modulus	ISO 527-1, -2	1350	MPa
Tensile Stress at Yield	ISO 527-1, -2	32	MPa
Tensile Strain at Break	ISO 527-1, -2	> 50	%
Tensile Strain at Yield	ISO 527-1, -2	10	%
Impact			
Charpy unnotched impact strength	ISO 179		
(23 °C, Type 1, Edgewise)		105	kJ/m²
(0 °C, Type 1, Edgewise)		25	kJ/m²
Charpy notched impact strength (23 °C, Type 1, Edgewise, Notch A)	ISO 179	2	kJ/m²
Hardness			
Ball indentation hardness (H 358/30)	ISO 2039-1	70	MPa
Thermal			
Heat deflection temperature B (0.45 MPa) Unannealed	ISO 75B-1, -2	90	°C
Vicat softening temperature	ISO 306		
(B50 (50°C/h 50N))		85	°C
(A50 (50°C/h 10N))		154	°C

Ellastolan C85A (TPU)

Typical Properties of Elastollan®	ASTM Test Method	Units	Typical Values
All the physical properties reported here are measured on injection molded samples. Properties of sheet or film samples of this product are also available upon request.			
Specific Gravity	ASTM D 792	g/cm^3	1.19
Shore Hardness	ASTM D 2240	Shore A or D	85A
Taber Abrasion	ASTM D 1044	mg loss	25
DIN Abrasion	DIN 53516	mm^3 loss	25
E-Modulus	ASTM D 412	psi	3000
Flexural Modulus	ASTM D 790	psi	3600
Tensile Strength	ASTM D 412	psi	6000
Tensile Stress at 100% Elongation	ASTM D 412	psi	1000
Tensile Stress at 300% Elongation	ASTM D 412	psi	2200
Ultimate Elongation	ASTM D 412	%	590
Tear Strength	ASTM D 624, Die C	lb/in	620
Compression Set 22h at 70ºC 22h at 23 ºC	ASTM D 395 "B"	% of original deflection	35 25
Glass Transition temperature*	BASF Analytical Method	ºC	-40
Vicat Softening Temperature	ASTM D 1525	ºC	110
DMA Softening Temperature	BASF Analytical Method	ºC	100

*Measured with Dynamic Mechanical Analysis (DMA). DMA profile is available upon request.
Above values are shown as typical values and should not be used as specifications.

PS 168N/L (PS)

Property, Test Condition	Standard	Unit	Values
Rheological Properties			
Melt Volume Rate, 200 °C/5 kg	ISO 1133	cm³/10 min	1.5
Mechanical Properties			
Charpy Unnotched, 23° C	ISO 179	kJ/m²	<25
Tensile Stress at Yield, 23° C	ISO 527	MPa	59
Tensile Strain at Break, 23° C	ISO 527	%	3
Tensile Modulus	ISO 527	MPa	3300
Tensile Creep Modulus (1000h)	ISO 899	MPa	2600
Tensile Creep Modulus (1h)	ISO 899	MPa	3300
Flexural Strength	ISO 178	MPa	106
Hardness, Ball Indentation	ISO 2039-1	MPa	150
Thermal Properties			
Vicat Softening Temperature, B/1 (120°C/h, 10N)	ASTM D 1525	°C	108
Vicat Softening Temperature, B/2 (120°C/h, 50N)	ASTM D 1525	°C	101
Heat Deflection Temperature A; (annealed, 1.8 MPa)	ISO 75	°C	86
Heat Deflection Temperature B; (annealed, 0.45 MPa)	ISO 75	°C	98
Coefficient of Linear Thermal Expansion	ISO 11359	10^(-6)/°C	80
Thermal Conductivity	DIN 52612-1	W/(m K)	0.17

Property, Test Condition	Standard	Unit	Values
Other Properties			
Density	ISO 1183	kg/m³	1040
Water Absorption, Saturated at 23°C	ISO 62	%	<0.1
Moisture Absorption, Equilibrium 23°C/50% RH	ISO 62	%	< 0.1

Terluran Hi-10 (ABS)

Typical values [1] at 23°C	Test method [2]	Unit	Values
Properties			
Polymer abbreviation	-	-	**ABS**
Density	ISO 1183	kg/m³	1030
Filler content: Glass fiber (GF)	-	%	-
Water absorption, equilibrium in water at 23°C	similar to ISO 62	%	1.03
Moisture absorption, equilibrium 23°C/50% r.h.	similar to ISO 62	%	0.21

Flammabillity			
UL94 rating at 1.6 mm thickness	UL 94	class	HB
Automotive materials (thickness d >= 1mm)	-	-	+
Mechanical Properties			
Tensile modulus	ISO 527-1/-2	MPa	1900
Yield stress, 50 mm/min	ISO 527-1/-2	MPa	38
Yield strain, 50 mm/min	ISO 527-1/-2	%	2.8
Nominal strain at break, 50 mm/min	ISO 527-1/-2	%	9
Flexural strength	ISO 178	MPa	56
Charpy impact strength (23°C)	ISO 179/1eU	kJ/m²	N
Charpy impact strength (-30°C)	ISO 179/1eU	kJ/m²	140
Izod notched impact strength (23°C)	ISO 180/1A	kJ/m²	36
Izod notched impact strength (-30°C)	ISO 180/1A	kJ/m²	14
Charpy notched impact strength (23°C)	ISO 179/1eA	kJ/m²	35
Charpy notched impact strength (-30°C)	ISO 179/1eA	kJ/m²	13
Izod notched impact strength, method A (23°C)	ASTM D 256	J/m	410
Ball indentation hardness	ISO 2039-1	MPa	74
Force	ISO 2039-1	N	358
Duration	ISO 2039-1	s	30
Thermal properties			
HDT A (1.80 MPa)	ISO 75-1/-2	°C	96
HDT B (0.45 MPa)	ISO 75-1/-2	°C	101
Vicat softening temperature VST/A/50	ISO 306	°C	103
Vicat softening temperature VST/B/50	ISO 306	°C	90
Max. service temperature (short cycle operation)	-	°C	80
Coefficient of linear thermal expansion, longitudinal (23-80)°C	ISO 11359-1/-2	E-4/°C	0.8 - 1.1
Thermal conductivity	DIN 52612-1	W/m*K	0.17

Evatan® 28-05 (EVA)

Characteristics	Value	Test method
Vinyl Acetate content	27-28 wt%	FTIR
Melt Index (190 C / 2.16 kg)	5-8 g/10min	ISO 1133 / ASTM D1238
Density (23 °C)	0.95 g/cm³	ISO 1183
Melting Point	72 °C	ISO 11357-3
Vicat softening point (10 N)	40 °C	ISO 306 / ASTM D1525
Ring&Ball temperature	160 °C	ASTM E28 / NF EN 1238
Elongation at break	700-1000 %	ISO 527 / ASTM D638
Tensile strength at break	24 MPa	ISO 527 / ASTM D638
Hardness Shore A	80	ISO 868 / ASTM D2240

PLA 4032D (PLA)

| Typical Material & Application Properties [1, 2, 3]			
Film Properties		**Ingeo 4032D**	**ASTM Method**
Density		1.24 g/cc	D1505
Tensile Strength	MD	15 kpsi	D882
	TD	21 kpsi	D882
Tensile Modulus	MD	500 kpsi	D882
	TD	550 kpsi	D882
Elongation at Break	MD	180%	D882
	TD	100%	D882
Elmendorf Tear	MD	17 g/mil	D1922
	TD	14 g/mil	D1922
Spencer Impact		2.5 joules	
Transmission Rates	Oxygen	675 cc-mil/m^2-24hr-atm	D1434
	Carbon Dioxide	2,850 cc-mil/m^2-24hr-atm	Internal
	Water Vapor	375 g-mil/m^2-24hr-atm	F1249
Optical Characteristics	Haze	2.1%	D1003
	Gloss, 20°	90	D1003
Thermal Characteristics	Melting Point	155-170°C	D3418

(1) Typical properties; not to be construed as specifications.

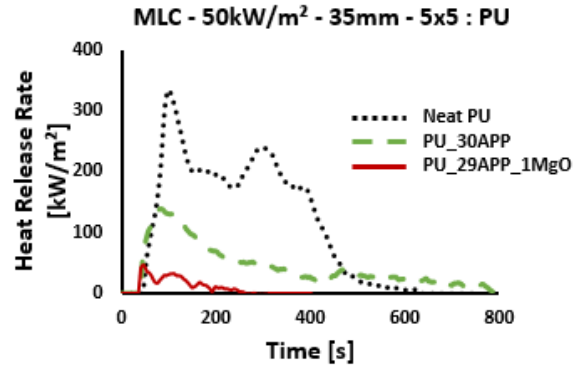(2) All properties measured on 1.0 mil film.

(3) Typical values for a film oriented 3.5x in MD and 5x in TD.

Appendix 2. Data obtained by standard or reduced MLC for PU and EVA formulations
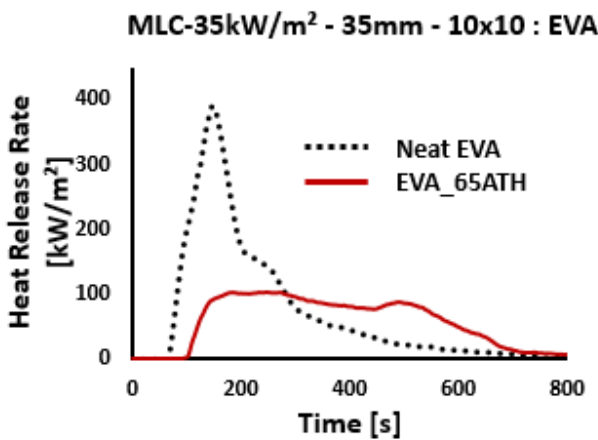
Formulations based on PU
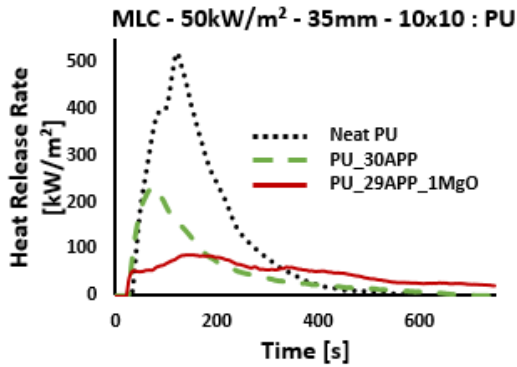
	TTI [s]	TOF [s]	pHRR [kW/m²]	THR [MJ/m²]	Residue [wt.%]
Neat PU	33	411	520	78	7%
PU_30APP	28	649	233	37	41%
	-5	238	-55%	-52%	34%
PU_29APP_1MgO	25	867	86	40	43%
	-8	456	-83%	-49%	36%

	TTI [s]	TOF [s]	pHRR [kW/m²]	THR [MJ/m²]	Residue [wt.%]
Neat PU	48	479	336	80	13%
PU_30APP	38	752	128	32	52%
	-10	273	-62%	-60%	39%
PU_29APP_1MgO	37	132	46	4	80%
	-11	-347	-86%	-95%	67%

Formulations based on EVA

	TTI [s]	TOF [s]	pHRR [kW/m²]	THR [MJ/m²]
Neat EVA	71	698	391	58
EVA_65ATH	105	669	104	47
	34	-29	-73%	-20%
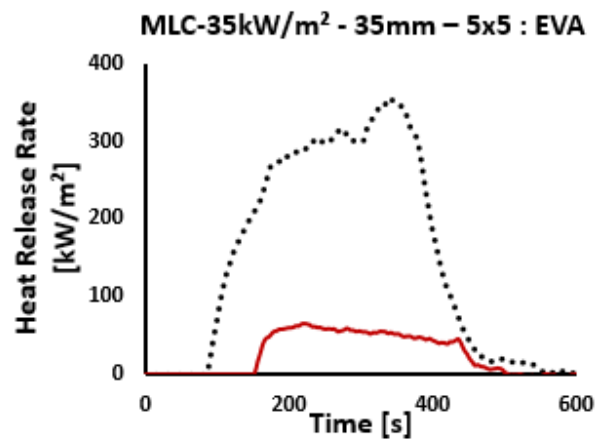
	TTI [s]	TOF [s]	pHRR [kW/m²]	THR [MJ/m²]
Neat EVA	86	442	356	90
EVA_65ATH	154	436	65	16
	68	-6	-82%	-83%

Appendix 3. TGA-FTIR spectra of ABS/lignin formulations at different temperatures
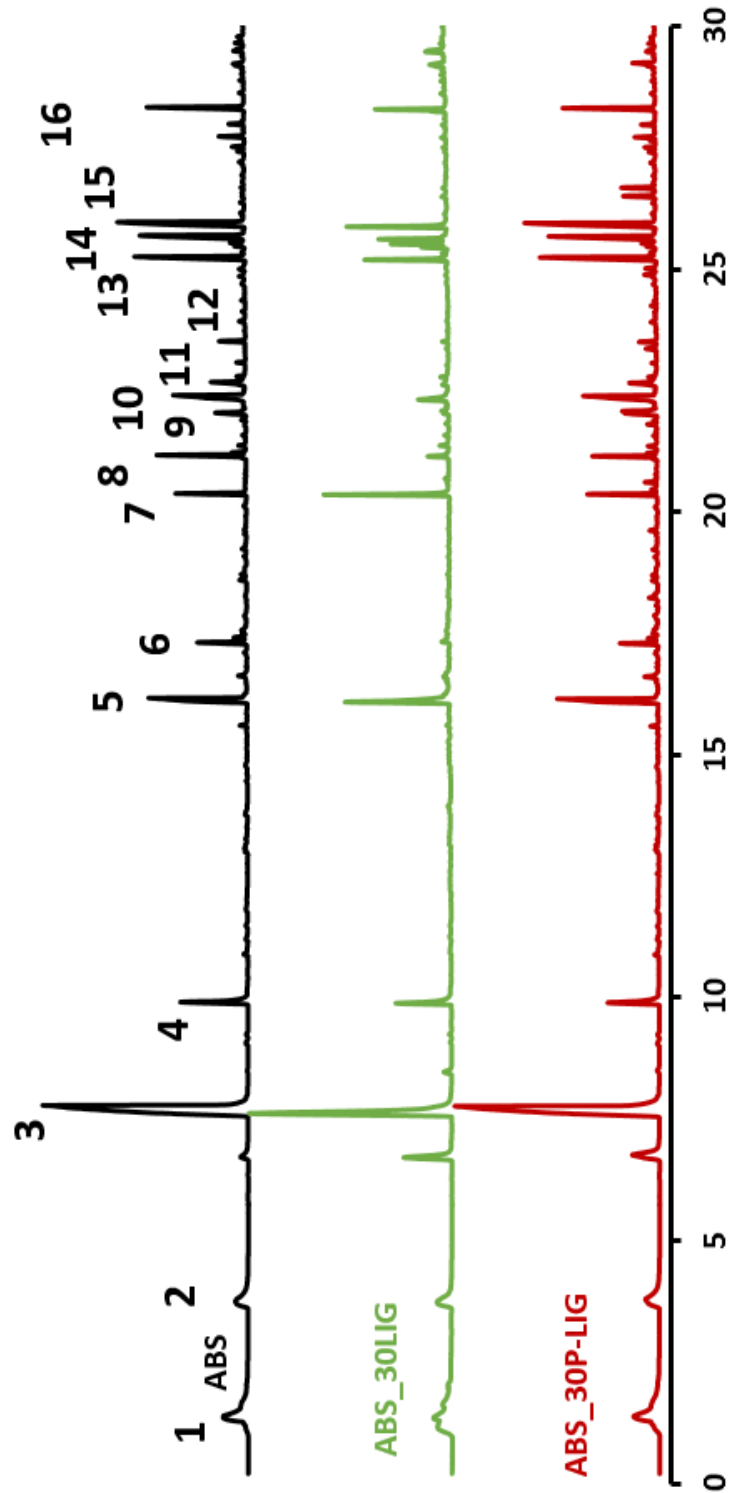
Thermo-oxidation
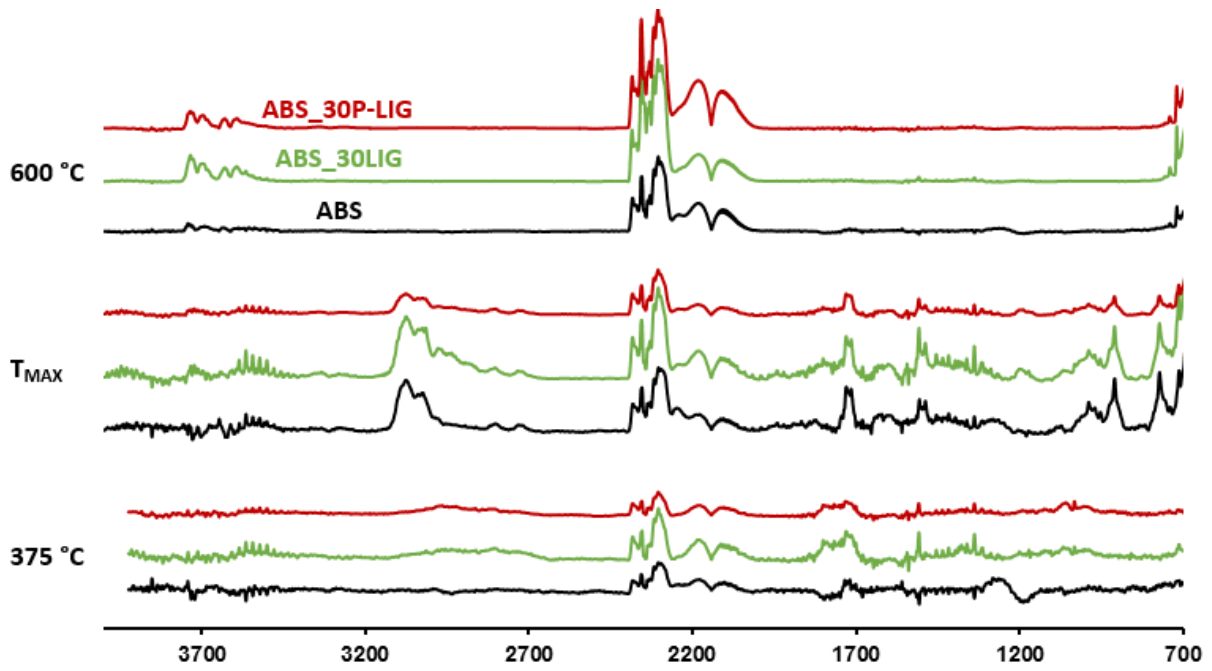
Pyrolysis
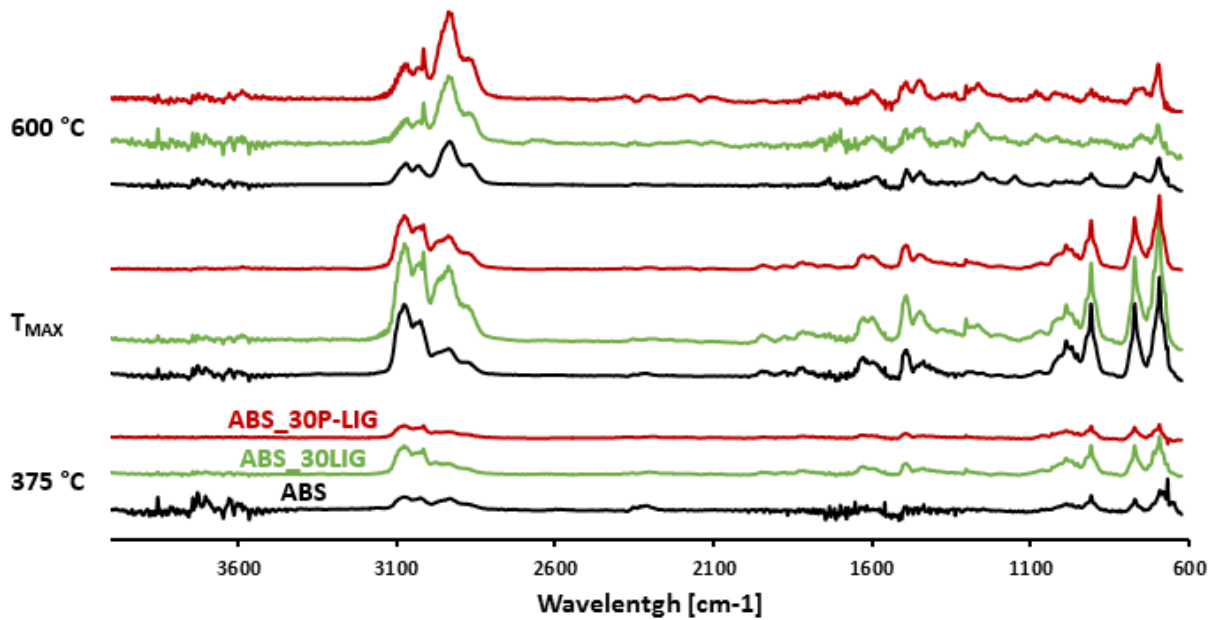
Appendix 4. Py-GCMS of ABS formulations treated at 475 °C

Py-GCMS spectra of neat ABS and ABS/lignin composites at 475 °C. Attribution numbers are detailed in Table 41, p202.

Comparison of ABS, ABS/lignin composites chromatograms obtained 475 °C